DEVELOPMENT OF A TRUSS-ARCH MODEL UNIFIED FOR FLEXURE AND SHEAR-CRITICAL INTERACTION OF STRUCTURAL CONCRETE MEMBERS

A Dissertation

by

JUDONG LEE

Submitted to the Office of Graduate and Professional Studies of
Texas A&M University
in partial fulfillment of the requirements for the degree of

DOCTOR OF PHILOSOPHY

Chair of Committee,	John B. Mander
Committee Members,	Stefan Hurlebaus
	Mary Beth Hueste
	Julian Kang
Head of Department,	Robin Autenrieth

December 2020

Major Subject: Civil Engineering

ABSTRACT

Based on force-deformation behavior computed using the Compatibility Strut and Tie Model (C-STM), a theoretical limit analysis model is developed to predict the ultimate shear-carrying capacity of shear-critical structural concrete beams with and without transverse reinforcement. The Truss-Arch Model Unified (*TAMU*) is validated based on experimental observations and from previous studies reported in the literature. The limit analysis approach assumes the failure mechanism occurs when the principal diagonal arch reaches its softened peak strength. Two truss models, with a vertical tie or an inclined tie, are used depending on whether the members are reinforced with or without shear steel, respectively. Explicit solutions for the principal strain ratio and ultimate shear strength are derived based on truss and arch contribution to flexibility and strength. A large database of test data consisting of 839 beams is assembled for the substantiation of the proposed method and also to conduct a comparative assessment of existing code-based shear analysis methods. The proposed *TAMU* approach predicts well the limit load capacities against the database. When compared with existing code-based shear analysis approaches, the *TAMU* based approach demonstrates superior accuracy with less dispersion due to modeling and aleatory uncertainty in both D-and B-regions.

The *TAMU* approach is further extended to account for axial strain effects which may be present due to the presence of either prestress, axial load, or both. A full-scale experimental program is conducted on reinforced and prestressed concrete bent caps to investigate the effect of prestressing force, shear reinforcement spacing, interior voids, and axial loads on the bent cap. The specimens are analyzed by the *TAMU* method and other existing code-based analysis methods. The C-STM and *TAMU* analysis methods are able to accurately predict the experimental test outcomes somewhat better than existing code analysis approaches.

DEDICATION

I dedicate this work to my lovely wife Jieun,

who has been a constant source of support, encouragement, and love

throughout this journey.

ACKNOWLEDGEMENTS

CONTRIBUTORS AND FUNDING SOURCES

Birely, A.C., Yole, K.J., **Lee, J.D.**, McKee, C.D., and Mander, J.B. (2020). "Experimental Behavior of Reinforced Concrete and Pretensioned Concrete Bent Caps," *Journal of Bridge Engineering*, V.25(2)

TABLE OF CONTENTS

LIST OF FIGURES

LIST OF TABLES

1. INTRODUCTION

1.1　Background and Motivation

Over the past few decades, a number of experimental and theoretical studies have been performed to investigate the mechanism and primary parameters of shear failure in structural concrete beams under flexure-shear interaction. Due to the effort of many researchers, various shear designs have been proposed from empirical and theoretical approaches. However, the determination of the ultimate shear-carrying capacity of structural concrete beams is still open to discussion because various parameters which may affect the shear mechanism of concrete beams are not properly accounted for. Given the nature of the shear failure that could occur without warning, the accurate prediction of shear capacity of concrete structures is necessary to avoid an unexpected brittle failure that could result in a catastrophe.

Structural concrete members may be categorized into several types depending on their geometry with the shear resistance mechanism depending on slenderness, shear intensity, and loading. Figure 1-1 presents commonly accepted classifications of beams based on the shear span-depth ratio, a/d. In general, a member is considered slender if $a/d \geq 2.5$ or very deep if $a/d < 1.0$, and are governed generally by flexure and shear, respectively. Between these limits, intermediate beams may be governed by the interacting effects of both flexure and shear (Kani 1964, Zsutty 1971, Zararis and Papadakis 2001, and Choi et al. 2007).

The two distinct actions are generally recognized as the principal mechanisms related to shear resistance within a structural concrete element: 1) truss action, which dominates the shear resistance in slender beams; and 2) arch action, which governs the shear mechanism in deep beams. Truss action is generally associated with shear resistance provided by transverse reinforcement, whereas arch action is associated with shear resistance provided by a diagonal concrete compressive strut which follows the principal load path between the applied load and the supports.

1
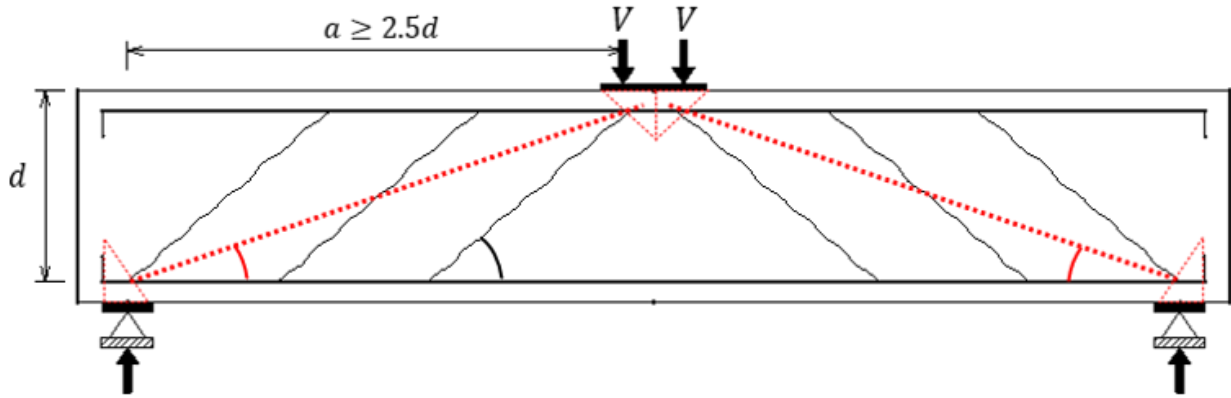
(a) Slender beam; behavior is governed by truss action
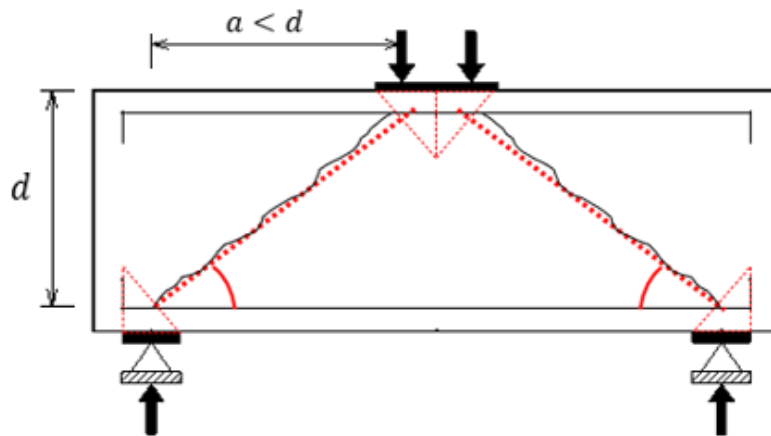
(b) Squat beam; behavior is governed primarily by arch action
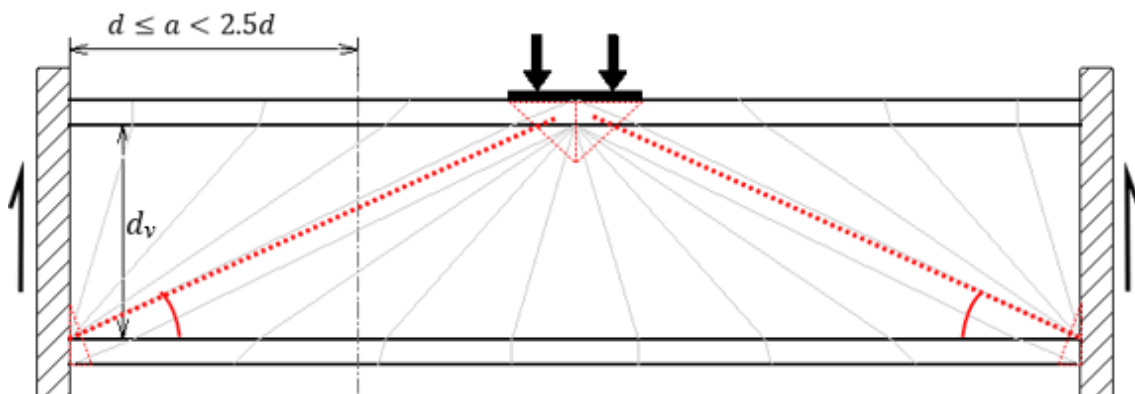
(c) Intermediate beam; behavior is governed primarily by combined truss-arch action

Figure 1-1. Determination of slender, intermediate, and deep beams.

Historically, sectional shear theories have been used to design RC beams. However, these shear theories are generally derived by considering truss action and do not take arch action into account. Also, in the sectional model, it is assumed that the forces such as shear, flexure, and torsion at a particular section are independent of each other, thus, the required reinforcement is determined separately instead of considering the coupled effect of these actions. Schlaich et al., (1987) introduced the concept of B-and D-regions, where B stands for 'Beam' or 'Bernoulli', and D stands for 'Discontinuity' or 'Disturbed'. While the sectional model may be used in designing B-regions as the strain distribution is linear, it is not strictly applicable to D-regions because the shear-flexure interaction causes the high irregularity of internal stress and nonlinear strain distribution (Mander et al., 2012).

The current American Association of State Highway and Transportation Officials (AASHTO) LRFD and American Concrete Institute (ACI) design provisions suggest using Strut-and-Tie Model (STM) to design D-regions (AASHTO, 2017, and ACI 318, 2019). However, recent works by Scott et al., (2012a) and Liu et al., (2017) have shown that the use of STM could result in an exceedingly conservative design. Because the STM satisfies force equilibrium only and is formulated as a lower bound plastic solution, the critical failure mode is often elusive to the designer.

A big research question arises: "Is there a more comprehensive way to directly accommodate the flexure-shear interaction in the shear design for shear-critical reinforced concrete members with both D- and B- regions?". To answer this question, this dissertation is dedicated to investigating the flexure-shear behavior of reinforced concrete beams and also to suggest a comprehensive shear design procedure for them.

Additionally, this dissertation is focused on the introduction of prestressing technology for precast bent caps (referred to as 'precast, prestressed concrete bent caps'). Since the mid-1990s, the Texas Department of Transportation (TxDOT) has been well aware of on-site construction delays caused by the use of cast-in-place (CIP) reinforced concrete (RC) bent caps. To this end, precast reinforced concrete bent caps have been developed and successfully used in certain standard bridge projects in Texas. Advantages of precast RC bent caps over CIP bent caps include; 1) accelerated bridge construction; 2) efficient production with high-quality concrete; 3) Reduced traffic disruption; 4) accommodation of special construction conditions with harsh environments and difficult access; and 5) less impact on the environment by reducing construction waste.

However, as progress to date has generally been limited to reinforced concrete, the next step to improve and maximize serviceability, durability, and sustainability of bridge substructures may be to introduce prestressing to precast bent caps. In addition to the abovementioned advantages of precast concrete, the use of prestressing force in precast bent caps can bring improved resistance to cracking and enhanced flexural and shear strengths. With better cracking and flexural resistance, the use of an interior void to reduce weight may be additionally achieved. Thus, another significant research question is raised: "Can precast concrete bent caps be effectively prestressed and accommodate a large void and how do these caps perform, especially in shear?".

1.2   Research Objectives

The major objectives of this study are as follows:

- Develop an appropriate shear design model to account for flexure-shear interaction in shear-critical reinforced concrete beams.

4

- Establish simple and straightforward shear analysis and design procedures based on the proposed method, providing the ultimate shear-carrying capacity of shear-critical RC members.

- Develop a large shear database from previous experimental studies to verify the proposed method.

- Evaluate the adequacy of existing code-based shear designs for shear-critical RC beams using the shear database.

- Perform C-STM using the versatile program, *OpenSees* (Version 3.2.2, 2020), and compare the results with the proposed method and the test results.

- Understand and realize the performance advantages of PSC bents cap over RC bent caps.

- Investigate the possibility to lighten the weight of bent caps without compromising the cracking moment or shear resistance.

1.3   What Then Is Particularly New in This Research?

1.3.1   Analytical Program

The Compatibility Strut-and-Tie Method has been previously demonstrated as an efficient nonlinear modeling approach to accurately predict the overall load-deformation response of shear-critical reinforced concrete members. However, one might hesitate to use the C-STM for design as it is highly computational. To overcome this difficulty, the C-STM is reduced in scope to be more executable in performing strength analysis amenable to computation by hand. This reduced model, which need not track overall force-deformation behavior, is herein referred to as the *Truss-Arch Model Unified* (or *TAMU*).

The *TAMU* model accounts for the strength reduction of the principal diagonal concrete arch, which is softened due to the transverse principal tensile strain. It is thus assumed the structure

loses its ultimate load-carrying capacity when the principal diagonal arch fails. Thus, the *TAMU* approach is geared to estimate the limit load of the diagonal arch, which often leads to a sudden or brittle collapse of a shear-critical system. This simplified *TAMU* method is developed and verified for beams with and without transverse reinforcement using a large database of shear tests.

Not only is the C-STM simplified in the present study but also its use is expanded. Previously, the C-STM analysis was implemented using a commercially available structural analysis program, SAP2000. In the present study, the more versatile program, *OpenSees* (Version 3.2.2), is used to model the C-STM, allowing users to choose more accurate constitutive models for materials. As a result, a more accurate analysis is performed on large scale physical tests on bridge piers. The displacement-based C-STM analysis is further developed to capture the performance of solid and hollow prestressed concrete bent caps.

1.3.2 Experimental Program

Prestressing is introduced to precast concrete bents to minimize time and to maximize the economy using factory-like production. The verification of the performance of precast prestressed concrete bent caps is made through full-scale experimentation on bent cap subassemblies. Previous experimental studies of reinforced bent caps have used a sub-assemblage that consisted of a single column with the bent cap cantilevered from both sides. In this test setup, the demands were limited to the negative moment region, and the shear-moment demand ratios did not accurately reflect those in actual bent systems. For this reason, the test setup is specially devised to simulate both positive and negative critical regions with similar shear-moment demand ratios.

Other benefits of prestressed bent caps are the possibility for improved resistance to cracking as a result of the prestressing force and reduced weight through the use of interior voids. The large size of the bent cap does not have a weight issue if the cast-in-place method is used.

However, the weight of long precast bent caps may be restricted for shipping and erection as well. It may be practical to adapt an interior void to avoid the problem of weight exceedance for the broad use of the precast prestressed bent caps. This study examines the possibility of applying interior voids in bent caps through previous experimental programs and develops an ideal size that ensures the serviceability of bent caps without compromising the overall performance.

To accommodate the opening for the bent-column connection, a side configuration of longitudinal reinforcement is proposed. The interference among the longitudinal reinforcement in the bent cap and column and the precast connection can be avoided by using this configuration, maximizing the benefit of precast concrete. Also, uniformly distributed reinforcement may control cracks effectively

1.4 Organization

The dissertation is organized into a total of seven chapters. Following this introductory chapter, Chapter 2 presents a comprehensive literature review of the previous research regarding various reinforced concrete shear theories, state-of-practice on shear designs, state-of-practice on the use of precast bent caps.

Chapter 3 introduces the concept of the *TAMU* shear analysis approach. The *TAMU* approach estimates the ultimate shear-carrying capacity of the concrete member by focusing on the failure of the principal diagonal arch due to the softening effect. The explicit solution for the implementation of the method is presented and verified through previous experimental results of large-scale bridge piers.

Chapter 4 presents further broad substantiation of the *TAMU* approach. A shear database is developed via a comprehensive literature review and a total of 540 reinforced concrete beams which failed in flexure-shear interaction are collected. The *TAMU* approach is tested against the

shear database to estimate the ultimate shear strengths, and the analysis results are compared with the test results as well as three existing code-based shear analysis methods

In Chapter 5, the proposed *TAMU* method is modified to apply to beams without transverse reinforcement. To capture the truss mechanism, a simple truss consisting of a single concrete tie perpendicular to the principal diagonal arch represents the lumped concrete tension field. Formulae to calculate the maximum shear strength are derived using shear deformations of truss and arch actions. A shear database consisted of 380 shear-critical beams without transverse reinforcement is used to verify the modified *TAMU* approach as well as three existing code-based shear strength analysis methods.

Chapter 6 presents the experimental test of prestressed concrete bent caps. Full-scale bent cap subassemblies are tested to verify the improved performance of prestressed concrete caps over reinforced concrete caps. The experimental program is designed to investigate the effect of prestressing force, the shear reinforcement, and an interior void on the bent cap, and the test results are analyzed by each parameter. The maximum shear strengths and failure locations of specimens are predicted using the C-STM and *TAMU* analyses and compared with the test results.

Finally, Chapter 7 presents a summary of the analytical and experimental studies and the key findings from the present study. Major conclusions from each section are made, and recommendations for future work are presented.

In addition to the abovementioned chapters, two appendices are presented, following the references. Appendix A provides the shear database for both cases with and without transverse reinforcement developed to verify the proposed *TAMU* method. Appendix B provides detailed information regarding the experimental program, including material properties and specimen design.

2. LITERATURE REVIEW

2.1 Overview

This chapter provides the results of a comprehensive literature review of previous investigations to help understanding and accomplishing the study objectives. Specific technical objectives include: a) understanding various theories and models that explain the internal mechanism of the flexure-shear interaction; b) investigating available test data under combined flexure-shear loading RC beam; c) developing the shear mechanism and design procedure for shear-critical reinforced and prestressed concrete members; d) examining performance of precast, prestressed bent caps; and e) investigating appropriate ways to lighten the member's weight.

This literature reviews also traces the evolution of shear theories in conjunction with flexure and points out the folly of treating the two separately. It then goes on to outline attempts a few investigators have made in trying to unify the flexure-shear interaction and then makes the case for a new theory which is the subject of this research.

In this literature review, the following are specific areas of focus: (i) Truss models to capture shear and flexure behavior; (ii) Shear-flexure interaction based on diagonal cracks; (iii) Various parameters affecting the shear capacity of RC beams; (iv) State-of-practice on shear designs; (v) Use of precast bent cap in Texas; and (vi) Methods to reduce bent cap weight.

Various truss models to explain the flexure-shear interaction are introduced in Section 2.2. Section 2.3 focuses on a relation between the interaction and diagonal shear crack. Design variables affecting the shear strength of concrete strengths are presented in Section 2.4, followed by the state-of-practice on the shear design found in AASHTO LRFD provision in Section 2.5. A background and current use of precast bent caps in Texas are given in Section 2.6. Finally, research questions arising from this literature review are discussed in Section 2.7

2.2   Truss Models to Capture Shear and Flexure Behavior

Truss models have been considered as an understandable and reasonable way to explain the behavior of reinforced concrete structures and extensively used to the design and analyze them. In this section, various truss models are categorized in terms of two aspects: 1) plasticity; and 2) compatibility, and studies regarding each aspect are described in chronological order in the following subsections.

2.2.1   Plastic Truss Models

Since the truss analogy was first introduced by Ritter (1899) and Mörsch (1909) nearly 120 years ago, it has been adapted by various shear design procedures for structural concrete all over the world. In the truss analogy, it is assumed that a cracked reinforced concrete beam behaves like a truss consisting of 1) compression and tension chords in the longitudinal direction; 2) diagonal concrete strut in the web; and 3) transverse steel ties as shown in Figure 2-1.
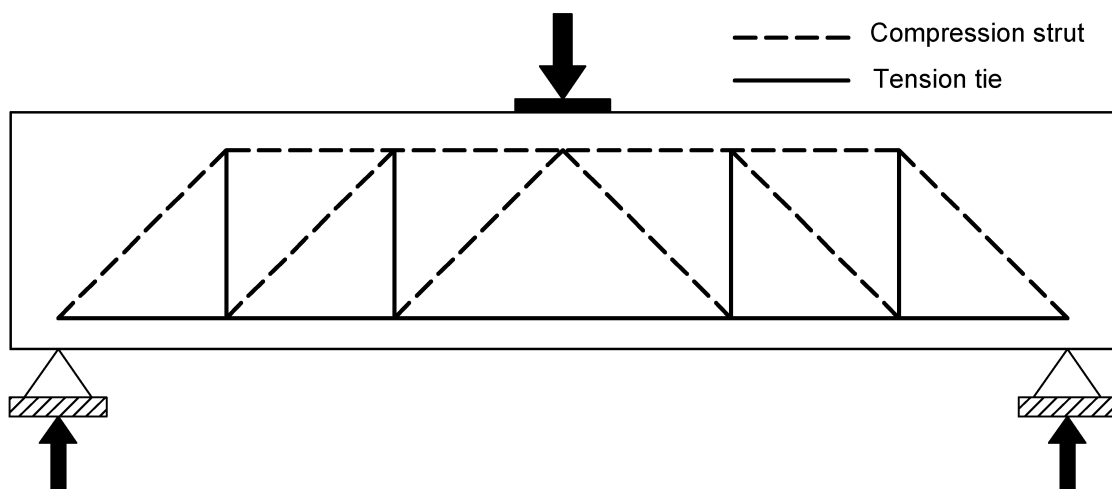
Figure 2-1. Truss analogy model

When shear is applied to this truss model, compression is resisted by a longitudinal compression chord at the top formed by concrete. In a similar manner, tension is resisted by a longitudinal tension chord formed by the bottom reinforcement. Shear forces transferred through diagonal compressive force are carried by concrete and transverse steel ties. Mörsch assumed the angle of the diagonal concrete strut to be 45-degree after he found it was not possible to determine the angle mathematically.

Based on plasticity theory, the fundamental equilibrium equations for shear were derived by Nielsen (1967) and Lampert and Thurlimann (1968). The authors developed the plasticity truss model for beams to consider the yielding of the steel reinforcement.

The strut-and-tie model (referred to as STM) was promoted by Marti (1985) based on his study regarding the application of consistent equilibrium and ultimate strength considerations for the design and detailing of reinforced concrete beams. Marti used the truss model to examine the equilibrium among applied forces, reactions, and internal forces in concrete and reinforcement. Based on the truss model, he proposed a design method applicable to arbitrary geometries of the structural concrete under various loading conditions. His work was recognized as the first attempt in the development of the STM which can be found in ACI and AASHTO design provisions today.

However, the application of initial STM was limited to only a few types of structures so that the need for a unified design that can be adaptable to all parts of structures in a consistent manner arose. In order to meet these needs, Schlaich et al. (1987) extended Marti's work by generalizing the truss analogy method for beams. With this extended STM, all parts of structures could be modeled and analyzed regardless of whether the considered beam is in the B-region or D-region. The authors explained how to construct STM with a load path method and also provided some examples demonstrating the application of STM to structures with significant D-regions.

11

Collins and Mitchell (1991) and Macgregor (1992) strongly encouraged to use the STM for the design of D-regions. However, the main problem with this approach is it ignores the beneficial effects of shear steel in D-regions and is thus quite conservative.

2.2.2 Compatibility Truss Models

Plastic truss models described in Section 2.2.1 have been extensively used as handy and reasonable computational tools for the design and analysis purpose as they provided some degree of insight regarding the shear strength of reinforced concrete members. However, limited effort has been used to account for the shear deformation of the concrete structure, and this is an important aspect that must be considered to assure the ductility of structures.

Kupfer (1964) investigated the crack angle, θ, to explain the shear-flexural interaction by minimizing the strain energy in an idealized single truss model of a cracked T-beam element. The test results reveleated that the 45-degree truss model by Mörsch 's (1909) tended to overestimate the required shear design by 15–25%. Leonhardt (1965) used the truss analogy to explain the mechanism of failure of structural concrete members at the ultimate level and found that the angle of shear cracks changed significantly rather than kept constant 45-degree.

Paulay (1969 and 1971) tested several coupling beams under cyclic loading and concluded that there was a complex interaction among the concrete struts between cracks, longitudinal, and transverse reinforcement based on the observation from the test. To identify this complex interaction, Paulay deliberated the effect of shear-flexure interaction, shear carrying mechanisms, deformation characteristics, and stiffness of beams. He identified four major components regarding shear transfer mechanisms and the consequent distortions in cracked coupling beams. Those include 1) truss action and consequent distortions, 2) arch action and compression across the main diagonal of the beam, 3) flexure and associated rotations, and 4) tying action of flexural

reinforcement and consequent elongation of the beam. A variable angle truss model was suggested to incorporate the abovementioned components, and the stiffness of the beam after the formation of diagonal cracks was obtained with reasonable accuracy.

Mander (1983) introduced a nonlinear column analysis model to account for both flexure and shear. Further development was achieved by Chang and Mander (1994) for a better understanding of the shear portion in the analysis, and it was called the Cyclic Inelastic Strut-and-Tie model (CIST). In the study, an advanced constitutive relationship model for concrete was also proposed. Kim and Mander (1999 and 2000a) explored the application of the CIST model for structural concrete members subjected to combined shear and flexure. The authors investigated two different truss models with (a) constant angle and (b) variable angle, and both models were found to be practical methods when determining the shear stiffness. The Two-Point Gauss truss model was used to unify the flexure-shear interaction for both B-regions and D-regions. In the following study (Kim and Mander, 2000b), the nonlinear performance of beam-column joints was predicted using a theoretical framework of the STM. The authors pointed out that the post-elastic behavior of beam-column joints can be effectively modeled by the STM with a fan-shaped crack pattern. While a piecewise linear elastic approach to material modeling provided a good response, nonlinear material models were more refined.

With advances in computing abilities, there was a considerable potential to apply interactive computer programs for the further development of truss models by considering appropriate nonlinear behavior of truss members. Based on that, a nonlinear STM computational tool was developed by To et al. (2001, 2002 and 2003) to assess the behavior of reinforced concrete beams and columns with transverse reinforcement under monolithic and cyclic loading through

force-deformation response. The authors verified the effectiveness of the model using large-scale experimental data.

Brown et al. (2006) evaluated the application of STM to structural reinforced concrete members. The authors concluded that the shear span-to-depth ratio was a prominent parameter in consideration of shear capacity. Struts that formed at shallower angles experienced reduced ultimate capacities. They also found that cracking loads were unaffected by reinforcement crossing over cracks. Additionally, direct struts between the point of load application and support were found to be a good representation of behavior for $a/d < 2$.

Scott et al., (2012a) proposed the compatibility strut-and-tie model (C-STM) as a minimalistic computational method in an effort to reduce computation when performing nonlinear analysis of reinforced concrete bridge piers with significant D-regions. This method separates truss and arch action, and an arch-breadth scalar, η, is used to consider the contribution of combined truss and arch action to the shear strength of structural concrete members by adapting the variable truss model suggested by Kim and Mander (1999; 2005; and 2007). The authors proposed formulas to define the axial rigidities of the concrete and steel elements and to take account of the softening effect in the diagonal concrete struts due to the orthogonal tensile strains.

Scott et al. (2012b) analyzed experimental data to verify C-STM analysis using a commercial structural analysis program (SAP2000 v.14, 2009) by following procedures: 1) definition of nodal zones; 2) assignment of element properties; 3) assignment of nonlinear constitutive relationships; 4) load case definition; 5) analysis execution; and 6) post-analysis investigations. Post-analysis investigations involve evaluating axial forces and displacements. Based on the application of C-STM to experimental data, C-STM analysis provided a suitable computational prediction of the force-deformation response with a reasonable degree of accuracy.

However, a major shortcoming of the C-STM analysis technique was identified by the authors. Specifically, it is not possible to account for the compression softening effects on the diagonal concrete struts directly into an incremental force-based analysis procedure, resulting in the inability to predict the force and displacement corresponding to post-peak (softening) behavior.

To overcome this issue, Karthik et al., (2015) proposed two key extensions to the C-STM technique suggested by Scott et al., (2012a): (i) to take a softened model of the diagonal concrete struts into consideration to be used in the analysis procedure directly; and (ii) to conduct a displacement-control analysis. The validity of the proposed modifications to the C-STM was examined against the experimental study by Bracci et al., (2000) for the case of monotonic loading and Paulay (1969 and 1971) for cyclic loading. With these modifications, a prediction of the failure of the shear-critical reinforced concrete member was possible using C-STM analysis with good accuracy.

Baie (2017) examined the concept of a generalized moment-curvature approach (referred to as 'Z-section analysis') along with the C-STM to analyze the spliced continuous prestressed concrete girder bridges. In the Z-section analysis, the moment-curvature analysis was conducted along a diagonal crack plane instead of a transverse plane to directly account for the effects of flexure-shear interaction. Formulas are provided to calculate the nominal capacity of such sections. The author also advanced the C-STM approach to investigate the behavior of slab-on-spliced prestressed concrete bridges where significant shear and flexure interaction may affect the overall performance of the system, especially near spliced regions. Both the Z-section analysis and advanced C-STM approach were validated using results from the full-scale test.

2.2.3 Modified Compression Field Theory (MCFT)

Mitchell and Collins (1974) proposed a theoretical model for reinforced concrete members in pure torsion called the diagonal compression field theory (CFT) which became a basis of modified compression field theory (MCFT) found in AASHTO LRFD Bridge Design Specifications. In this theory, the inclination angle of the diagonal compressive strut was determined by minimizing external displacement. The prediction of the post-cracking torsional response of structural concrete members could be made using this model with a wide variety of symmetric cross-sections.

The CFT was then extended by Collins (1978) to account for shear in reinforced concrete members. The major assumption in this modification was that after the formation of cracks the concrete element was unable to resist any tension, and the shear was carried by a diagonal compression field. The average strains in both longitudinal and transverse directions were related to each other by Mohr's circle of strain and the angle of principal compression was determined using the conditions of compatibility. Collins regarded the ultimate shear strength of reinforced concrete members as either when the longitudinal reinforcement yields or when the average principal compressive stress of concrete reaches its limit.

Vecchio and Collins (1986) further extended the CFT to accommodate tensile stresses in concrete between cracks; this is now known as the 'Modified Compression Field Theory (MCFT)'. The authors formulated compatibility, equilibrium, stress-strain relationships of the cracked concrete using average stresses and strains. The relations of stress and strain of concrete were explained in terms of geometry relation and mechanics approach, and several assumptions were made to develop MCFT. The developed theory was validated with an additional experimental program which included some 30 reinforced concrete specimens. The test program was carefully

16

designed to represent and compare the tensile attributes in cracked concrete through several variables. The MCFT was also validated by other researchers (Iida et al., 1984; and Ang, 1985).

Vecchio and Collins (1988) incorporated the concepts of the MCFT into a fiber element model to analyze the full response of reinforced and prestressed concrete beams under combined shear, flexure, and axial loads for the further implementation. The authors proposed an iterative solution procedure to obtain rational longitudinal strains and shear stress distributions that can be applied to any type of beam sections subjected to various loading conditions. In the model, an assemblage of concrete and longitudinal reinforcement elements represented the whole beam section and each element was analyzed by satisfying conditions of compatibility and equilibrium. Using this fiber element model, Bentz (2000) developed a computer program 'Response 2000' that was capable of predicting overall load-deformation behavior of reinforced and prestressed concrete members.

The MCFT is an effective tool and background for non-linear finite element analysis, however, it was not appropriate for use in day-to-day engineering calculations because it includes fifteen equations that must be solved simultaneously. For further application of the MCFT to the design, Collins et al., (1996) simplified the MCFT with several assumptions and proposed a simple and unified method. In this method, in lieu of solving 15 equations to calculate variable θ and β that are required to estimate concrete and transverse reinforcement contribution on shear, the authors provided tables with values of θ and β as functions of the longitudinal strain, ε_x, and the shear stress level, v/f'_c. This MCFT with tables was validated using 528 tests which displayed experimental shear failures. In recognition of the simplicity with tabulated values for β and θ and physical significance to the parameters being calculated, the work of Collins et al (1996) was

adopted by the Canadian Standards Association Concrete Design Code (CSA Committee A23.3, 1994), and the AASHTO LRFD specifications (1994).

Although the early application of MCFT with tables was adapted in many design provisions and resulted in efficient shear designs, it was rather complicated for conducting hand analysis. Because it was not possible to remember the values in the tables for the back-of-the-envelope calculations, many engineers preferred simple equations to tables (Hawkins et al., 2005). To overcome this difficulty, Bentz et al. (2006) suggested the simplified MCFT that uses simple equations instead of tables. Those equations for θ and β were determined from the basic expression of the MCFT, and this simplified MCFT improved ease of predicting the shear strength of a wide range of reinforced concrete elements with almost equivalent accuracy as the full theory. The simplified MCFT has also been adopted by the bridge and building design provisions in Canada (CSA, 2010), the fib Model Code 2010, and the AASHTO LRFD Bridge Design Specification (AASHTO LRFD, 2010). However, there are some concerns of the use of MCFT and Simplified MCFT such as 1) inadequacy to use for deep beams; 2) excessively overestimated shear strength in some cases; and 3) uncertainty on the equation to calculate longitudinal strain, ε_x and hence θ.

2.3 Shear-Flexure Interaction Focusing on Diagonal Cracks

Concrete structural members are typically subjected to combined flexure and shear rather than pure flexure or shear; therefore, it is desirable to take the interaction of these two actions into consideration (Russo et al., 1991). Once it was assumed that shear and flexure act on structures separately, resulting in neglecting the interaction between them; however, a number of experimental and theoretical investigations have shown the strong relation between shear and flexure (Kani, 1964; Krauthammer and Hall, 1982; and Ahmad and Lue, 1987).

The shear-flexure interaction of a structural member is mostly dependent on its loading condition, shear span length, a ($=M/V$), and geometry, depth of the member, d, that the shear span-depth ratio, a/d, is perhaps the major factor that affects shear–flexure interaction. A simply supported beam with symmetrical loads applied at two points is shown in Figure 2-2 as an example. As seen in the figure, as the shear span-depth ratio, a/d, increases, the moment produced by the load increases while the shear remains constant, leading the beam prone to be governed by flexure. Conversely, as the shear span-depth ratio, a/d, decreases, the moment on the beam decreases, resulting in the beam inclined to be governed by shear (Kani, 1964; Kang et al., 2012 and Massone et al., 2013).

(a) with relatively large shear span length, a   *(b) with relatively small shear span length, a*
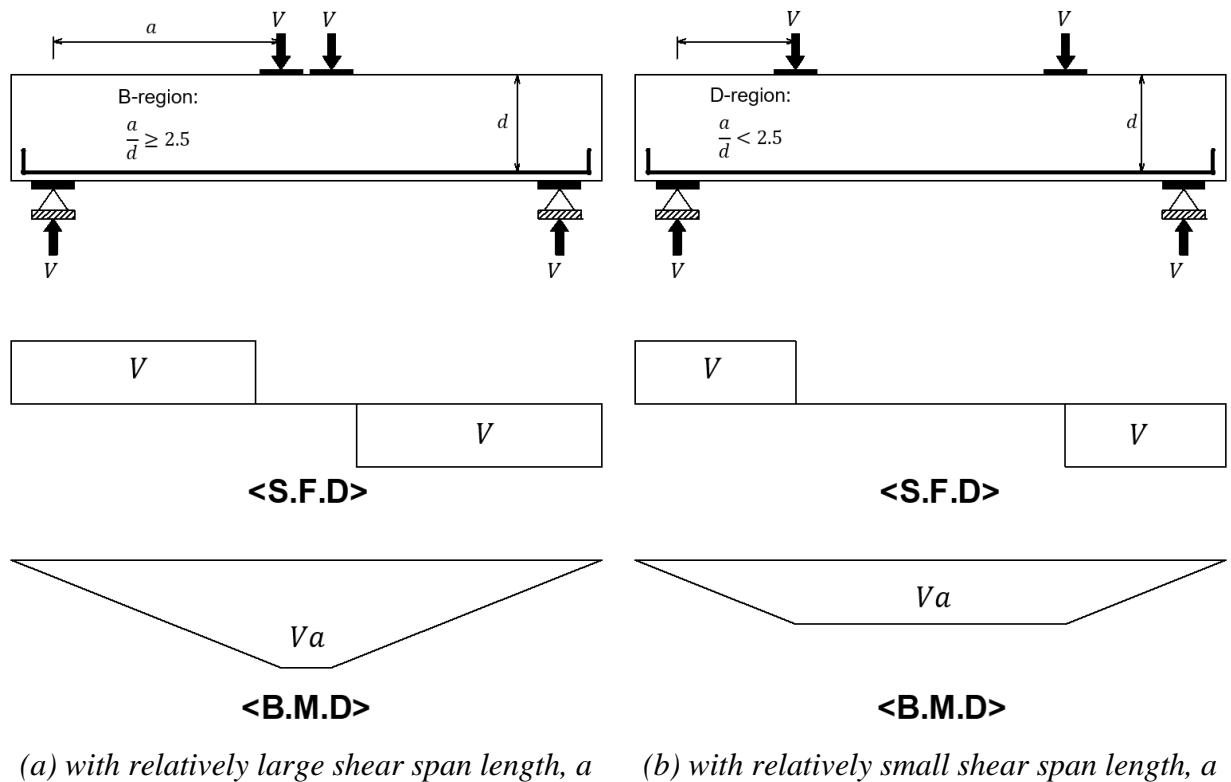
Figure 2-2. Simply supported beam with symmetrical loads

While the shear-flexure interaction of slender beams has been extensively investigated both analytically and experimentally (Leonhardt and Walther, 1962 and Kani, 1966), that of intermediate and deep beams remained unresolved because conventional beam theory cannot be easily applied for such beams owing to the "disturbed nature" of the internal stress and nonlinear strain distribution.

For this reason, this study mainly focuses on the flexure-shear interaction of intermediate beams and deep beams. A concrete structure with a small shear span-depth ratio, a/d, is drawn diagrammatically in Figure 2-3(a). This kind of structure can commonly be found in bent caps in bridges, transfer girders, offshore structures, plant structures, and foundation pile caps (Demir et al., 2019). As shown in Figure 2-3, these structures may be categorized into two different beam regions based on the geometries and boundary conditions; (a) cantilever beam region as shown in Figure 2-3(b); and (b) fixed-fixed beam region shown in Figure 2-3(c) (This is often referred to as squat beam when the shear span-depth ratio, a/d, is small). The main difference between the two regions is that double curvature occurs in the fixed-fixed beam region while single curvature is found in the cantilever beam region.

(a) Schematic representation of the considered structural concrete

(b) Cantilever Beam Region

(c) Fixed-Fixed Beam Region
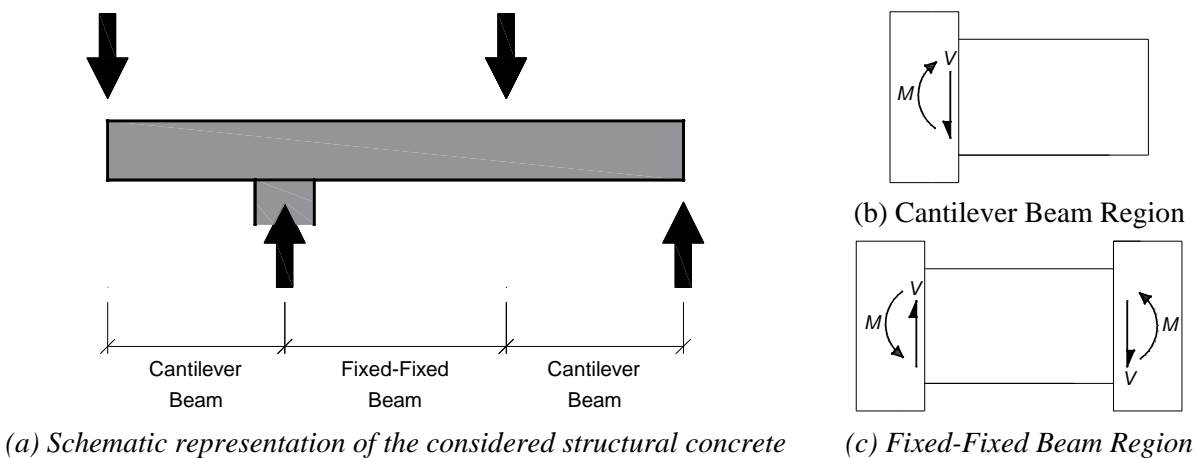
Figure 2-3. Categorization of structural concrete with small *a/d* ratio

For squat beams (fixed-fixed beams), a significant shear force can be found near the joint depending on the location of applied force, leading to a similar behavior with coupling beams with a small shear span-depth ratio ($a/d \leq 2.5$). Double curvature and high shear forces can be found in these members and they are prone to be vulnerable to shear failures that occur along wide diagonal cracks, following the yielding of the transverse reinforcement as drawn in Figure 2-4(a). A large amount of shear reinforcement may be provided in squat beams to avoid diagonal tension failures. However, members fail at the end sections due to the significant shear-flexure interaction, resulting in the concrete crushing prior to or right after the yielding of the flexural reinforcement. The failure is often followed by sliding deformations as shown in Figure 2-4(b) (Paulay and Priestley, 1992, and Mihaylov and Fransse, 2017).
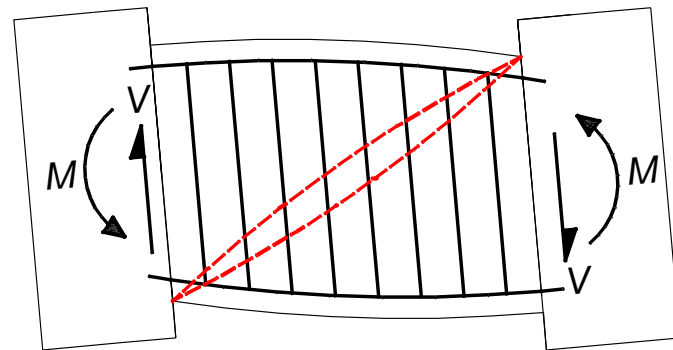
(a) Flexure-Shear Failure along with diagonal cracks
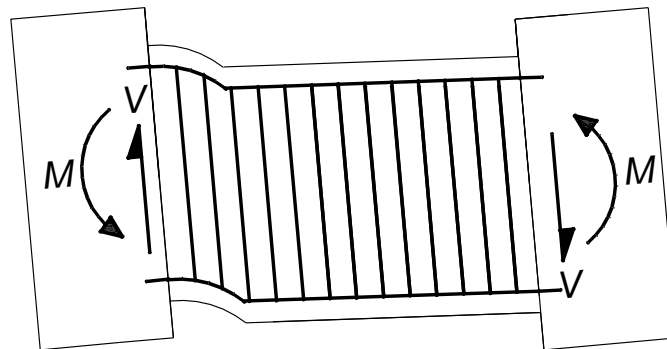
(b) Hinge-Shear Failure in the end section

Figure 2-4. Shear failure modes in fixed-fixed end beam (adapted from Paulay and Priestley, 1992)

Figure 2-5 (a) presents a cantilever beam behavior with a small shear span-depth ratio, a/d. Diagonal cracks commonly form along compressive struts in such members as depicted in Figure 2-5(b). As indicated, a diagonal crack angle, θ, does not always correspond to shear span-depth angle, α, due to the complex interaction of shear and flexure. Considering that the diagonal shear crack angle, θ, is considered as an important factor affecting the post-cracking behavior of concrete members (Kim and Mander, 2005), estimating a precise crack angle is necessary to predict combined shear and flexure resistance of concrete structures.

(a) Cantilever behaved beam   *(b) Failure along with diagonal cracks*
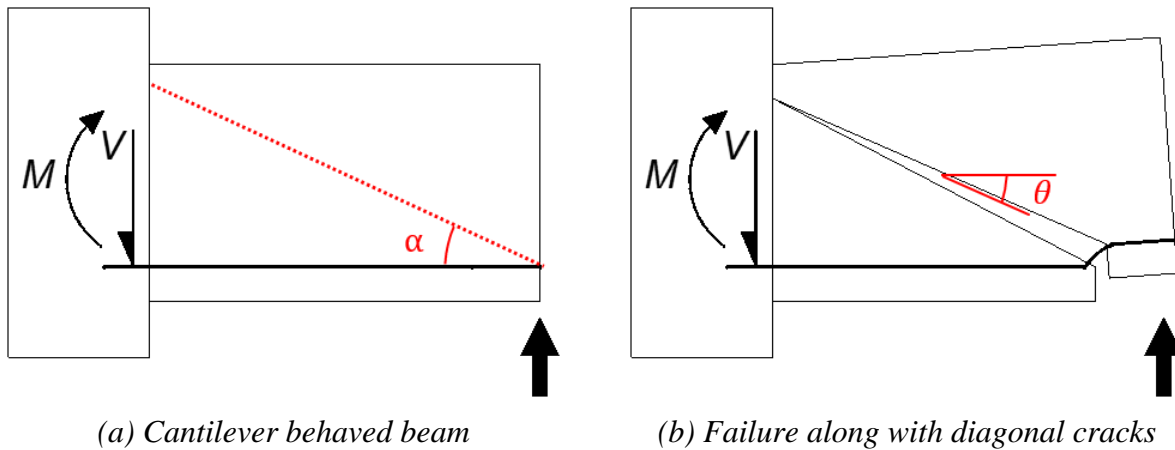
Figure 2-5. Shear failure mode in cantilever beam

Many researchers and engineers have proposed various truss models to predict an accurate diagonal crack angle, θ, since the traditional 45-degree truss model analogy was first introduced by Ritter (1899) and Mörsch (1909) some 120 years ago. Among them, Kim and Mander (1999 and 2007) proposed both the constant angle truss model (CATM) and variable angle truss model (VATM) to analyze shear stiffness of concrete beams and columns for B-region and D-region, respectively. Kim and Mander (2007) proposed formulae to predict the diagonal crack angle that creates the minimum amount of energy for both constant and variable angle truss models as:

22

- Continuum truss model with the constant angle truss

$$tan\theta = \left(\frac{(\rho_v A_v)}{0.61(\rho_t A_g)\Lambda}\right)^{1/4} \geq tan\alpha = \frac{d}{a} \tag{2-1}$$

- Discrete truss model with the variable angle truss

$$tan\theta = \frac{d_c/s}{N_h} \geq tan\alpha = \frac{d}{a} \tag{2-2}$$

where θ = angle of crack plane inclined to the longitudinal axis; ρ_v = volumetric ratio of shear steel to concrete; A_v = shear area of concrete section; ρ_t = volumetric ratio of longitudinal steel to concrete; A_g = gross section area; Λ = end fixity parameter, taken as $\Lambda = 1$ for fixed-pinned and $\Lambda = 2$ for fixed-fixed ends; d_c = center to center hoop depth or pitch diameter of hoop steel; s = center to center spacing of transverse reinforcement; α = corner-to-corner diagonal angle; d = effective depth; a = shear span length; and N_h = exact number of hoops that traverse the inclined crack plane.

Kim and Mander (2007) verified the formulae using the test results of 24 concrete column specimens, and analytical prediction showed reasonable agreement with the crack angle observed from the tests. In this study, the proposed model by Kim and Mander is further investigated for the application in the design stage and may be simplified if possible. With a reasonably reliable diagonal crack angle, shear and flexure interaction may be further examined.

2.4 Primary Parameters Affecting the Shear Capacity of RC Beams

Once it was believed in the early 1900s that shear stress at failure, v_u, for reinforced concrete beams without stirrups was a constant property only dependent on the compressive strength of concrete, f'_c. This was based on the concept that shear failure in reinforced concrete beams was a tensile phenomenon suggested by Mörsch (1904). Thus, the early design specifications related the

nominal shear stress to the cylinder strength of concrete, resulting in providing the maximum allowable nominal shear stress such as $0.02f'_c$.

Talbot (1909) found an increasing trend of shear stress when beams were stiffer, shorter, and deeper from the test results from over a hundred of reinforced concrete beams. Based on the findings, he concluded that the percentage of reinforcement and the shear length-to-depth ratio are critical variables related to shear and diagonal tension strength of reinforced concrete beams and pointed out the folly of the procedure in the early design specifications. However, his findings did not attract the attentions of designers and researchers at that time as he failed to support them with mathematical terms.

Talbot's work had forgotten in the interval between 1920 and the late 1940s until enormous research conducted in the 1940-50s brought about a clear realization that shear and diagonal tension is a complex problem involving many variables. Attention to the forgotten fundamentals first arose when Morretto (1945) conducted a series of beam tests with several variables including 1) the size and inclination of the stirrups; 2) the type of concrete; and 3) the ratio of longitudinal reinforcement. Morretto (1945) found a significant effect of the ratio of longitudinal reinforcement and took it into consideration in his empirical equation for the estimation of the shear strength of reinforced concrete beams.

Clark (1951) investigated shear resistance through a series of tests using various ratios of web reinforcement, two cross-sections, 4 span lengths, and concrete strengths ranged from 14 to 42 MPa. Based on the observation from the test, he introduced an empirical equation that implemented the span-to-depth ratio, a/d, to estimate the shear strength of reinforced concrete beams for the first time. In his equation, the shear resistance was expressed in terms of the square root of the ratio of transverse reinforcement, ρ_v, the compressive strength of the concrete, f'_c, the

ratio of effective depth of beam to distance from the plane of the nearest concentrated load point to plane of the support, a/d, and the ratio of longitudinal reinforcement, ρ_t, as follows:

$$v_c = 7{,}000\rho_t + \left(0.12f'_c\right)\frac{d}{a} + 2{,}500\sqrt{\rho_v} \qquad (2\text{-}3)$$

Although the development of the a/d ratio was considered as a great step forward in a more reasonable estimation of the shear strength of reinforced concrete beams, the use of the term was limited due to the difficulty of defining the shear span, a, for numerous loading conditions. In the early 1950s, the difficulty was resolved when theories based on the M/Vd ratio were first introduced at the University of Illinois. The terms M/Vd has a physical significance not only for single point load and two symmetrical loads but also for any other loading conditions. For this reason, the development of the M/Vd ratio was considered as a breakthrough toward an empirical solution of a shear design problem. Besides that, other variables were known to affect shear strength such as a presence of axial load, a type of cross-sections, a type of bearing plates, and type of reinforcement. Several equations were introduced that included the considerations of the ratio of width to depth b/d; the elastic modular ratio, n; the ratio of length to depth L/d; and use of $\sqrt{f'_c}$ instead of f'_c.

Although a variety of shear tests had been conducted in the 1950s, it was not possible to find any meaningful and reliable interpolation using those data because of the lack of consistency in those tests or too many variables related to the shear failure mechanism, resulting in a need for the extensive test program. According to the need, a series of studies were done by Kani in the 1960s. He uncovered many variables associated with the shear strength of reinforced concrete and his work became an important background in the many reinforced concrete design provisions.

Kani (1964; 1966 and 1967) conducted a series of shear tests on beams with variables including effective depth, d, width, b, shear span, a, and the longitudinal reinforcement ratio, ρ_t. Through the series of experimental programs, Kani discovered that shear stress, v_u, is not a constant quantity, and also the effect of concrete strength on shear was relatively insignificant compared to other factors. Kani concluded that effective depth, shear span, and longitudinal reinforcement are closely related to the shear strength of the RC members while beam width had only a slight effect based on the test observation. Not only that, but Kani also demonstrated two totally different and unrelated mechanisms that govern the strength of concrete beams distinguishable at the a/d ratio of 2.5.

Following Kani's intensive experimental studies, many researchers agreed that concrete strength, f'_c, longitudinal reinforcement ratio, ρ_t, and the shear depth-span ratio, a/d, are the basic parameters affecting the shear strength of concrete beams. In the following sections, several studies conducted to reveal the relations between the abovementioned variables and the shear capacity of RC members are presented.

2.4.1 Concrete Compressive Strength

The compressive strength of concrete has been regarded as one of the most important parameters influencing the shear behavior of concrete members. In the 1960s, many studies have observed the increasing trend of shear strength of concrete members as the concrete compressive strength increases. Based on this finding, $0.17\sqrt{f'_c}\,b_w d$ was taken as the shear strength of RC members in the ACI Building code to represent a conservative estimate (ACI Committee 318, 1963; ACI-ASCE Committee 326, 1962, and Angelakos et al. 2001). The relation of the normalized shear strength, v_u, and concrete compressive strength, f'_c, of the test results by Moddy (1954) is presented along with the curve of $0.17\sqrt{f'_c}\,b_w d$ in Figure 2-6(a) and it clearly shows the trend.
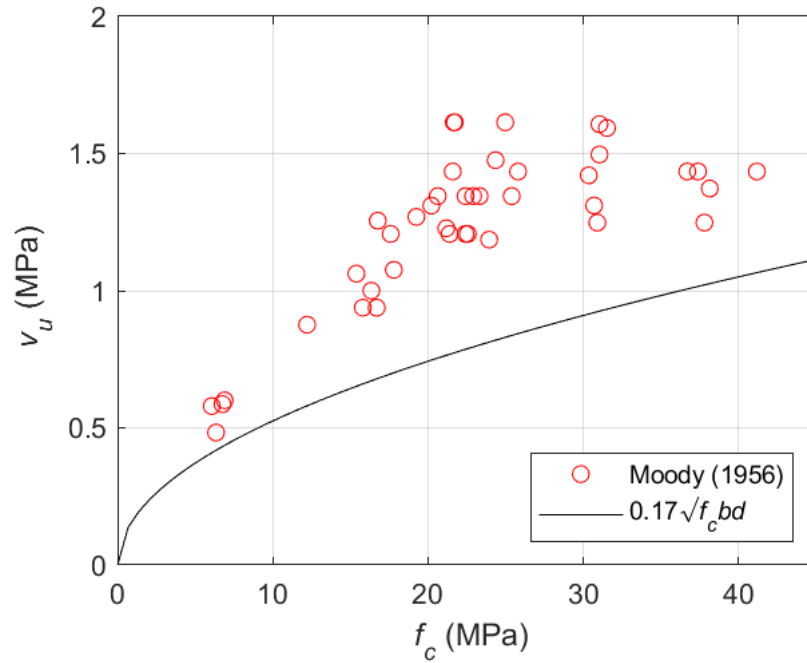
(a) Concrete strength, f'_c vs. shear stress, v_u
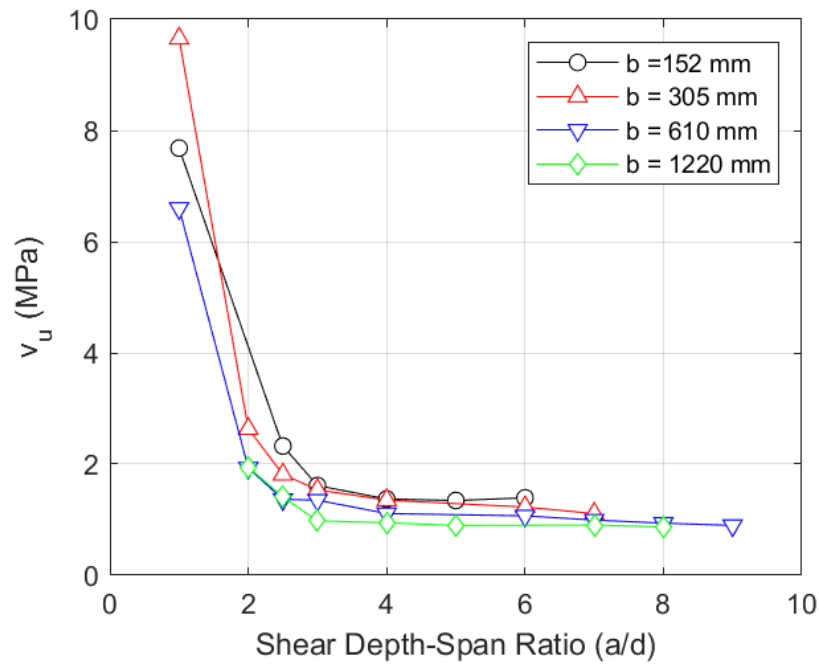
(b) Shear depth span ratio, a/d vs. shear stress, v_u

Figure 2-6. Influence of concrete strength and *a/d* ratio on the ultimate shear stress

This empirical equation still can be found in ACI 318-19 and AASHTO LRFD specification in a simplified shear design equation as:

$$V_c = 0.17 \sqrt{f'_{c\,(\text{MPa})}} bd \qquad (2\text{-}4)$$

However, it was pointed out that the increasing trend cannot be applied when the concrete compressive strength is higher than 70 MPa (Johnson and Ramirez, 1989; Roller and Russell, 1990; and Perera and Mutsutoshi, 2013). Collins and Kuchma (1999) conducted an extensive experimental program to investigate the size effect and high compressive strength concrete in shear on reinforced concrete members and found a trend that as the depth of the beams increased, the shear stress at failure decreased. The authors demonstrated that the empirical equation could be extremely unconservative by showing several specimens whose ultimate strengths were only about 40% of predicted strengths. Based on the concerns with the use of this traditional empirical equation to beams with high-strength concrete, ACI code provided an upper limit on the failure of shear stress and required a minimum area of stirrup for beams when the factored shear demand, V_u, exceeds $0.5V_c$.

Angelakos et al., (2001) argued that large and lightly reinforced concrete specimens designed based on the empirical equation with considering failure shear stress limit and minimum area of stirrup only showed 70% of the predicted shear strength. Finally, the authors suggested not using the empirical equation when designing large and lightly reinforced concrete with high-strength concrete.

2.4.2 Shear Span-Depth Ratio

Kani (1967) found a significant increase in ultimate shear strength when a beam has a small shear-span-depth ratio, *a/d*, less than 2.5 as shown in Figure 2-6(b) through his experimental program. Based on the observation, Kani concluded the significant increment of maximum shear-carrying

capacity is attributed to the tied arch action that transferred the shear force rather than the truss action. Since then the shear-span-depth ratio, *a/d*, is recognized as the most important factor influencing the shear behavior of the concrete members because it determines how the shear force is transferred to adjacent support through the member. For this reason, various design provisions, such as ACI 318 and AASHTO consider the shear span-depth ratio in their shear designs.

Oh and Shin (2001) provided another set of tests that revealed the significant influence of the shear-span-depth ratio to the shear strength of concrete members. In the study, fifty-three reinforced concrete deep beams were tested for a deep understanding of their diagonal cracking and ultimate shear capacities. The specimens were tested symmetrically under two-point loading as shown in Figure 2-7.

(a) a/d = 0.5   *(b) a/d = 0.85*

(c) a/d = 1.25   *(d) a/d = 2.0*
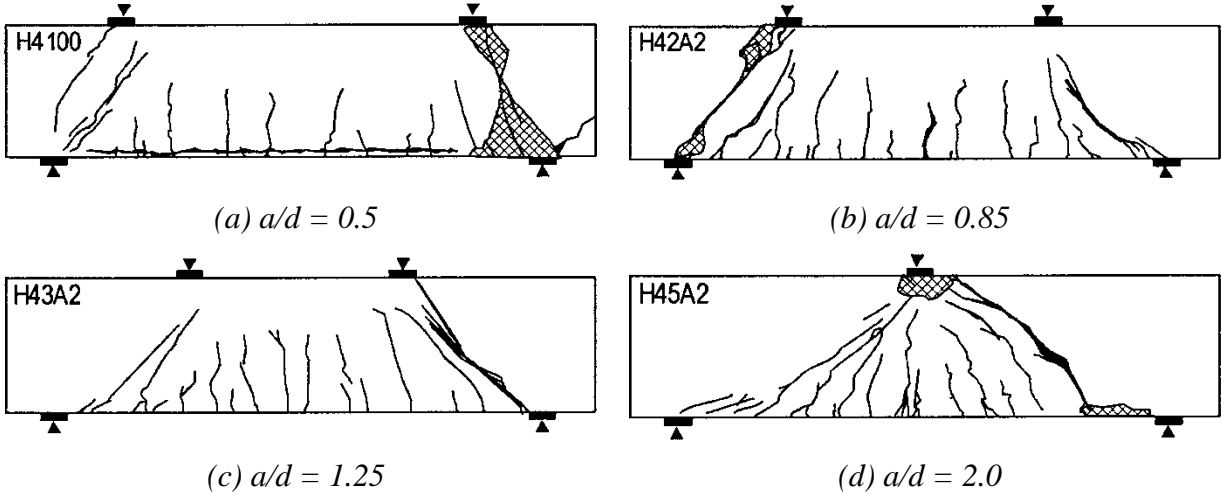
Figure 2-7. Crack pattern at failure with various *a/d*

Design parameters included: 1) concrete compressive strength from 23 to 74 MPa; 2) effective span-depth ratio, l_e/d from 3.0 to 5.0; 3) shear span-depth ratio, *a/d*, from 0.5 to 2.0; 4) longitudinal reinforcement ratio of 0.0129 and 0.0156; 5) vertical reinforcement ratio varying

from 0 to 0.0034; 6) horizontal reinforcement (skin reinforcement) ratio from 0 to 0.0094; and 7) size of the section. More details regarding the material and geometric properties of the specimens and the test result such as maximum load capacity, and the failure mode are available in Oh and Shin (2001).

The test results indicated that the ultimate shear strength of deep beams was predominantly affected by the shear-span-depth ratio, *a/d.* The ACI design provisions were used to predict the specimen strength and showed conservative results by underestimating the effect of concrete compressive strength and longitudinal steel reinforcement.

Based on the observation observed in the experimental program, several conclusions were made: 1) failure mode was not changed by the concrete compressive strength in deep beams; 2) for the specimen with the small *a/d* ratio, strut type cracking patterns controlled, and while shear friction cracking patterns controlled as the *a/d* ratio increased; 3) the *a/d* ratio was the most influential parameter affecting the ultimate shear strength, and l_e/d also affected the shear capacity to some degree; 4) vertical shear reinforcement increased the shear capacity as the *a/d* ratio increased; however, the effect of horizontal shear reinforcement was insignificant.

2.4.3 Flexural Reinforcement Ratio

Moddy (1954) conducted shear tests on simple beams with different longitudinal reinforcement ratios, ranging from 0.082 to 0.0217. From the experimental test observation, the author found a prominent increase in the failure load when a higher longitudinal reinforcement ratio was provided, and the same trend was observed in his follow-up study (Moddy, 1955). Since Moddy's finding shed light on another parameter related to the shear capacity of reinforced concrete structures, the effect of the longitudinal reinforcement ratio has been investigated by many researchers through numerous experimental tests.

Kani (1966) tested a series of rectangular beams to determine the effect of three parameters, including, (a) compressive concrete strength; (b) longitudinal reinforcement ratio; (c) shear span-depth ratio, a/d. Four different longitudinal reinforcement ratios (ρ_t = 0.005, 0.008, 0.0188, and 0.0280) were used in the test. Kani also found the increasing trend of ultimate shear strength as ρ_t increased in his tests although the effect of the longitudinal reinforcement ratio to the ultimate shear strength was not as significant as the compressive strength concrete and shear span-depth ratio. The obtained trend from Kani's test can be seen in Figure 2-8.
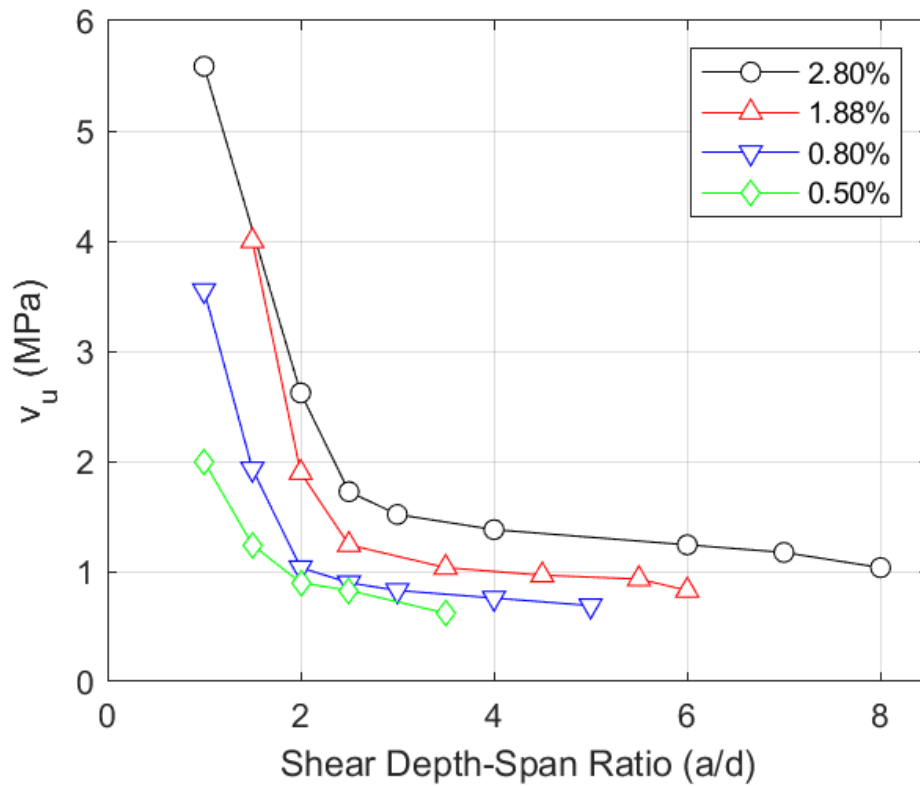
Figure 2-8. Ultimate shear capacity varied by ρ_t

Ahmad and Lue (1987) pointed out that the effect of the longitudinal reinforcement is rather quantitative than qualitative since it determines the ultimate load level at which a particular failure mode occurs, rather than the failure mode itself.

Angelakos et al. (2001) observed the longitudinal axial strain and the crack angle in reinforcement concrete members influence the shear strength and strength margin after diagonal cracking when minimum transverse reinforcement is provided. The higher longitudinal reinforcement ratio reduces overall longitudinal strain in reinforcement, and this leads to a larger concrete contribution to the shear. The author used the variable angle truss model to explain the effects of longitudinal axial strain and crack angle.

Lee and Kim (2008) investigated the effects of longitudinal reinforcement ratio and shear-span-depth ratio in reinforced concrete beams with the minimum transverse reinforcement as per the ACI design provision (ACI 318-05). The authors tested twenty-six RC beams, and the shear ratio (V_n of the beam with minimum transverse reinforcement / V_n of the beam with no transverse reinforcement) were obtained for all specimens. Based on the observation from the test, the authors concluded that the shear ratio increased as the longitudinal reinforcement ratio increased and the shear span-depth ratio, *a*/*d*, decreased.

Jeong et al., (2017) pointed out that previous studies regarding longitudinal reinforcement ratio, ρ_t, focused mostly on typical types of beams with a ratio of less than 0.03 or beams with a ratio higher than 0.03 and an effective depth of less than 400 mm. To investigate the effect of longitudinal reinforcement ratio exceeding 0.03 and the size effect on the shear resistance of reinforced concrete beams, the authors conducted shear tests with varied longitudinal reinforcement ratios and effective depths. The test results showed that the shear capacity of specimens increased as the longitudinal reinforcement ratio increased, and this tendency was more

remarkable for beams with relatively small effective depths. Based on the test results, the authors proposed formulas to predict the shear strength of RC beams considering the size effect for beams whose ratio of longitudinal reinforcement exceeds 0.03.

2.5   State-of-Practice on Shear Design in AASHTO

Concrete is a composite material consisting of cement, aggregate, and water. Even with the same concrete mix, the compressive strength and tensile of concrete may vary as much as 10-20% from an average value depending on the characteristic of mixed materials, curing process, and temperature. Because the shear resistance of concrete members is dependent largely on the material properties of concrete, an accurate assessment of shear strength is difficult. This high uncertainty and variability lead many research groups to keep developing and improving theories regarding shear strength. Although intensive research on shear has been done to understand and reveal the shear failure mechanism over a few decades, there are still disagreements amongst various theories. For these reasons, there is no unified theory that can be used to estimate ultimate shear strength and also to assess the shear failure mechanism while the flexural behavior of concrete can be predicted with a good agreement.

Significant efforts have been made by many researchers and engineers: 1) to reveal various factors contributing shear resistance in structural concrete; 2) to explain shear failure mechanisms; and 3) to develop a unified shear design model. In this section, those efforts are introduced chronologically, and limits are pointed out.

AASHTO LRFD Bridge Design Specification (2017) provides two different shear design models, including 1) the conventional sectional model in AASHTO 5.8.3; and 2) the Strut-and-Tie model in AASHTO 5.6.3. The conventional sectional model applies to the design of typical bridge components where the assumptions of traditional beam theory can be valid (referred to as 'B-

region') such as girders and slabs. The Strut-and-Tie model is more appropriate to deep beams or disturbed regions (referred to as 'D-region') where the flexure-shear interaction causes the high irregularity of internal stress and nonlinear strain distribution (Mander et al., 2012).

The main difference between the two models is that the sectional model assumes the factored forces, V_u, M_u, and T_u, at a particular section are independent of each other and affect the required transverse reinforcement, separately, however, the Strut-and-Tie Model takes the mechanical interaction among these actions into account. It is well known that the direct strut action governs when the shear span-depth ratio, a/d, is less than 2.5 (Kani 1967, Matamoros and Wong 2003, He et al. 2012, and Tuchscherer et al. 2014). Thus, the AASHTO design provision recommends using the Strut-and-Tie Model when the distance between the centers of applied load and the supporting reaction is less than twice of the member depth ($a \le 2h$).

The current AASHTO LRFD Bridge Design Specification provides three different approaches in the sectional design to estimate shear resistances of concrete and transverse reinforcement. All different design procedures based on sectional and strut-and-tie models in the current AASHTO design provision are introduced in the following sections.

2.5.1 Sectional Design

In the sectional design approach, the shear resistance of a reinforced and prestressed member, V_n, is assumed as the sum of shear resistances provided by the tensile stresses of concrete, V_c, the tensile stresses of transverse reinforcement, V_s, and the vertical component of the prestressing force, V_p. The upper limit of V_n is also provided to avoid the concrete crushing in the web of the concrete member prior to the yielding of the transverse reinforcement. The factored shear resistance, ϕV_n, is then compared to the factored shear force, V_u, at several shear critical sections along its entire

34

length (usually near the supports and the tenth points of the span). The basic equations consisting of the shear design are given by:

$$V_n = V_c + V_s + V_p \tag{2-5}$$

$$V_n = 0.25 f'_c b_v d_v + V_p \tag{2-6}$$

$$\phi V_n \geq V_u \tag{2-7}$$

where V_n = nominal shear resistance of the section considered; V_c = nominal shear resistance provided by tensile stresses in the concrete; V_s = shear resistance provided by shear reinforcement; V_p = component in the direction of the applied shear of the effective prestressing force; ϕ = shear resistance factor, taken as 0.9 for normal weight concrete; and V_u = factored shear force at section.

The current AASHTO LRFD design provision provides three complementary methods to evaluate shear resistances of concrete, V_c, and transverse reinforcement, V_s, respectively, and those include:

- Method 1: Simplified Procedure for Nonprestressed Sections (Section 5.8.3.4.1)
- Method 2: General Procedure (Section 5.8.3.4.2 and Appendix B5)
- Method 3: Simplified Procedure for Prestressed and Nonprestressed Sections (Section 5.8.3.4.3)

In Method 1 and 2, the expressions for V_c and V_s are functions of variables β and θ, which differ by the applied loading and the properties of the section. The concrete contribution is a function of the factor β, and the transverse steel contribution is established from the amount of steel traversing a crack angle θ (measured from the longitudinal member axis) as shown:

$$V_c = 0.083\beta \sqrt{f'_{c\,(MPa)}} b_v d_v \tag{2-8}$$

35

$$V_s = A_v f_y \frac{d_v}{s} \cot \theta \qquad (2\text{-}9)$$

where β = factor relating effect of longitudinal strain on the shear capacity of concrete; f'_c = compressive strength of concrete for use in design; b_v = effective web width taken as the minimum web width within the depth d_v; d_v = effective shear depth; A_v = area of a transverse reinforcement within distance, s; f_y = yield stress of transverse reinforcement; θ = angle of inclination of diagonal compressive stresses (degrees); and s = spacing of transverse reinforcement measured in a direction parallel to the longitudinal reinforcement.

In Method 3, V_c is calculated from a direct equation in lieu of using the parameter, β, and V_s is calculated using Eq. (2-9) as the same as the former two methods. In the following subsections, the historic developments of these three procedures are discussed, and details and equations used are introduced.

2.5.1.1 Simplified Procedure for Nonprestressed Section

Ritter (1899) first introduced the truss model and later Mörsch (1909) expanded the model in the first design specification of structural concrete to estimate the shear strength of reinforced concrete members (MacGregor, 1992). In the truss model, Mörsch regarded the concrete beam as an equivalent Howe truss whose compression and tension members are modeled with concrete and steel, respectively. Thus, the compression forces in compression chords and struts are carried by concrete while the tension forces in tension chords and vertical ties are resisted by longitudinal and transverse reinforcement, respectively. For simplicity, the angle of the compression struts was conservatively to be 45-degree. This well-known truss model was considered to be conservative when estimating the shear capacity of concrete members because shear resistance contributed by shear friction and tensile strength of concrete were neglected.

To overcome the limits of Mörsch's truss model, Richart (1927) suggested an empirical equation to estimate the shear resistance by the tensile strength of concrete, while the shear resistance by the transverse steel reinforcement was found through the truss model. The current simplified procedures for non-prestressed members found in the AASHTO LRFD Bridge Design Specifications (2017) and the ACI 318-19 Building Code are based on this truss model. This procedure specified that for the non-prestressed beams containing at least the minimum amount of transverse steel reinforcement, values of $\beta = 2.0$ and $\theta = 45$-degree can be used. Thus, the nominal shear strength, V_n, and shear resistances contributed by concrete and transverse reinforcement are given by:

$$V_n = V_c + V_s \tag{2-10}$$

$$V_c = 0.17 \sqrt{f'_{c\,(\text{MPa})}} b_v d_v \tag{2-11}$$

$$V_s = A_v f_y \frac{d}{s} \tag{2-12}$$

Note: V_p in Eq. (2-5) is taken as zero as there is no prestressing force; transverse reinforcement orthogonal to the longitudinal axis of the member is considered in Eq. (2-12).

This is a simple and handy approach to approximate the shear contribution of concrete and transverse reinforcement. However, it is noted that this method is applicable only to a non-prestressed concrete section not subjected to axial tension and with at least the minimum amount of transverse reinforcement or with an overall depth not greater than 400 mm.

2.5.1.2 *General Procedure Based on MCFT*

Vecchio and Collins (1986) suggested the modified compression field theory (MCFT) to explain shear failure mechanism based on tests on shear panel. When MCFT was first introduced in AASHTO in 1994, the tables were provided to find several variables required to estimate shear

resistance of concrete and transverse reinforcement. The procedure was then simplified by replacing tables with equations for the better and easier calculation as suggested by Bentz et al. (2006). This simplified procedure based on the MCFT is provided as the general procedure in Section 5.7.3.4.2 of the current version of the AASHTO LRFD Bridge Design Specification (2017). More details regarding the historic developments of modified compression field theory are previously addressed in Section 2.2.3.

The general procedure provides two equations to estimate the factor relating to the effect of longitudinal strain on the shear capacity of concrete, β, based on the amount of transverse reinforcement provided in the concrete section. For sections with the minimum amount of transverse reinforcement, the parameters β is calculated by:

$$\beta = \frac{4.8}{1 + 750\varepsilon_s} \tag{2-13}$$

where ε_s = net longitudinal tensile strain in the section at the centroid of the tensile reinforcement and determined as explained later.

For sections without the minimum amount of transverse reinforcement, β is determined as:

$$\beta = \frac{4.8}{(1 + 750\varepsilon_s)} \frac{51}{(39 + s_{xe})} \tag{2-14}$$

where s_{xe} = crack spacing parameter to consider the size effect and determined by:

$$s_{xe} = s_x \left(\frac{1.38}{a_g + 0.63}\right) \le 2{,}000 \ mm \tag{2-15}$$

where s_x = lesser of either d_v or the maximum distance between crack control reinforcement, where the area of the reinforcement in each layer is not less than $0.003b_v s_x$; and a_g = maximum aggregate size.

The crack angle in both cases is given by:

$$\theta = 29 + 3500\varepsilon_s \qquad (2\text{-}16)$$

The net longitudinal tensile strains, ε_s, in Eqs. (2-13), (2-14), and (2-16) is determined by:

$$\varepsilon_s = \frac{\left(\frac{|M_u|}{d_v} + 0.5N_u + |V_u - V_p| - A_{ps}f_{po}\right)}{E_s A_s + E_p A_{ps}} \qquad (2\text{-}17)$$

If ε_s from Eq. (2-17) is less than zero, then it should be taken as zero or recalculated by:

$$\varepsilon_s = \frac{\left(\frac{|M_u|}{d_v} + 0.5N_u + |V_u - V_p| - A_{ps}f_{po}\right)}{E_s A_s + E_p A_{ps} + E_c A_{ct}} \qquad (2\text{-}18)$$

where $|M_u|$ = absolute value of factored moment, not to be taken less than $|V_u - V_p|$; N_u = factored axial force, taken as positive for tensile and negative for compressive, respectively; V_u = factored shear force; V_p = component in the direction of the applied shear of the effective prestressing force; A_{ps} = area of prestressing steel on the flexural tension side of the member; f_{po} = parameter taken as modulus of elasticity of prestressing tendons multiplied by the locked in difference in strain between the prestressing tendons and the surrounding concrete; E_s = modulus of elasticity of reinforcing bars; A_s = area of non-prestressed steel on the flexural tension side of the member at the section under consideration; E_p = modulus of elasticity of prestressing strands; A_{ct} = area of concrete on the flexural tension side of the member; and E_c = modulus of elasticity of concrete.

The nominal shear capacity from this general procedure (AASHTO LRFD 5.7.3.4.2) is simple, however, it is less accurate and can be excessively conservative in some cases (Hawkins et al. 2005, and Birely et al., 2018). For this reason, Table B5.2.1 and B5.2.2 in AASHTO Appendix B5 may be also used to obtain the parameters β and θ as an alternative (rigorous) method. Figure 2-9 gives a flowchart of shear design using the general procedure based on MCFT.
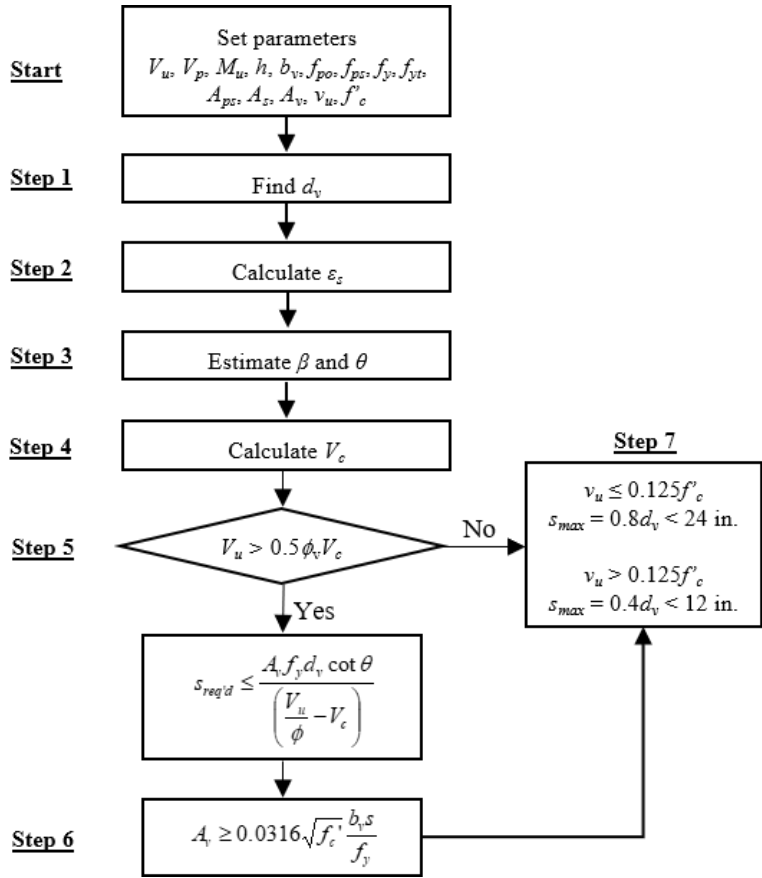
Figure 2-9. Shear design flowchart for the general procedure based on MCFT

2.5.1.3   Simplified Procedure for Prestressed and Nonprestressed Sections

MacGregor et al. (1965) suggested the simplified procedure to predict the diagonal shear cracking

of prestressed concrete sections, and ACI Code 318 (ACI, 1965) and AASHTO Bridge Design

Standard adapted his equation at that time. Hawkins et al. (2005) then modified the equation to be

applicable to non-prestressed concrete sections as well, and the current AASHTO LRFD design

provision adapted that change. Thus, this current modified simplified procedure found in Section

5.8.3.4.3 can be applied to both non-prestressed and prestressed concrete sections.

In this method, the nominal shear resistance, V_n, at the given section is the sum of shear

resistances provided by concrete, V_c, and steel, V_s, as the same as the two former methods, and the

determination of V_c and V_s depends on the type of inclined cracking occurred. Hawkins et al. (2005) took two types of diagonal cracking: 1) flexure-shear cracking, and 2) web-shear cracking into consideration and associated them with two different nominal concrete shear resistances, V_{ci} and V_{cw}, respectively.

Web-shear cracking initiates in the web of the member adjacent to the support and extends toward the center of the beam. An equation is suggested to calculate the shear stress in the web when the web-shear cracking forms based on Mohr's circle analysis. The shear capacity of the section with the formation of web-shear cracking is calculated by:

$$V_{cw} = \left(0.16 \sqrt{f'_{c \text{ (MPa)}}} + 30 f_{pc} \right) bd + V_p \tag{2-19}$$

where V_{cw} = nominal shear resistance when inclined cracking results from excessive principal tension in web; f_{pc} = compressive stress in concrete); and V_p = effective prestressing force in direction of shear.

Flexural-shear cracking initiates from existing flexural cracks and extends toward the support. During this process, vertical flexure cracks change its angle of inclination to become a diagonal shear crack. The empirical equation to calculate shear capacity of the section with the formation of flexural-shear cracking is suggested as shown:

$$V_{ci} = 0.0525 \sqrt{f'_{c \text{ (MPa)}}} bd + V_d + \frac{V_i M_{cr}}{M_{max} \sqrt{f'_c}} \geq 0.16 \sqrt{f'_{c \text{ (MPa)}}} bd \tag{2-20}$$

in which V_{ci} = nominal shear resistance of concrete when inclined cracking results from shear and moment; V_d = shear force at section due to unfactored dead load; V_i = factored shear force at section due to externally applied loads; M_{cre} = moment causing flexural cracking at section due to

externally applied loads; and M_{max} = maximum factored moment at section due to externally applied loads.

M_{cre} is given by:

$$M_{cre} = S_c \left(f_r + f_{cpe} - \frac{M_{dnc}}{S_{nc}} \right)$$

(2-21)

where f_{cpe} = compressive stress in concrete due to effective prestress forces at the extreme fiber of section where tensile stress is caused by externally applied loads; M_{dnc} = total unfactored dead load moment acting on the section; S_c is the section modulus for the extreme fiber of the composite section where tensile stress is caused by externally applied loads; and S_{nc} = section modulus for the extreme fiber of the section where tensile stress is caused by externally applied loads.

The lesser of V_{cw} and V_{ci} is taken as V_c, and the inclined angle, θ, required to calculate V_s in Eq. (2-9) is determined based on which governs V_c. If V_{ci} is greater than V_{cw}, $\cot\theta = 1$ is used or otherwise $\cot\theta$ is calculated by:

$$\cot \theta = 1.0 + 1.14 \left(f_{pc} / \sqrt{f'_{c\,MPa}} \right) \leq 1.8$$

(2-22)

It is noted that V_p in Eq. (2-5) is taken as zero since the prestressing effect is already taken into consideration when calculating V_c as shown in Eq. (2-19). There are a few conditions that need to be met to use this method that: 1) the section must not be subjected to a significant axial tension force, and 2) the section must contain at least the minimum amount of transverse reinforcement as per AASHTO 5.7.2.5.

2.5.2 Strut-and-Tie Model

When the concrete members are subjected to a combination of high shear and flexure, flexural and diagonal cracks may form and expand, resulting in a loss of shear-carrying capacity. In such

regions, the overall performance of the members deteriorates, and the conventional beam theory fails to capture the coupling effects of shear and flexure. Therefore, there has been a need for an advanced design and analysis model that can be applicable to such regions by taking account of the flexure-shear interaction. To satisfy the need of an alternative design for such regions, AASHTO LRFD Bridge Design Specifications and ACI 318 first adapted a strength-based design model called the 'Strut-and-Tie' model in 1994 and 2002, respectively. This strut-and-tie model was based on a generalized truss model that was suggested by Marti (1985) and later expended by Schlaich et al. (1987).

In the STM, it is assumed that the applied load in a structure is transferred to the supports in the form of compression and tension through a truss-like model that simulates load paths. The truss is assembled with concrete compressive struts and steel tension ties interconnected at nodal regions as shown in Figure 2-10. The applied forces are required to be in equilibrium with resisting forces of the system provided by concrete compression struts and steel tension ties, meaning the lower bound theorem of plasticity is taken into account. The plastic theory considers the case when the maximum load-carrying capacity and deformation capacity of the member are not exceeded, thus it provides the lower bound limit of the member but not a dependable insight regarding expected failure location and mechanism (MacGregor, 1992).

The strut-and-tie design procedure includes determination of 1) a truss model; 2) required widths of the struts and ties; and 3) required sizes of nodal regions, reflecting the equilibrium with the external load and the size of the bearings at the nodal regions. The solution from the STM method can be varied as the determination of the truss layout is subjective. Schlaich et al., (1987) suggested that the model with the minimum strain energy may be the most effective solution.
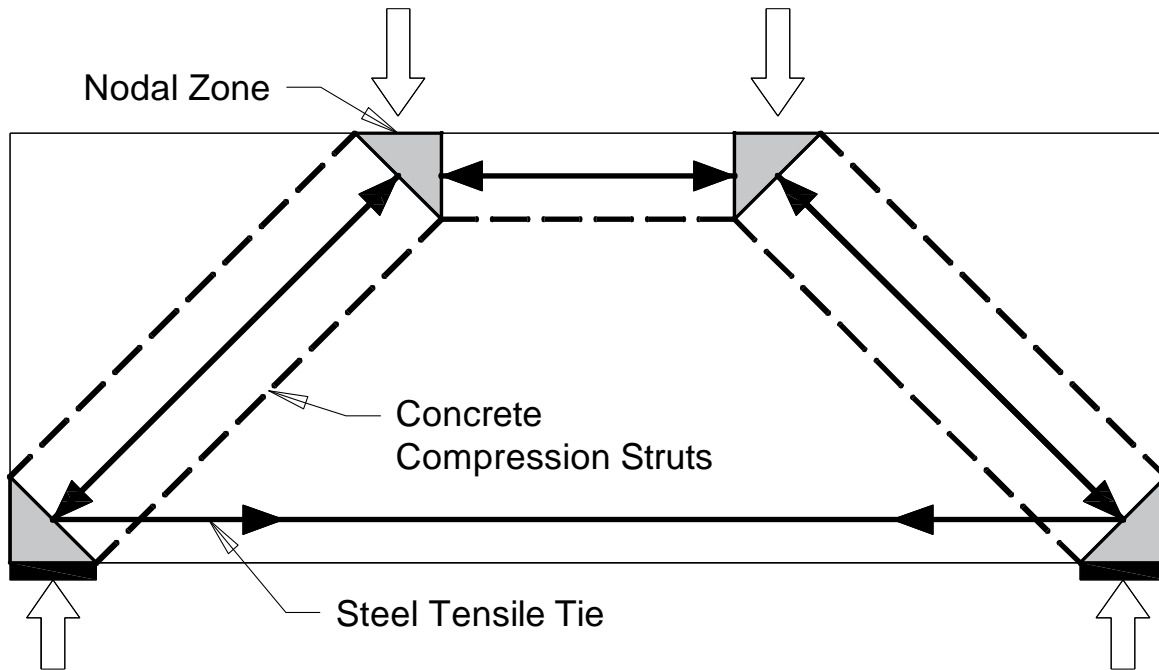
Figure 2-10. Strut-and-Tie model for a deep beam

The basic design philosophy of the STM is that the factored resistance must be greater than the demand:

$$P_u \leq \phi P_n = P_r \qquad (2\text{-}23)$$

where P_u = force in strut, tie, and node due to factored load; P_r = factored resistance of strut, tie, and node; P_n = nominal resistance of strut, tie, and node; and ϕ = resistance factor for tension or compression.

The nominal resistance of unreinforced / reinforced compressive strut is taken as:

$$P_n = f_{cu}A_{cs} + f_y A_{ss} \qquad (2\text{-}24)$$

where P_n = nominal resistance of a compressive strut; f_{cu} = limiting compressive stress; A_{cs} = effective cross-sectional area of strut; f_y = specified yield strength of reinforcing bars; and

A_{ss} = area of reinforcement in the strut, if reinforcement parallel to the strut is not provided in the compressive strut then $f_y A_{ss}$ in Eq. (2-24) is taken as 0.

The compressive stress of the concrete, f_{cu} is limited by:

$$f_{cu} = \frac{f'_c}{0.8 + 170\varepsilon_1} \leq 0.85f'_c \qquad (2\text{-}25)$$

$$\varepsilon_1 = \varepsilon_s + (\varepsilon_s + 0.002)\cot^2\alpha_s \qquad (2\text{-}26)$$

where f'_c = specified compressive strength of concrete; ε_1 = principal tensile strain in cracked concrete; ε_s = tensile strain in the concrete in the direction of the tension tie; and α_s = smallest angle between the compressive strut and adjoining tension ties.

The nominal resistance of a tension tie is calculated by:

$$P_n = A_{st}f_y + A_{ps}[f_{pe} + f_y] \qquad (2\text{-}27)$$

where A_{st} = total area of longitudinal mild steel reinforcement in the tie; A_{ps} = area of prestressing steel; and f_{pe} = stress in prestressing steel due to prestress after losses.

For proportioning of node regions, AASHTO specifies three reduction factors based on the type of nodal zones connected to struts and ties. The concrete compressive stress limit in the node regions is given as:

- For node regions bounded by compressive struts and bearing area $\qquad 0.85\ \phi f'_c$

- For node regions anchoring a one-direction tension tie: $\qquad 0.75\ \phi f'_c$

- For node regions anchoring tension ties in more than one direction: $\qquad 0.65\ \phi f'_c$

2.6 State-of-Practice on Precast Concrete Bent Cap

The state-of-practice on precast concrete bent cap is discussed in this section. Several projects that the use of precast concrete bent cap had brought successful outcomes are first introduced in Section 2.6.1. Previous studies conducted concerning bent cap that influenced TxDOT bent cap design are summarized in Section 2.6.2. Section 2.6.3 provides an in-depth review of the state-of-the-practice of bent cap-column connections.

2.6.1 The Use of Precast Bent Caps in Texas

In the mid-1990s, the needs of prefabrication for unique construction projects have led the use of precast bent caps in Texas, and the use of precast bent capS has become very popular. Currently, TxDOT allows contractors to select the type of bent caps between cast in place concrete and precast concrete bent caps, depending on the project characteristics. Precast bent caps have been successfully used in many standards and also unique bridge constructions by showing great benefits over RC bent caps. There are several projects completed successfully, and the following discussions summarize them.

An example of how the employment of precast concrete bent cap can reduce the construction time can be found in US 290 Ramp G construction in 1994 shown in Figure 2-11(a). The conventional cast-in-place bent cap was an original construction plan and 41-day of construction was first estimated. To avoid traffic congestion due to high volume of traffic, accelerated construction was necessary. The contractor used precast inverted T-bent caps in the construction, and this alternative precast construction reduced the construction to 6 hours.

46

(a) US 290 Ramp G (1994)

(b) Redfish Bay (1994)

Figure 2-11. Use of precast concrete bent caps in Texas

Another example of the implementation of precast bent caps is the Redfish Bay and Morris & Cummings Cut Bridges construction in 1994 shown in Figure 2-11(b). In this project, the 0.5-mile bridge had to be constructed across over Gulf Coast and the contractor used 44 identical rectangular precast bent caps to minimize casting over water. The use of precast caps eliminated significant construction time over the water and also the casting of concrete. The repeatable pattern led to maximize the advantages with fabricated identical bent caps by removing critical path from the construction timeline. The connection between precast bent caps and precast trestle piles consisted of two U-shaped reinforcing bars epoxy grouted into ducts at the top of precast piles, and projected into two voids built along the full depth of the bent cap. Concrete was placed into the voids after the placement of the cap (Freeby et al. 2003).

The Pierce Street Elevated Project in 1996 also used precast bent caps. In the project, 113 superstructures and bent caps were replaced. Connections between precast bent cap and columns were made with post-tensioned bars embedded in the column and projected from the column top to corrugated ducts built in the precast bent cap. The ducts were grouted and the bars were anchored at the cap top.

2.6.2   Previous Research on Bent Caps

Research to investigate the performance of Texas bent caps and to improve the design detailing preceded efforts to develop options for precast bent caps. Ferguson (1964) investigated bent caps through an experimental test program of 36 specimens that varied parameters such as the shear span dimensions, anchorage length of longitudinal steel in the end regions, web reinforcement, and material properties. Key outcomes of the study included recommendations for minimum extension of reinforcing bars and recommendations for calculating the strength of the bent caps. In particular, Ferguson commented on the limited contribution of shear reinforcement at small

shear span ratios. Ferguson made important observations on the distribution of strains in the connection region and the importance of adequate skin steel to minimize side cracks.

For TxDOT project 0-1851, Bracci et al. (2000) constructed a total of sixteen full-size specimens and tested them under quasi-static monotonic loading. The major purpose of the research was to investigate the reasons for the occurrence of unexpected cracks in the multi-column RC bent cap at overhang region. Field investigations indicated typical crack patterns consisted of small flexural cracks within the width of the column support and large shear or flexure-shear cracks within the shear span region. The specimens were designed to be representative for several parameters which were thought to be an important factor for crack control such as concrete strength, stress in the flexural reinforcement, arrangement of flexural and skin reinforcement, shear reinforcement detailing, and the critical section for design. The experimental crack patterns were similar to that observed in the field, and measured strains, displacements, crack widths and crack patterns obtained throughout the test program were analyzed.

Research on the performance of RC bent caps has also been conducted outside Texas. Fonseca et al. (2003) tested deteriorated RC rectangular bent caps that were significantly deteriorated while in service in Utah. For the bent caps tested, flexural response was found to dominate the response (no D-regions existed) but the damage did not compromise the load capacity on account of the fact that corrosion had not occurred. A number of studies (e.g., Restrepo et al. 2011) have evaluated performance of bent caps under earthquake loading, either evaluation of existing bridges, retrofit, or the development of designs for new construction; these studies are not summarized here.

2.6.3   State-of-Practice on Bent Cap-Column Connection

A number of state department of transportation (DOTs) have used precast bent caps in bridge constructions for various projects owing to many advantages over reinforced concrete bent caps such as accelerated construction, reduced on-site hazards, improved quality control ability. In the design stage, the determination of an appropriate connection type to effectively connect the precast bent cap and the pier columns is one of the major keys leading to successful bridge construction. In traditional cast in place concrete bridge bent, bent cap-column connections are constructed in the following procedures.

- Construct the reinforcement concrete column with the extended longitudinal reinforcement beyond the top of the column

- Complete the formwork for reinforced concrete bent cap (typically on falsework)

- Install the bent cap reinforcement and pour the concrete

With this traditional cast in place concrete construction, a monolithic (rigid) connection between the bent cap and column is secured since extended longitudinal reinforcement in the column is bonded to the bent cap concrete. However, for precast concrete bent cap this traditional monolithic connection is not suitable as concrete is generally poured at an off-site while the connection between the bent cap and column is formed at an on-site, separately. An alternative connection is desired that can be equivalent to the monolithic connection in cast-in-place concrete construction. In this study, several feasible options for precast bent cap are classified into two broad categories: a) emulative connections; and b) jointed connections, and these are described in the following.

Emulative connections have been mostly used in the connections in precast bent cap system. In emulative connections, a rigid connection almost equivalent to the conventional monolithic

50

connection found in cast in place concrete bridge is created. Typically, the emulative connection is designed to be stronger than the adjoining bent cap and columns, leading to be applicable in seismic zone also. Emulative connections include: a) Grouted pocket connection; b) Grouted vertical duct connection; c) Pocket connection; d) Bolted connection; and e) Grouted sleeve coupler connection.

Jointed connections are a relatively new way of connecting precast concrete members. The major difference with the emulative connections is that jointed connections use a weaker connection than the adjacent bent cap and columns. Due to the weaker joint, jointed connections can provide protection of connected precast members from being damaged by slight joint opening and closing under lateral load or differential settlement. Although jointed connections have not been used as widely as emulative connections, extensive research has been done in recognition of its potential. Jointed connections include: a) Partially prestressed (hybrid) connection; b) Armored damage avoidance connection; and c) pretensioned rocking bridge bent.

An extensive amount of literature regarding these various connection types is provided by Culmo (2009), Marsh et al. (2011), Ziehl et al. (2011), Kapur et al. (2012), Mehrsoroush et al. (2017), and Birely et al. (2018). In this dissertation, the merits of one type of connection relative to others are not of primary focus, as there are advantages and disadvantages of each connection with selection for a project or jurisdiction ultimately driven by a number of factors such as loading conditions, substructure type and detailing, and local preferences for design and construction practice. Instead, a new type of narrow pocket connection was adopted which can offer an additional option for emulative connections, motivated by a preference for ease of construction and use within pretensioned bent caps for multi-column bents in non-seismic regions.

2.7 Research Question Arising

Based on the literature review on theories regarding flexure-shear interaction in reinforced concrete elements and bent cap members, the following research questions arise:

Is it possible to develop a simple strength shear design method for shear-critical reinforced concrete members?

Extensive previous studies were conducted to develop a unified shear design model and various design procedures have been suggested. However, each method is based on a different shear failure mechanism theory, and procedures are not simple but too complicated to use for practitioners. Furthermore, suggested design procedures are often limited or varied based on the shear span-depth ratio and presence of prestressing forces. Some procedures require iteration, leading to a need for automation.

A survey conducted of 26 different state DOTs and federal lands bridge design agencies on the use of the LRFD Sectional Design Model revealed that designers were often losing their physical feel for shear design due to the increasing complexity of the design provision and the resulting automation. This leads to a loss of confidence when checking designs because the method cannot be readily executed by hand (Hawkins et al. 2005).

Therefore, for design office use the analysis procedure must be simple (but not simplistic) and sufficiently straightforward to be done easily by hand. This study aims to provide a strength-based shear design procedure for the shear-critical members, and it is not limited by a/d ratio.

Can Flexure-Shear interaction be considered readily?

In practice, structural concrete members are subjected to loads causing shear as well as bending. Thus, it is desirable to consider flexure-shear interaction when determining flexure and shear strengths. The current design philosophy imposes a fictitious separation between the shear

resistance and the moment resistance of the structural concrete members. In the design, one evaluates the amount of shear reinforcement needed to minimize the influence of shear on the flexural performance of reinforced concrete members. The design methods do not relate a certain level of moment capacity with a certain amount of shear reinforcement. This separation between shear and moment resistances of a member may result in a design that prevents the development of the full moment capacity. Therefore, it is reasonable to expect that if methods could be developed for predicting the moment capacity a function of shear influence or vise versa, one could compute the optimum amount of shear reinforcement that will ensure attainment of full moment capacity of the member. Furthermore, the incorporation of such methods into a numerical procedure will result in improved methods for evaluating the performance of such members.

Can wide and deep beams with a relatively small shear span-depth ratio such as bent caps be designed in accordance with AASHTO LRFD provisions?

The AASHTO LRFD shear design approach was developed with roots in the Modified Compression Field Theory (MCFT). The MCFT was based on tests of shear panel in which truss action mainly governed the shear transfer and does not take the direct strut action into account. Therefore, the use of the diagonal crack angle in accordance with AASHTO provisions in calculating the shear resistance, while appropriate for slender beams, may be inadmissible for intermediate and certainly for squat beams where direct strut action governs the shear resistance. For this reason, the study verifies the validation of AASHTO provision and furthermore suggested an appropriate design method.

Can the flexure and shear performance of reinforced and prestressed bent caps which have an interior void be adequately predicted?

TxDOT standard bent caps with rectangular cross-sections and without skews range from 24 to 44 ft. The large size bent caps do not have a weight issue if the cast-in-place method is used. However, the weight of long precast, pretensioned bent caps may be restricted for shipping and erection as well. Since a particular bridge project may require a longer bent cap to cope with a wider bridge deck, it may be practical to adopt an interior void in bent caps to avoid the problem of weight exceedance for the broad use of precast, pretensioned bent cap. This study examines the possibility of applying interior void in bent caps through previous experimental programs and develops an ideal size and details of void that ensures the serviceability of bent caps without compromising the overall performance.

3. THEORY DEVELOPMENT FOR FLEXURE-SHEAR INTERACTION WITH TRANSVERSE REINFORCEMENT

3.1 Chapter Summary

While the Compatibility Strut-and-Tie Method has been previously demonstrated as an efficient nonlinear modeling approach to accurately predict the overall load-deformation response of flexure-shear interaction in shear-critical reinforced concrete members, it has limited utility as the approach is highly computational. This chapter presents a reduced form which is based on limit analysis principles to assess the ultimate strength. Amendable for hand methods of analysis, the approach is herein referred to as the *Truss-Arch Model Unified* (or *TAMU*).

The *TAMU* approach accounts for the failure mechanism of the principal diagonal concrete arch which is softened due to the transverse principal tensile strain. Instead of providing overall force-deformation behavior, this model focuses on estimating the ultimate load-carrying capacity by assuming the failure mechanism occurs when the principal diagonal arch reaches its softened maximum strength in shear-critical beams.

This chapter derives an explicit solution for the principal strain ratio, which is required to estimate the concrete softening coefficient. Using the calculated concrete softening coefficient and axial rigidities of the arch and truss members, formulae for the ultimate load-carrying capacity are derived. The validity of the formulae is verified through a comparison of the predicted ultimate shear strength with those measured from previous experimental results on large scale physical tests of bridge piers. The *TAMU* approach is then compared with other code-based strength analysis methods and shows better predictions of the maximum shear strength.

3.2   Introduction

Fenwick and Paulay (1968) were among the first to define the two distinct actions which dominate the shear resistance within a structural concrete element: 1) *truss action* associated with the shear resistance provided by the transverse reinforcement; and 2) *arch action* associated with the shear resistance provided by a diagonal concrete compressive strut (arch) that follows the principal load path between the applied load and the supports (or reactions). The diagonal concrete compression arch is tied with longitudinal and transverse reinforcement after the crack formation, forming a structure like a compound truss. While truss action may be dominant in slender and intermediate beams ($a/d > 2.5$), arch action becomes more prevalent in deeper beams ($a/d \leq 2.5$).

This concept of arch and truss action was popularized and mainstreamed after the publication of the authoritative Park and Paulay (1975) textbook. Chang and Mander (1994) developed a compatibility-based analysis model called 'Cyclic Inelastic Strut-and-Tie Model' (CIST) to account for flexure-shear interaction in beam-column members. Kim and Mander (1999, 2000a, and 2000b) later explored the application of the CIST model. Based on experimental evidence, two different continuum truss models, (i) Constant angle and (ii) variable angle, were postulated. These were then simplified for numerical analysis using a two-point Gauss truss model to unify the cracked elastic flexure-shear interaction for both B- and D-regions.

Following the cracked elastic analysis contributions of the work of Kim and Mander (1999, 2000a, and 2000b), Scott et al. (2012a, 2012b) and Karthik et al. (2016) extended this as the Compatibility Strut and Tie Model (C-STM) to capture overall elastic and inelastic truss and arch actions in structural concrete deep beams up to failure. By using nonlinear constitutive relations for cracked reinforced concrete, they showed that the C-STM is capable of capturing the nonlinear force-deformation response including post-peak behavior of concrete structures remarkably well.

In spite of several advantages and appeal of this approach, one might hesitate to use the C-STM for design as its use remains cumbersome and is more intended for advanced analysis requiring computational methods. For example, Scott et al. (2012b) and Karthik et al. (2016) used a structural analysis program, SAP2000 v.14 (2009) and v.17 (2014), to implement the C-STM.

In this chapter, the C-STM is reduced in scope to be more amenable to performing strength analysis using hand methods of analysis. This reduced model which need not track overall force-deformation behavior is herein referred to as the *Truss-Arch Model Unified* (or *TAMU*). This model accounts for the strength reduction of the principal diagonal concrete arch which is softened due to the transverse principal tensile strain, ε_1. It is thus assumed the structure loses its ultimate load-carrying capacity when the principal diagonal arch fails. Thus, the *TAMU* approach is geared to estimate the limit load of the diagonal arch, which often leads to a sudden or brittle collapse of a shear-critical system.

In the following discussions, the *TAMU* approach is elaborated upon whereby truss and arch actions are discussed and how these two actions may be combined and apportioned to define the limit failure loads. From this, an explicit solution to estimate a concrete softening coefficient is proposed. A parametric study on the softening coefficient of concrete, ζ, is presented to identify what factors are prevalent in governing the softening effect. The proposed *TAMU* approach is then verified using data from a previous large-scale experimental program of Bracci et al. (2000) and also compared with existing code-based methods of limit (ultimate strength) analysis.

3.3 Development of a Truss and Arch Model Unified (*TAMU*) Approach

Figure 3-1 presents the structural modeling basis for the *TAMU* approach. As mentioned, following cracking, a truss-like structure forms by a diagonal concrete compression arch tied by steel reinforcement. The shear mechanism of the truss is associated with a load transfer path. In this

simplified *TAMU* approach, a compound truss is formed such that when the parts are treated separately, they consider the diagonal arch and the truss which encompasses the transverse reinforcement. To model the combined truss and arch structure, the single-point cantilever Gauss quadrature model of Scott et al. (2012a) is simplified whereby the transverse steel is lumped midway along the principal diagonal arch.

3.3.1 Truss and Arch Model with a Vertical Tie

Figure 3-1(a) shows a simply supported beam under two-point loads with different shear-span depth ratios, *a*/*d*. The beam is overlaid by truss and arch actions represented by red and blue lines, respectively (Collins, 1991). The solid and dashed lines respectively show members in tension and compression. As shown in the figure, a shear is resisted by truss and arch actions, and transverse reinforcement provided within the shear span, *a*, is assumed to be clustered at the center of the principal diagonal arch. Figure 3-1(b) represents a shear-resisting mechanism along with truss and arch action for a cantilever beam. As the same as the simply supported beam above, the transverse reinforcement is considered to be clustered at the center of the shear span, $0.5a$. This figure also shows the strains of transverse reinforcement, ε_v, and diagonal arch, ε_2, where transverse to the axis of the principal diagonal arch is subjected to softening due to the principal tensile strain, ε_1. The *TAMU* approach is based on this simplified cantilever beam model.

When transverse reinforcement is provided, a truss is formed with the longitudinal steel. This truss action complements the diagonal concrete compression arch after initial diagonal cracking develops. However, the truss dilates transverse to the action of the arch. It is this dilatation that in turn softens the concrete and eventually leads to tensile fracture along the axis of the arch member. In the following discussion, the important concepts and steps to implement the *TAMU* approach are introduced.
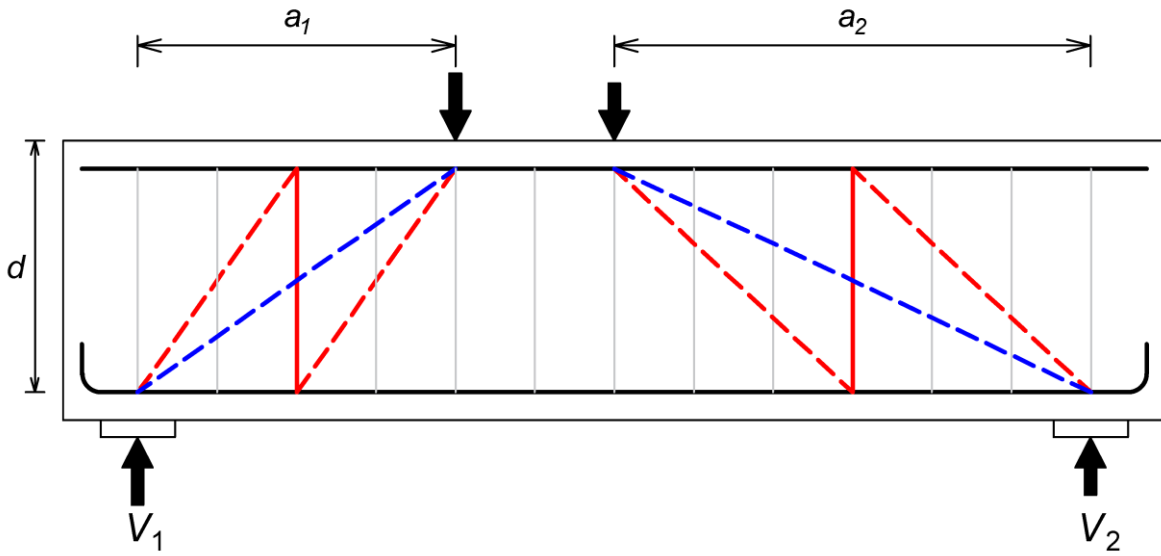
(a) Simply supported beam depicting to different shear span aspect ratios
(a/d ≈ 1.0 left, and a/d = 2.5 right)
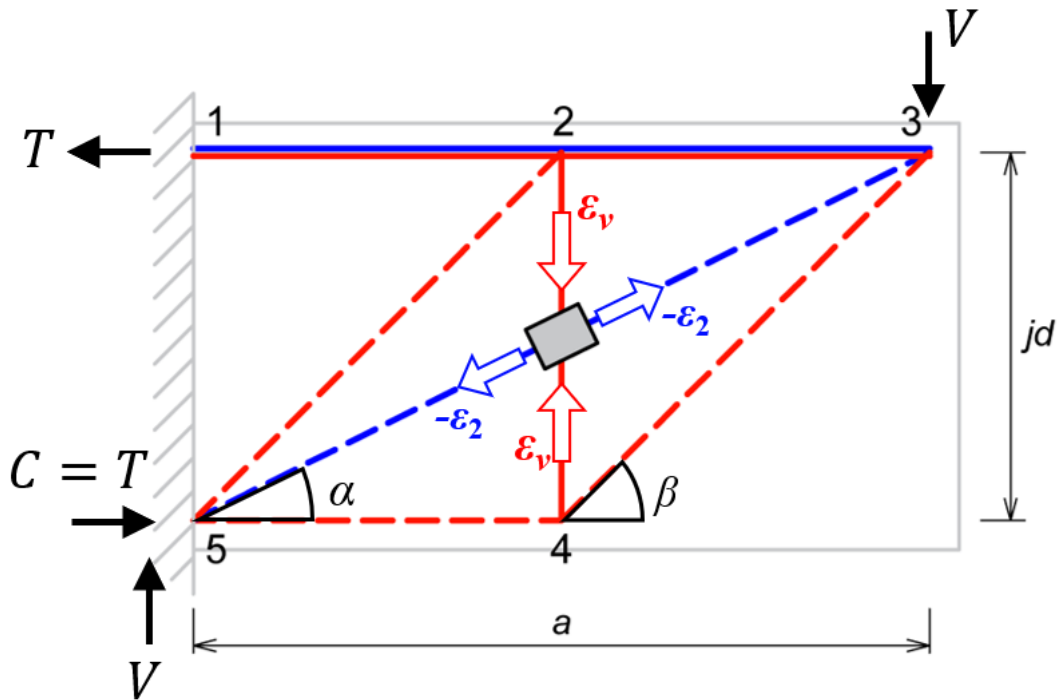
(b) Cantilever beam

Figure 3-1. Beams modeled with truss and arch members

Based on over 200-panel tests, Vecchio (2000) proposed an empirical equation which is the function of the ratio of the principal tensile and compressive strains, $\varepsilon_1/\varepsilon_2$, to find concrete softening coefficient. Based on Vecchio's work, Karthik et al. (2016) defined the magnitude of concrete arch softening, ζ, through:

$$\zeta = \frac{1}{1 + 0.25|\varepsilon_1/\varepsilon_2|}$$

(3-1)

where ζ = concrete softening coefficient; ε_1 = principal diagonal tensile strain transverse to the axis of the arch; and ε_2 = principal diagonal compressive strain at the center of the arch.

Based on the proposed C-STM approach described in Scott et al. (2012a), the axial strain of the vertical tie member 2-4 which represents transverse reinforcement in the truss model (red line in Figure 3-1(b)), is considered as the vertical transverse strain, ε_v, and axial diagonal strain of the concrete arch member 3-5 is taken as the principal compressive strain, ε_2. Using a Mohr's circle analysis, Scott et al. (2012a) showed that the principal strain ratio, $\varepsilon_1/\varepsilon_2$, could be inferred from the ratio of $\varepsilon_v/\varepsilon_2$ as follows:

$$\left|\frac{\varepsilon_1}{\varepsilon_2}\right| = \left(\tan^2 \alpha + \frac{|\varepsilon_v/\varepsilon_2|}{\cos^2 \alpha}\right)$$

(3-2)

where ε_v = transverse tie strain; and α = corner-to-corner diagonal angle.

The determination of each action's relative contributions is an important step in the *TAMU* approach. There have been several studies to accurately estimate the portion of truss and arch action using different parameters such as: (a) strength (Paulay, 1971); (b) stiffness (Kim and Mander, 1999; and Zhu et al., 2003); (c) geometry (Hwang et al., 2000); and (d) the shear span-to-internal lever arm ratio (FIP-Commission 3, 1996). Scott et al. (2012a) investigated each parameter's effect on the force-deformation response and made two conclusions:

- Only minor differences are observed in the elastic force-deformation response by varying the proportions of arch and truss actions.

- Significant differences are observed for non-linear response of the flexure-shear failure mechanisms.

Based on these observations, Scott et al. (2012a) proposed to apportion the arch and truss mechanisms for beams with transverse reinforcement using: (a) the ratios of longitudinal and transverse reinforcement to account for strength; and (b) the ratios of the member's length and height to account for geometry. Both of these components are proportional to the longitudinal and transverse reinforcement as:

$$V_{arch} = f_y A_s \tan \alpha = \rho_L f_y b_w d \tan \alpha \qquad (3\text{-}3)$$

$$V_{truss} = f_{yh} A_v \frac{a}{s} = \rho_v f_{yh} b_w d \cot \alpha \qquad (3\text{-}4)$$

in which V_{arch} = maximum shear force resisted by arch action; V_{truss} = maximum shear force resisted by truss action that is proportional to the transverse reinforcement; f_y = yield strength of the longitudinal steel; f_{yh} = yield strength of the transverse steel; A_s = area of longitudinal reinforcement contributing to the tension tie; A_v = area of one set of stirrups; a = shear span; s = spacing of transverse reinforcement α = corner-to-corner diagonal angle; ρ_L = volumetric ratio of longitudinal steel to concrete, where $\rho_L = A_s/b_w d$; ρ_v = ratio of area of transverse steel to area of concrete for one hoop spacing, where $\rho_v = A_v/b_w s$; b_w = beam width; and d = effective depth of the beam from the extreme concrete compression fiber to the centroid of the tension steel.

By considering these two parameters, it is expected to accurately account for the flexure and shear interaction. An arch breadth scalar proposed by Scott et al. (2012a) is given by:

$$\eta = \frac{V_{arch}}{V_{arch} + V_{truss}} = \frac{\rho_L f_y}{\rho_L f_y + \rho_v f_{yh} \cot^2 \alpha} = \frac{1}{1 + \frac{\rho_v f_{yh}}{\rho_L f_y} \left(\frac{a}{d}\right)^2} \qquad (3\text{-}5)$$

Scott et al. (2012) and Karthik et al. (2016) showed that the C-STM analysis results using the arch breadth scalar in Eq. (3-5) captured the combined truss and arch action quite well. For this reason, the breadth scalar proposed in Scott et al. (2012a) is adopted herein.

In addition to apportioning the arch and truss mechanisms appropriately, the deformations from these mechanisms also need to be taken into consideration when they are combined. This is because overall displacements from both arch and truss mechanisms must be compatible. In the C-STM analysis, a structural analysis software automatically accounts for the compatibility of the combined truss and arch members based on their stiffness as elements are constrained between nodes in the modeling. However, these different displacements by each mechanism need to be directly taken into account in the *TAMU* approach. A force distribution factor, μ, is determined based on the stiffness of each member to meet the compatibility of the whole system such that:

$$\mu = \frac{\delta_{truss}}{\delta_{arch} + \delta_{truss}} \qquad (3\text{-}6)$$

where μ= force distribution factor; δ_{truss} = displacement of the truss mechanism caused by the unit load; and δ_{arch} = displacement of the arch mechanism caused by the unit load.

3.3.2 Arch Action

The force flow in the arch mechanism of the considered cantilever beam adopted in the *TAMU* approach is depicted by blue lines in Figure 3-1(b). As shown in the figure, the compressive stress field is formed throughout the diagonal corner-to-corner concrete arch (strut) running between the applied force and the support (or reaction). This principal diagonal arch is assumed to carry all the

compressive force in this arch mechanism. It has been observed in previous experimental tests that reinforced concrete beams are still capable of carrying additional load even after an initial diagonal shear crack propagates (Bracci et al. 2000; Matsumoto et al. 2001; and Birely et al. 2018). This indicates that the tensile failure of the principal concrete arch may not be a governing mechanism at the ultimate (peak) load and beyond post-peak behavior to failure. It is postulated that the strength prediction based on concrete tensile strength may create an acceptable lower bound solution but not necessarily the peak force prior to failure.

In the failure mechanism of the principal diagonal arch, tensile cracking may develop diagonally from the middle outwards due to tensile splitting, resulting in an unzipping effect. Due to the marked drop in transverse tensile stiffness, a significant increase in the principal tensile strain occurs. This tensile unzipping promotes an accelerated concrete softening effect. As the tensile strength along the arch strut fades, the concrete arch takes over and resists the external force in compression. The concrete strut then soon reaches its softened maximum compressive strength limit and finally fails in a non-ductile (brittle) fashion. This failure mechanism gives a reasonable explanation for D-regions in beams which display an abrupt shear failure following a significant diagonal crack along the strut length.

For this reason, the C-STM approach considers the compressive failure of the principal concrete arch as one of the potential failure mechanisms in shear-critical beams with D-region. When estimating the compressive strength of the arch, Karthik et al. (2016) directly accounted for the softened concrete due to the softening effect via the softened concrete constitutive relationship in their C-STM analysis. The deformation-controlled C-STM analysis by Karthik et al. (2016) predicted the overall force-displacement response quite well of a bent cap specimen from Bracci et al. (2000) by considering the concrete softening effect. In the C-STM analysis, an abrupt

compressive failure of the principal diagonal arch was expected following the yielding of longitudinal and transverse reinforcement. The C-STM force-deformation results showed good agreement with the experimental observations by capturing the post-peak behavior well too. This strongly supports the failure mechanism of the diagonal principal arch, as explained above.

To estimate the maximum force achievable by the principal diagonal arch, it is important to correctly size the effective area of the arch via width, w_s and breadth, b_w, in the present *TAMU* analysis. The strut breadth is estimated using Eq. (3-5) proposed by Scott et al. (2012a), and an appropriate strut width, w_s, needs to be evaluated for the *TAMU* approach. Figure 3-2 presents some strut widths according to different approaches. Marti (1985) introduced the classic strut-and-tie model (STM) based on the observation from many previous experimental studies that only a limited strut width along the diagonal compressive strut between the point of load application and support resists to a significant portion of compressive force. In the STM approach, instead of considering the entire section depth, a certain strut width, w_s, is assumed to resist the compressive force applied to the strut, and a strut width is determined by considering the anchorage condition at the end of the strut. The feasible uniform strut width for D-regions based on the STM approach is depicted in Figure 3-2(a).

However, the STM approach does not account for the truss action formed by the transverse reinforcement. Furthermore, the recent works by Scott et al., (2012a) and Liu et al. (2017) showed that the use of STM for deep beams may result in an exceedingly conservative design. This may imply that the strut width, w_s, used in the STM approach does not reflect well the effective strut width appropriately, and this can be improved.
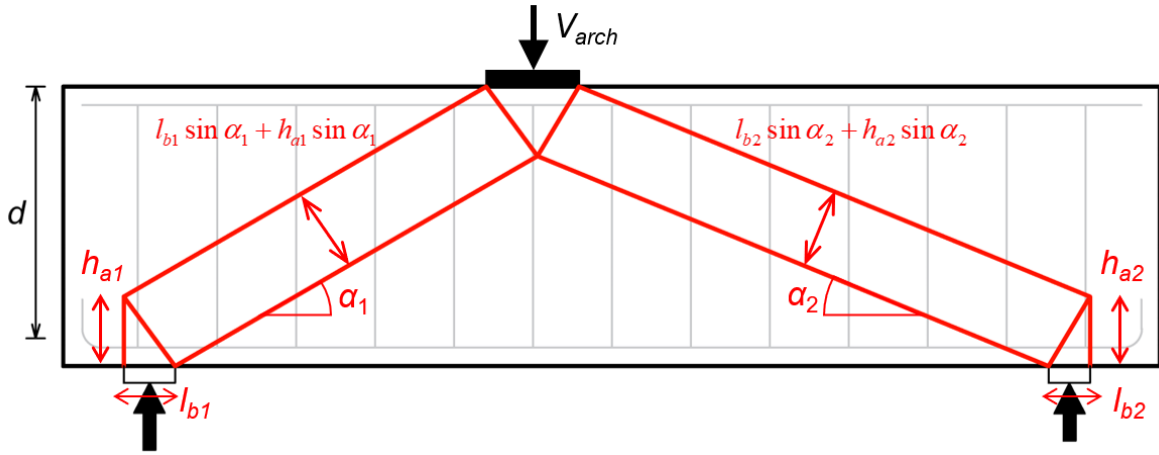
(a) Strut width in the STM approach
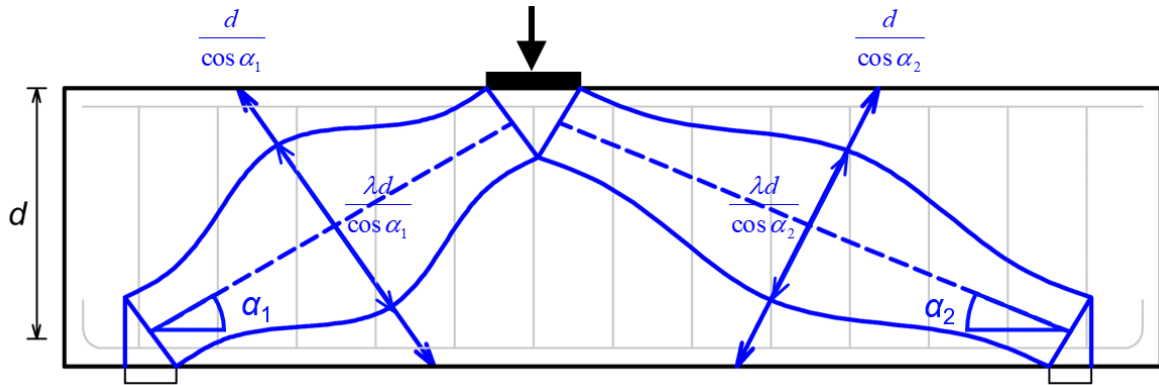
(b) Bottle-shape strut widths proportional to d/cosα
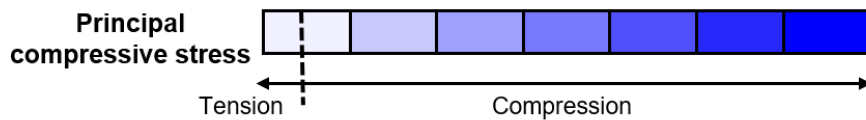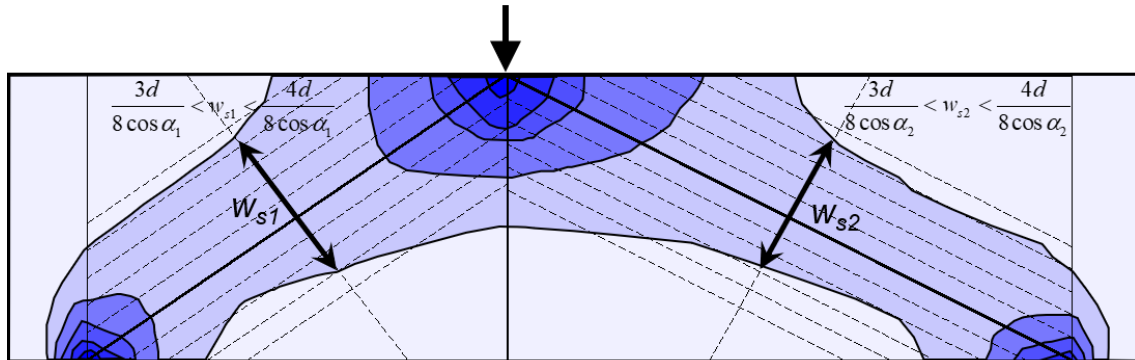
(c) Compressive strut distribution from the FEM analysis

Figure 3-2. Determination of strut width, w_s

65

Figure 3-2(b) displays a bottle-shape strut width introduced by Schlaich et al. (1987). The bottle-shape strut has a convex profile with non-uniform and non-linear variation along its cross-section. According to the bottle-shape strut, the stresses disperse in the lateral direction as they flow the concrete member in D-regions. This bottle-shape strut is a prevalent approach to understand stress flows in deep beams and has been adopted by many studies (Brown and Bayrak, 2008; Sahoo et al. 2010; He et al. 2012; and Birrcher et al. 2014). To estimate the width of the bottle-shape strut at the middle, the *TAMU* approach assumes that the strut width is proportional to the section depth, *d*, and the shear span, *a*. Also, there is a certain coefficient about the width, λ, which remains almost constant regardless of other variables. Thus, the proposed strut width can be expressed as:

$$\frac{w_s}{d} = \lambda \sec \alpha = \lambda \sqrt{1 + \left(\frac{d}{a}\right)^2} \tag{3-7}$$

where w_s = principal diagonal strut width; d = effective depth; λ = strut width scalar (< 1.0); and a = shear span.

The bottle-shape strut is expressed in a form of ($d\sec\alpha$ = overall width) with an arbitrary strut width scalar, λ, in Figure 3-2(b). To further investigate λ, use of the commercial finite-element method (FEM) analysis program, RISA 3D, is made to estimate an appropriate strut width, w_s. The deep beam is modeled with two different *a*/*d* ratios to investigate the strut width varied by them. The left-hand side of the beam simulates a deep beam with *a*/*d* ≈1.0, whereas the right-hand side has an intermediate beam with *a*/*d* ≈ 2.5. The principal compression stress distribution from the FEM analysis is depicted in Figure 3-2(c). The stress distribution shows that a majority of compression force is transferred through a strut width, w_s.

Comparing strut widths at the mid-depth of the beam from different a/d ratios shows that the strut width is proportional to the depth and length of the shear span. Several alternative widths in a form of $(d\sec\alpha)$ are drawn along with the stress distribution. The alternative widths are varied at every $0.0625\ d\sec\alpha_i$ ($d/16\cos\alpha_i$). Measuring the strut width from the FEM analysis shows that the strut width is slightly greater than $0375\ d\ \sec\alpha$ but less than $0.5d\ \sec\alpha$ for both sides. To provide an appropriate estimation with some modest conservativeness, a strut width scalar of $\lambda = 0.375$ is adopted herein for further investigation, thus the arch width is:

$$\frac{w_s}{d} = \frac{3}{8}\sec\alpha \tag{3-8}$$

The proposed strut width of $0.375d\sec\alpha$ is used in the *TAMU* analysis to estimate an ultimate force inducing the compressive failure of the arch concrete strut. This is based on the assumption that the maximum load-carrying capacity is accomplished when the softened concrete reaches its maximum compressive stress and then fades away. An additional empirical verification regarding the suitability of this strut width with $\lambda = 0.375$ is provided in Section 4.4.1.

Table 3-1 summarizes elastic axial rigidities and the virtual work components of the arch action over the individual members shown in Figure 3-3(a). The force applied and strain induced in two elements in the arch action are determined using geometry and axial rigidities. The shear deformation of the arch model is the sum of deformations of a tension chord and concrete arch. The arch displacement by the unit load is needed to estimate the force distribution factor, μ, in Eq. (3-6). Using elastic axial rigidities and the virtual work components and recalling that $\cot\alpha = a/d$, the displacement of the arch model by the unit load, δ_{arch}, is calculated as:

$$\delta_{arch} = \sum_{i=1}^{2}\frac{f^2 L}{EA} \tag{3-9}$$

67

Expanding Eq. (3-9) using the items in the rightmost column in Table 3-1 gives:

$$\delta_{arch} = \frac{a}{E_c b_w d} \psi_{arch} \tag{3-10}$$

where ψ_{arch} = flexibility coefficient for arch displacements defined by:

$$\psi_{arch} = \frac{cot^2\alpha}{\rho_L n} + \frac{8}{3sin^2\alpha}\left(1 + cot^2\alpha \frac{f_{yh}\rho_v}{f_y \rho_L}\right) \tag{3-11}$$

where $cot\alpha = a/d$; and $sin\alpha = d/\sqrt{a^2 + d^2}$.

3.3.3 Truss Action

When transverse reinforcement is provided, truss action is specifically related to the shear mechanism associated with diagonal concrete struts and a vertical tie which represents a clustered transverse reinforcement as shown in Figure 3-3(b). Based on Kim and Mander (1999), the area of the concrete strut (members 2-5 and 3-4) in the truss action is defined by:

$$A_{2-5} = A_{3-4} = \frac{0.5 b_w d}{\sqrt{x + tan^2\beta}} = \frac{0.5 b_w d}{\sqrt{0.5 + (2d/a)^2}} \tag{3-12}$$

in which $x = 0.5$ which is normalized coordinate of the integration point; β = strut angle relative to longitudinal reinforcement ($tan\beta = 2d/a$).

The obtained concrete strut area is then multiplied by the apportioned truss breadth, $(1 - \eta)$, for the truss strut area using Eq.(3-5). As mentioned earlier, transverse reinforcement provided along the shear span, a, is assumed to be clustered at $0.5a$. Thus, the vertical tie (member 2-4 in Figure 3-3b) considers a total sectional area of transverse reinforcement within the shear span by using a number of the vertical hoop, N_h. Elastic axial rigidities and the virtual work components over the individual members in the truss mechanism are summarized in Table 3-2.

Table 3-1. Virtual work analysis on arch model with a vertical tie

Member	Rigidity (EA)	Length (L)	Unit Load (f)	Strain $(\varepsilon = F/EA)$	Deformation by f $(f^2 L/EA)$
1-3	$nE_c\rho_L b_w d$	$d\cot\alpha$	$\cot\alpha$	$\dfrac{\mu V \cot\alpha}{nE_c\rho_L b_w d}$	$\dfrac{\cot^3\alpha/\rho_L}{nE_c b_w}$
3-5	$\dfrac{0.375E_c\eta b_w d}{\cos\alpha}$	$\dfrac{d}{\sin\alpha}$	$-\dfrac{1}{\sin\alpha}$	$\dfrac{-\boldsymbol{\mu V}\cot\boldsymbol{\alpha}}{\mathbf{0.375}E_c\boldsymbol{\eta b_w d}}$	$\dfrac{\cot\alpha}{0.375\eta\sin^2\alpha\,E_c b_w}$

Table 3-2. Virtual work analysis on truss model with a vertical tie

Member	Rigidity (EA)	Length (L)	Unit Load (f)	Strain $(\varepsilon = F/EA)$	Deformation by f $(f^2 L/EA)$
1-2	$nE_c\rho_L b_w d$	$d\cot\beta$	$2\cot\beta$	$\dfrac{2(1-\mu)V\cot\beta}{nE_c\rho_L b_w d}$	$\dfrac{5\cot^3\beta/\rho_L}{nE_c b_w}$
2-3	$nE_c\rho_L b_w d$	$d\cot\beta$	$\cot\beta$	$\dfrac{(1-\mu)V\cot\beta}{nE_c\rho_L b_w d}$	
2-5	$\dfrac{0.5E_c(1-\eta)b_w d}{\sqrt{0.5+\tan^2\beta}}$	$\dfrac{d}{\sin\beta}$	$-\dfrac{1}{\sin\beta}$	$\dfrac{-(1-\mu)V\sqrt{0.5+\tan^2\beta}}{(1-\eta)0.5E_c b_w d\sin\beta}$	$\dfrac{4\sqrt{0.5+\tan^2\beta}}{(1-\eta)\sin^3\beta\,E_c b_w}$
3-4	$\dfrac{0.5E_c(1-\eta)b_w d}{\sqrt{0.5+\tan^2\beta}}$	$\dfrac{d}{\sin\beta}$	$-\dfrac{1}{\sin\beta}$	$\dfrac{-(1-\mu)V\sqrt{0.5+\tan^2\beta}}{(1-\eta)0.5E_c b_w d\sin\beta}$	
2-4	$nE_c\rho_v b_w a$	d	1	$\dfrac{\boldsymbol{(1-\mu)V}}{\boldsymbol{nE_c\rho_v b_w a}}$	$\dfrac{\tan\alpha/(\rho_v)}{nE_c b_w}$
4-5	$(kd)b_w E_c$	$d\cot\beta$	$-\cot\beta$	$\dfrac{-(1-\mu)V\cot\beta}{(kd)b_w}$	$\dfrac{\cot^3\beta}{kb_w E_c}$

Note: N_h = number of hoops within the shear span, and s = spacing of transverse reinforcement;

(a) Arch model   *(b) Truss model*
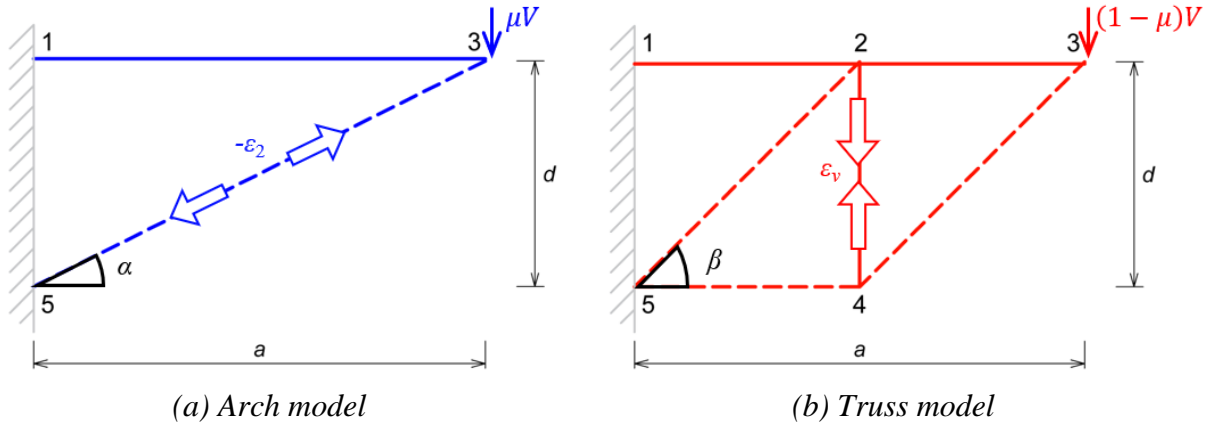
Figure 3-3. Arch and truss model with a vertical tie

The shear deformation of the truss model with a vertical tie is the sum of component deformations. Using elastic axial rigidities and the virtual work components and recalling that $\cot\beta = a/2d$, the shear deformation of the truss caused by the unit load, δ_{truss}, is calculated by:

$$\delta_{truss} = \sum_{i=1}^{6} \frac{f^2 L}{EA} \tag{3-13}$$

Expanding Eq. (3-13) using unit displacement components in Table 3-2 gives:

$$\delta_{truss} = \frac{a}{E_c b_w d} \psi_{truss} \tag{3-14}$$

where ψ_{truss} = flexibility coefficient for truss displacements defined by:

$$\psi_{truss} = \cot^2\alpha \left(\frac{5k + \rho_L n}{8k\rho_L n} \right) + \frac{\tan^2\alpha}{\rho_v n} + \frac{\sqrt{8 + 16\tan^2\beta}}{\sin^3\beta \cot\alpha} \left(\frac{f_y \rho_L}{f_{yh} \rho_v} \tan^2\alpha + 1 \right) \tag{3-15}$$

in which k = elastic compression zone coefficient defined by:

70

$$k = \sqrt{(\rho_L + \rho'_L)^2 n^2 + 2\left(\rho_L + \left(\frac{d'}{d}\right)\rho'_L\right)n} - (\rho_L + \rho'_L)n \qquad (3\text{-}16)$$

where $d' = $ depth from the extreme compression fiber to the centroid of the compression reinforcement; $\rho'_L = $ ratio of compression reinforcement; and $n = $ modular ratio of steel to concrete.

Using Eqs. (3-9) and (3-13), arch and truss shear deformations by the unit load, Δ_{arch} and Δ_{truss}, are calculated, respectively, and these are used to determine the arch-truss force distribution, η, according to Eq. (3-6).

3.3.4 Explicit Solution of Concrete Softening Coefficient

The overall behavior of the considered *TAMU* model is the amalgamation of truss and arch actions, and strains from both actions are used to estimate the magnitude of the concrete softening effect. Earlier in Eq. (3-1), the softening coefficient was defined using, ε_1, and ε_2. This is now formed in terms of ε_v and ε_2 based on Eq. (3-2). In the previous sections, equations required to estimate all the member's strains in the truss and arch actions are provided, thus, an explicit solution of the principal strain ratio, $\boldsymbol{\varepsilon_1/\varepsilon_2}$, can be evaluated using those strains. For the combined truss and arch model with a vertical tie, $\boldsymbol{\varepsilon_v}$ and $\boldsymbol{\varepsilon_2}$ can be interred using equations regarding the axial strain of member (3-5) in Table 3-1 and member (2-4) in Table 3-2. It is noted that the total shear load, V, is distributed to the arch and truss mechanisms, respectively, based on the arch-truss force distribution so that (η) and $(1 - \eta)$ are taken into consideration in the strains in the tables. ε_v, and ε_2 are given by:

$$\varepsilon_v = \frac{(1 - \mu)V}{nE_c b_w \rho_v a} \qquad (3\text{-}17)$$

$$\varepsilon_2 = -\frac{\mu V \cot \alpha}{0.375 E_c \eta b_w d} \qquad (3\text{-}18)$$

where V is shear force applied; μ = force distribution factor defined by Eq. (3-6).

Dividing ε_v by ε_2 gives:

$$\left|\frac{\varepsilon_v}{\varepsilon_2}\right| = \left(\frac{1-\mu}{\mu}\right)\frac{0.375\eta\tan^2\alpha}{\rho_v n} = \frac{0.375}{\rho_v n}\left(\frac{\rho_L f_y}{\rho_L f_y + \rho_v f_{yh}\cot^2\alpha}\right)\tan^2\alpha\left(\frac{\psi_{arch}}{\psi_{truss}}\right) \qquad (3\text{-}19)$$

By substituting Eq. (3-19) into Eq. (3-2), the explicit solution for the principal strain ratio is given by:

$$\left|\frac{\varepsilon_1}{\varepsilon_2}\right| = \tan^2\alpha\left(1 + (\sec^2\alpha)\left(\frac{\rho_L f_y}{\rho_L f_y + \rho_v f_{yh}\cot^2\alpha}\right)\left(\frac{\psi_{arch}}{\psi_{truss}}\right)\left(\frac{0.375}{\rho_v n}\right)\right) \qquad (3\text{-}20)$$

The principal strain ratio is expressed in terms of a few variables such as a/d ratio, ratios of longitudinal and transverse reinforcement, ρ_L and ρ_v, and the elastic modulus ratio of steel reinforcement to concrete, n; and yield stresses of longitudinal and transverse reinforcement, f_y and f_{yh}. Substituting (3-20) into Eq. (3-1) gives an explicit solution for the concrete softening coefficient, ζ. The force transferred to the arch action, $C_{arch} = \mu V \csc\alpha$, is resisted by softened concrete compressive strength, $\zeta f'_c$, multiplied by the effective area of strut $A_{arch}(= \eta b_w w_s)$. Thus, the maximum nominal shear capacity for the arch compression critical failure, V_n^{arch}, is expressed as:

$$V_n^{arch} = \frac{3}{8}\frac{\zeta\beta_1 f'_c b_w d}{\left(1 + \frac{\rho_v f_{yh}}{\rho_L f_y}\cot^2\alpha\right)}\tan\alpha\left(1 + \frac{\psi_{arch}}{\psi_{truss}}\right) \qquad (3\text{-}21)$$

where V_n^{arch} = maximum nominal shear capacity inducing compressive failure of the principal diagonal arch; β_1 = ratio of the depth of the equivalent uniformly stressed compression zone; and f'_c = concrete compressive strength.

3.3.5 *TAMU* Analysis Procedure

Based on the proposed *TAMU* method, the ultimate shear strength of the shear-critical concrete beams (deep or intermediate beams) can be calculated. The main procedures to implement the *TAMU* analysis are as follows:

(1) Determine basic parameters needed to implement the *TAMU* analysis including geometrical parameters (h, b_w, d, a), material and design properties (f'_c, E_c, f_y, f_{yh}, E_s, A_s, A_v, and s).

(2) Find the maximum shear forces resisted by arch action, V_{arch}, and truss action, V_{truss}, using Eqs. (3-3) and (3-4), respectively, and calculate arch-breath scalar, η, based on Eq. (3-5).

(3) Calculate displacements of truss and arch actions by the unit load, Δ_{truss} and Δ_{arch}, according to Eqs. (3-9) and (3-13) and force distribution factor using Eq. (3-6).

(4) Determine the principal strain ratio, $\varepsilon_1/\varepsilon_2$, using and Eq. (3-20).

(5) Find concrete softening coefficient, ζ, using Eq. (3-1).

(6) Calculate the maximum shear capacity, V_n^{arch}, by Eq. (3-21)

3.4 Verification of *TAMU* Approach with Large Scale Experimental Study

A large-scale experimental study conducted by Bracci et al. (2000) is first analyzed using the computational C-STM approach to obtain the overall force-deformation behavior. Next, the *TAMU* strength limit analysis approach is applied and the results are compared with peak forces obtained in C-STM. Both are compared with the experimental data as well as two existing code methods of analysis.

3.4.1 Summary of the Bracci et al. (2000) Experimental Tests
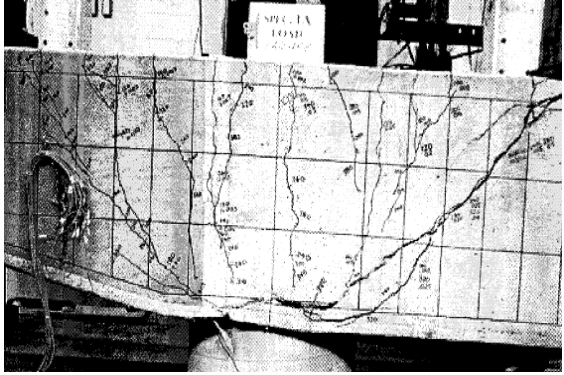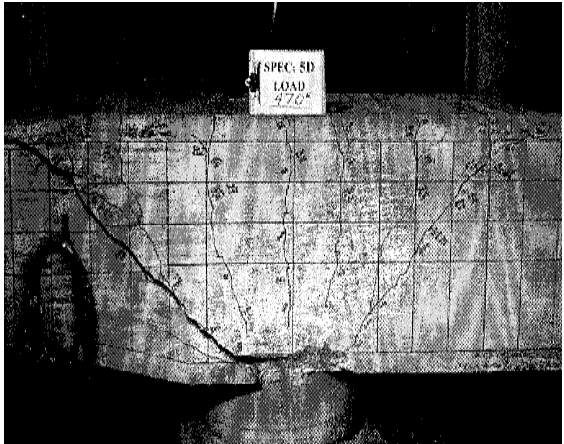
Bracci et al. (2000) tested a total of sixteen full-scale rectangular reinforced concrete bent cap specimens (838 mm by 914 mm) under quasi-static monotonic loading until failure. The main object of the experimental test was to investigate the cause of the unexpected flexural and diagonal

cracks at overhang region of hammer-head pier bents and to determine their nonlinear performance through to failure. The brief explanations needed to understand and analyze the test program such as test matrix, test setup, and summary of the test results are presented here. More details about the experimental program including specimen design, specimen construction, connection details, and material properties are available in Bracci et al. (2000) and Young et al. (2002).

The specimens were divided into three groups depending on the variables, and Table 3-3 summarizes these variables. The specimens were designed to be representative for several parameters which were thought to be an important factor for crack control such as concrete strength, and detailing of flexural, skin, and shear reinforcement. The photographs in Table 3-3 show the failure mode category of the specimens in that grouping. Generally, shear failure occurred between the applied loading and the supporting column along the principal diagonal arch (strut) for all three groups. The ductility displayed differed by each group due to the variables, but it is apparent that the failure was governed by a flexure-shear failure mechanism for each case. This shear failure mechanism is further explained in the C-STM analysis.

Figure 3-4(a) presents the details of the cross-section for each group and Figure 3-4(b) shows the layout of the reinforcement overlaid by truss and arch actions adapted in the C-STM and *TAMU* analyses. As shown in the figure, specimens were cantilevered from both sides with a single column to represent an exterior part of the bent cap where the diagonal shear crack formation is frequently observed. Identical loads were applied through two vertical actuators symmetrically located at a distance of 1,067 mm from the column center to simulate loads from girders, resulting in the equivalent shear demand on both sides and the maximum negative moment at the centerline of the column.

Table 3-3. Test matrix and failure mechanism of experimental study reprinted from Bracci et al. (2000)

	ID	Flex. Reinf.	Skin Reinf.	f'_c, (MPa)	Shear reinf.	Photo taken after the failure
Group A	1A	8-D25	4-D16	42.9	2-D16	
	1B	8-D25	4-D16	40.1	2-D16	
	2A	8-D25	6-D13	42.9	2-D16	
	2B	8-D25	6-D13	40.1	2-D16	
Group B	3C	11-D22	6-D13	41.6	2-D16	
	3D	11-D22	6-D13	38.0	2-D16	
	4C	7-D32	6-D13	41.6	2-D16	
	4E	7-D32	6-D13	53.2	2-D16	
	5D	11-D25	6-D13	38.0	2-D16	
	5E	11-D25	6-D13	53.2	2-D16	
Group C	6F	5-D32	6-D13	37.6	4-D16	
	6G	5-D32	6-D13	36.7	4-D16	
	7F	11-D25	6-D13	37.6	4-D16	
	7H	11-D25	6-D13	39.5	4-D16	
	8G	8-D25	6-D13	36.7	4-D16	
	8H	8-D25	6-D13	39.5	4-D16	

Group 1   *Group 2*   *Group 3*

(a) Representative cross-section

(b) Test layout and C-STM model
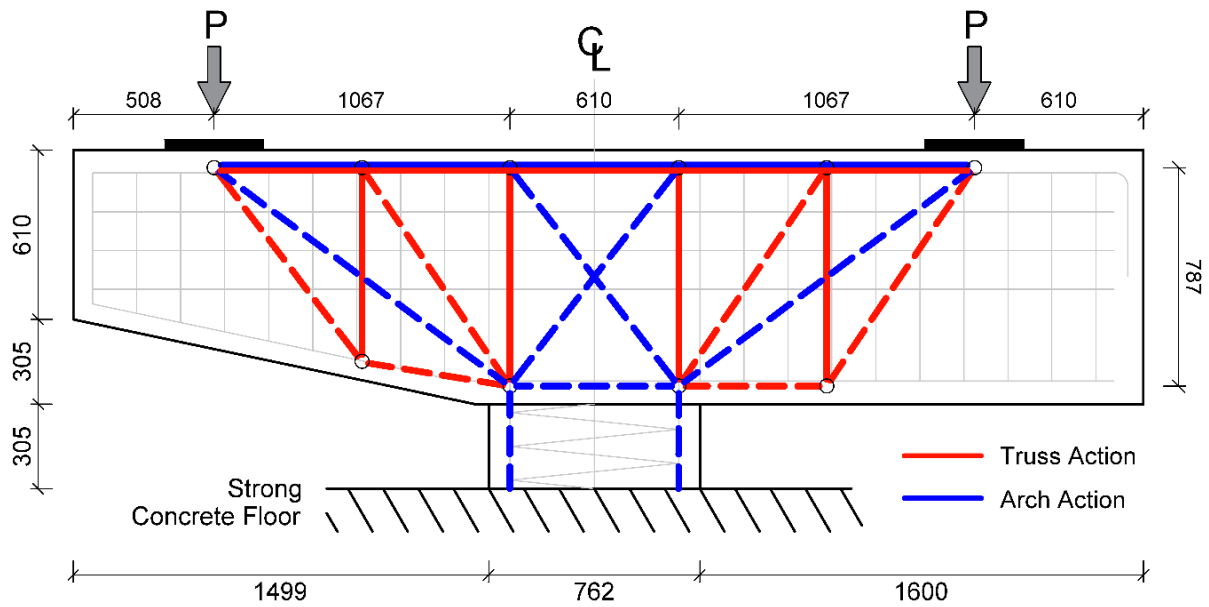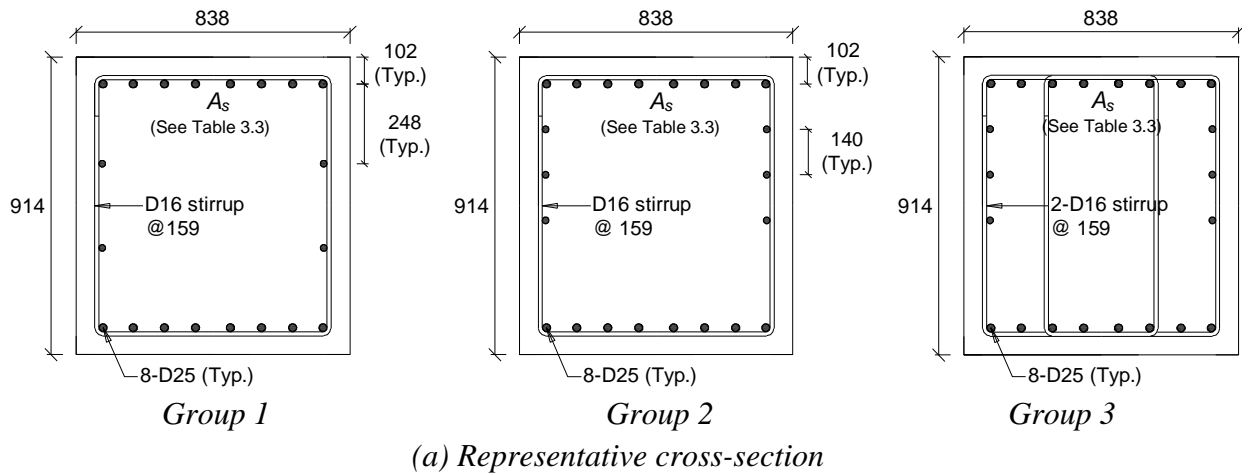
Figure 3-4. RC-bent cap used to verify C-STM and *TAMU*

76

3.4.2   C-STM Analysis

A C-STM analysis was performed using a nonlinear analysis program (*OpenSees*, Version 3.2.3).

Figure 3-5(a) represents truss and arch models used in the C-STM analysis. Each truss and arch

member in the C-STM is comprised of concrete and steel elements, and their constitutive material

models are provided in Figure 3-5(b) and (c), respectively. In the analysis, these concrete and steel

elements are constrained together to create the combined response. The C-STM geometry and axial

rigidities of truss and arch members are determined based on Scott et al. (2012a).

To properly account for the concrete softening effect, the C-STM analysis was performed

twice. First, by running the C-STM analysis, the respective principal compressive and tensile

strains, ε_2 and ε_1, were obtained from the diagonal concrete arch member and a dummy member

(whose axial rigidity is set to $EA = 1.0$) placed perpendicular to that arch, respectively. The

concrete softening coefficient calculated by using the $\varepsilon_1/\varepsilon_2$ of ratio and Eq. (3-1) then applied in

the second C-STM analysis.

Figure 3-6 presents the results of the C-STM displacement control analysis conducted for

three specimens, representing each group: Specimen 2A, 5D, and 8H. Force-displacement

response and force-internal strain of flexural reinforcement are obtained, and the simulated results

are compared to experimental data. The force-internal strain of the principal diagonal concrete

arch from the analysis is also presented to help understanding of the failure mechanism even

though there is no data available to compare with it. The analysis predicted several nonlinear hinge

formations and those are indicated in the figure using different types of markers. The nonlinear

events include: a) concrete cracking at the tensile chord (member 1-2); b) yielding of longitudinal

reinforcement (member 1-2); c) yielding of transverse reinforcement (member 2-4); and d)

crushing of the principal diagonal concrete arch (member 3-5).
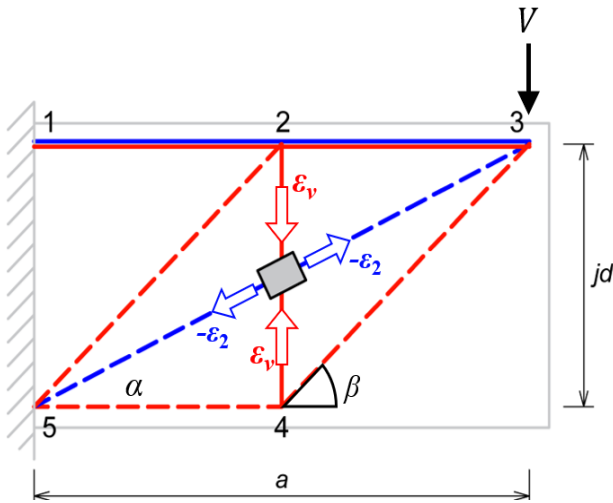
Member	Steel A	Concrete A
1-2	A_s	$b_w(kd)$
2-3	A_s	$b_w(kd)$
2-5	-	$\dfrac{0.5E_c(1-\eta)b_w d}{\sqrt{0.5+\tan^2\beta}}$
3-4		
2-4	$N_h A_{sh}$	$(4c+2d_h)N_h s$
4-5	A'_s	$b_w(kd)$
3-5	-	$\dfrac{0.375E_c\eta b_w d}{\cos\alpha}$

(a) Simulated model and sectional area of each member
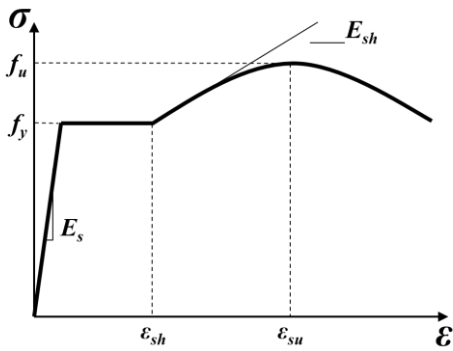
(b) Steel Model
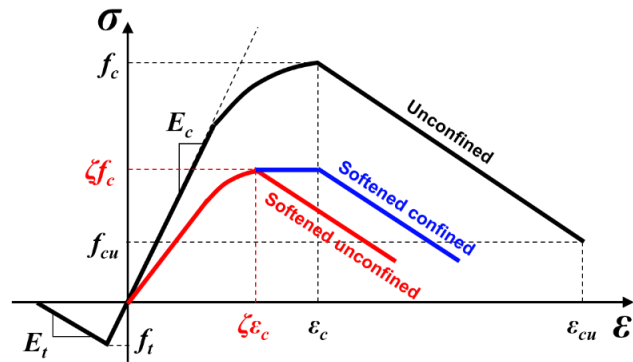
(c) Concrete Model with softening effect
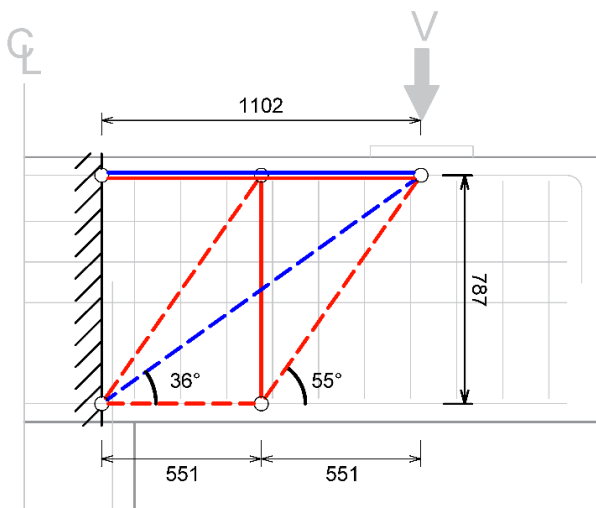
(d) TAMU application to bent cap and fixed variables

Given geometry variables

$a = 1{,}102$ mm; $d = 787$ mm;

$h = 914$ mm; $b_w = 838$ mm;

$\alpha = 36$ deg.; $\theta = 55$ deg.; $N_h = 6$

Section and Material properties

f'_c varies by specimen;

$E_c = 4{,}459\sqrt{f'_c}$ in MPa;

A_s varies by specimen;

$A'_c = 4{,}077$ mm^2; $f_y = 448$ MPa;

$E_s = 200$ GPa

Figure 3-5. Detailing of OpenSees modeling and nonlinear constitutive models used

78

For Specimen 2A, analysis results from the same class of analysis by Karthik et al. (2016) are superimposed in a blue line on Figure 3-6 (a). Note Karthik et al. (2016) used the software, SAP2000 v.17 (2014), whereas herein the present analysis uses the more versatile *OpenSees* v. 3.2.2 (2020). Analysis results are discussed for each specimen with experimental observations given in the following discussion.

Good agreement between the experiment results and the C-STM analyses is found in both force-displacement response and strain-force behavior for Specimen 2A as shown in Figure 3-6(a). The C-STM analysis captures well the overall behavior of the specimen, and in particular the challenging post-peak behavior of the descending branch. Slightly better agreement is achieved in the current study than Karthik et al. (2016), and this may be due to: 1) smooth material models used for steel and concrete; and 2) different event-to-event solution strategies that each program is based upon.

The obtained $\varepsilon_1/\varepsilon_2$ ratio from the first performance of the C-STM was -7.3, resulting in the concrete softening coefficient of 0.36. The C-STM analysis predicted a diagonal shear failure along the strut in arch action after yielding of longitudinal and transverse reinforcement as shown in the force-displacement curve in Figure 3-6 (a). According to the C-STM analysis, the peak load is achieved when the concrete arch reaches its softened maximum strength, and the load-carrying capacity starts decreasing gradually while maintaining some ductility. This prediction corresponds to the observation reported by the authors that the specimen exhibited some ductile response by yielding of longitudinal reinforcement prior to a sudden shear failure.
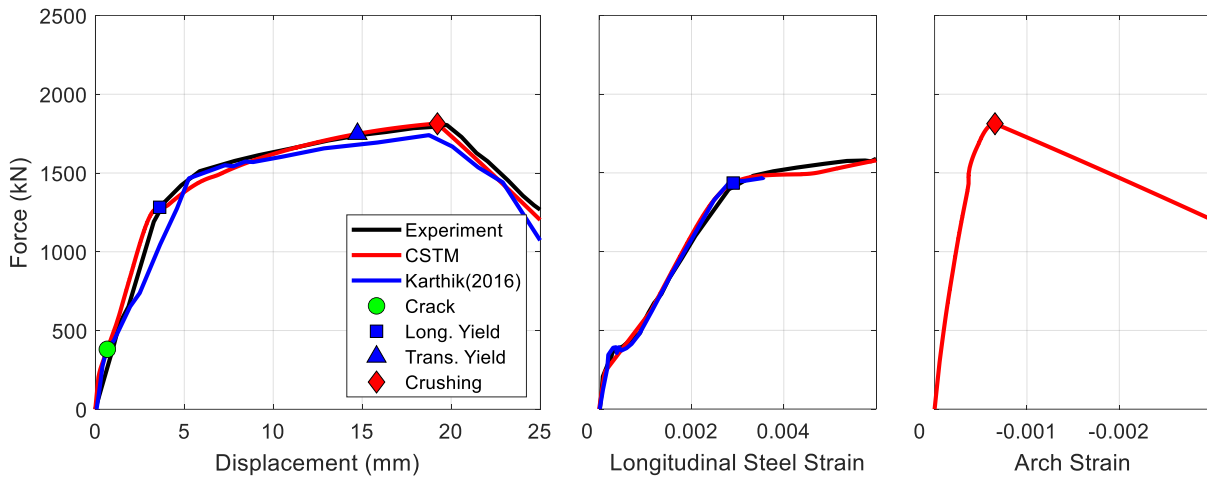
(a) Group A: Specimen 2A
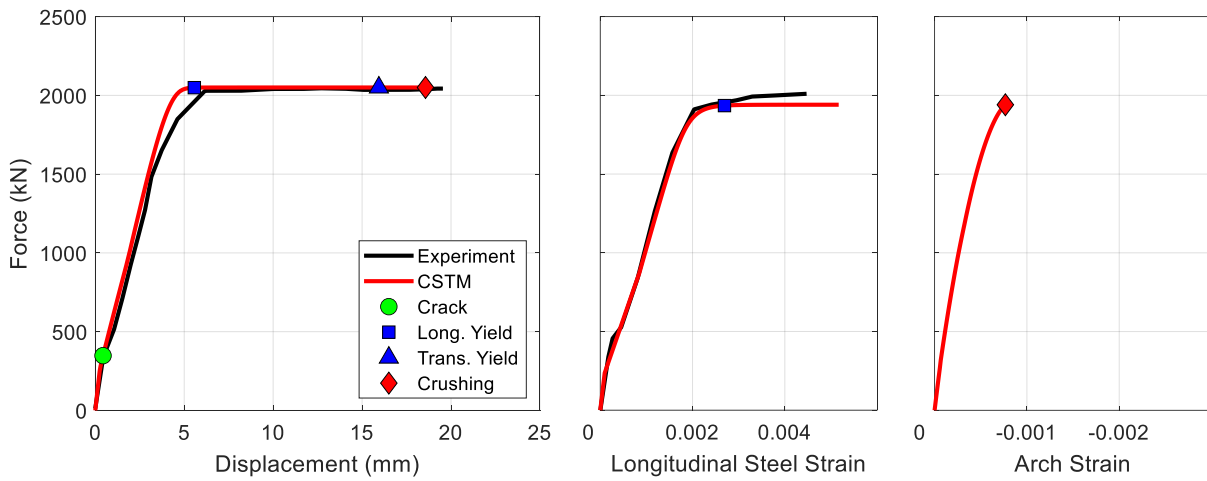
(b) Group B: Specimen 5D
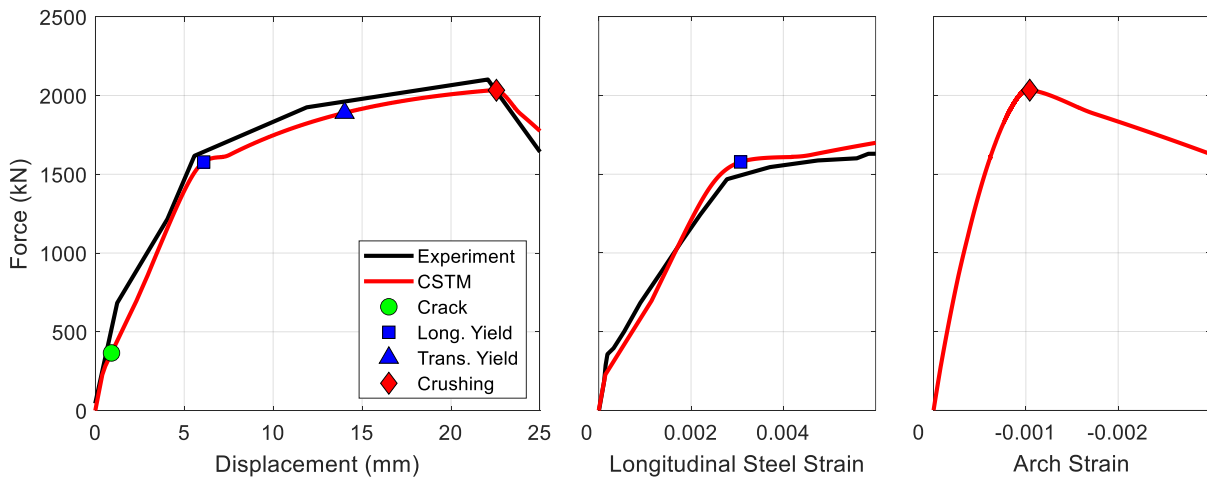
(c) Group C: Specimen 8H

Figure 3-6. Test vs. C-STM analysis

As shown in Figure 3-6(b), the C-STM analysis on Specimen 5D also shows an acceptable agreement with the test results. About 40% more longitudinal reinforcement was provided in this specimen compared to specimens in Group A and C, and the other variables remained almost the same. The force-displacement curve from the C-STM analysis shows that although yielding of both longitudinal and transverse reinforcement takes place, neither of them reaches into the strain-hardening range. Because of that, the specimen lost its load-carrying capacity as soon as the principal diagonal arch attained its softened maximum strength and faded away, resulting in the abrupt failure. In the test, although the ultimate shear capacity at failure increased some 15% compared to Specimen 2A, Specimen 5D failed in a very brittle shear mode. This test observation is consistent with the prediction made by the C-STM analysis. Bracci et al. (2000) also reported that the specimen did not reach its full flexural capacity although some initial flexural yielding took place just prior to the shear failure. The C-STM analysis is able to explain these nuances observed in the test well. Note the concrete softening coefficient increased from $\zeta = 0.36$ to 0.41 due to the additional flexural reinforcement (this is evident in the force-strain of the principal diagonal concrete curve); this aspect is discussed in the next subsection.

Figure 3-6(c) displays the C-STM analysis results of Specimen 8H which was strengthened by using twice as much transverse (shear) reinforcement than the other specimens in Groups A and B; the results agree rather well with the experimental test observation. Specimen 8H reached its full flexural strength with a considerably increased deformation capacity by deterring the brittle shear failure mechanism. The delayed shear failure was considered due to the increased concrete softening coefficient which to $\zeta = 0.43$. According to the C-STM analysis, the increased concrete softening coefficient allowed both longitudinal and transverse reinforcement to enter their strain-hardening regions. Due to the strain-hardening effect, the truss action was able to resist the force

to some degree while the resistance of the concrete arch faded away. This process may provide some ductility. This increased concrete softening coefficient is clearly seen in the force vs. arch strain curve as the peak load is achieved at the higher strain in Specimen 8H compared to Specimen 2A and 5D.

The full computationally intensive C-STM analysis on these three bent cap specimens demonstrates quite well the versatility of the C-STM approach; in particular, the peak strength and the associated displacement are well captured, and most commendably the post-peak performance until failure.

3.4.3 *TAMU* Analysis

The Truss-Arch Model Unified (*TAMU*) analysis is implemented herein to analyze all specimens tested by Bracci et al. (2000). The same geometry and axial rigidities used in the C-STM analysis earlier in Figure 3-5(a) are used for the *TAMU* analysis. Both the left and right sides of the specimen are symmetric to the column center and identical, except for a battered end in the left part. Therefore, the specimen is considered as a cantilever beam by emulating the right-half of the specimen in the analysis. This cantilever beam is depicted in Figure 3-5(d) along with geometry variables, and section and material properties used in the analysis.

The analysis is done by following the step-by-step guidelines provided in Section 3.3.5. The *a/d* ratio of 1.4 is used for all specimens and meets the requirement to implement the *TAMU* approach. By substituting given variables into Eqs. (3-3) and (3-4), maximum shear forces resisted by arch action, V_{arch}, and truss action, V_{truss}, are calculated, respectively. Eq. (3-5) is then used to determine arch breadth scalar, η, and the force distribution factor, η, is calculated by Eq. (3-6). Maximum shear capacity inducing shear failure is obtained by Eq. (3-21). The calculated values in the analysis are summarized in Table 3-4 along with the measured shear strengths and shear

strength ratio (V_{test}/V_{pred}). The C-STM analysis results of three specimens (2A, 5D, and 8H) are also presented with an asterisk in the table.

The accuracy of the *TAMU* analysis can be evaluated by assessing the shear strength ratios, V_{test}/V_{pred}. The average of V_{test}/V_{pred} is 1.07 with a median of 1.06, and the lognormal standard derivations, given by the dispersion factor, $\beta = 0.08$. These average and median values close to 1.0 and low β indicate that the *TAMU* approach is capable of predicting the ultimate shear strength precisely. Although the *TAMU* analysis overestimated the maximum strength in a few cases (4 of 16), differences are not significant (1 to 9%), thus this unconservative aspect may be covered by an appropriate strength reduction factor when taken into consideration. The ultimate shear strengths of three specimens (2A, 5D, and 8H) predicted by the C-STM are quite close to the test results so that the ratios of V_{test}/V_{pred} are almost 1.0. Compared to the *TAMU* approach, the C-STM shows only slightly better agreement.

The concrete softening coefficients obtained from the *TAMU* and C-STM analyses are 0.33 and 0.36 for Specimen 2A, 0.38 and 0.41 for Specimen 5D, and 0.41 and 0.43 for Specimen 8H, respectively. These coefficients are not exactly the same but reasonably close, showing the versatility of the explicit solution to estimate the concrete softening coefficient derived in Sec. 3.3.4. The concrete softening coefficient tends to be greater when a higher ratio of longitudinal and transverse reinforcement is provided. Further investigation regarding the effect of design variables on the concrete softening coefficient is made in Section 3.5. The *TAMU* approach provided overall a reasonable prediction of the maximum shear capacities regardless of flexural and shear reinforcement ratios and concrete compressive strength. Thus, the *TAMU* approach may be used as a simple analysis procedure for checking structural capacity.

Table 3-4. Summary of *TAMU* analysis results for large scale RC bent cap tests by Bracci et al. (2000)

ID	V_{arch}, kN	V_{truss}, kN	η	μ	$\varepsilon_1/\varepsilon_2$	ζ	V_{pred}, kN	V_{test}, kN	$\dfrac{V_{test}}{V_{pred}}$
RC-1A	1,305	883	0.61	0.75	8.58	0.33	1,690	1,668	**0.99**
RC-1B	1,305	883	0.61	0.75	8.32	0.33	1,646	1,815	1.10
*RC-2A	1,305	883	0.61	0.75	8.58	0.33 *0.36	1,690 *1,813	1,797	1.06 *0.99
RC-2B	1,305	883	0.61	0.75	8.32	0.33	1,646	1,695	1.03
RC-3C	1,363	883	0.62	0.76	8.25	0.33	1,708	1,873	1.10
RC-3D	1,363	883	0.62	0.76	7.92	0.34	1,655	2,042	1.24
RC-4C	1,836	883	0.69	0.81	6.9	0.38	2,002	1,908	**0.95**
RC-4E	1,836	883	0.69	0.81	7.75	0.35	2,224	2,024	**0.91**
*RC-5D	1,795	883	0.68	0.81	6.72	0.38 *0.41	1,913 *2,050	2,069	1.08 *1.00
RC-5E	1,795	883	0.68	0.81	7.86	0.35	2,198	2,140	**0.97**
RC-6F	1,311	1,765	0.44	0.61	5.92	0.41	1,739	1,913	1.10
RC-6G	1,311	1,765	0.44	0.61	5.82	0.41	1,713	1,788	1.04
RC-7F	1,795	1,765	0.52	0.68	5.18	0.44	1,988	2,224	1.12
RC-7H	1,795	1,765	0.52	0.68	5.27	0.44	2,020	2,126	1.05
*RC-8G	1,305	1,765	0.44	0.61	5.83	0.41	1,713	1,926	1.13
RC-8H	1,305	1,765	0.44	0.61	6.03	0.41 *0.43	1,762 *2,033	2,104	1.19 *1.03

Notes: An asterisk (*) indicates the C-STM analysis results; Unconservative predictions are bold; Median = Median value; and β = dispersion factor.

Median	1.06
β	0.08

3.4.4   Comparison with Code-Based Shear Analysis Approaches

The *TAMU* approach is now compared with other code-based strength analysis methods provided in ACI 318-19 (2019) and AASHTO LRFD Bridge Design Specification (2017). The code-based approaches are referred to as ACI and AASHTO methods in this study. The general procedure using equations in AASHTO 5.7.3.4.2 is used as the AASHTO method. The analysis results are presented and compared herein, and the detailed analysis procedures of these two code-based strength analysis methods can be found in Sec.2.5.1. It is noted that strength reduction factors are not applied to all cases.

Table 3-5 summarizes shear strengths predicted by the three methods along with shear strength ratios, V_{test}/V_{pred}. The median and dispersion factor (β) of the shear strength ratios are also provided in the table. The comparison indicates that *TAMU*, ACI, and AASHTO generally give conservative estimates of the nominal strengths, as the median values of the shear strength ratio are 1.07, 1.02, and 1.23, respectively. The low dispersion factor, β, for all methods implies predicted strengths are more likely within the acceptable range.

A noticeable unconservative aspect was found in the ACI approach for all specimens in Group C which were strengthened by applying twice as much transverse reinforcement. The ACI analysis overestimated these heavily shear-reinforced bent caps as much as 11 to 36%, and it is not acceptable even after considering the strength reduction factor (ϕ_v=0.75). This contrasts with AASHTO based analysis as only 1 to 3% of results were unconservative for these specimens. In the ACI analysis, the shear resistance by transverse reinforcement, V_s, increases proportionally by the amount of transverse reinforcement, and this may cause the uncertainties. On the other hand, the effect of heavy transverse reinforcement was also taken into consideration by altering the concrete softening coefficient in the *TAMU* or by adjusting the crack angle in the AASHTO.

Table 3-5. Comparison with code-based strength analysis methods

ID	V_{test}, kN	V_{pred}, kN			V_{test}/V_{pred}		
		TAMU	ACI	AASHTO	*TAMU*	ACI	AASHTO
RC-1A	1,668	1,690	1,638	1,315	**0.99**	1.02	1.27
RC-1B	1,815	1,646	1,612	1,305	1.10	1.13	1.39
RC-2A	1,797	1,690	1,638	1,322	1.06	1.10	1.36
RC-2B	1,695	1,646	1,612	1,317	1.03	1.05	1.29
RC-3C	1,873	1,708	1,633	1,344	1.10	1.15	1.39
RC-3D	2,042	1,655	1,601	1,327	1.24	1.28	1.54
RC-4C	1,908	2,002	1,644	1,504	**0.95**	1.16	1.27
RC-4E	2,024	2,224	1,738	1,541	**0.91**	1.16	1.31
RC-5D	2,069	1,913	1,618	1,478	1.08	1.28	1.40
RC-5E	2,140	2,198	1,742	1,528	**0.97**	1.23	1.40
RC-6F	1,913	1,739	2,444	1,854	1.10	**0.78**	1.03
RC-6G	1,788	1,713	2,439	1,847	1.04	**0.73**	**0.97**
RC-7F	2,224	1,988	2,475	2,146	1.12	**0.90**	1.04
RC-7H	2,126	2,020	2,491	2,155	1.05	**0.85**	**0.99**
RC-8G	1,926	1,713	2,449	1,840	1.13	**0.79**	1.05
RC-8H	2,104	1,762	2,471	1,855	1.19	**0.85**	1.13
Notes: Unconservative predictions are bold				Median	1.06	1.02	1.23
				β	0.08	0.19	0.15

Figure 3-7 shows the data points of the shear strength ratios, V_{test}/V_{pred} connected with a solid line for three methods. The data points are sorted by V_{test}/V_{pred}, and distributed evenly to obtain the cumulative probability. Shear analysis approaches are distinguished by colors (Black for *TAMU*; Red for ACI; and Blue for AASHTO). The median and dispersion factor (β) values are presented on the left in the figure. As shown in the figure, the *TAMU* method shows the most concentrated data points near $V_{test}/V_{pred} = 1.0$ due to the median value close to 1.0 and the low dispersion, $\beta = 0.08$. Both ACI and AASHTO shear approaches show a similar trend in the figure owing to close β values, but the AASHTO distribution is shifted to the right, resulting in more conservative assessment.

3.5 Discussion and Significance

Through a series of experimental programs, Kani (1964, 1966, and 1967) found there is a transition area called 'Shear Valley' where a structure may fail in shear prior to reaching its flexural capacity; diagonal shear failure governs the failure mechanism. In this shear valley, a significant increase of ultimate shear load carrying capacity is observed as the shear span-depth ratio decreases, beginning at *a/d* = 2.5. This significant change of ultimate shear capacity based on *a/d* ratio may be physically explained by the concrete softening effect. In this section, parameter studies on the concrete softening coefficient are conducted using the explicit solution proposed in this study.

Kani conducted a series of shear tests on beams with variables including effective depth, *d*, width, *b*, shear span, *a*, and the longitudinal reinforcement ratio, ρ_L. Through the series of experimental programs, Kani discovered that shear stress, v_u, is not a constant quantity, and also the effect of concrete strength on shear was relatively insignificant compared to other factors. Kani concluded that effective depth, shear span, and longitudinal reinforcement are closely related to the shear strength of RC members while beam width had only a slight effect based on the test
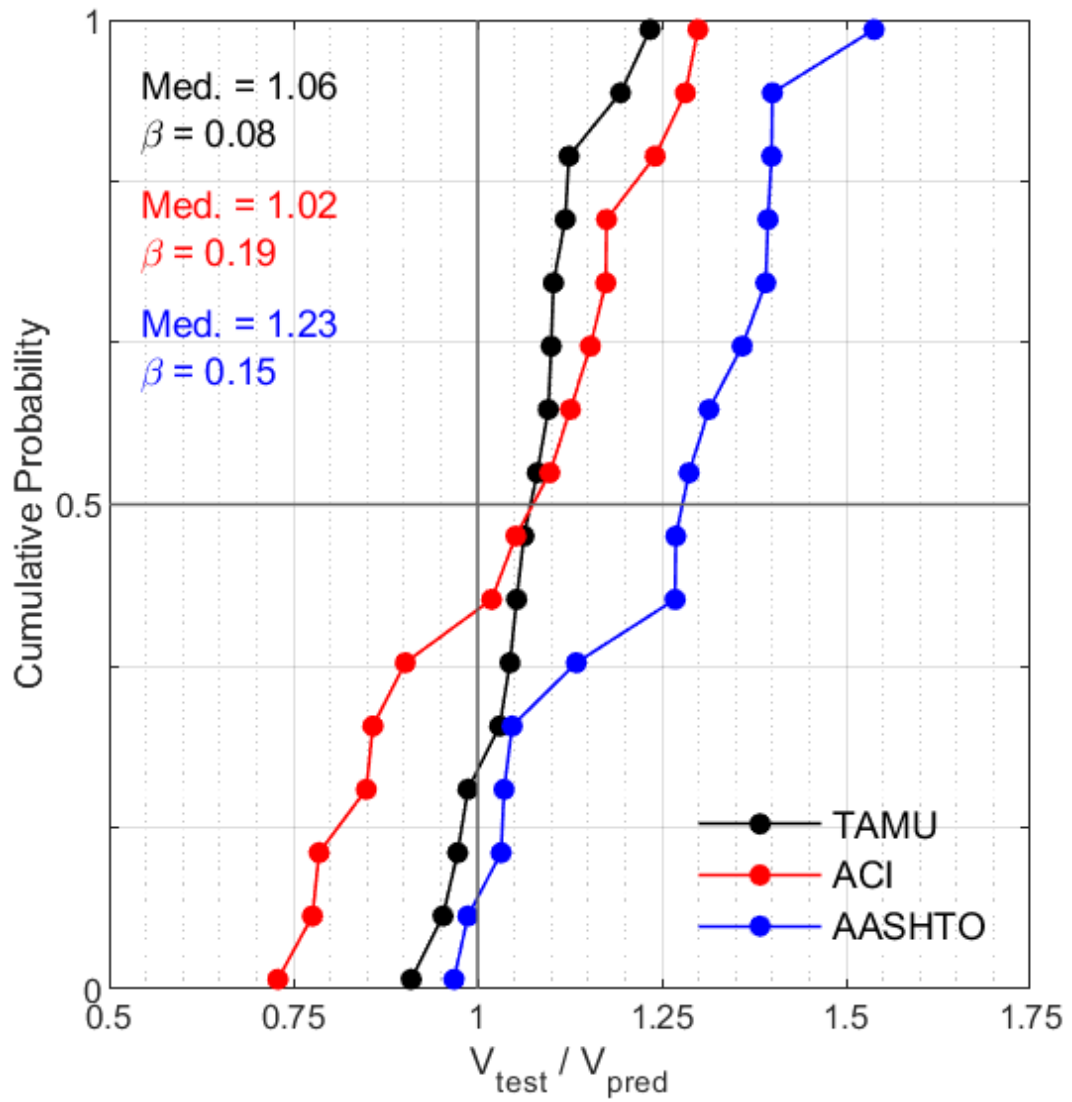
Figure 3-7. Cumulative probability based on plotted data points

observation. This corresponds to the explicit solution in Eq. (3-20) as the equation includes effective depth, d, shear span, a, and longitudinal reinforcement ratio, ρ_L, to calculate the principal strain ratio. The equation also contains shear reinforcement ratio, ρ_v, elastic modulus ratio of steel and concrete, n. Therefore, the following parameters are considered in this parametric study to check if the suggested explicit solution provides reasonable estimations: (1) a/d ratio; (2) longitudinal reinforcement ratio, ρ_L ; (3) concrete compressive strength, f'_c; (4) depth to width ratio, b/d; and (5) shear reinforcement ratio, ρ_v. It is noted that the yielding stress of 420 MPa is used for both longitudinal and transverse reinforcement throughout the parametric study, and $E_c = 4{,}700\sqrt{f'_{c\,(MPa)}}$ is used to estimate the elastic modulus of concrete in accordance with AASHTO LRFD (2017).

To facilitate comparison with the experimental studies by Kani (1964), the same geometry and material properties are used for a control beam. The control beam has a 152 mm x 305 mm rectangular section ($h/b = 2.0$) with $f'_c = 25$ MPa and steel ratios of $\rho_L = 0.01$ and $\rho_v = 0.005$. In the parameter study, parameters vary as: $a/d = 0.75$ to 3.75; $\rho_L = 0.005$ to 0.02; $\rho_v = 0.0025$ to 0.01; $f'_c = 20$ to 35 MPa; and $h/b = 0.5$ to 2.0;

Figure 3-8 shows relations of shear stress ($v_u = V_u/bd$) and a/d ratio based on varying parameters. Regardless of other variables, the shear stress changes significantly according to a/d ratio throughout all four cases in the parametric study, demonstrating that a/d ratio is the most influential parameter affecting the ultimate shear strength (Kani 1964, 1966, 1967, and Oh and Shin 2002).
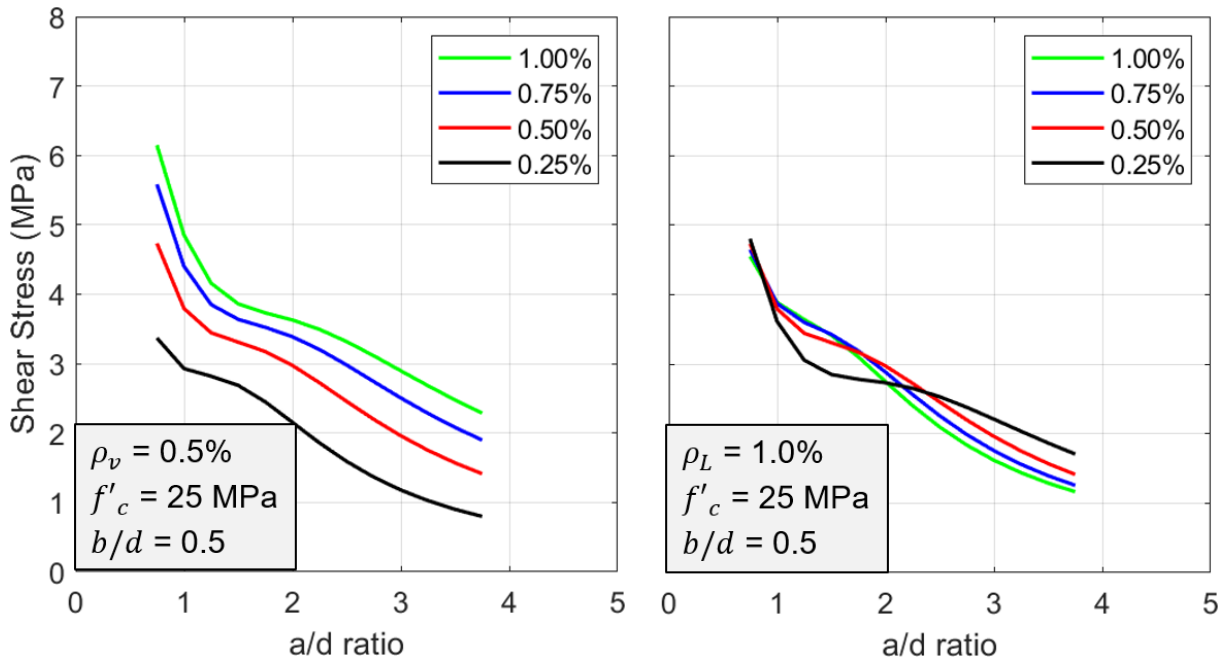
(a) Flexural Reinforcement Ratio (ρ_L)

(b) Shear Reinforcement Ratio (ρ_v)
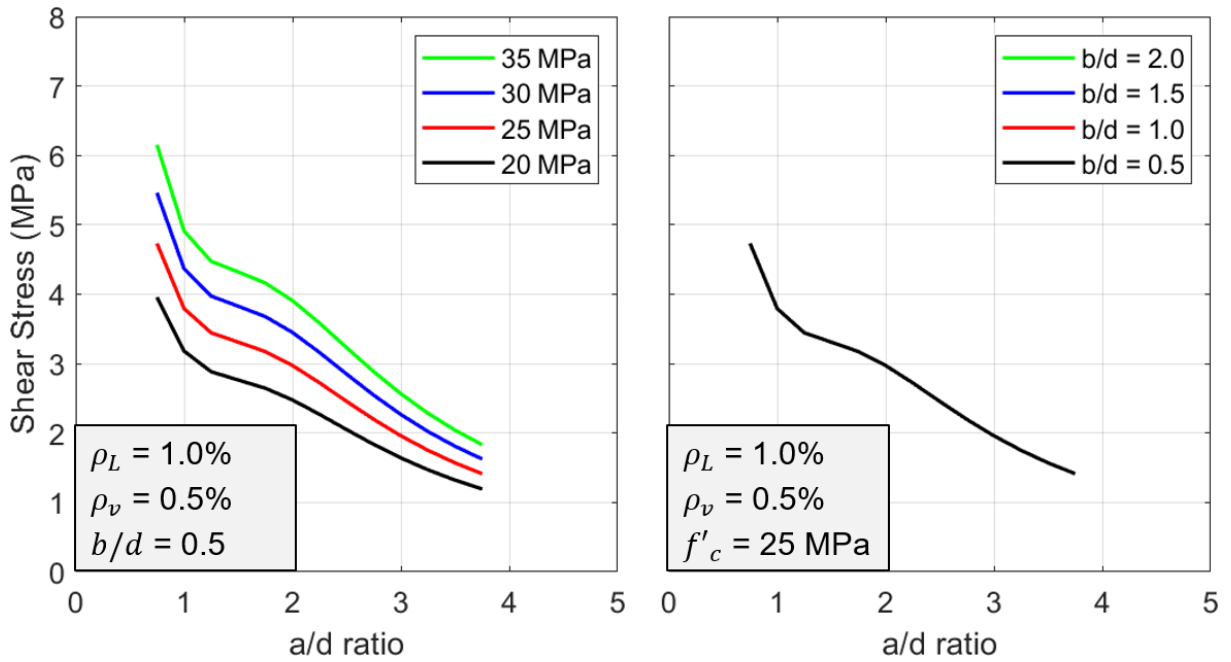
(c) Concrete Compressive Strength (f_c)

(d) Depth to Width Ratio (b/d)

Figure 3-8. Results of parameter studies

The effect of longitudinal reinforcement on shear capacity can be found in Figure 3-8(a). The ultimate shear stress, v_u, increases substantially as more longitudinal reinforcement is provided. The increasing trend associated with longitudinal reinforcement continues regardless of the *a/d* ratio. This corresponds to the observation by Kani (1966) that longitudinal reinforcement is one of the most significant factors regarding ultimate shear stress. The effect of transverse reinforcement is ambiguous as more transverse reinforcement does not always lead to the increase of shear resistance as shown in Figure 3-8(b). This contrasts with the broadly used 45-degree truss model where shear reinforcement proportionally increases the shear resistance. However, many experimental studies have revealed that providing more shear reinforcement does not improve shear capacity in deep beams (Oh and Shin, 2001; and Birely et al., 2018).

The stronger concrete strength tends to increase the ultimate shear stress but this increasing trend due to the concrete strength fades away as the *a/d* ratio increases as shown in Figure 3-8(c). This observation contradicts the classic shear theory in that the concrete strength proportionally increases the shear resistance contributed by concrete, V_c in that theory. However, many studies have already shown that the effect of concrete strength on shear is not as significant as geometry, *a/d* ratio, and it is also affected by other variables (Kani 1964, Vecchio and Collins, 1986, 1988). This has been considered in many design provisions. For example, in AASHTO LRFD (2017), the shear resistance contributed by concrete, V_c, is not only increased by the concrete strength but also varies by *a/d* ratio, flexural reinforcement properties, and longitudinal strain of tensile reinforcement by the applied force. The width of the section has no influence on the ultimate shear stress as shown in Figure 3-8(d), and this agrees with the experimental observation reported by Kani (1964) and Oh and Shin (2002).

3.6   Closure and Key Findings

The Truss and Arch Model Unified (*TAMU*) is developed to estimate the maximum force carrying capacity of shear-critical concrete beams. The proposed method has its roots in the C-STM which provides a deeper insight into the nature of flexure-shear interaction in D-regions. The *TAMU* analysis method proposed herein adopts formulations regarding axial rigidities of truss and arch components and the concrete softening effect due to the orthogonal tensile strains from C-STM. However, *TAMU* does neither use nonlinear constitutive material model nor track overall force and deformation behavior. Instead, it only focuses on seeking the ultimate force that may cause an abrupt shear failure in the principal diagonal concrete strut. As a result, the *TAMU* approach requires a straightforward calculation to predict the ultimate shear strength and can be readily executed by hand analysis.

The explicit solution of the concrete softening coefficient is numerically derived using the virtual work method, and its versatility is validated by comparing with the experimental test conducted by Bracci et al. (2000). The C-STM is also implemented using a nonlinear analysis program, *OpenSees* v. 3.2.2 (2020), and the results show a great agreement with the test data. The concrete softening coefficients from the proposed explicit solution and C-STM analysis are reasonably close. In comparison with code-based strength analysis methods including ACI (2019) and AASHTO (2017), more exact predictions are found in the *TAMU* approach against the experimental test by Bracci et al. (2000). In the parametric study, the explicit solution catches the trends in the ultimate shear stress due to several parameters quite well. The analysis results show that the proposed *TAMU* approach is capable of predicting the ultimate failure load of shear-critical concrete members with good accuracy.

4. APPLICATION AND EXAMINATION OF PROPOSED TRUSS-ARCH MODEL UNIFIED USING SHEAR DATABASE

4.1 Chapter Summary

A shear strength analysis model called Truss-Arch Model Unified (*TAMU*) for beams with transverse reinforcement was proposed for shear-critical reinforced concrete (RC) beams in the previous chapter. The proposed model is a simplified version of the Compatibility Strut-and-Tie Model (C-STM) approach which is overall force-deformation computational modeling so that a limit analysis can be executed by hand methods. While the tensile stress of concrete is generally taken into account to evaluate the shear strength of concrete beams, the *TAMU* limit analysis focuses on the strength reduction of the principal diagonal concrete arch due to the transverse principal tensile strain.

To further substantiate the validity of the *TAMU* approach, a shear database is assembled for beams with transverse reinforcement for an aspect ratio range of $0.5 < a/d < 4.5$ from previous works reported in the literature. Comparative *TAMU* analysis results show satisfactory agreement with the ultimate strengths observed in 460 beam tests regardless of D- and B-regions, demonstrating the method's ability to predict the maximum load-carrying capacity for shear-critical beams. Additionally, the *TAMU* approach shows better accuracy and consistency against the database compared to other code-based shear analysis methods including ACI and AASHTO. The probability of reasonable prediction of the *TAMU* method is 92% in D-regions and 78% in D-regions, respectively. This is significantly higher than code-based shear analysis methods, especially in D-regions.

4.2 Introduction

Evaluating a proposed shear theory using a database on experimental tests has been a commonly used method in many studies. Collins et al. (1996) suggested a unified method for the shear design based on the Modified Compression Field Theory (MCFT) and demonstrated the validity of the design method using the experimental results from 528 tests. Lee and Watanabe (2000) proposed a shear design equation considering two different shear failure modes based on the yielding of shear reinforcement. The proposed equation was validated by comparing with the experimental results of 92 beams. Tureyen et al. (2003) developed a simple method for the design of fiber-reinforced polymer (FRP) reinforced beams. The applicability of the method was then verified by comparing with the experimental strengths of 370 specimens. Bentz et al. (2006) proposed a simplified analysis method based on the MCFT and demonstrated its utility with over 100 pure shear tests in reinforced concrete panels. Brown and Bayrak (2008) assembled a database of 596 tests of reinforced concrete beams with shear span-depth ratios less than 2.0 and used this to evaluate strut-and-tie models (STM). Hsu et al. (2010) used test results of 148 prestressed concrete beams by 14 groups of researchers to verify an equation for the shear strengths of prestressed concrete beams proposed by Laskar et al. (2010). Choi et al. (2016) proposed a shear strength model based on 'Compression Zone Failure Mechanism' and verified the model using 942 non-prestressed beams with and without transverse reinforcement and 46 prestressed beams.

There have been significant efforts by many researchers in the United States, Canada, and Germany to build shear databases on experimental tests that can provide a tool to evaluate shear strength analysis expressions. A partnership for these efforts between ACI and the German Committee for Reinforced Concrete (DAfStb) was launched and four different evaluation databases were created including: 1) slender RC beam without shear reinforcement (Reineck et al.,

2013); 2) Slender RC beam with shear reinforcement (Reineck et al., 2014a); 3) non-slender RC members with shear reinforcement (Reineck et al., 2014b); 4) Non-slender RC members without shear reinforcement (Todisco et al., 2015). It was noted that test results that passed certain criteria (for example, beams that met minimum size limits, had specified material properties, and did not fail in flexure) were only collected in those databases.

By the same efforts, a shear database for prestressed concrete members (referred to as "UTPCSDB") was developed at the University of Texas (Nakamura et al., 2013). The database includes a total of 1,696 shear tests on prestressed concrete members from North America, Japan, and Europe. The authors also filtered the database using specific criteria such as concrete strength, member size, shear span-depth ratio, and finally used the database to validate five current shear design provisions including ACI 318-11, AASHTO LRFD 2010, CSA A23.3-04, JSCE 2007, and fib MC 2010.

In this chapter, a database on shear tests in reinforced concrete (RC) beams is assembled and used to verify the proposed Truss-Arch Model Unified (*TAMU*) approach. RC beams with transverse reinforcement failed by flexure-shear interaction are only collected in the database, and those include not only deep beams with $a/d < 2.0$ but also some intermediate and slender beams. A comprehensive literature review is conducted, and a total of 460 shear-critical concrete beams which failed with a significant diagonal shear crack are collected from 28 references. The shear database is divided into two data sets: one is for (i) shear-reinforced concrete beams with D-regions, and the other is for (ii) shear-reinforced concrete beam section with B-regions. In the following sections, both data sets are evaluated using the *TAMU* approach, to investigate if the method can also be used for intermediate beams (B-regions).

The development of the shear database is first presented with statistical analysis concerning variables. The accuracy and stability of the *TAMU* method is assessed by using statistics of the shear strength ratio, V_{test}/V_{pred}, which is calculated by dividing the observed ultimate shear strength, V_{test}, by the predicted shear strength, V_{pred}. The *TAMU* approach is then compared with other code-based methods using the database and is adjusted for uncertainties via the well-known code-based resistance reduction factor (ϕ-factor) approach.

4.3   Development of Shear Test Database

Experimental data on shear tests from 28 references in the literature were collected to verify whether the proposed shear theory is capable of predicting the ultimate shear capacity of reinforced concrete beams with transverse reinforcement. Several parameters needed to implement the proposed theory are depicted in Figure 4-1. A majority of the specimens were simply supported rectangular beams subjected to a single or two-point load as shown in the figure. Additionally, a few specimens had a single column with cantilevered beams on both sides, and these are considered as a cantilever. In developing the shear database, shear critical members where *a*/*d* < 4.5 and failed in shear with a diagonal cracking are only collected. The maximum shear loads achieved during the entire test are considered as the ultimate shear capacity.

A total of 460 beams with transverse reinforcement in 28 references published from 1951 to 2005 were collected in the shear database (340 beams with D-regions and 120 beams with B-regions). The list of all collected references for test data is summarized in Table 4-1 with brief information: authors, published year, and a number of specimens collected. The references and detailed information used to develop the shear database can be found in Appendix A. Some specimens in the listed references are filtered out when information is not sufficient to implement the proposed theory or if the failure mode is not clearly specified as the shear failure.
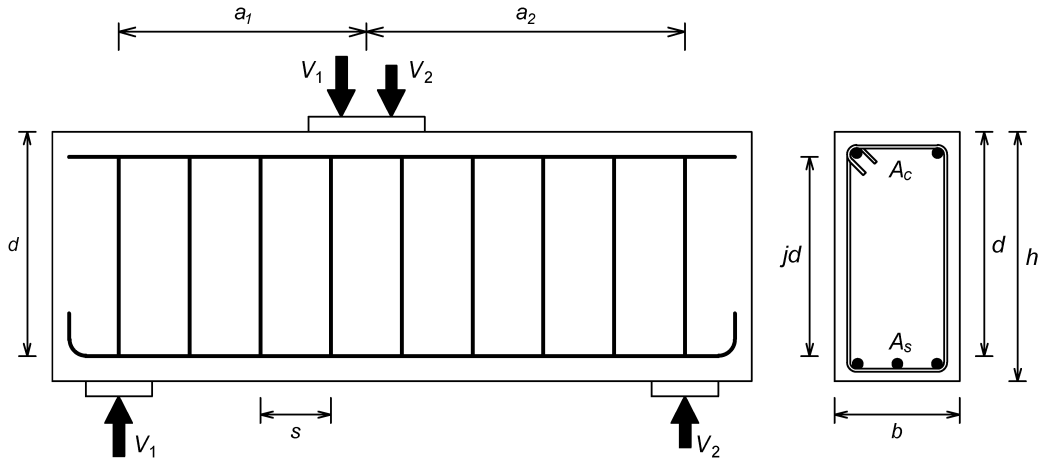
Note: $a/d \approx 1.0$ on the left-hand side beam, and $a/d \approx 2.5$ on the right-hand side beam

Figure 4-1. Parameters in the shear database

Table 4-1. List of references for beams with transverse reinforcement

Authors	Year	Number	Authors	Year	Number
Anderson and Ramirez	1989	3	Mphonde and Frantz	1984	20
Angelakos et al.	2001	6	Oh and Shin	2002	54
Bracci et al.	2000	16	Ozcebe et al.	1999	7
Bresler and Scordelis	1963	3	Peng	1999	7
Brown	2005	14	Podgorniak	1998	2
Clark	1951	50	Rodriguez et al.	1959	9
Collins and Kuchma	1999	2	Roller and Russell	1990	7
Debaiky and Eliniema	1982	7	Sarsam and Al-Musawi	1992	14
Elzanaty et al.	1968	3	Shin et al.	1999	24
Gabrielsson	1993	21	Smith and Vantsiotis	1982	47
Johnson and Ramirez	1989	6	Tan et al.	1995	19
Kong and Rangan	1998	48	Tanimura and Sato	2005	36
Kong et al.	1970	10	Xie et al.	1994	9
Kriski	1996	7	Yoon et al.	1996	9
			Total	-	460

Generally, six variables are considered as the most influential factors contributing shear strength of reinforced concrete members: (i) Concrete compressive strength, f'_c; (ii) member height, h; (iii) member width, b; (iv) shear span-depth ratio, a/d; (v) ratio of flexural reinforcement, ρ_L; (vi) ratio of shear reinforcement, ρ_v. Ranges of variables in the database are classified to assess the effect of each variable on the accuracy of the *TAMU*. By comparing results by variables' ranges, it can be determined if the *TAMU* underestimates or overestimates certain variables.

Figure 4-2 presents frequency distributions of those six variables for the 460 RC beams with transverse reinforcement in the shear test database. The range of six significant experimental variables are: (i) 14 to 149 MPa with a mean of 49 MPa for concrete compressive strength f'_c; (ii) 200 to 1000 mm with a mean of 452 mm for member height, h; (iii) 76 to 838 mm with a mean of 224 mm for member width, b; (iv) 0.27 to 4.5 with a mean of 1.96 for a/d ratio; (v) 0.004 to 0.070 for longitudinal (flexural) reinforcement ratio with a mean of 0.023; and (vi) ρ_L; and 0.001 to 0.024 with a mean of 0.004 for transverse reinforcement ratio, ρ_v.

Concrete strengths within 20-40 MPa that have been historically in common use in construction account for most of the specimens, and high strength concrete as strong as 149 MPa are also used. Thus, it can be assessed whether the proposed method can be used for high strength concrete without compromising accuracy. Most specimens represent regular size beams used in buildings and some specimens represent bridge members whose height and width are as large as 1,000 mm, and 838 mm, respectively. By analyzing a wide range of height and width of members, the effect of member size on the *TAMU* approach can be assessed. The influence of a/d ratio and both flexural and shear reinforcement ratios is also investigated.
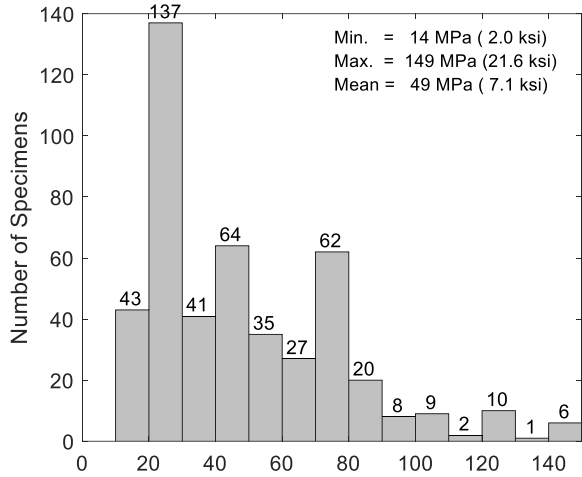
(a) Concrete compressive strength, f′c (MPa)
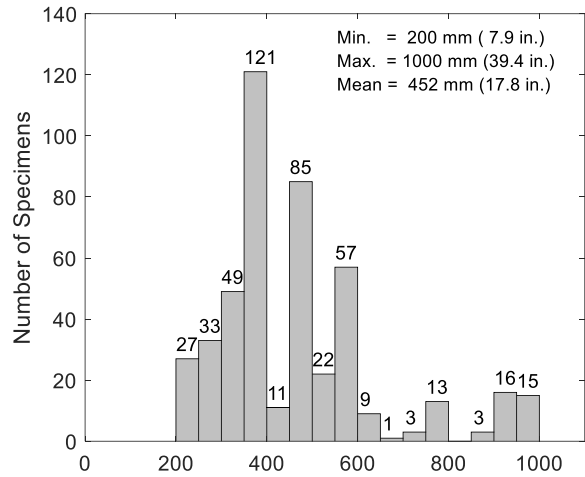
(b) Member height, h (mm)
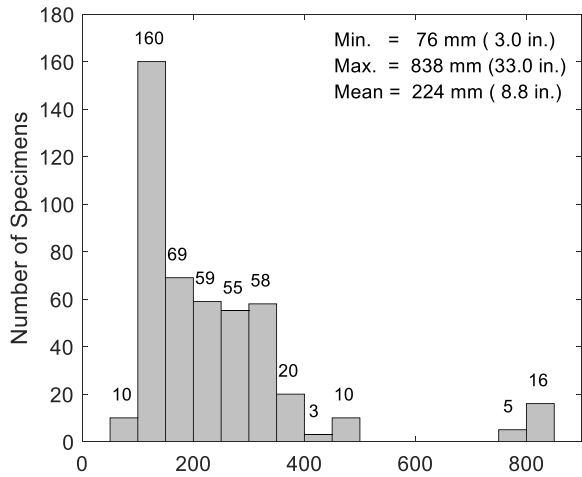
(c) Member width, b (mm)
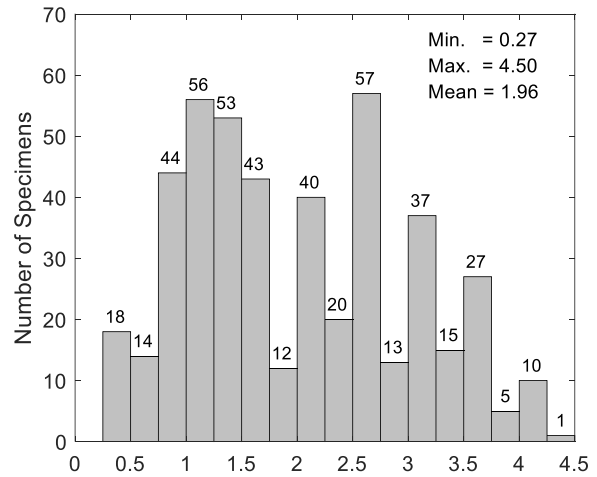
(d) a/d ratio
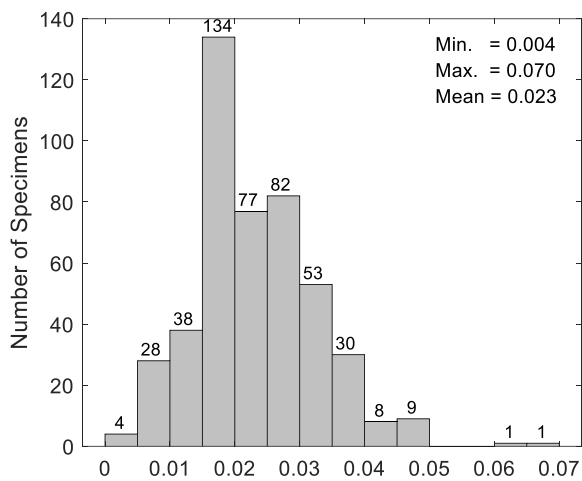
(e) Flexural reinforcement ratio (ρ_L)
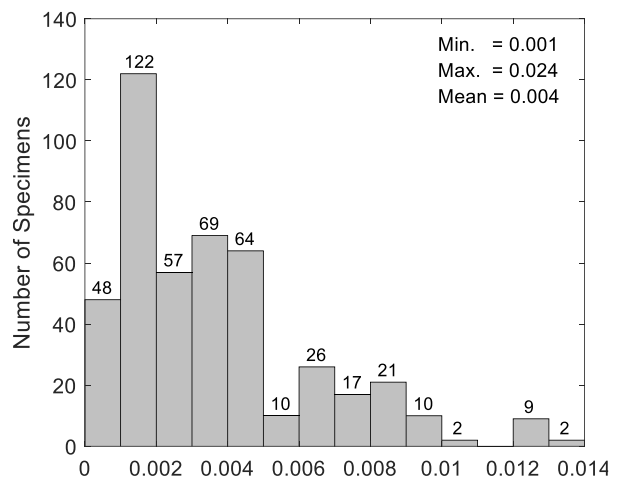
(f) Shear reinforcement ratio (ρ_v)

Figure 4-2. Distribution of experimental variables in the database with transverse reinforcement

99

4.4   Verification of *TAMU* with Transverse Reinforcement Using Shear Database

The shear database developed in Section 4.3 is used to validate the proposed *TAMU* approach. The model is mainly evaluated using statistics of the shear strength ratio, V_{test}/V_{pred}, which is calculated by dividing the ultimate shear force carried by test specimen, V_{test}, by the shear strength predicted with the shear model, V_{pred}. The accuracy of the analysis can be estimated by comparing three statistical parameters of the shear strength ratio: a) mean; b) the dispersion factor (β); and c) the percentage of unconservative and over-conservative predictions. The shear strength ratio with a mean value close to 1.0 is considered accurate, however, the ratio greater than 1.0 is preferred to avoid unconservative prediction. A low dispersion factor (β) is desirable as it indicates low variation in the use of the shear design. The low percentage of unconservative designs (V_{test}/V_{pred} < 1.0) is preferred to prevent unexpected failure, however, overly conservative designs are not desirable. Thus, the percentage of both unconservative and over-conservative designs are evaluated. The factored shear strength ratio greater than 2.0 is considered overly conservative ($V_{test}/V_{pred} > 2.0$) in this study. The procedures and formulae needed for the *TAMU* analysis to estimate the ultimate shear strength of the shear-critical beam are as follows:

- Step 1: Find the maximum shear forces resisted by arch action, V_{arch}, and truss action, V_{truss}, and calculate arch-breath scalar, η, using:

$$V_{arch} = f_y A_s \tan \alpha = \rho_L f_y b_w d \tan \alpha \tag{4-1}$$

$$V_{truss} = f_{yh} A_v \frac{a}{s} = \rho_v f_{yh} b_w d \cot \alpha \tag{4-2}$$

$$\eta = \frac{V_{arch}}{V_{arch} + V_{truss}} = \frac{\rho_L f_y}{\rho_L f_y + \rho_v f_{yh} \cot^2 \alpha} \tag{4-3}$$

in which V_{arch} = maximum shear force resisted by arch action; V_{truss} = maximum shear force resisted by truss action that is proportional to the transverse reinforcement; f_y = yield strength of the longitudinal steel; f_{yh} = yield strength of the transverse steel; A_s = area of longitudinal reinforcement contributing to the tension tie; A_v = area of one set of stirrups; $\cot\alpha = a/d$ where a = shear span; s = spacing of transverse reinforcement α = corner-to-corner diagonal angle; ρ_L = volumetric ratio of longitudinal steel to concrete, where $\rho_L = A_L/b_w d$; ρ_v = ratio of area of transverse steel to area of concrete for one hoop spacing, where $\rho_v = A_v/b_w s$; b_w = effective width of beam; and d = effective depth of the beam from the extreme concrete compression fiber to the centroid of the tension steel.

- Step 2: Determine a force distribution factor, μ, by:

$$\mu = \frac{\delta_{truss}}{\delta_{arch} + \delta_{truss}} = \frac{\psi_{truss}}{\psi_{arch} + \psi_{truss}} \tag{4-4}$$

where μ= force distribution factor; δ_{truss} = displacement of the truss mechanism caused by the unit load; and δ_{arch} = displacement of the arch mechanism caused by the unit load; ψ_{truss} and ψ_{arch} flexibility coefficient for truss and arch displacements given by:

$$\psi_{arch} = \frac{\cot^2\alpha}{\rho_L n} + \frac{8}{3\sin^2\alpha}\left(1 + \cot^2\alpha\frac{f_{yh}\rho_v}{f_y\rho_L}\right) \tag{4-5}$$

$$\psi_{truss} = \cot^2\alpha\left(\frac{5k + \rho_L n}{8k\rho_L n}\right) + \frac{\tan^2\alpha}{\rho_v n} + \frac{\sqrt{8 + 16\tan^2\beta}}{\sin^3\beta\cot\alpha}\left(\frac{f_y\rho_L}{f_{yh}\rho_v}\tan^2\alpha + 1\right) \tag{4-6}$$

- Step 3: Calculate the principal strain ratio, $\varepsilon_1/\varepsilon_2$ using:

$$\left|\frac{\varepsilon_1}{\varepsilon_2}\right| = \tan^2\alpha\left(1 + (\sec^2\alpha)\left(\frac{\rho_L f_y}{\rho_L f_y + \rho_v f_{yh}\cot^2\alpha}\right)\left(\frac{\psi_{arch}}{\psi_{truss}}\right)\left(\frac{0.375}{\rho_v n}\right)\right) \tag{4-7}$$

- Step 4: Find the concrete softening coefficient, ζ according to:

$$\zeta = \frac{1}{1 + 0.25|\varepsilon_1/\varepsilon_2|} \tag{4-8}$$

where ζ = concrete softening coefficient; ε_1 = principal diagonal tensile strain transverse to the axis of the arch; and ε_2 = principal diagonal compressive strain at the center of the arch.

- Step 5: Calculate the maximum shear capacity by:

$$V_n^{arch} = \frac{3}{8} \frac{\zeta \beta_1 f'_c b_w d}{\left(1 + \frac{\rho_v f_{yh}}{\rho_L f_y} \cot^2 \alpha\right)} \tan \alpha \left(1 + \frac{\psi_{arch}}{\psi_{truss}}\right) \tag{4-9}$$

where V_n^{arch} = maximum nominal shear capacity of the principal diagonal arch; β_1 = ratio of the depth of the equivalent uniformly stressed compression zone; and f'_c = concrete compressive strength.

The ultimate shear strength is predicted according to the above-mentioned procedures for RC beams in the database. The predicted strength is then compared with the measure peak force during the test.

4.4.1 Verification of a Strut Width, w_s

In the previous chapter, it was shown that a significant force is transferred through only a limited strut width, w_s, and an appropriate strut width estimation based on a principal compressive stress distribution obtained from the FEM analysis in Section 3.3.2. As a result, a strut width proportional to the depth and length of a beam was proposed as:

$$\frac{w_s}{d} = \frac{3}{8} \sec \alpha \tag{4-10}$$

where w_s = principal diagonal strut width; λ = strut width scalar (< 1.0); d = effective depth; and a = shear span.

This proposed width is identical to what has been previously used for C-STM analysis where the ability of the C-STM analysis in predicting the failure mechanism, ultimate shear strength, and full deformation response was validated through experimental tests with good accuracy (Scott et al. 2012b, and Karthik et al. 2016). However, no clear verification was made regarding Eq. (4-10) for calculating a strut width in the C-STM, and also there is no evidence if the same width can be used for the *TAMU* method. For this reason, the *TAMU* analysis is conducted against the shear database by varying a strut width from $0.325d\sec\alpha$ to $0.425d\sec\alpha$ at every $0.050d\sec\alpha$. This parameter study is intended to verify whether the *TAMU* approach based on the proposed strut width gives reasonable predictions for ultimate shear strength.

Figure 4-3 provides lognormal cumulative distribution functions (CDFs) of the shear strength ratio, $V_{test}/V_{pred.}$ differed by arch widths. The *TAMU* predicts the ultimate shear strength of 460 specimens with transverse reinforcement and the predicted values are compared with the test data to obtain statistical parameters of the shear strength ratio. As shown in the figure, median values are smaller for larger strut widths but no significant difference is observed in the dispersion factor, β. A larger strut width creates a larger strut area to resist the applied force in the strut, resulting in a more unconservative prediction. Given that the shear strength ratio, V_{test}/V_{pred}, is preferred to be close (but slightly greater than 1.0) for both accuracy and safety, strut widths less than $0.425d\sec\alpha$ may be an ideal suggestion. Therefore, it is concluded that $0.375d\sec\alpha$ creates a reasonable estimation for a strut width, and may this be used for the *TAMU* analysis. A smaller strut width may reduce some unconservative aspects to secure better safety, however, it may be also achieved by considering an appropriate strength reduction factor.
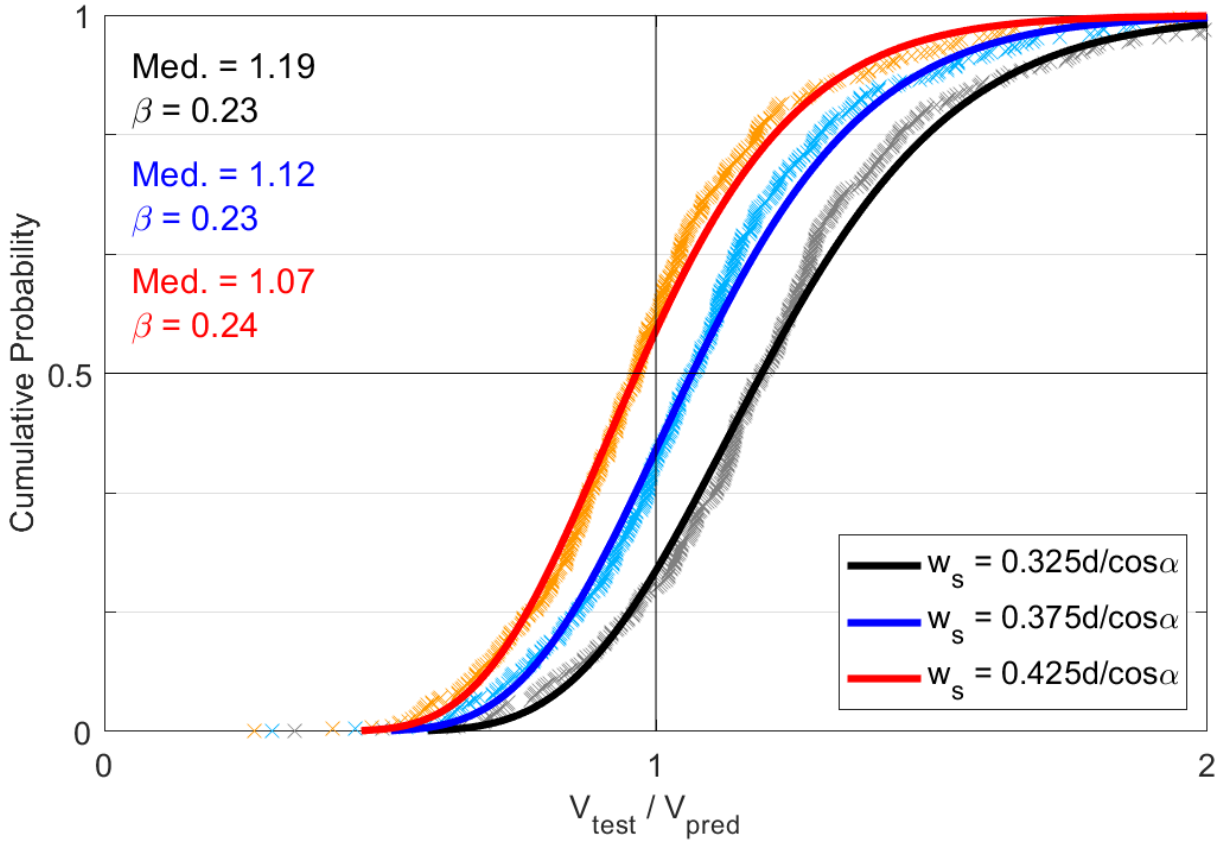
Figure 4-3. Verification of the strut width

4.4.2   Assessment of Primary Variables

The influence of the six major variables on the *TAMU*'s accuracy is assessed in this section. Considered variables are: (i) Concrete compressive strength, f'_c; (ii) member height, h; (iii) member width, b; (iv) shear span-depth ratio, a/d; (v) ratio of flexural reinforcement, ρ_L; and (vi) ratio of shear reinforcement, ρ_v.

Figure 4-4 shows the trends in shear strength ratios, V_{test}/V_{pred}, for the *TAMU* approach analysis as a function of all variables. As shown in the figure, the overall shear strength ratios are distributed evenly between 0.5 and 2.3, regardless of variables. There is no significant change found on the shear strength ratio based on variables, implying the *TAMU* approach manages to consider all variables appropriately. There is a number of matters that need discussing for each variable.

Figure 4-4(a) shows the variation of the shear strength ratio, V_{test}/V_{pred} by the a/d ratio. Even though the *TAMU* approach is originally aimed to analyze for deep and intermediate beams ($a/d \leq 2.5$), it also gives reasonable predictions for some slender beams. In transition regions near $a/d = 2.5$, shear still dominates the failure mechanism so that the truss and arch model can capture its force transfer path well, resulting in reasonable predictions. However, the failure mechanism is more governed by flexure rather than shear when the a/d ratio is greater than 3.5, and the truss and arch model may no longer capture the failure mechanism satisfactorily. This may explain why overly conservative aspects are found in beams with $a/d > 3.5$. Generally, the *TAMU* analysis provides satisfactory predictions for deep and intermediate beams both, thus, it may be also used for some slender beams as long as a/d ratios are less than 3.5.

(a) a/d ratio

(b) Concrete compressive strength, f'_c

(c) Member depth (size effect), d

(d) Member width, b

(e) Longitudinal reinforcement ratio, ρ_L

(f) Transverse reinforcement ratio, ρ_v
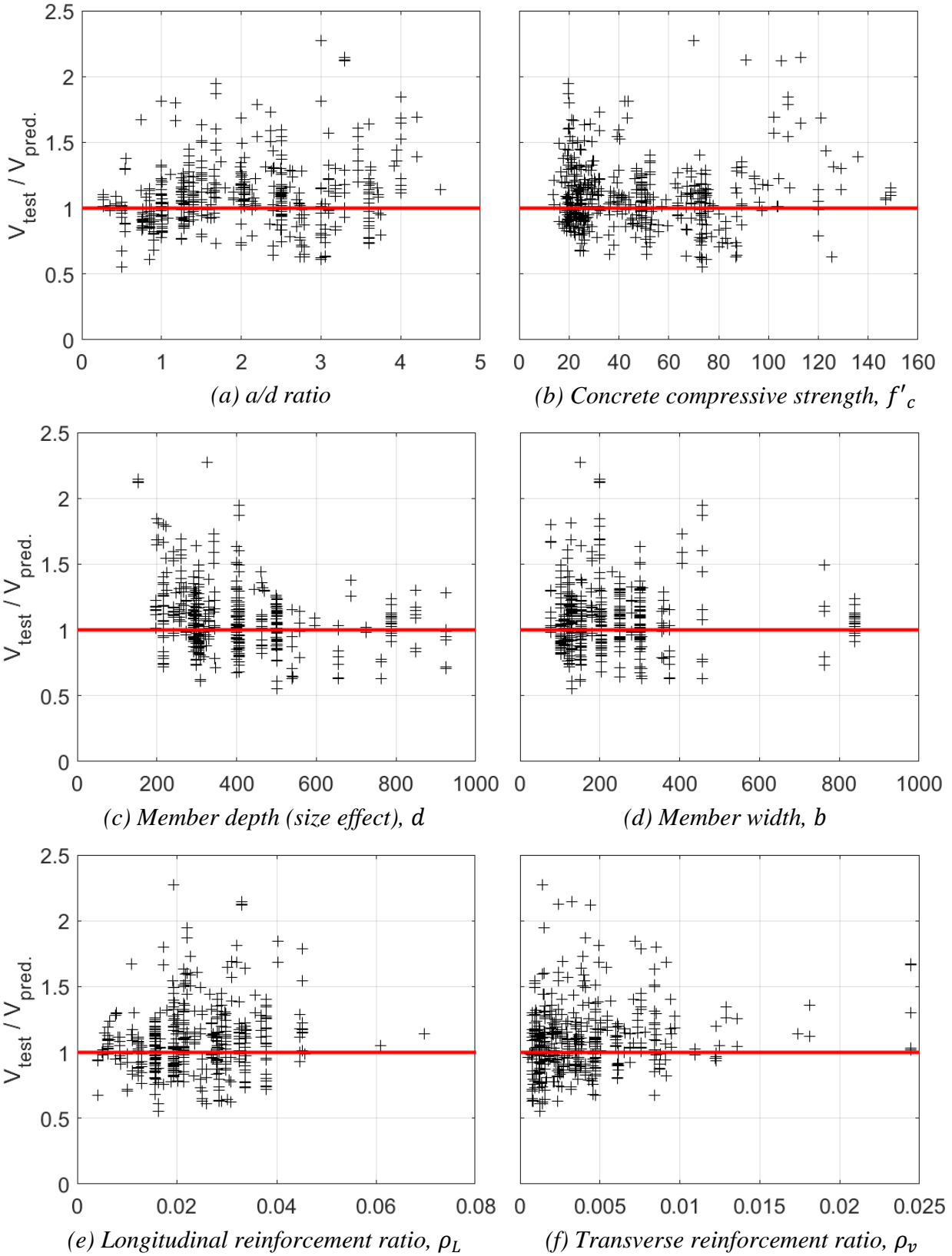
Figure 4-4. Distribution of shear strength ratio against the shear test database

Figure 4-4(b) shows that the shear strength ratios are distributed evenly across all concrete strength ranges. This may indicate that a contribution of concrete on shear is reasonably estimated by considering the concrete softening coefficient regardless of concrete strength. The reasonable predictions are found for cases with high strength concrete whose compressive strength is greater than 60 MPa although some overly conservative predictions ($V_{test}/V_{pred} > 2.0$) are shown for a few beams. One hesitates to conclude that the *TAMU* approach is applicable to high strength concrete as only limited cases are taken into consideration. However, it is considered advantageous if a single shear design method can be used for any concrete strength ranges without additional consideration; this matter is worthy of further investigation.

Figure 4-4(c) and (d) show the accuracy of the *TAMU* approach based on the size of beams, effective depth, *d*, and width, *b*. Regardless of the size of beams, most shear strength ratios are located near 1.0 with some underestimated or overestimated. The predicted values for wider beams tend to be more accurate; no overly conservative predictions are made when the depth and width are greater than 500 mm. It has been previously demonstrated that the method may be used for large bridge members such as the bent caps in Section 3.4.3.

The shear strength ratio varied by ratios of longitudinal and transverse reinforcement can be seen in Figure 4-4(e) and (f). The shear strength ratios are scattered quite evenly for all cases including lightly-reinforced and over-reinforced beams, and no significant characteristic is found based on the steel ratios. The *TAMU* approach does not account for the effect of longitudinal and transverse reinforcement directly but indirectly by considering their effect on the magnitude of the concrete softening. This concept differs from commonly used design provisions such as AASHTO and ACI where the contribution of shear reinforcement on shear is accounted for directly. Having no bias on the results may imply that the *TAMU* properly takes account of the effect of longitudinal and transverse steel reinforcement on the shear capacity of RC beams.

107

4.4.3 Statistics and Accuracy of the Predictions for the *TAMU* Method

The analytical results of the proposed *TAMU* against the shear test database are further investigated in this section. To examine the effect of the *a/d* ratio on the proposed method's accuracy, the test data is categorized into two cases: a) D-regions with transverse reinforcement and b) B-regions with transverse reinforcement. The different symbols and colors are used to distinguish D- and B-regions (gray 'x' for D-regions and light gray '+' for B-regions).

The overall analysis results of the *TAMU* analysis including both D- and B- regions are first presented in Figure 4-5. The scatter graph of *a/d* ratio vs. V_{test}/V_{pred} is shown in Figure 4-5(a) for all ranges of *a/d* ratios. V_{test}/V_{pred} values are dispersed evenly between 0.55 and 1.94 with a mean value of 1.08. No apparent bias trends can be observed across the spectrum of the *a/d* ratio. The lognormal cumulative distribution for the combined D- and B-regions is presented in Figure 4-5(b). The versatility of the *TAMU* approach is evident, showing the median value of 1.06 and lognormal standard derivation of $\beta = 0.21$. Considering concrete strength commonly has a coefficient of variation of 15% or more, the outcome is considered acceptable.

Load and resistance factor design (LRFD) uses partial safety factors to account for uncertainties in the load, and undercapacity (ϕ-factors) to account for the uncertainty in the material resistance. An appropriate strength reduction factor (ϕ_v factor) for the proposed *TAMU* analysis is thus proposed. Herein an undercapacity factor of $\phi_v = 0.75$ is chosen and drawn in the figure with a red dotted line. The non-exceedance and over-exceedance probabilities (at $2\phi_v$) are 5.4% and 6.9%, respectively, for these combined regions. This indicates that the *TAMU* approach analysis may be able to predict the ultimate shear strength of shear-critical beams regardless of B -and D-regions.
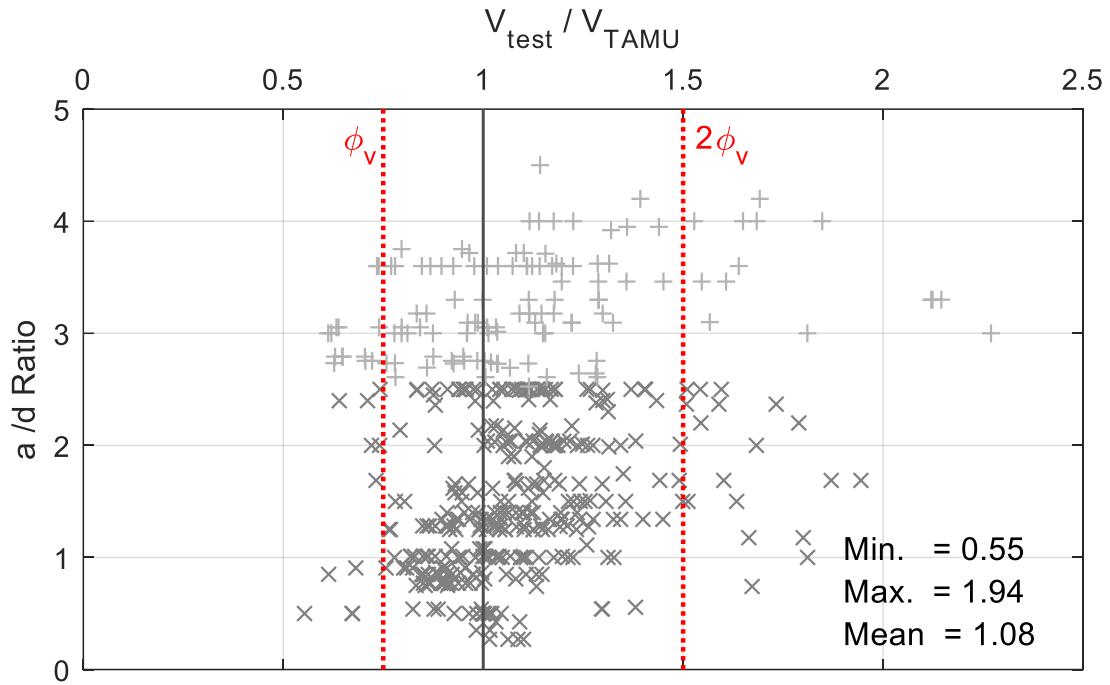
(a) Scatter of V_{test}/V_{pred} by a/d ratios
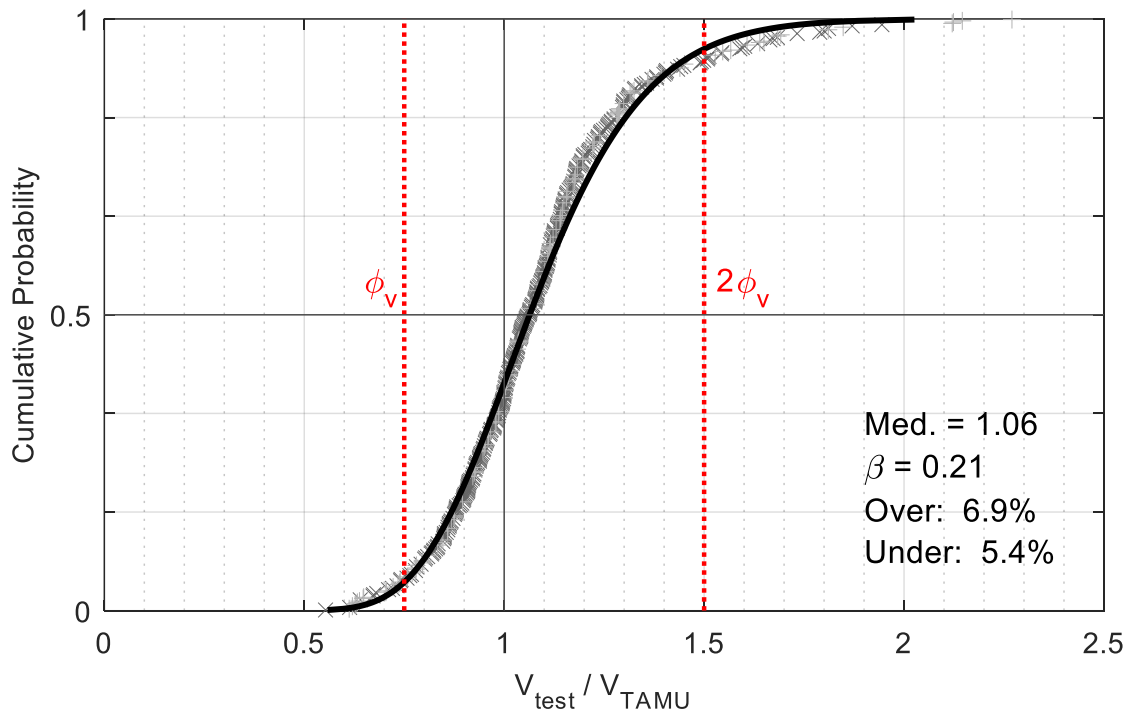
(b) Lognormal cumulative distribution

Figure 4-5. Overall analysis results of the proposed method

109

To investigate the accuracy of the proposed method based on a/d ratio, the *TAMU* analysis results are categorized into D- and B-regions. Figure 4-6 shows the scatter plot and lognormal cumulative distribution for each categorized data. In the figure, dark-gray and light-gray colors are used to distinguish D-and B-regions, respectively. The analysis results of D- and B-regions are presented in the graph on the left and right columns, respectively. As shown in Figure 4-6(a), the proposed *TAMU* method shows the shear strength ratios, V_{test}/V_{pred}, range between 0.55 and 1.94 for D-regions and 0.61 and 2.27 for B-regions. Good agreement with experimental test results is evident in both scatter plots as mean values are 1.08 and 1.11 for D- and B-regions, respectively, thus, no significant difference is found on the accuracy of the method based on a/d ratio.

In Figure 4-6(b), the data points are plotted with a lognormal cumulative probability distribution. Overall good agreement between the computed data points and the fitted cumulative lognormal distribution is evident. Both obtained lognormal cumulative distributions shown in Figure 4-6(b) have a median value of 1.06. Slightly better accuracy is observed in D-regions as the lognormal standard derivations, given by the dispersion factor, β, are 19% and 28% for D-and B-regions, respectively. Given concrete strength commonly has a coefficient of variation of 15% or more, such dispersion of results is to be expected. Note, that an ideal model fit would occur if the median was 1.0. Given the median is 1.06, there is a slight measure of conservatism in the results consistent with Figure 4-3.

The results of the adjustment for uncertainty are also presented for both regions in the figure. The non-exceedance probability (when $V_{test}/V_{pred} < \phi_v$) is 3% and 11%, and the over-exceedance probability (when $V_{test}/V_{pred} > 2\,\phi_v$) is 3% and 11% for D- and B-regions, respectively.
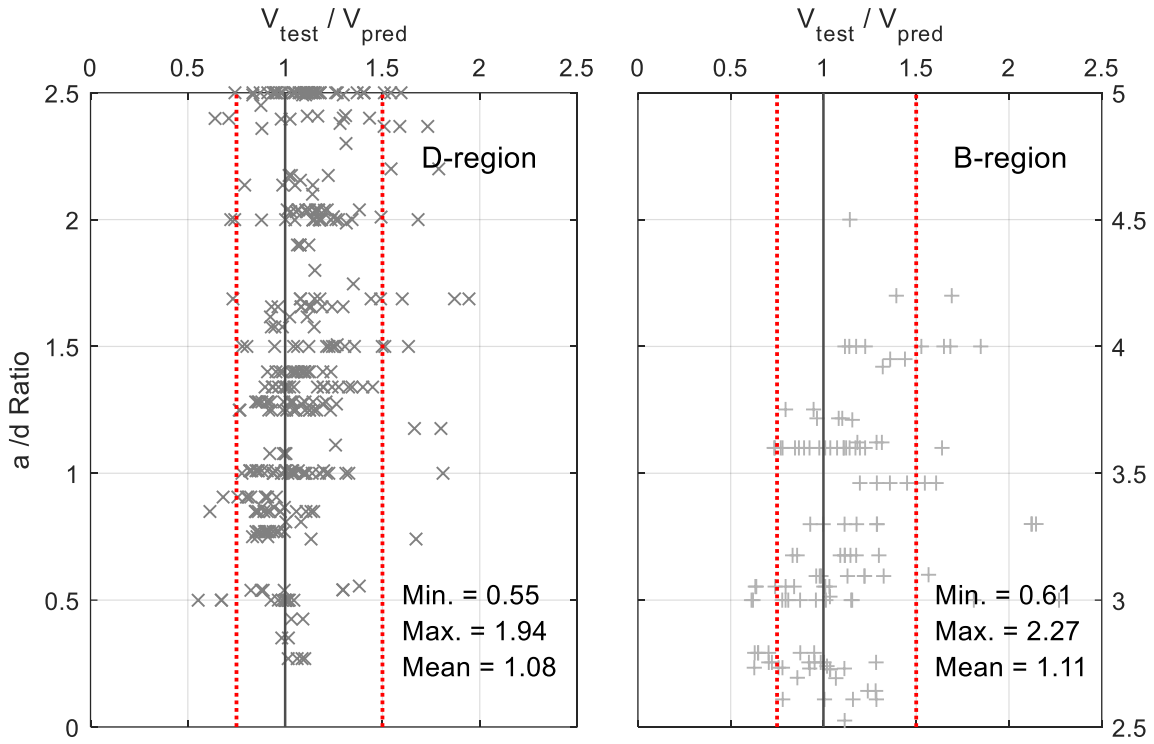
(a) Scatter of V_{test}/V_{pred} by a/d ratios (Left: D- and Right: B-regions)
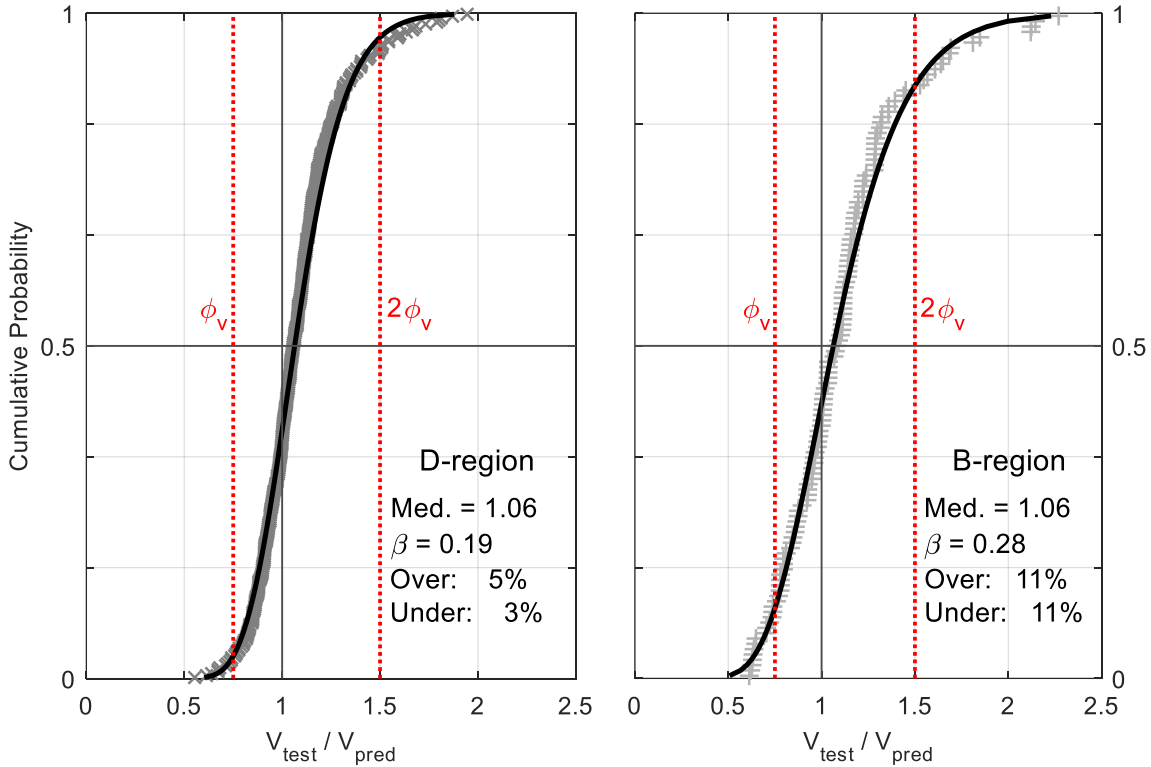
(b) Lognormal cumulative distribution of V_{test}/V_{pred} (Left: D- and Right: B-regions)

Figure 4-6. Analysis results of the proposed method separated by D- and B-regions

111

4.5 Comparison with Code-Based Analysis Approaches

The current shear design provisions based on the sectional design approach in ACI 318-19 (2019) and AASHTO LRFD Bridge Design Specifications (2017) are evaluated using the shear database and compared with the proposed *TAMU* approach in this section. ACI 318-19 shear provision is based on the classic shear approach, assuming a 45-degree truss model. AASHTO LRFD shear provisions are nowadays based on a simplified version of the original Modified Compression Field Theory (MCFT) which is referred to as the sectional method in AASHTO 5.7.3. In the current AASHTO LRFD provision, two methods may be used to obtain θ and β which are the coefficients needed to estimate contributions of concrete and transverse reinforcement on the shear resistance. The first method is a simplified method using equations in AASHTO LRFD 5.8.3.4.2 (referred to as 'simplified MCFT'), and the second method is an iterative method using tables in AASHTO LRFD Appendix B5 (referred to as 'full MCFT'). Both methods are taken into consideration in the following discussions.

4.5.1 Analysis Procedures for Code-Based Sectional Design Approaches

In the sectional design approach, the shear resistance of a reinforced and prestressed member, V_n, is assumed as the sum of shear resistances provided by the tensile stresses of concrete, V_c, the tensile stresses of transverse reinforcement, V_s, and the vertical component of the prestressing force, V_p, as:

$$V_n = V_c + V_s + V_p \tag{4-11}$$

where V_n = nominal shear resistance of the section considered; V_c = nominal shear resistance provided by tensile stresses in the concrete; V_s = shear resistance provided by shear reinforcement; and V_p = component in the direction of the applied shear of the effective prestressing force.

112

The upper limit of V_{n1} is provided to avoid the concrete crushing in the web of the concrete member prior to the yielding of the transverse reinforcement as:

$$V_{n1} = 0.25f'_c b_w d_v + V_p \tag{4-12}$$

The factored shear resistance, ϕV_n, is then compared to the factored shear force, V_u, at a number of shear critical sections along its entire length (usually near the supports and the tenth points of the span) as follows:

$$\phi V_n \geq V_u \tag{4-13}$$

where ϕ = shear resistance factor, taken as 0.9 for normal weight concrete; V_u = factored shear force at section

In the sectional method, the expressions for V_c and V_s are functions of variables, β, and θ which differ by the applied loading and the properties of the section. The concrete contribution is a function of the factor, β, and the steel contribution is established from the amount of steel across the crack angle, θ, as shown:

$$V_c = 0.083\beta \sqrt{f'_{c\,(\text{MPa})}}\, b_w d_v \tag{4-14}$$

$$V_s = A_v f_y \frac{d_v}{s} \cot\theta \tag{4-15}$$

where β = factor relating effect of longitudinal strain on the shear capacity of concrete; f'_c = compressive strength of concrete; b_w = effective web width taken as the minimum web width within the depth d_v; d_v = effective shear depth; A_v = area of a transverse reinforcement within distance, s; f_y = yield stress of transverse reinforcement; θ = angle of inclination of diagonal compressive stresses; and s = spacing of transverse reinforcement measured in a direction parallel to the longitudinal reinforcement

The following discussions explain how these concrete coefficient and crack angle are determined by each design method.

4.5.1.1   ACI Approach

In the ACI method, $\beta = 2.0$ is commonly used, and $\theta = 45$-degree is implied given $\cot 45° = 1$, and Eqs. (4-14) and (4-15) become:

$$V_c = 0.17 \sqrt{f'_{c\,(MPa)}} b_w d \tag{4-16}$$

$$V_s = A_v f_y \frac{d}{s} \tag{4-17}$$

4.5.1.2 Simplified MCFT Approach: 5.7.3 Sectional Design Model in AASHTO LRFD (2017)

The simplified MCFT in AAHSTO (2017) provides two equations to estimate the concrete, β.

For sections with the minimum amount of transverse reinforcement, β is calculated by:

$$\beta = \frac{4.8}{1 + 750\varepsilon_s} \tag{4-18}$$

The crack angle in both cases is given by:

$$\theta = 29 + 3500\varepsilon_s \tag{4-19}$$

The net longitudinal tensile strains, ε_s, in Eqs. (4-18) and (4-19) is determined by:

$$\varepsilon_s = \frac{\left(\frac{|M_u|}{d_v} + 0.5N_u + |V_u - V_p| - A_{ps}f_{po} \right)}{E_s A_s + E_p A_{ps}} \tag{4-20}$$

where $|M_u|$ = absolute value of factored moment; N_u = factored axial force; V_u = factored shear force; V_p = component in the direction of the applied shear of the effective prestressing force; A_{ps} = area of prestressing steel on the flexural tension side of the member; f_{po} = parameter taken

114

as modulus of elasticity of prestressing tendons; E_s = modulus of elasticity of reinforcing bars; A_s = area of non-prestressed steel on the flexural tension side of the member at the section E_p = modulus of elasticity of prestressing strands; and E_c = modulus of elasticity of concrete.

By substituting β and θ into Eqs. (4-14) and (4-15), shear contribution by concrete, V_c, and transverse reinforcement, V_s, can be estimated.

4.5.1.3 Full MCFT Approach: Appendix B5 in AASHTO LRFD (2017)

Table 4-2 presents AASHTO Table B5.2-1 containing the values of θ and β used in the full MCFT approach. The table is used for beams with more than minimum transverse reinforcement.

Table 4-2. Values of θ and β for section with transverse reinforcement

$\dfrac{v_u}{f_c'}$	$\varepsilon_x \times 1,000$								
	≤-0.20	≤-0.10	≤-0.05	≤ 0	≤ 0.125	≤ 0.25	≤ 0.50	≤ 0.75	≤ 1.00
≤ 0.075	22.3	20.4	21.0	21.8	24.3	26.6	30.5	33.7	36.4
	6.32	4.75	4.10	3.75	3.24	2.94	2.59	2.38	2.23
≤ 0.100	18.1	20.4	21.4	22.5	24.9	27.1	30.8	34.0	36.7
	3.79	3.38	3.24	3.14	2.91	2.75	2.50	2.32	2.18
≤ 0.125	19.9	21.9	22.8	23.7	25.9	27.9	31.4	34.4	37.0
	3.18	2.99	2.94	2.87	2.74	2.62	2.42	2.26	2.13
≤ 0.150	21.6	23.3	24.2	25.0	26.9	28.8	32.1	34.9	37.3
	2.88	2.79	2.78	2.72	2.60	2.52	2.36	2.21	2.08
≤ 0.175	23.2	24.7	25.5	26.2	28.0	29.7	32.7	35.2	36.8
	2.73	2.66	2.65	2.60	2.52	2.44	2.28	2.14	1.96
≤ 0.200	24.7	26.1	26.7	27.4	29.0	30.6	32.8	34.5	36.1
	2.63	2.59	2.52	2.51	2.43	2.37	2.14	1.94	1.79
≤ 0.225	26.1	27.3	27.9	28.5	30.0	30.8	32.3	34.0	35.7
	2.53	2.45	2.42	2.40	2.34	2.14	1.86	1.73	1.64
≤ 0.250	27.5	28.6	29.1	29.7	30.6	31.3	32.8	34.3	35.8
	2.39	2.39	2.33	2.33	2.12	1.93	1.70	1.58	1.50

As shown in the table, the values of θ and β are specified by longitudinal strain, ε_x, and the ratio of shear stress and concrete strength, v_u/f'_c. The longitudinal strain, ε_x, and the shear stress, v_u, are determined as:

$$\varepsilon_s = \frac{\left(\frac{|M_u|}{d_v} + 0.5N_u + 0.5|V_u - V_p| - A_{ps}f_{po}\right)}{2(E_s A_s + E_p A_{ps})} \tag{4-21}$$

$$v_u = \frac{(V_u - \phi V_p)}{\phi b_v d_v} \tag{4-22}$$

Linear interpolation between the values given in the table may be used to provide a more exacting prediction. Obtained θ and β values are used for Eqs. (4-14) and (4-15) to estimate V_c and V_s, respectively.

4.5.2 Comparison of Four Shear Analysis Approaches

In the following discussions, shear strengths are calculated following the above-mentioned procedure for the ACI, simplified MCFT, and full MCFT methods. The test data is categorized into two cases (D- and B-regions) to investigate the effect of the *a/d* ratio on each analysis.

Figure 4-7 shows the comparisons of four shear analysis methods against the shear database. For better comparison, each method is presented with a representative color (*TAMU*: gray, ACI: orange; Full MCFT: blue; and Simplified MCFT: green), and slightly brighter colors are used to indicate B-regions. Red dotted lines are drawn in the figures to indicate non-exceedance probability (when $V_{test} < \phi_v V_{pred}$) and over-exceedance probability (when $V_{test} > 2\phi_v V_{pred}$). The resistance reduction factors of 0.90 and 0.75 are used for the AASHTO and ACI methods, respectively according to the recommendation, each method is based upon. To be consistent with the ACI approach, an undercapacity factor of $\phi_v = 0.75$ is also adopted for the *TAMU* analysis.
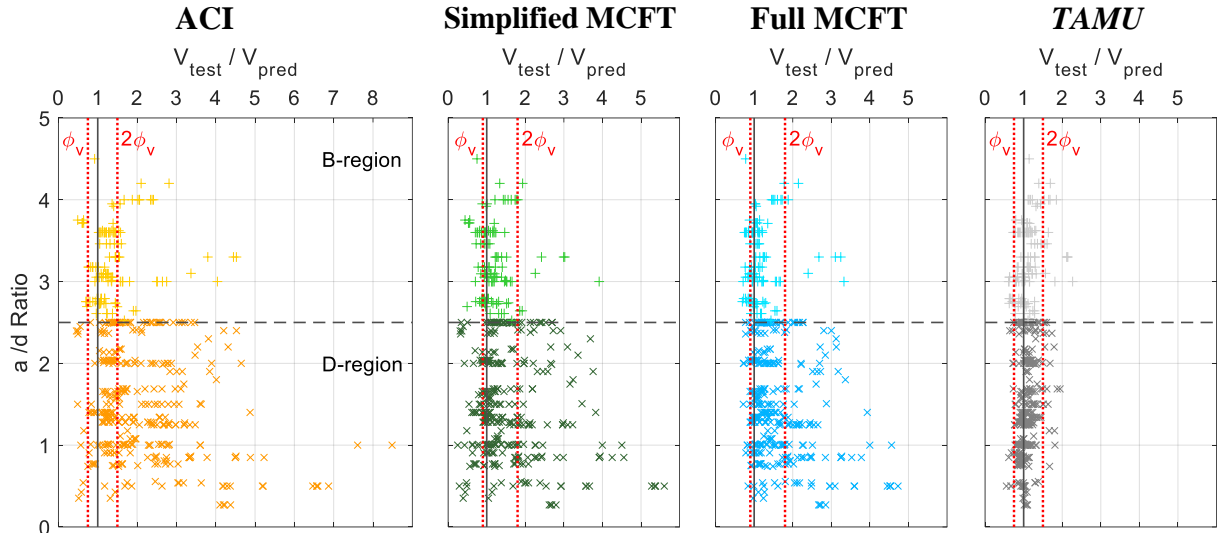
(a) Scatter plot of V_{test}/V_{pred} vs. a/d ratio
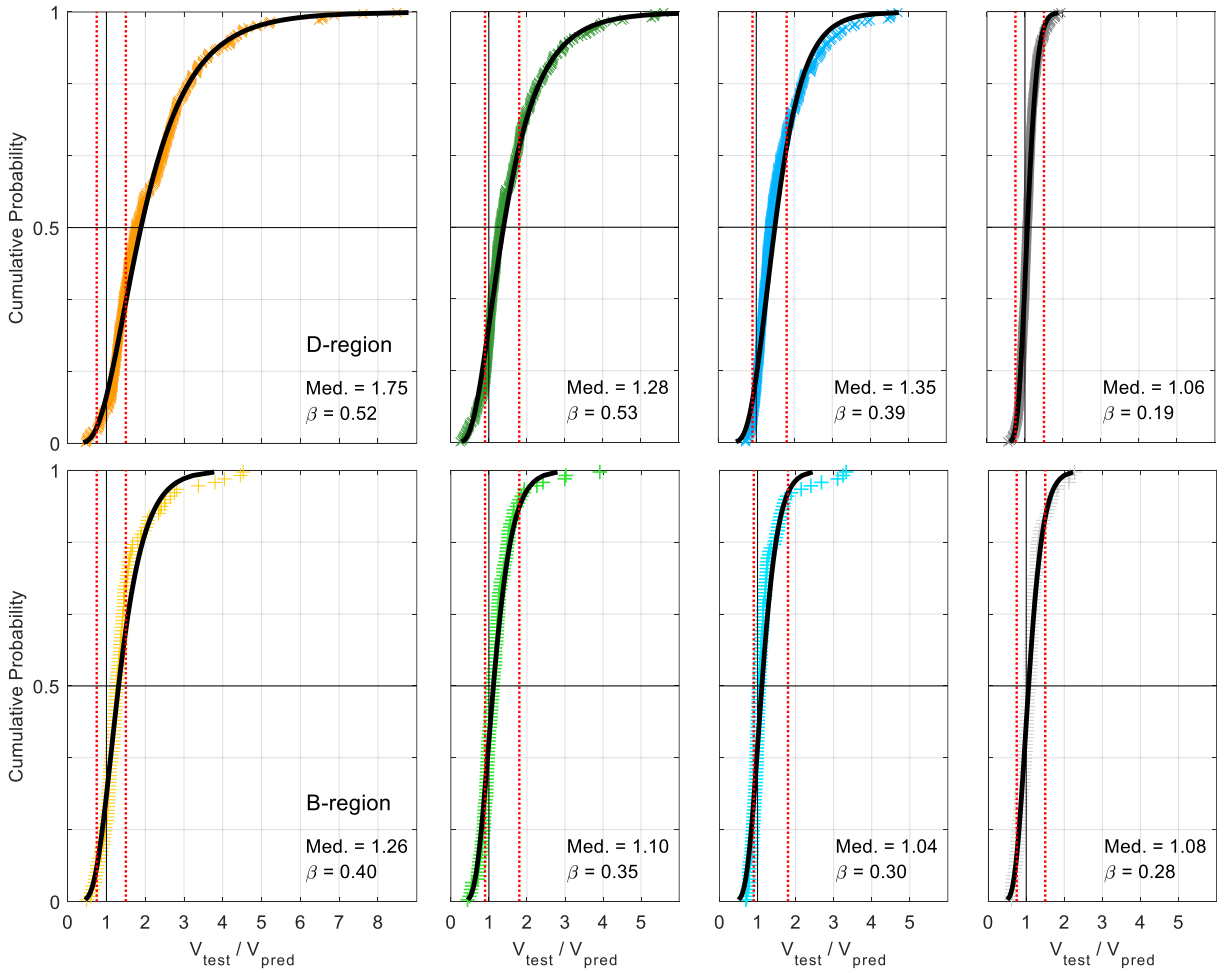
(b) Lognormal cumulative distribution function of V_{test}/V_{pred}

Figure 4-7. Comparison of four shear analysis methods for beams with shear reinforcement

117

The analysis results are presented in the order of the ACI, simplified MCFT, full MCFT, and the *TAMU* approach according to the level of sophistication of the method. As shown in the scatter graphs of *a*/*d* ratio vs. V_{test}/V_{pred} in Figure 4-7(a), the *TAMU* approach shows V_{test}/V_{pred} values concentrated near 0.5-2.0 regardless of the *a*/*d* ratio. However, the three code-based shear approaches display remarkably different results based on the *a*/*d* ratio. All three code-based shear strength methods show significantly conservative aspects without consistency in D-regions, and excessively conservative results are alleviated somewhat in B-regions. Compared to the full MCFT, the simplified MCFT produces more conservative or unconservative results in some cases, corresponding to comments made by Hawkins et al. (2005) and Birely et al. (2018).

Figure 4-7(b) shows the data points plotted along with lognormal cumulative probability distributions. The lognormal cumulative distributions that agree well with the overall data points are chosen to check both unconservative and over-conservative aspects more accurately. The comparisons of four shear methods are presented, respectively, with D-regions on the top and B-regions on the bottom.

The ACI-318 shear analysis method shows some conservative aspects in D-regions where the median = 1.75 and $\beta = 0.52$. In D-regions, over 60% of ACI predictions are overly conservative, and some shear strength ratios are as great as 8.7. At the same time, unconservative predictions are also found. Based on this observation, the ACI shear approach is not recommended for D-regions. However, this excessively conservative aspect is alleviated in B-regions. In B-regions, the median value is 1.26 and the dispersion factor, β, is reduced to 0.4. This is still a large margin from an accuracy point-of-view; however, this method may be used in B-regions given that this is a simple and straightforward analysis approach that may be easily done by hand analysis and it mostly gives a conservative solution.

Both MCFT methods show similar results in D- and B-regions although the full MCFT tends to be more accurate. Both methods show nearly 30% over-conservative predictions in D-regions. This implies the MCFTs may not account for the shear mechanism appropriately when that occurs within a D-region. The simplified MCFT provides substantially unconservative predictions in a few cases that are not found in the full MCFT. The accuracy and consistency of both MCFT methods are enhanced as the *a*/*d* ratio increases. In B-regions, better agreement with the test results is observed for both MCFT methods. The simplified and full MCFT methods show median values of 1.10 and 1.04 with $\beta = 0.35$ and $\beta = 30\%$, respectively.

The over-conservative aspects found in D-region are reduced to less than 10% for both methods. This observation implies that the MCFTs are capable of capturing the behavior of structural concrete quite well in B-regions. The better accuracy and consistency of the *TAMU* over the code-based analysis methods are evident in D-regions as the median value is 1.05 with $\beta = 0.19$. The probability of providing a reasonable prediction of the *TAMU* method is over 90% in D-regions.

In B-regions, all code-based analysis approaches show reasonable accuracy, and the *TAMU* approach provides more accurate predictions. In the analysis results of four strength analysis approaches, it is evident that more sophisticated (or complicated) methods have better accuracy in the order of the *TAMU*, full MCFT, simplified MCFT, ACI.

Table 4-3 summarizes statistics of the analysis results such as median values, and probabilities for unconservative, over-conservative, and reasonable predictions. The probabilities from data points of V_{test}/V_{pred} and fitted lognormal cumulative distribution functions are both provided. According to the table, probabilities of creating reasonable predictions based on three code-based strength analysis methods are evidently low within the D-region (38%, 53%, and 64%

119

for the ACI, simplified MCFT, and full MCFT, respectively) compared to that of the *TAMU* method (92%). Given low probabilities, the use of the code-based shear approaches is not recommended for beams with D-regions. However, all code-based methods show better outcome probabilities for reasonable solutions in B-regions (64%, 70%, and 74% for the ACI, current MCFT, and appendix MCFT, respectively) although the *TAMU* method still has slightly superior results (78%). The distinct difference in the accuracy of code-based strength analysis methods between D- and B-regions is due to the shear mechanism they are based on. All the sectional shear designs, including, those three methods, are generally based on the truss action and do not take the direct arch action into consideration. Therefore, the use of these code-based strength analyses, while appropriate for slender beams, may be inadmissible for D-region where a direct arch action governs the shear strength behavior.

Table 4-3. Summary of the analysis results for beams without transverse reinforcement

Assessment criteria	Method	ACI	AASHTO (MCFT)		*TAMU*
			Simplified	Full	
	ϕ_v	0.75	0.9	0.9	0.75
$\phi_v < \dfrac{V_{test}}{V_{pred}} < 2\phi_v$ (Overall-Reasonable)	D-region	38%	53%	64%	**92%**
	B-region	67%	70%	74%	**78%**
$\dfrac{V_{test}}{V_{pred}} < \phi_v$ (Unconservative)	D-region	3%	14%	5%	3%
	B-region	6%	22%	21%	11%
$\dfrac{V_{test}}{V_{pred}} > 2\phi_v$ (Overconservative)	D-region	64%	33%	31%	5%
	B-region	26%	7%	6%	11%

Note: Percentage of reasonable predictions over 75% are bold

4.6 Closure and Key Findings

A shear test database was developed through an intensive literature review and used to validate the proposed *TAMU* shear analysis approach as well as three code-based strength analysis methods, including the ACI, full MCFT, and simplified MCFT. The accuracy and conservativeness of each shear analysis approach are assessed by using statistics of the shear strength ratio, V_{test}/V_{pred}. The key observations and findings from this section are summarized below:

- The strut width of $w_s = 0.375d\sec\alpha$ is acceptable to be used in the *TAMU* analysis as it provides reasonable predictions which are slightly conservative.

- The *TAMU* method is capable of predicting the maximum shear strength regardless of *a/d* ratios given the mean value of the shear strength ratios close to 1.0 and the reasonably low dispersion values for both D-and B-regions. The slight unconservative aspect of the *TAMU* is adjusted by the resistance reduction factor of ϕ_v =0.75 in design.

- The results of three code-based strength analysis methods have high dispersion values due to many unconservative or over-conservative results in D-regions. Such an inconsistency leads to the suggestion that these code-based analysis methods are certainly not appropriate for D-regions as these code-based approaches are founded on tensile strength of concrete and do not directly address arch action.

- In B-regions, reasonable agreement with the test results is found for all three code-based shear analysis methods. The ACI approach provides more conservative predictions while the two MCFT approaches give more accurate solutions. As tension and truss actions govern the shear behavior over the arch action in B-regions so that these code-based strength analysis methods are able to predict the maximum strength more accurately.

- The probabilities of providing reasonable predictions ($\phi_v < V_{test}/V_{pred} < 2\phi_v$) are the order (highest to lowest) of the *TAMU*, full MCFT.

- In both B-and D-regions, the *TAMU* method gives the most accurate and tight estimates of the ultimate shear capacity of beams with transverse reinforcement. Given that statistics of shear strength ratio, the tight fit with the test data is considered to be a significant improvement. The probability of providing a reasonable solution is over 90% and 75% for D-and B-regions, respectively; this is significantly higher than other code-based strength analysis methods. Thus, the *TAMU* method may be a viable improvement as an alternative strength analysis method for shear-critical reinforced concrete beams with transverse reinforcement.

5. MODIFICATION OF THEORY FOR CASES WITHOUT
TRANSVERSE STEEL

5.1   Chapter Summary

A new shear strength analysis approach referred to as '*Truss and Arch Model Unified* (or *TAMU*)' is developed for shear-critical beams with transverse reinforcement in Chapter 3. That *TAMU* approach considers vertical transverse reinforcement provided within a shear span, *a*, as a clustered vertical tie at the center of the shear span in the truss model. The *TAMU* approach needs to be modified to be applicable for beams without transverse reinforcement because the force transfer path with a vertical tie is not strictly valid without transverse steel. Thus, modifications are made so that the *TAMU* analysis may be conducted for reinforced concrete beams without transverse reinforcement.

To capture the concrete tensile field, a simple truss consisting of a single concrete tie perpendicular to the principal diagonal arch is used at the center of the shear span. The equilibrium and compatibility conditions of the combined truss and arch models are investigated to develop an explicit solution for the concrete softening coefficient. As a result, formulae to calculate the maximum shear strength are derived using shear deformations of truss and arch actions. A shear database consisting of 379 shear-critical beams without transverse reinforcement is assembled and used to verify the modified *TAMU* approach as well as three code-based strength analysis methods. The comparison of predicted strengths with experimentally measured maximum strengths shows reasonable accuracy of the proposed *TAMU* method. Compared to other sectional shear analysis approaches, the modified *TAMU* analysis shows better agreement with the test results than ACI and AASHTO in both D- and B-regions.

5.2   Introduction

Kani (1966) conducted a series of shear tests on beams without transverse reinforcement using

several variables such as effective depth, d, member width, b_w, shear span, a, and the longitudinal

reinforcement ratio, ρ_L. Through the results of the experimental programs, Kani discovered that

shear stress, v_u, is not a constant quantity, and also the effect of concrete strength on shear stress

was relatively insignificant compared to other factors. Kani concluded that effective depth, shear

span, and longitudinal reinforcement are closely related to the shear strength of RC members

without transverse reinforcement while beam width had only a slight effect based on the test

observation.

Based on the ultimate shear stress from the test rests, Kani (1967) found there is a transition

area called the 'Shear Valley' where structure failed prior to reaching its flexural capacity, with

diagonal shear failure governing the failure mechanism. In this shear valley, a significant increase

of ultimate shear load carrying capacity is observed as the shear span-depth ratio decreases,

beginning at $a/d = 2.5$. Following the work of Kani (1966 and 1967), many studies have been

conducted to reveal the different shear failure mechanisms depending on a/d ratio (Schlaich et al.

1987; Cook and Mitchell 1988; Zararis and Papadakis 2001; Choi et al. 2007; and He et al. 2012).

Since then it has become well understood that the shear mechanism is governed by arch action

within the D-region (or non-slender beams whose $a/d \leq 2.5$), whereas tension and truss action (or

beam action) governs behavior in the B-region (or non-slender beam whose $a/d > 2.5$).

The significant change of ultimate shear capacity based on a/d ratio may be physically

explained by the concrete softening effect. In Chapter 3, an explicit solution for the concrete

softening coefficient is derived for beams with transverse reinforcement. However, this solution is

derived by considering the truss model with a vertical tie so that it may not be appropriate for

beams without transverse reinforcement. Thus, the *TAMU* approach with a vertical tie is modified herein to be applicable to shear-critical beams without transverse reinforcement.

A truss model suggested by Kim and Mander (1999) is simplified to represent the truss mechanism without transverse reinforcement. The equilibrium and compatibility conditions of the combined truss and arch models are investigated to develop an explicit solution for the concrete softening coefficient. The modified *TAMU* approach is then validated using the shear database developed in Chapter 4 and compared with other code-based methods.

5.3   Truss and Arch Model with an Inclined Tie

Kim and Mander (1999) suggested the two-point Gauss quadrature truss model with inclined ties for the concrete only mechanism. In this truss model, the inclined ties represent the concrete tension field lumped at the center of the span length, and the diagonal struts represent the concrete compression field stabilizing the truss model. The truss model by Kim and Mander is modified to the single-point cantilever model whereby a single concrete tie represents the lumped concrete tension field and it is perpendicular to the principal diagonal arch.

Figure 5-1 shows truss and arch mechanisms with the inclined concrete tie for some different beam types. Truss and arch actions are represented by red and blue lines, respectively. Members in tension and compression are respectively distinguished by solid and dotted lines. Arch action is considered as the same as beams with transverse reinforcement, as discussed in Chapter 3. The simply supported beam with two different *a*/*d* ratios is drawn in Figure 5-1(a). As shown in that drawing, the concrete tensile ties (red solid line) are perpendicular to the principal arch (blue strut dotted line). These concrete tensile ties bridge the concrete struts and tension chord by transferring the force in tension. It is thought that the concrete softening effect may be more pronounced with this inclined concrete tie than the vertical steel reinforcement tie since concrete is weak in tension.

Figure 5-1(b) depicts the shear resisting mechanism with an inclined tie in a cantilever beam, which the *TAMU* approach with an inclined tie is based on. For consistency, struts and ties are numbered in the same fashion as Figure 3-1(b). The axial strain of the inclined concrete tie (member 2-4) represents the principal tensile strain, ε_1, which acts across the crack plane and induces the concrete softening in the diagonal arch. The principal compressive strain, ε_2, is the strain of the diagonal arch (member 3-5).

In Chapter 3, the arch breadth scalar, η, proposed by Scott et al. (2012), is used in the *TAMU* approach with a vertical tie. However, the same arch breadth scalar cannot be used in this model with the inclined concrete tie since it is defined by the ratio of transverse reinforcement, which is not provided in this case. From many studies, different parameters have been suggested to estimate the portion of truss and arch action, including (a) strength (Paulay, 1971); (b) stiffness (Kim and Mander, 1999, and Zhu et al., 2003); (c) geometry (Hwang et al., 2000); and (d) the shear span-to-internal lever arm ratio (FIP-Commission 3, 1996). Scott et al. (2012) investigated those parameters and concluded that only minor differences are expected by varying the proportions of arch and truss actions in the elastic analysis. Since the *TAMU* approach is a strength analysis method based on the elastic range of materials, the use of the shear span-to-depth ratio, *a/d*, to apportion the truss and arch actions may be appropriate. For this reason, the arch breadth scalar is replaced with *d/a* (= tanα) in this model. To meet the geometry of an inclined perpendicular to the arch, an upper limit of 1.0 is used as shown:

$$\eta = \frac{d}{a} = \tan\alpha < 1.0 \tag{5-1}$$
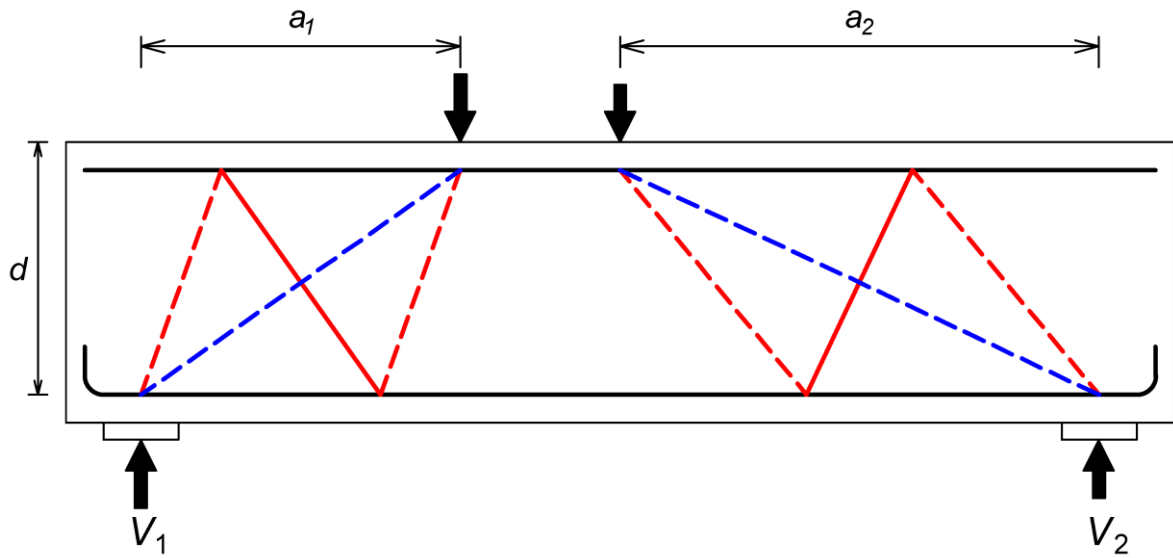
(a) Simply supported beam depicting to different shear span aspect ratios (a/d ≈1.0 left, and a/d = 2.5 right)
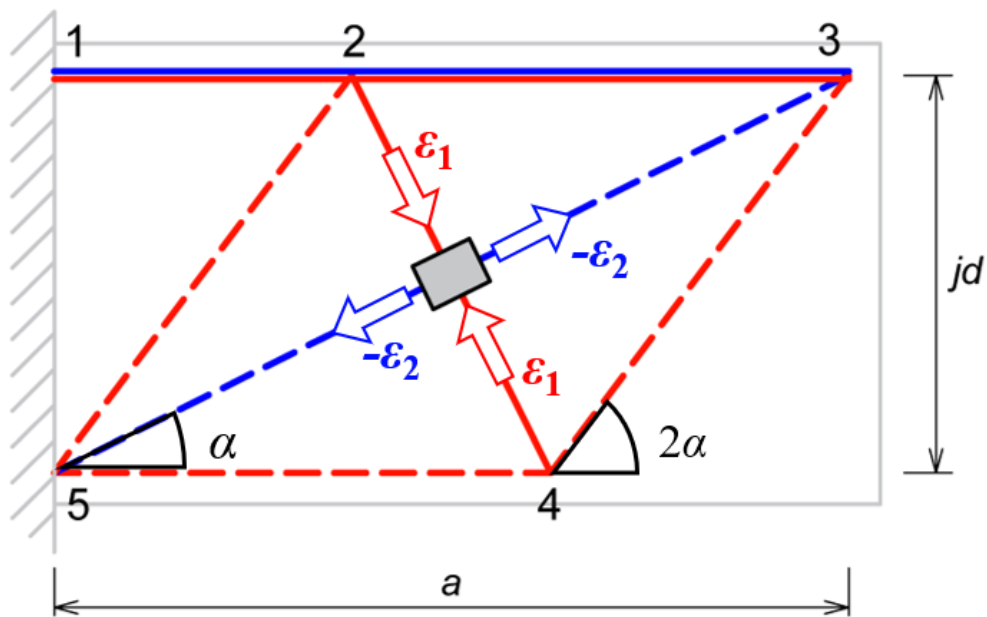
(b) Cantilever beam

Figure 5-1. *TAMU* **model with an inclined tie**

To achieve the integrity of the combined truss and arch models, the force distribution factor, μ, needs to be considered in this model. In the same fashion as the *TAMU* approach with a vertical tie, shear deformations of both truss and arch actions by the unit load are determined based on the Virtual Work method, and the factor is calculated using:

$$\mu = \frac{\delta_{truss}}{\delta_{arch} + \delta_{truss}} \tag{5-2}$$

where μ = force distribution factor; δ_{truss} = displacement of the truss mechanism caused by the unit load; and δ_{arch} = displacement of the arch mechanism caused by the unit load.

As shown in Figure 5-2(a), the arch mechanism remains as the *TAMU* with the vertical tie, however, the arch displacement by the unit load, δ_{arch} is not the same due to the changed the arch breadth scalar, η. Table 5-1 summarizes elastic axial rigidities and the virtual work components of the arch action for beams with an inclined tie. Using elastic axial rigidities and the virtual work components, the displacement of the arch model by the unit load, δ_{arch}, is given by:

$$\delta_{arch} = \sum_{i=1}^{2} \frac{f^2 L}{EA} \tag{5-3}$$

Substituting unit deformation components in the rightmost column in Table 5-1 into Eq. (5-3) gives:

$$\delta_{arch} = \frac{a}{E_c b_w d} \psi_{arch} \tag{5-4}$$

where ψ_{arch} = flexibility coefficient for arch displacements defined by:

$$\psi_{arch} = \frac{\cot^2 \alpha}{\rho_L n} + \frac{8\cot\alpha}{3\sin^2 \alpha} \tag{5-5}$$

128

Table 5-1. Virtual work analysis on arch model with a vertical tie

Member	Rigidity (EA)	Length (L)	Unit Load (f)	Strain ($\varepsilon = F/EA$)	Deformation by f (f^2L/EA)
1-3	$nE_c\rho_Lb_wd$	$d\cot\alpha$	$\cot\alpha$	$\dfrac{\mu V\cot\alpha}{E_sA_s}$	$\dfrac{\cot^3\alpha/\rho_L}{nE_cb_w}$
3-5	$\dfrac{0.375E_c\eta b_wd}{\cos\alpha}$	$\dfrac{d}{\sin\alpha}$	$-\dfrac{1}{\sin\alpha}$	$\dfrac{-\boldsymbol{\mu V\cot\alpha}}{\mathbf{0.375}E_c\boldsymbol{\eta b_wd}}$	$\dfrac{\cot^2\alpha}{0.375\sin^2\alpha\,E_cb_w}$

Note: arch breadth scalar, η, on the rightmost column is replaced with $d/a =\tan\alpha$

Table 5-2. Virtual work analysis on truss model with an inclined tie

Member	Rigidity (EA)	Length (L)	Unit Load (f)	Strain ($\varepsilon = F/EA$)	Deformation by f (f^2L/EA)
1-2	$nE_c\rho_Lb_wd$	$d\cot 2\alpha$	$2\cot 2\alpha + \tan\alpha$	$\dfrac{V(1-\mu)(2\cot 2\alpha + \tan\alpha)}{E_sA_s}$	$\dfrac{(2\cot 2\alpha + \tan\alpha)^2\cot 2\alpha}{\rho_LnE_cb_w}$
2-3	$nE_c\rho_Lb_wd$	$\dfrac{d}{\sin 2\alpha}$	$\cot 2\alpha$	$\dfrac{V(1-\mu)(\cot 2\alpha)}{E_sA_s}$	$\dfrac{(\cot 2\alpha)^2/\rho_L}{nE_cb_w\sin 2\alpha}$
2-5	$\dfrac{0.5E_c(1-\eta)b_wd}{\sqrt{0.5+\tan^2 2\alpha}}$	$\dfrac{d}{\sin 2\alpha}$	$-\dfrac{1}{\sin 2\alpha}$	$\dfrac{-V(1-\mu)\sqrt{2+4\tan^2 2\alpha}}{E_c(1-\eta)b_wd\sin 2\alpha}$	$\dfrac{\sqrt{8+16\tan^2 2\alpha}}{(1-\tan\alpha)\sin^3 2\alpha E_cb_w}$
3-4	$\dfrac{0.5E_c(1-\eta)b_wd}{\sqrt{0.5+\tan^2 2\alpha}}$	$\dfrac{d}{\sin 2\alpha}$	$-\dfrac{1}{\sin 2\alpha}$	$\dfrac{-V(1-\mu)\sqrt{2+4\tan^2 2\alpha}}{E_c(1-\eta)b_wd\sin 2\alpha}$	
2-4	$\dfrac{E_{ct}(1-\eta)b_wd}{4\sin\alpha\sqrt{0.5+\tan^2 2\alpha}}$	$\dfrac{d}{\cos\alpha}$	$\dfrac{1}{\cos\alpha}$	$\dfrac{\mathbf{4}\boldsymbol{V(1-\mu)}\sqrt{\mathbf{0.5}+\boldsymbol{\tan^2 2\alpha}}}{\boldsymbol{(1-\eta)E_{ct}b_wd\cot\alpha}}$	$\dfrac{\tan\alpha\sqrt{8+16\tan^2 2\alpha}}{(1-\tan\alpha)\cos^2\alpha E_{ct}b_w}$
4-5	$E_c(kd)b_w$	$\dfrac{d}{\sin 2\alpha}$	$\cot 2\alpha + \tan\alpha$	$\dfrac{V(1-\mu)(\cot 2\alpha + \tan\alpha)}{(kd)b_w}$	$\dfrac{(\cot 2\alpha + \tan\alpha)^2}{k\sin 2\alpha E_cb_w}$

where a = shear span length; b_w = beam width; and d = effective depth of the beam; ρ_L = volumetric ratio of longitudinal steel to concrete, where $\rho_L = A_L/b_wd$; A_s = area of longitudinal reinforcement contributing to the tension tie; α = corner-to-corner diagonal angle; E_c = modulus of elasticity of concrete in compression; E_{ct} = modulus of elasticity of concrete in tension; n = modular ratio of steel to concrete; and n' = modular ratio of concrete in tension to concrete in compression.

(a) Arch model   (b) Truss model
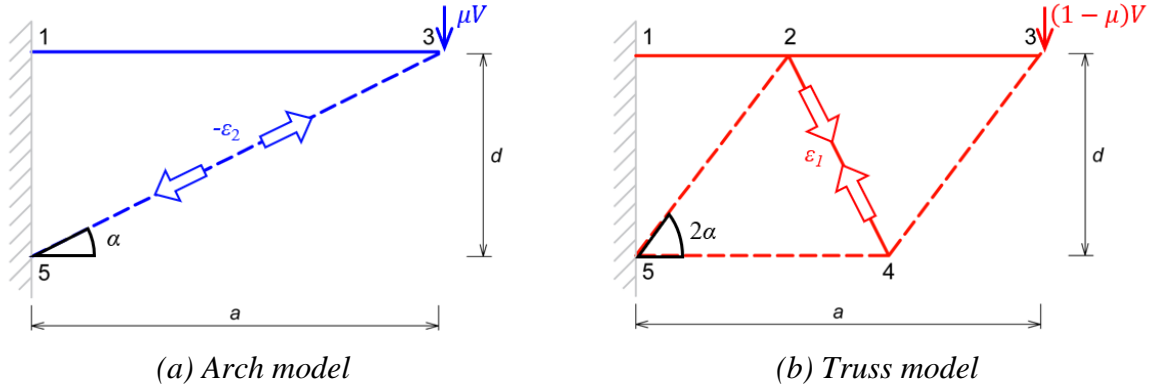
Figure 5-2. Arch and truss model with an inclined tie

As shown in Figure 5-2(b), the truss mechanism has an inclined tie perpendicular to the

principal diagonal arch. Due to this different geometry, an equation for the displacement of the

truss model by the unit load changes significantly compared with Eq. (3-13) for the *TAMU* with

the vertical tie. The axial rigidities and virtual work components of the truss action are provided

in Table 5-2. The shear deformation of the truss model with an inclined concrete tie is the sum of

component deformations. Using elastic axial rigidities and the virtual work components, the shear

deformation of the truss by the unit load, δ_{truss}, is calculated by:

$$\delta_{truss} = \sum_{i=1}^{6} \frac{f^2 L}{EA} = \frac{a}{E_c b_w d} \psi_{truss} \tag{5-6}$$

Expanding Eq. (5-6) using the components in the rightmost column in Table 5-2 gives:

$$\delta_{truss} = \frac{a}{E_c b_w d} \psi_{truss} \tag{5-7}$$

where ψ_{truss} = flexibility coefficient for arch displacements given by:

$$\psi_{truss} = \frac{(\cot\alpha - 1)}{2\rho_L n} - \frac{\cot^2 2\alpha}{2\rho_L n \cos^2\alpha} + \frac{\sec^4\alpha}{8k\sin^2\alpha} + \frac{\sqrt{16\tan^2 2\alpha + 8}}{8\cos^4\alpha(1 - \tan\alpha)}\left(\csc^2\alpha + \frac{8\sin^2\alpha}{n'}\right) \tag{5-8}$$

130

Based on the empirical equation proposed by Karthik et al. (2016), the concrete softening coefficient, ζ, is given by:

$$\zeta = \frac{1}{1 + 0.25|\varepsilon_1/\varepsilon_2|} \tag{5-9}$$

where ζ = concrete softening coefficient; ε_1 = principal diagonal tensile strain transverse to the axis of the arch; and ε_2 = principal diagonal compressive strain at the center of the arch.

For the combined truss and arch model with an inclined tie, principal strains of ε_1 and ε_2 can be inferred using equations regarding the axial strain of member (3-5) and member (2-4) in Table 5-1 and Table 5-2, respectively. It is noted that the total shear load, V, is distributed to the arch and truss mechanisms, respectively, based on the arch-truss force distribution so that (η) and $(1 - \eta)$ are taken into consideration in the strains in the tables. ε_1, and ε_2 are given by:

$$\varepsilon_1 = \frac{4V(1 - \mu)\sqrt{0.5 + \tan^2 2\,\alpha}}{(1 - \eta)E_c b_w d\cot\alpha} \tag{5-10}$$

$$\varepsilon_2 = -\frac{\mu V \cot\alpha}{0.375 E_c \eta b_w d} \tag{5-11}$$

where V is shear force applied.

Dividing Eq. (5-10) by Eq. (5-11) gives the explicit solution for the principal strain ratio, $\varepsilon_1/\varepsilon_2$, as follows:

$$\frac{\varepsilon_1}{\varepsilon_2} = \frac{1.5n \tan^2\alpha \sqrt{0.5 + \tan^2 2\,\alpha}}{(\cot\alpha - 1)}\left(\frac{\psi_{arch}}{\psi_{truss}}\right) \tag{5-12}$$

Substituting Eq. (5-12) into Eq. (5-9) gives an explicit solution for the concrete softening coefficient, ζ. The force transferred to the arch action, $C_{arch} = \mu V \mathrm{cosec}\alpha$, is resisted by softened

concrete compressive strength, $\zeta f'_c$, multiplied by the effective area of strut $A_{arch}(= \eta b_w w_s)$.

Thus, the maximum nominal shear capacity for the arch compression critical failure, V_n^{arch}, is

calculated as:

$$V_n^{arch} = 0.375\zeta\beta_1 f'_c b_w d \tan^2 \alpha \left(1 + \frac{\psi_{arch}}{\psi_{truss}}\right) \qquad (5\text{-}13)$$

where V_n^{arch} = maximum nominal shear capacity the principal diagonal arch; β_1 = ratio of the

depth of the equivalent uniformly stressed compression zone; and f'_c = concrete strength.

5.4   Verification of *TAMU* without Transverse Reinforcement Using Shear Database

5.4.1   Shear Database for RC Beams without Transverse Reinforcement

To further verify the validity of the *TAMU* approach with an inclined tie for beams without

transverse reinforcement, a shear database is developed. Shear test data of reinforced concrete

beams with no transverse reinforcement, including both D-and B-regions, are collected to

investigate the accuracy of the method based on the *a/d* ratio and also to compare the results with

other code-based analysis methods. From 31 references, a total of 379 beams are collected (178

with D-regions, and 201 with B-regions). The literature used to develop this database is found in

Appendix A. Reinforced concrete beams that showed shear failure are only collected, and some

specimens in the literature are excluded due to unclarified failure mode and maximum shear loads.

Figure 5-3 presents the distributions of five experimental variables used in the database,

including, (a) f'_c = concrete compressive strength; (b) h = member height; (c) b = member width;

(d) a/d = shear span-depth ratio; and (e) ρ_L = ratio of flexural reinforcement. Since the effect of

these variables on the ultimate shear stress is evident (except for member width which has a minor

effect), it is of interest to assess the accuracy of this approach by each variable.
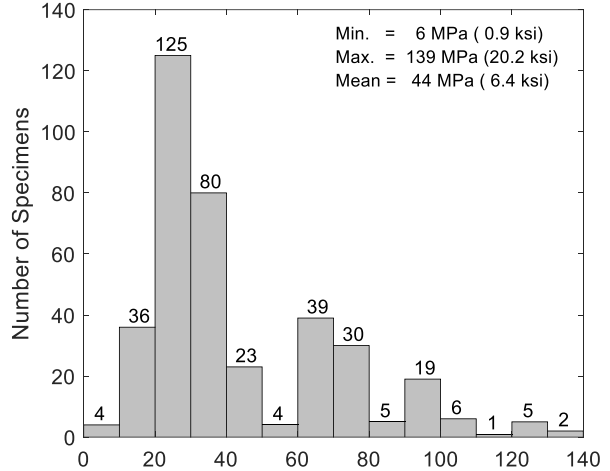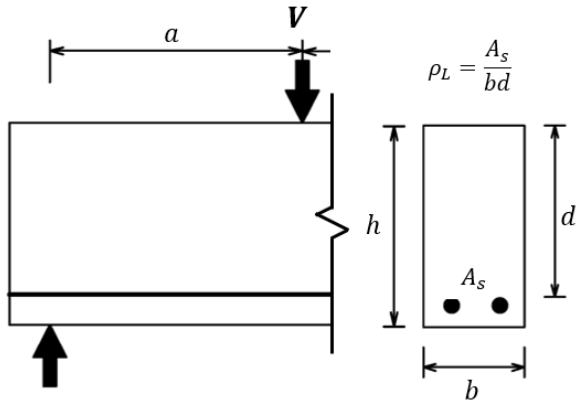
(a) Concrete compressive strength, f'_c (MPa)
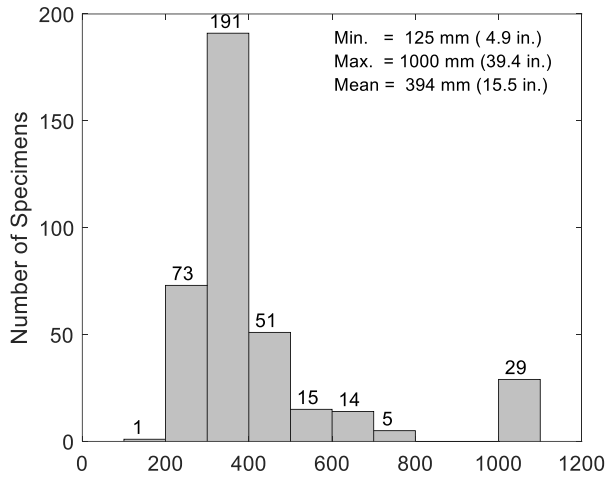
(b) Member height, h (mm)
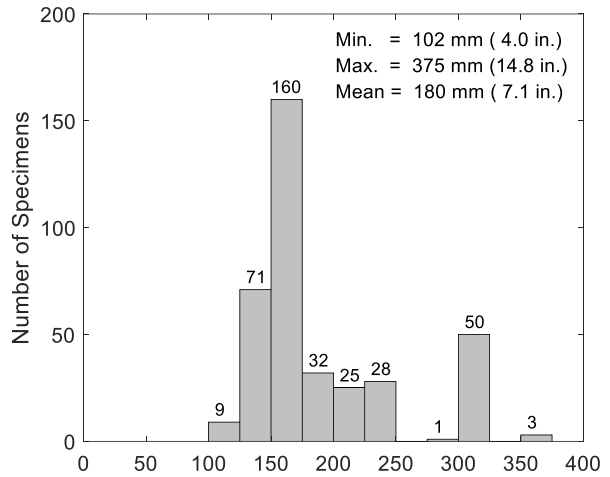
(c) Member width, b (mm)
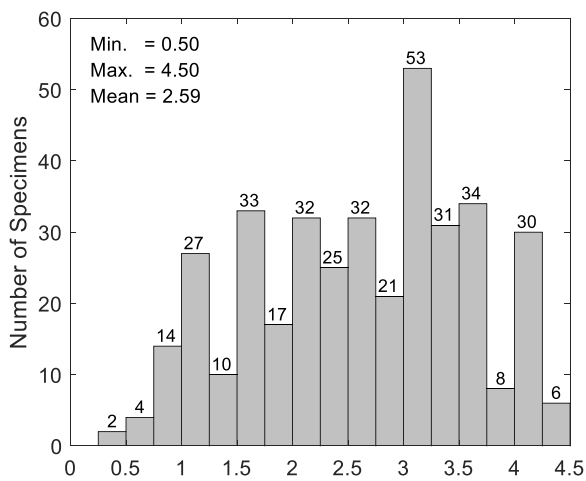
(d) a/d ratio
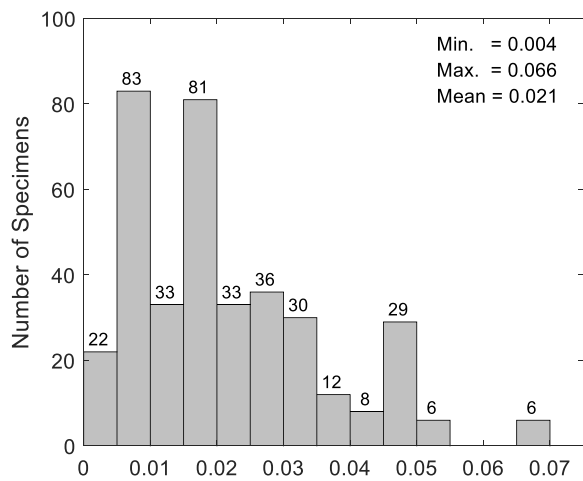
(e) Flexural reinforcement ratio (ρ_L)

Figure 5-3. Distribution of experimental variables in the database without transverse reinforcement

133

As shown in Figure 5-3 the ranges of variables are: f'_c = 6 to 139 MPa with a mean of 44 MPa for concrete compressive strength; h = 125 to 1000 mm with a mean of 394 mm for member height; b = 102 to 375 mm with a mean of 180 mm for member width; a/d ratio = 0.5 to 4.5 with a mean of 2.59; ρ_L = 0.004 to 0.066 with a mean of 0.021 for longitudinal (flexural) reinforcement ratio.

5.4.2   Statistics and Accuracy of the Predictions for the Modified *TAMU* Method

The *TAMU* approach analysis with an inclined tie for beams without transverse reinforcement is validated using the experimental shear database developed herein. The validation is made based on statistics of the shear strength ratio, V_{test}/V_{pred}, including mean, median, the lognormal standard derivations, given by the dispersion factor (β), and percentage of unconservative ($V_{test}/V_{pred} < \phi_v$) and over-conservative ($V_{test}/V_{pred} > 2.0\phi_v$) predictions. To investigate the effect of the a/d ratio on the accuracy of the modified *TAMU* approach, the analysis results are divided into two cases: a) D-regions without transverse reinforcement and b) B-regions without transverse reinforcement.

Figure 5-4 presents the overall analysis results of the *TAMU* approach against reinforced concrete beams without transverse reinforcement in the shear database for all ranges of a/d ratios. Figure 5-4(a) presents the trends in the shear strength ratios, V_{test}/V_{pred}, as a function of a/d ratio, ρ_L, f'_c, and b. No particular trend is evident with any of variables as the shear strength ratios are widely (randomly) scattered for the range of values used. As shown in the scatter plots, most of the shear strength ratios are located within 0.5 and 2.5 regardless of D- and B-regions and other variables. The mean of the overall shear strength ratio is 1.06 with a maximum of 2.46 and a minimum of 0.50.
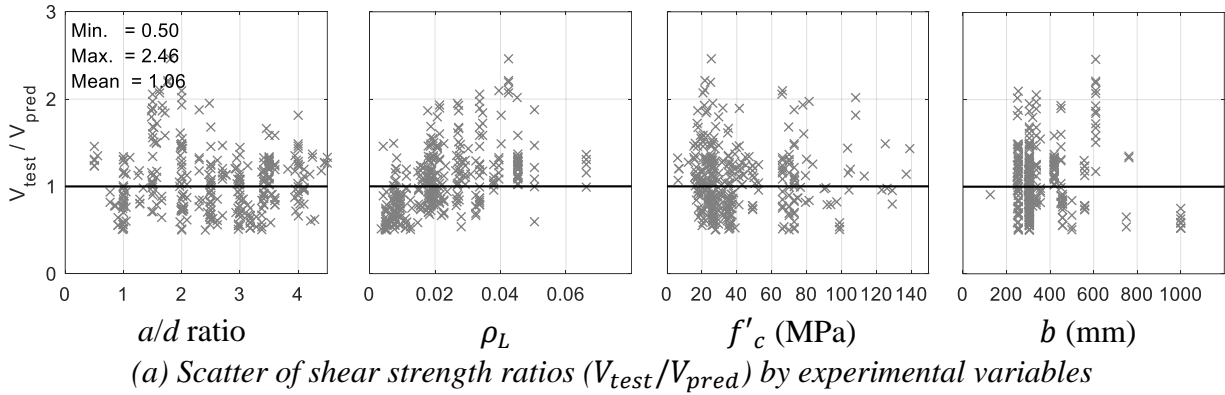
(a) Scatter of shear strength ratios (V_{test}/V_{pred}) by experimental variables
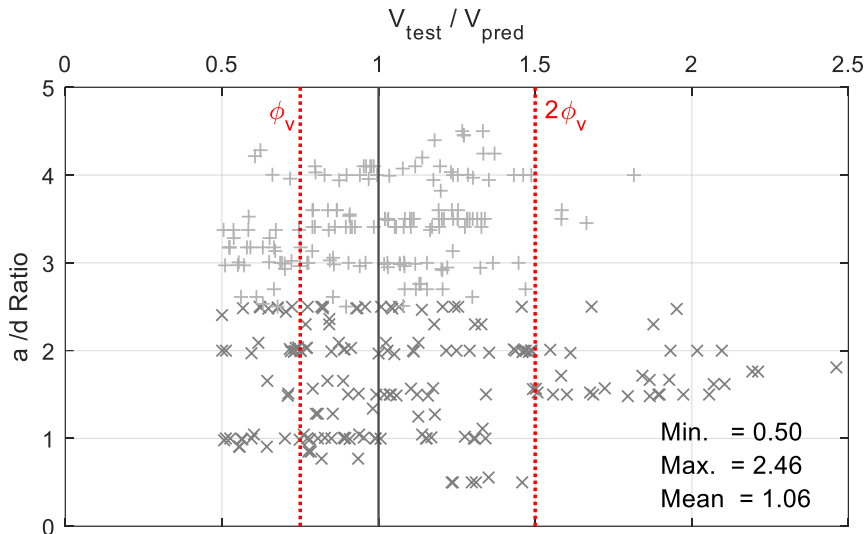
(b) Scatter of V_{test}/V_{pred} by a/d ratios
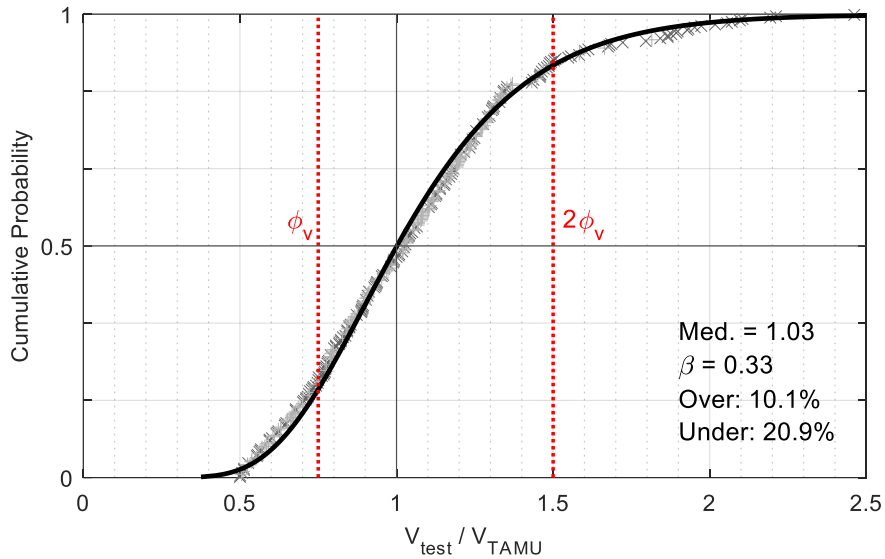
(c) Lognormal cumulative distribution of V_{test}/V_{pred}

Figure 5-4. Overall analysis results of the *TAMU* method with an inclined tie

Figure 5-4(b) presents the scatters of V_{test}/V_{pred} by a/d ratio with a summary of minimum, maximum, and mean of the data for all ranges of a/d ratio. An undercapacity factor of $\phi_v = 0.75$ is chosen herein to account for uncertainty in the material resistance, and this is the same as the factor used for beams with transverse reinforcement in Chapter 3 and ACI 318. The red dotted lines drawn along with the distribution indicate non-exceedance (when $V_{test} < \phi_v V_{pred}$) and over-exceedance (when $V_{test} > 2\phi_v V_{pred}$) probabilities, respectively. Although the median value is close to 1.0, there are some data points having unconservative or over-conservative predictions as shown in the figure. Both regions have a similar scatter pattern, however, D-regions have more data points exceeding the over-conservative criterion.

Figure 5-4(c) presents a lognormal cumulative distribution of the modified *TAMU* method against all data points. A distribution curve that matches well with the overall data points is selected. The median of V_{test}/V_{pred} is 1.03 and its dispersion factor, *β*, is 0.33. The respective over-conservative and unconservative probabilities are 10% and 21%. The overall dispersion of the analytical results is slightly greater than the *TAMU* approach for beams with transverse reinforcement.

Figure 5-5 presents the analytical results using the *TAMU* approach for RC beams without transverse reinforcement steel. The results are categorized into D- and B-regions to investigate the effect of *a/d* ratio on the accuracy and conservativeness of the method. Figure 5-5(a) presents the scatter graphs of *a/d* ratio vs. V_{test}/V_{pred} for D- and B-regions, respectively along with a summary of statistics, including minimum, maximum, and mean of the shear strength ratio. The mean values of the shear strength ratios are 1.12 and 1.00 for D- and B-regions, respectively, and some of the most conservative results are found when the *a/d* ratios are between 1.5 and 2.0. There is no significant difference, however, predictions in D-regions are dispersed more broadly.
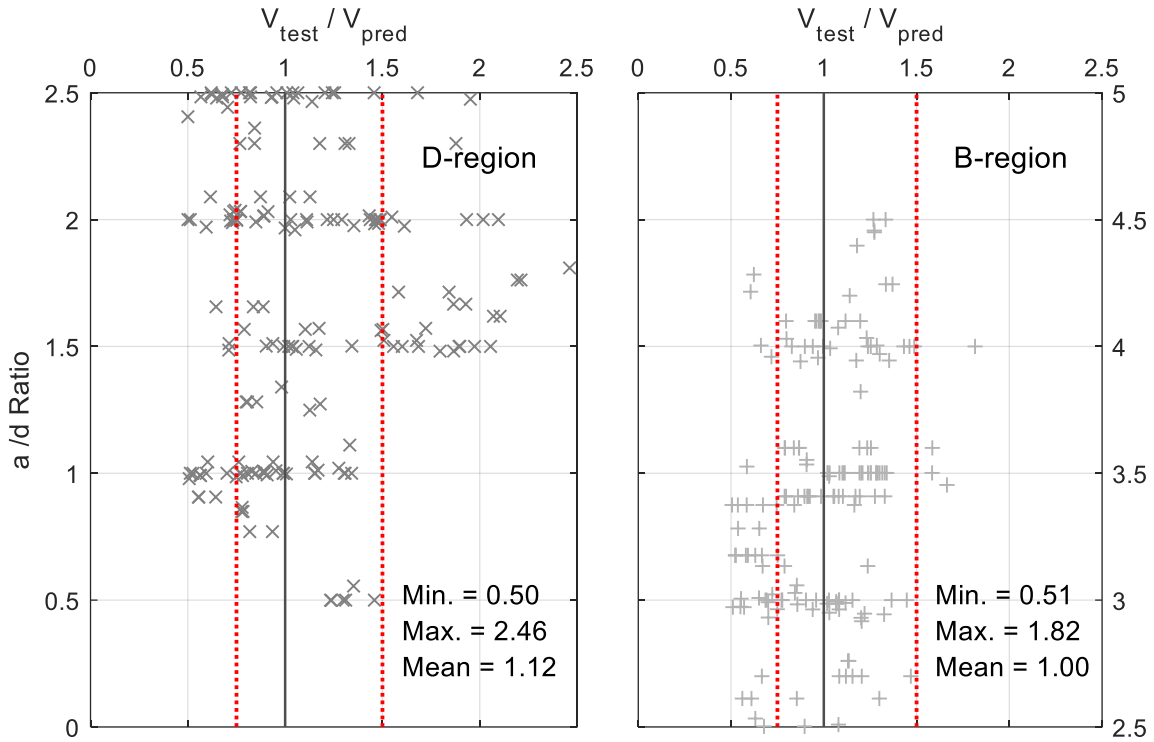
(a) Scatter of V_{test}/V_{pred} by a/d ratios (Left: D- and Right: B-regions)
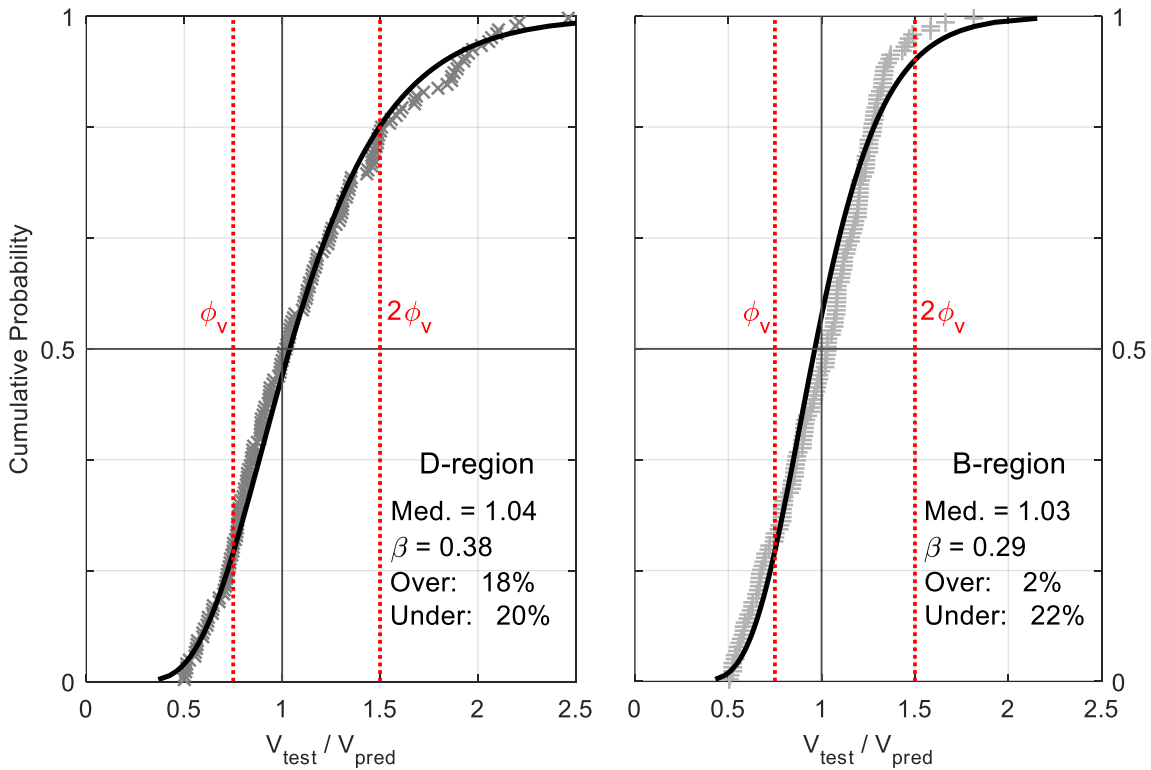
(b) Lognormal cumulative distribution of V_{test}/V_{pred} (Left: D- and Right: B-regions)

Figure 5-5. Analysis results of the *TAMU* method with an inclined tie for D- and B-regions

137

Figure 5-5(b) presents the lognormal cumulative distributions of D-and B-regions with corresponding data points. The cumulative distributions that agree well with the overall data points are chosen to evaluate conservativeness more precisely. The obtained lognormal cumulative distributions of D- and B- regions have median values of 1.04 and 1.03, respectively, and their lognormal standard derivations which are given by the dispersion factor are 0.38 and 0.29. In general, the *TAMU* approach with an inclined concrete tie has better accuracy in B-regions than D-regions.

More widely scattered data points with larger dispersion factors in both regions ($\beta = 0.38$ and 0.29) compared to those from the *TAMU* approach with a vertical tie ($\beta = 0.19$ and 0.28) in Chapter 4. Given that an ideal model fit has the median value close to 1.0, the *TAMU* method for beams without transverse reinforcement possesses a slight measure of conservatism in both regions. This result is considered to be appropriate as the shear strength needs to be estimated conservatively to prevent brittle shear failures.

Calculated probabilities of unconservative and over-conservative predictions are 20% and 18% for D-regions, and 22% and 2% for B-regions, respectively, meaning the *TAMU* approach would make reasonable predictions at 62% and 76% probabilities. Although the modified *TAMU* approach has better predictions in B-regions than D-regions, the difference is not significant, and the almost identical trend is observed in both regions. Thus, this method may be applicable to both D-and B-regions.

5.5 Comparison with Code-Based Strength Analysis Methods

The analysis results of the proposed *TAMU* approach for beams without transverse reinforcement are compared with three existing code methods of analysis. Three code-based shear methods include a) the classic shear method based on the 45-truss model in ACI 318-19; b) the full MCFT

method in AASHTO LRFD Appendix B5 (referred to as 'full MCFT'); and c) the simplified

MCFT method in AASHTO LRFD 5.8.3.4.2 (referred to as 'simplified MCFT'). These three

methods are based on the sectional design model. In the following sections, design procedures of

three existing code methods for beams without transverse reinforcement are introduced and their

results are compared with the simplified method.

5.5.1   Analysis Procedures for Code-Based Sectional Design Approaches

When transverse reinforcement is not provided, the shear resistance contributed by concrete (V_c)

alone is taken into account for all three code-based strength analysis methods:

$$V_c = 0.083\beta \sqrt{f'_{c\,(MPa)}} b_w d_v \tag{5-14}$$

where β = factor relating effect of longitudinal strain on the shear capacity of concrete;

f'_c = compressive strength of concrete; b_w = effective web width taken as the minimum web width

within the depth d_v; and d_v = effective shear depth.

Each design method has a respective procedure to estimate the concrete factor, β. The

classic shear method (ACI 318-19) uses a constant concrete coefficient of 0.17 regardless of the

presence of transverse reinforcement as:

$$V_c = 0.17 \sqrt{f'_{c\,(MPa)}} b_w d \tag{5-15}$$

where $d_v = d$ = effective shear depth.

Both simplified and full MCFT methods provide different procedures for β depending on

the existence of transverse reinforcement. The procedure for beams without transverse

reinforcement (or with less than minimum transverse reinforcement) is used herein. The simplified

MCFT method assumes concrete coefficient, β, is varied the tensile strain of the reinforcement, ε_s, and crack spacing, ε_s. as below:

$$\beta = \frac{4.8}{(1 + 750\varepsilon_s)} \frac{51}{(39 + s_{xe})} \tag{5-16}$$

The longitudinal tensile strain in the section at the centroid of the tension reinforcement, ε_s, is determined by:

$$\varepsilon_s = \frac{\left(\frac{|M_u|}{d_v} + 0.5N_u + |V_u - V_p| - A_{ps}f_{po}\right)}{\left(E_s A_s + E_p A_{ps}\right)} \tag{5-17}$$

where $|M_u|$ = absolute value of the applied factored moment; N_u = applied factored axial force; V_u = factored shear force; V_p = component in the direction of the applied shear of the effective prestressing force; A_{ps} = area of prestressing steel on the flexural tension side of the member; f_{po} = parameter taken as modulus of elasticity of prestressing tendons; E_s = modulus of elasticity of reinforcing bars; A_s = area of non-prestressed steel on the flexural tension side of the member at the section; and E_p = modulus of elasticity of prestressing strands.

The crack spacing parameter is given by:

$$s_{xe} = s_x \left(\frac{35}{a_g + 16}\right) \leq 2{,}000\text{mm} \tag{5-18}$$

where s_x = crack spacing which is taken as the lesser of either d_v or the maximum distance between crack control reinforcement; and a_g = maximum aggregate size.

The full MCFT method uses longitudinal strain in the web of the member, ε_x, instead of strain of the tension reinforcement, ε_s, and s_{xe} to estimate the concrete factor, β. Table 5-3 presents

AASHTO Table B5.2-2 containing the values of θ and β for beams with less than minimum transverse reinforcement required. Note, θ in the table is not used herein as beams without transverse reinforcement are only considered. As shown in the table, β is a function of s_{xe} and ε_x. Eq. (5-18) is used to estimate s_{xe}, and ε_x is given by:

$$\varepsilon_x = \frac{\left(\frac{|M_u|}{d_v} + 0.5N_u + 0.5|V_u - V_p|\cot\theta - A_{ps}f_{po}\right)}{\left(E_s A_s + E_p A_{ps}\right)} \quad (5\text{-}19)$$

Table 5-3. Values of θ and β for section without transverse reinforcement

s_{xe}, in.	$\varepsilon_x \times 1000$										
	$\leq$–0.20	$\leq$–0.10	$\leq$–0.05	$\leq$0	$\leq$0.125	$\leq$0.25	$\leq$0.50	$\leq$0.75	$\leq$1.00	$\leq$1.50	$\leq$2.00
$\leq$5	25.4	25.5	25.9	26.4	27.7	28.9	30.9	32.4	33.7	35.6	37.2
	6.36	6.06	5.56	5.15	4.41	3.91	3.26	2.86	2.58	2.21	1.96
$\leq$10	27.6	27.6	28.3	29.3	31.6	33.5	36.3	38.4	40.1	42.7	44.7
	5.78	5.78	5.38	4.89	4.05	3.52	2.88	2.50	2.23	1.88	1.65
$\leq$15	29.5	29.5	29.7	31.1	34.1	36.5	39.9	42.4	44.4	47.4	49.7
	5.34	5.34	5.27	4.73	3.82	3.28	2.64	2.26	2.01	1.68	1.46
$\leq$20	31.2	31.2	31.2	32.3	36.0	38.8	42.7	45.5	47.6	50.9	53.4
	4.99	4.99	4.99	4.61	3.65	3.09	2.46	2.09	1.85	1.52	1.31
$\leq$30	34.1	34.1	34.1	34.2	38.9	42.3	46.9	50.1	52.6	56.3	59.0
	4.46	4.46	4.46	4.43	3.39	2.82	2.19	1.84	1.60	1.30	1.10
$\leq$40	36.6	36.6	36.6	36.6	41.2	45.0	50.2	53.7	56.3	60.2	63.0
	4.06	4.06	4.06	4.06	3.20	2.62	2.00	1.66	1.43	1.14	0.95
$\leq$60	40.8	40.8	40.8	40.8	44.5	49.2	55.1	58.9	61.8	65.8	68.6
	3.50	3.50	3.50	3.50	2.92	2.32	1.72	1.40	1.18	0.92	0.75
$\leq$80	44.3	44.3	44.3	44.3	47.1	52.3	58.7	62.8	65.7	69.7	72.4
	3.10	3.10	3.10	3.10	2.71	2.11	1.52	1.21	1.01	0.76	0.62

Linear interpolation between the values given in the table may produce more accurate predictions but not necessarily recommended for hand calculations. For both simplified and full MCFT methods, the obtained β value is used for Eq. (5-14) to estimate concrete shear strength, V_c.

5.5.2 Comparison of Four Shear Strength Analysis Methods

In the following discussions, nominal shear strengths are calculated in accordance with the procedure provided in the previous section for the ACI-318 method, the simplified MCFT sectional method, and the full MCFT method. The calculated strengths are compared with the test results as well as the modified *TAMU* analysis results. Two cases, D- and B-regions, are compared separately to investigate the accuracy of each method by the *a*/*d* ratio.

Figure 5-6 presents the analysis results of each shear analysis method. The accuracy and adequacy of each method is evaluated by assessing the shear strength ratios, V_{test}/V_{pred}. Each method is presented with a representative color (*TAMU*: gray, ACI: orange; simplified MCFT: green, and full MCFT: blue), and slightly different brightness is used to distinguish D- and B-regions. Two red dotted lines indicate non-exceedance probability and over-exceedance probability, respectively. The used resistance reduction factors are 0.75 for the *TAMU* and ACI methods and 0.90 for both MCFT methods. The analysis results are presented in the order of the ACI, simplified MCFT, full MCFT, and *TAMU* based on the level of sophistication of the method.

In Figure 5-6(a), the ratios of V_{test}/V_{pred} against the *a*/*d* ratio are plotted. In D-regions, highly scattered data points are evident in the three code-based methods, compared to the *TAMU* approach where the ratios are limited between 0.5 and 2.5. When *a*/*d* ratio > 2.5, more accurate aspects start to appear in all code-based approaches. The dramatic change of conservatism in all code-based approaches near the *a*/*d* = 2.5 corresponds to the observation made by Collins et al. (2008). This distinct trend may be due to the change of the implicit tension-based shear mechanism. All code-based analysis methods are based on a tension ($\sqrt{f'_c}$) construct, resulting in a lack of accuracy in D-regions where a compression arch action dominates. On the other hand, both tension truss and arch actions are taken into account in the *TAMU* method, thus, it tends to have good accuracy in both regions.
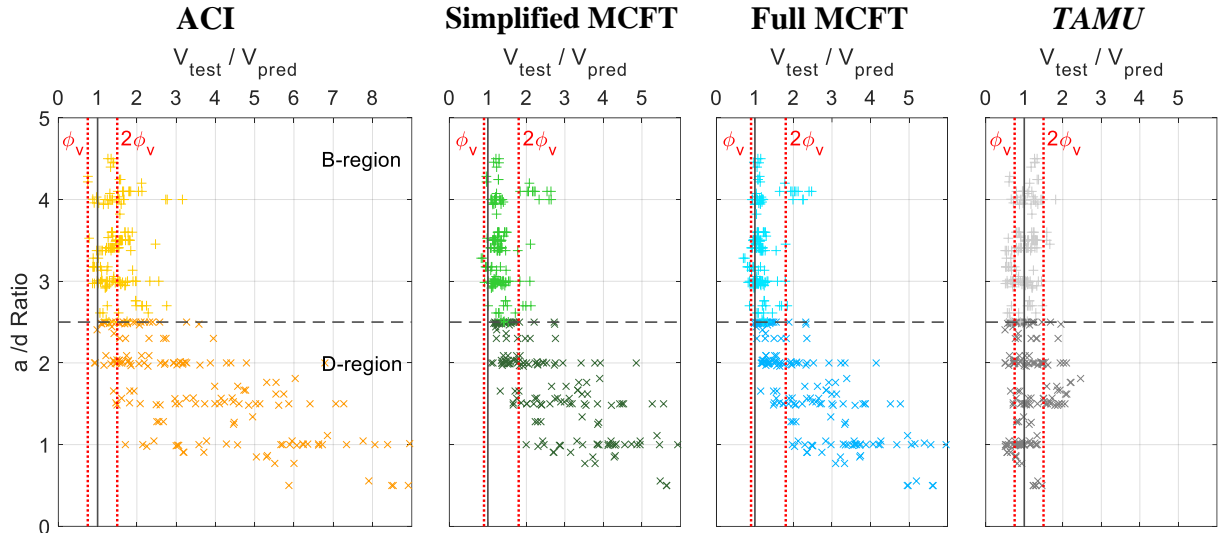
(a) Scatter plot of V_{test}/V_{pred} vs. a/d ratio
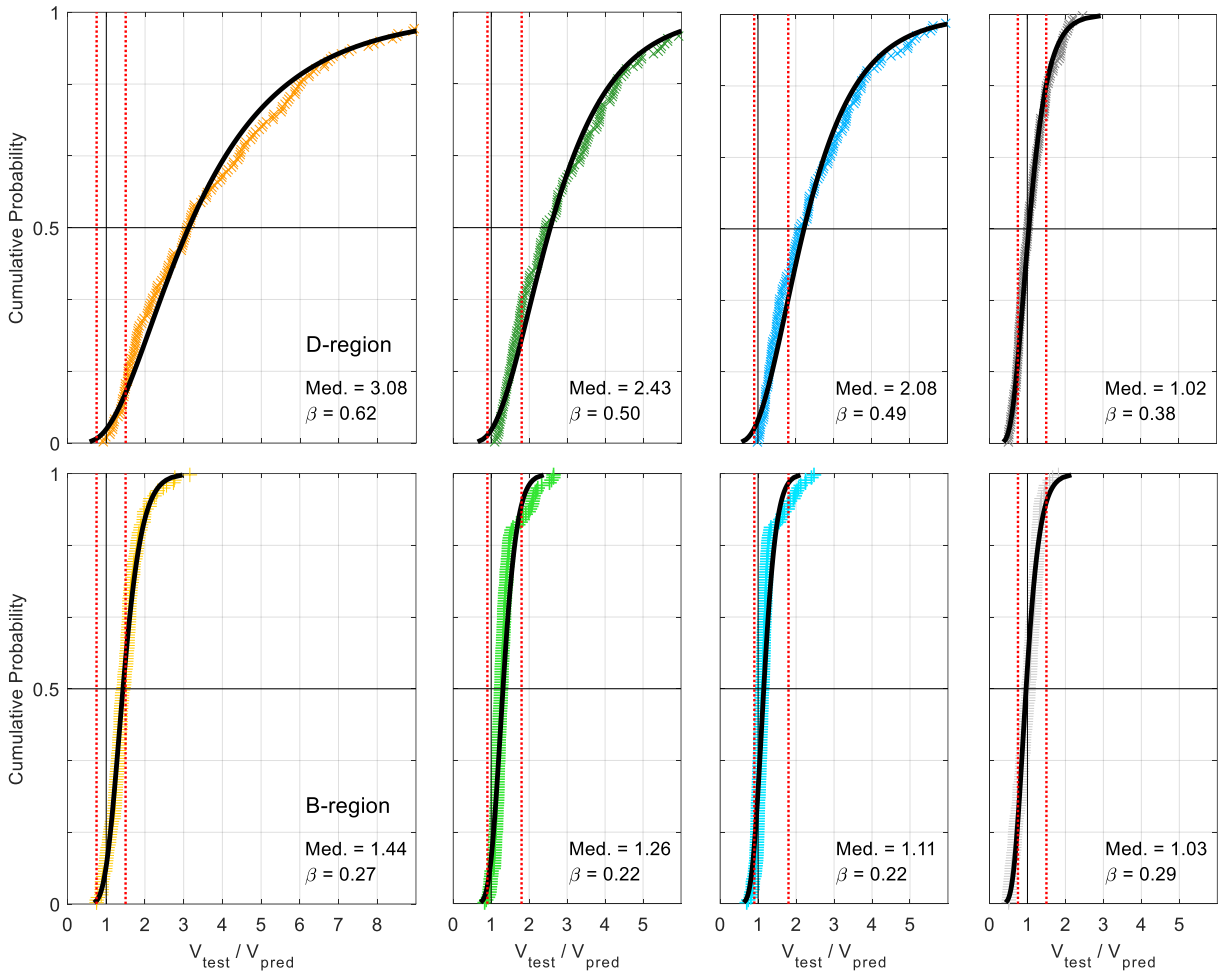
(b) Lognormal cumulative distribution function of V_{test}/V_{pred}

Figure 5-6. Comparison of shear analysis methods for beams without shear reinforcement

Figure 5-6(b) shows lognormal cumulative probability distributions of V_{test}/V_{pred} plotted with the data points. The lognormal distributions that agree well with the overall data points are selected for all methods to assess the unconservative and over-conservative aspects more precisely. In D-regions, an excessively conservative aspect is evident in the ACI method as its median is 3.08 with the dispersion factor (β) of 0.62. Over 83% of predictions are overly-conservative, and also some unconservative predictions exist at the same time. Similarly, both MCFT methods show conservative aspects for most of the data points in D-regions but not as over-conservative as the ACI method. Results show median values of 2.43 and 2.08 with dispersions of $\beta = 0.50$ and 0.49 for the simplified and full MCFT methods, respectively. A similar trend is observed in both MCFT methods, but better predictions with less over-conservative aspects are given in the full MCFT. Compared to code-based strength analysis methods, the *TAMU* method shows better agreement with the test results in D-regions. Although some unconservative aspects exist in the *TAMU* method, it may be removed if factored load and design strengths are considered in the design stage.

In B-regions, completely different aspects are evident for all the code-based strength analysis methods in Figure 5-6(b), as they now show overall reasonable predictions. The *TAMU* method also has good agreement with the test data. The median values of 1.44, 1.26, 1.11, and 1.03 are found in the *TAMU*, ACI, full MCFT, and simplified MCFT, respectively, with a dispersion ranging from $\beta = 0.22$ to 0.29. Generally, the more sophisticated shear analysis method generally creates better and more accurate analysis results in both regions. This is evident as the method on the right has a median value closer to 1.0 and smaller dispersion, β.

Table 5-4 summarizes the statistics of the shear strength ratios of three existing code-based shear analysis methods and the *TAMU* method. The statistics include median values, and probabilities of unconservative, over-conservative, and reasonable predictions. The accuracy of

the MCFT methods in B-regions is evident as they provide reasonable predictions over 85% although their accuracy significantly decreases in D-regions. The *TAMU* provides overall good predictions as 63% and 76% of its predictions are within reasonable ranges. Only 14% of predictions based on the ACI method are reasonable in D-regions, however, this increases to 55% in B-regions. Similar to the analysis results for beams with transverse reinforcement, the more sophisticated methods tend to be more accurate except for a few cases.

Table 5-4. Summary of the analysis results for beams without transverse reinforcement

Assessment criteria	Method	ACI	AASHTO (MCFT)		*TAMU*
			Simplified	Full	
	ϕ_v	0.75	0.9	0.9	0.75
$\phi_v < \dfrac{V_{test}}{V_{pred}} < 2\phi_v$	D-region	14%	32%	39%	63%
(Overall-Reasonable)	B-region	55%	**87%**	**88%**	**76%**
$\dfrac{V_{test}}{V_{pred}} < \phi_v$	D-region	0%	0%	0%	20%
(Unconservative)	B-region	0%	2%	6%	22%
$\dfrac{V_{test}}{V_{pred}} > 2\phi_v$	D-region	86%	68%	61%	12%
(Overconservative)	B-region	45%	11%	6%	2%

Note: Percentage of reasonable predictions over 75% are bold

5.6 Summary and Key Findings

In this section, the *TAMU* method with an inclined tie for reinforced concrete beams without transverse reinforcement is developed. The single-point cantilever model is used to capture the truss mechanism, whereby a single concrete tie perpendicular to the principal diagonal arch represents the lumped concrete tension field. Formulae to calculate the maximum shear strength are derived using shear deformations of truss and arch actions. To validate the proposed method, the test database of reinforced concrete beams with no transverse reinforcement is assembled and used. The key findings from this section are summarized below:

- The *TAMU* method with an inclined tie shows good agreement with the test result of over 380 beams with both D- and B-regions, demonstrating the ability to predict the maximum shear-carrying capacity of shear-critical beams without transverse reinforcement, regardless of the *a/d* ratio.

- The shear strength ratios, V_{test}/V_{pred}, are evaluated to investigate the effect of design parameters, *a/d* ratio, ρ_L, f'_c, and b, on the accuracy of the *TAMU* method. No trend is found based on any variables, indicating the method properly accounts for a contribution of each variable on the shear strength.

- Overall predictions made by code-based strength analysis methods for beams without transverse reinforcement are exceedingly conservative in D-regions, especially, when $a/d < 2.0$. Generally, all code-based strength methods tend to be more conservative for smaller *a/d* ratios. However, all code-based analysis methods show reasonable predictions in B-regions as they have median values close to 1.0 with a slight conservative aspect and low dispersion.

146

- The distinctly different trend in V_{test}/V_{pred} by the *a/d* ratio found in the code-based methods can be explained by the shear mechanism. The code-based strength analysis methods are derived from the truss action and do not account for the direct arch mechanism. Thus, code-based analysis methods do not capture the shear mechanism well in D-regions where an arch action tends to govern the shear mechanism. Unlike code-based strength analysis methods, the *TAMU* approach considers both compressive arch and tensile attributes, thus providing acceptable predictions in both D- and B-regions.

6. EXPERIMENTAL TEST AND ANALYSIS OF PRESTRESSED CONCRETE BENT CAPS[*]

6.1 Chapter Summary

Accelerated bridge construction using precast bridge systems have several advantages over cast-in-place concrete as it reduces traffic disruption and increases worker safety and quality of concrete. More benefits may be achieved by introducing prestressing to the precast bent caps. To verify the improved performance of prestressed caps, full-scale reinforced concrete (RC) and prestressed concrete (PSC) bent cap subassemblies were tested. The experimental program was designed to investigate the effect of prestressing force, the shear reinforcement spacing, and the added benefits of an interior void within the bent cap. Comparative test results showed superior performance of several solid and hollow PSC bent cap specimens to a benchmark RC specimen.

Advantages included the delay of initial flexural cracking, and overall reduced flexure and shear cracking with the ability to fully close existing cracks upon removal of live load. The spacing of the transverse reinforcement made only marginal difference in performance. When compared to the solid PSC specimens, the voided PSC caps showed similar flexural behavior, but the hollow specimen was more prone to shear cracking and exhibited a more brittle failure model. As each of the specimens approached their ultimate strength capacity, significant diagonal cracking was observed which in turn led to crushing along the principal diagonal arch/strut.

The observed behavior was further investigated using C-STM and *TAMU* analyses. The prestressing force used in PSC bent cap specimens was taken into account for both analyses. The

---

*The experiments described in Section 6.3 of this chapter were part of a large multi-investigation project of which the author was an integral part. Certain parts of that work are adapted herein with permission from Texas A&M Transportation Institute. Full details are given in: Birely, A. C., Mander, J. B., Lee, J. D., McKee, C. D., Yole, K. J., and Barooah, U. R. (2018). "Precast, Prestressed Concrete Bent Caps: Volume 1 Preliminary Design Considerations and Experimental Test Program," *Report No. FHWA/TX-18/0-6863-1*, Texas A&M Transportation Institute, College Station, Texas, USA. https://static.tti.tamu.edu/tti.tamu.edu/documents/0-6863-R1-Vol1.pdf

maximum shear strength and failure locations were predicted and in agreement with the experimental results. The results were also compared with existing code-based methods of analysis which showed more scatter and less accuracy.

6.2 Introduction

The construction of bridge piers is a significant part of overall bridge construction. Historically this process has been rather slow as most designs use cast-in-place (CIP) concrete. Much of this slowness is due to waiting times for concrete curing and certification prior to the erection of the bridge superstructure. Texas Department of Transportation (TxDOT) being aware of such concerns began exploring the use of precast reinforced bent caps to replace the use of cast-in-place reinforced concrete (RC) bent caps in the mid-1990s to reduce construction time. Since then, precast bent caps have become more popular in standard bridges and other special bridge projects in Texas. The introduction of the precast bent cap has brought numerous advantages over CIP bent cap, including 1) accelerated bridge construction, 2) efficient production with high-quality concrete, 3) reduced traffic disruption, 4) accommodation of special construction conditions within harsh environments with difficult access, and 5) less impact on the environment by reducing construction waste.

One further step to improve and maximize the serviceability, durability, and sustainability of bridge substructures may be achieved by introducing prestressing to the precast bent caps. In addition to the abovementioned advantages of precast reinforced concrete, the use of prestressed precast bent caps may improve resistance to cracking under service and also enhance the flexural and shear capacities. With better cracking and flexural resistance, the use of interior voids to reduce weight or reduction of columns may also be achieved.

The behavior of prestressed bent caps for multi-column bridge pier substructures is verified through an experimental analytical program described in this chapter. Special emphasis is placed

149

on: 1) analyzing the shear and flexure-shear interaction within the disturbed regions of the precast prestressed and reinforced bent caps, and 2) comparing the predictive capabilities of code-based shear strength analyses with advanced C-STM computational modeling as well as the limit analysis *TAMU* approach proposed in this research.

6.3   Full-Scale Experimental Investigation

6.3.1   Geometry of the Prototype Bridge Pier Substructure

The performance of full-scale precast bent caps under realistic loading conditions was investigated in this experimental test program. General bridge pier substructures for standard I-girder bridges in Texas have three or four columns, creating an indeterminate structure with negative moments near columns and positive moments near the center of spans. Although design demands are established from beams on knife-edge supports, the column stiffness influences the demands in an actual bent system, and the beam-column connection must provide sufficient strength for the transfer of moment from the beam to the column.

Figure 6-1(a) shows the shear and moment diagrams for a three-column bridge pier seating four-girders. To study the performance of bent caps, the experimental test setup must accurately simulate these demands. For this reason, the test specimens were designed as a full-scale subassembly of an entire pier consisting of the bent cap from the overhang to the second inflection point in the first span and the column from the bent to the inflection point. This region, indicated by a red dashed oval in Figure 6-1(a), allows for experimental evaluation of the performance under both positive and negative moment demands and the transfer of actions from the bent cap to the column. Figure 6-1(b) shows a schematic of the subassembly and the shear and moment demand produced by the loads.
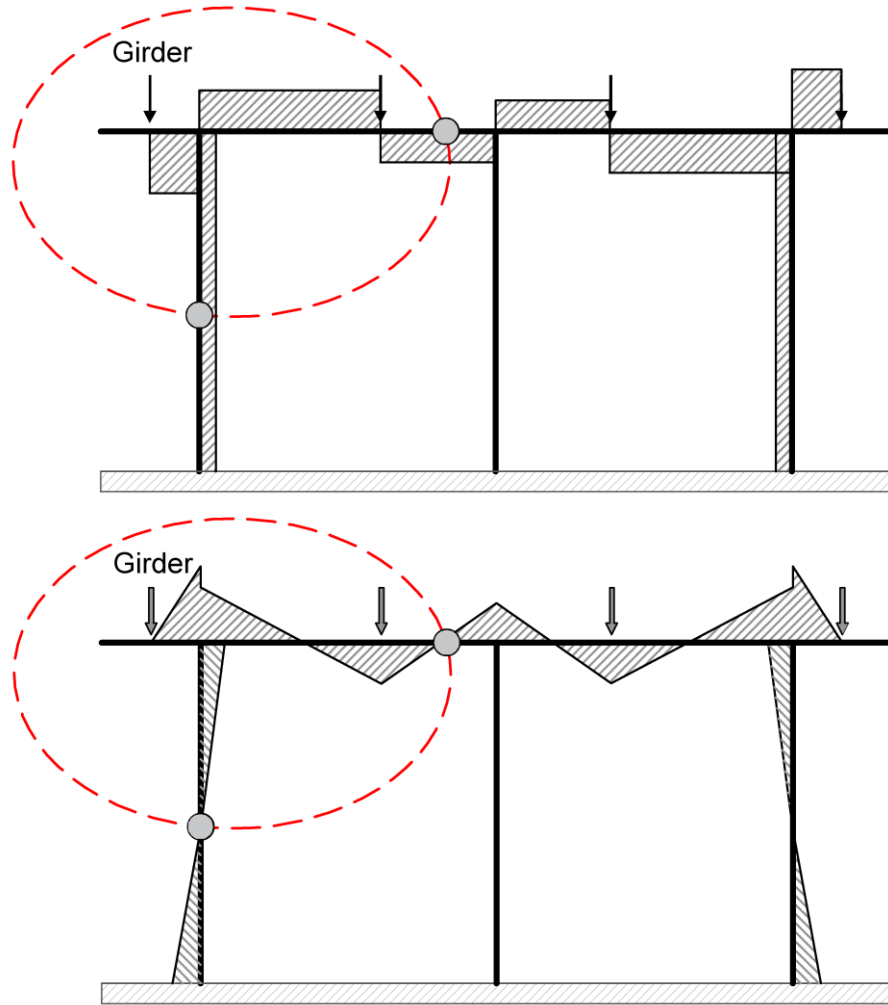
(a) Prototype bridge shear force diagram (top) and moment diagram (bottom)
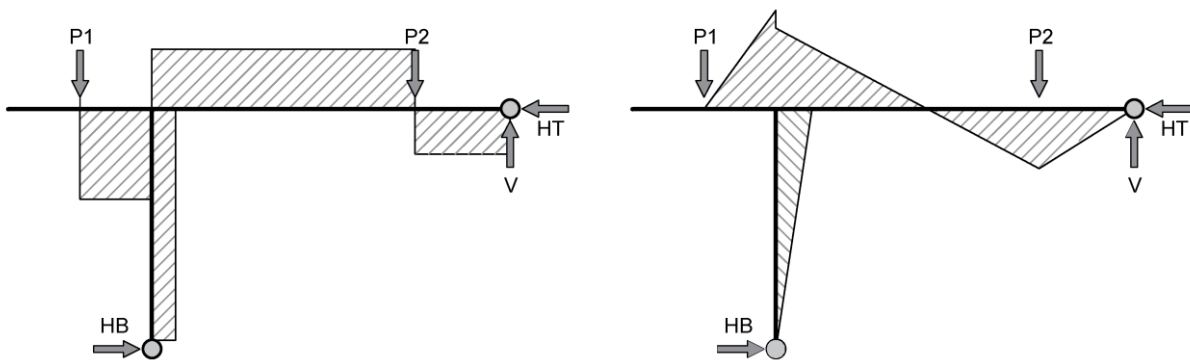
(b) Specimen shear force diagram (top) and moment diagram (bottom)

Figure 6-1. Shear and moment diagrams in prototype bridge and specimen

6.3.2 Experimental Test Setup

The experimental program presented herein consisted of six full-scale subassemblages, tested in two phases. Phase 1 tested one RC bent cap as a reference test and three 16 strand pretensioned bent caps. Phase 2 consisted of two longer specimens, both with 28 strands and interior voids. The present study only discusses Phase 1 specimens as Phase 2 specimens failed in flexure rather than shear. More details regarding the test as well as preliminary designs of bent cap specimens can be found in Birely et al. (2018), Lee et al. (2019), Birely et al. (2020), and McKee et al. (2020).

Figure 6-2 shows the experimental setup and cross-sections for all specimens. The test was conducted at the Texas A&M High Bay Structural and Materials Testing Laboratory (SMTL). The specimens had a bent cap length of 4,877 mm and a column height of 1,920 mm. As shown in the figure, a total of five actuators were used to simulate the actual bridge load applied to bent cap subassemblies. Two top vertical downward actuators, P1 and P2, simulated the girder load. The exterior (P1) and interior (P2) girders were located 610 mm and 2,134 mm from the column center, respectively. The bottom upward vertical actuator, V, was located 1,218 mm from the P2 actuator and acted as the shear at the bent cap inflection point. Horizontal actuators, HT and HB, were attached to horizontal load reaction frames and provided equilibrium of horizontal forces on the specimen.

As shown in Figure 6-2, a 1067 mm square concrete section was tested. Side reinforcement was uniformly distributed to control cracks effectively. There were 16 of 15 mm diameter strands provided in PSC specimens. To compare the overall performance of the PSC bent caps versus the RC bent caps, the RC specimen was designed to have the same steel configuration and similar strength to the pretensioned prototype, leading to the use of 16-D25 bars. A double leg stirrup made of D-16 was used as shear reinforcement for all the specimens.

Figure 6-2. Test setup and cross-section
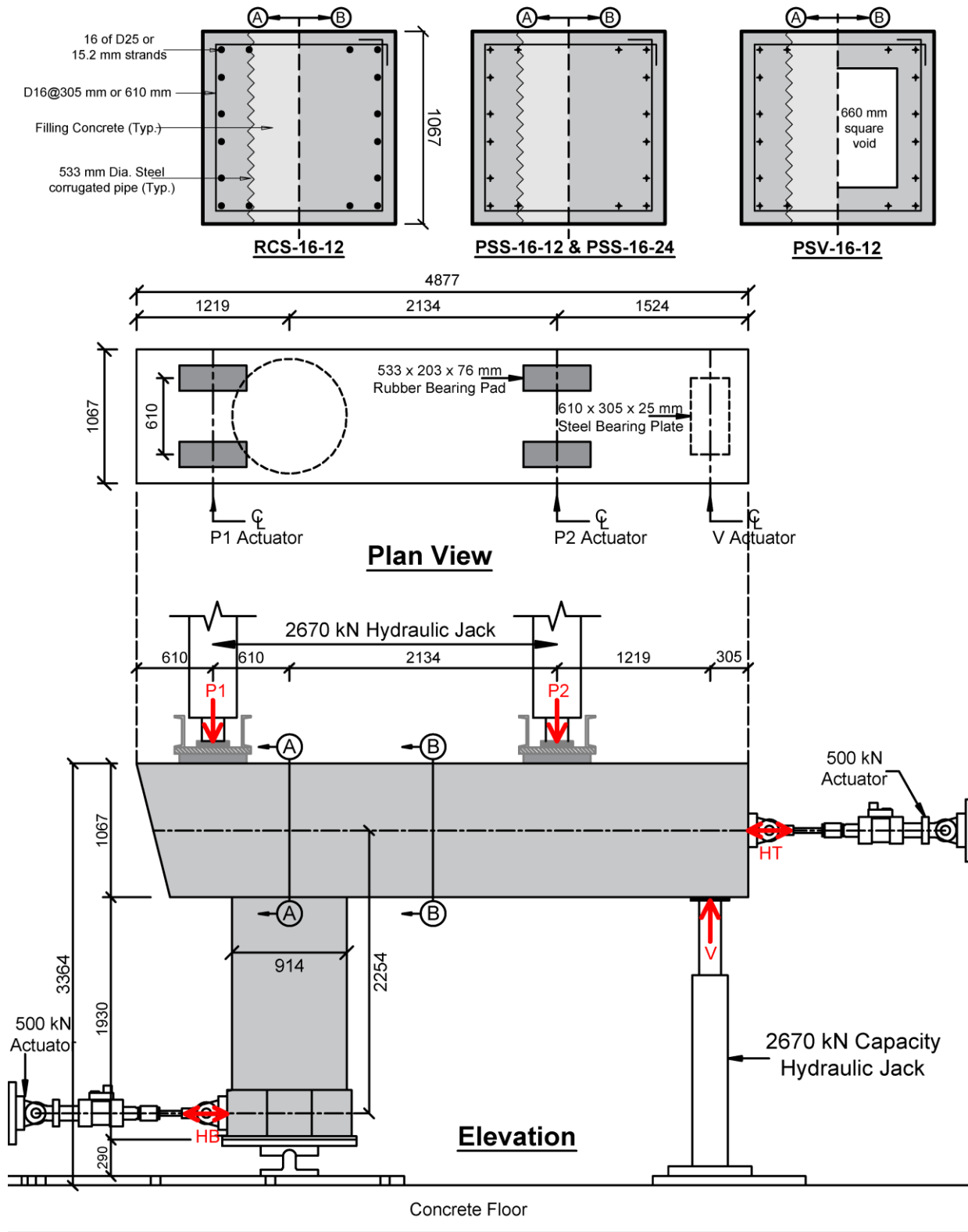
Note: 1 in. 25.4 mm; 1 kip = 4.448 kN

153

6.3.3 Test Matrix

The objective of the test matrix was to investigate a prestressed design, an equivalent RC design, and three design variations on the prestressed design. The considered variations are the transverse reinforcement spacing, a/d ratio ($a/d = 2.0$ for span region and $a/d = 1.5$ for end region shown in Figure 6-3), and the use of an interior void to reduce weight. Table 6-1 shows the names and characteristics of each test specimen. The naming of the specimens has the first set of characters showing the type of specimen (RCS = Reinforced Concrete Solid, PSS = Pretensioned Solid, and PSV = Pretensioned Void). The second set of characters shows the number of reinforcement bars or strands. The third set of characters indicates the spacing of transverse reinforcement provided in the span in inches. As shown in Table 6-1, two-legs of D16 were provided as the transverse reinforcement at 305 mm spacing for all specimens except for PSS-16-24 where 610 mm spacing was used. As-built concrete compressive strengths in Table 6-1 provide the strengths at the time of testing for each separately cast specimen. A 660 mm square interior void was provided in the voided bent cap (PSV-16-12).

6.3.4 Specimen Loading

All specimens were tested under multiple load patterns. The main pattern (Pattern A) generated shear and moment demands characteristics in keeping with the design service and ultimate load demands of the prototype multicolumn bridge bents. Patterns B and E were selected to generate the largest respective positive and negative moment demands permitted by the test setup. Joint opening and closing were conducted to test the connection performance, respectively. Finally, Pattern F was used to fail each specimen by using axial forces in the bent caps emulating side sway. To achieve each load pattern, P1, P2, V, and HT actuators were controlled through a mix of force and displacement control settings. Table 6-2 summarizes the actuator controls for each load pattern.
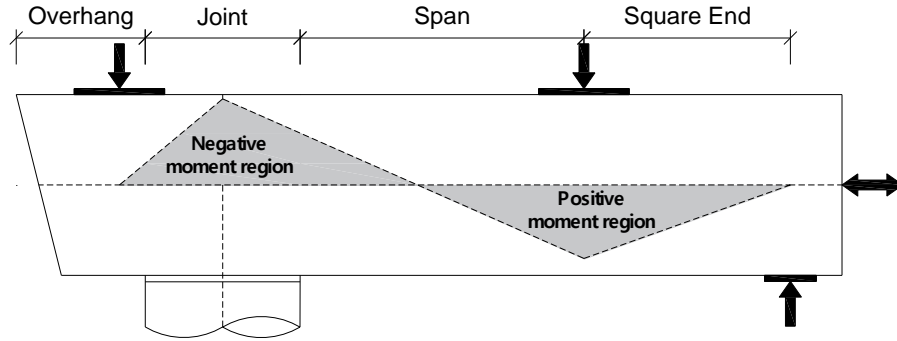
Figure 6-3. Moment region location

Table 6-1. Test matrix

Specimen	f'_c, MPa	Flex. Reinf.	Shear Reinf.	Description
RCS-16-12	38.6	16-D25	2-D16 @ 305 mm	RC design
PSS-16-12	55.2	16-15.2 mm 7 wire strands	2-D16 @ 305 mm	Prestressed design
PSS-16-24	60.8	16-15.2 mm 7 wire strands	2-D16 @ 610 mm	Less shear reinforcement
PSV-16-12	57.8	16-15.2 mm 7 wire strands	2-D16 @ 305 mm	660 mm square interior void

Table 6-2. Actuator control pattern

Load Pattern	P1 (kN)	P2 (kN)	V (kN)	HT (HB) (kN)
(A) Bridge Demands	Max.	Max.	0.48P2	$\Delta = 0$
(B) Max. Positive Moment	0	Max.	0.64P2	$\Delta = 0$
(C) Joint Opening	$\Delta = 0$	0	0	445 (T)
(D) Joint Closing	0	$\Delta = 0$	0	445 (C)
(E) Max. Negative Moment	Max.	$\Delta = 0$	0	445 (C)
(F) Failure	Max.	Max.	Max.	467 (T)

Note: Δ indicates the actuator is controlled by displacement to maintain zero change in displacement; Only compression force is applied in P1, P2, and V actuators

In Pattern A, dead load, P_D, and live load, P_L, were 710 kN and 490 kN, respectively. Service Limit State (SLS) demands were the sum of dead and live loads. The Ultimate Limit State (ULS) demands were based on $1.25 P_D + 1.75 P_L$ in accordance with AASHTO LRFD 3.4.1. Calculated ULS values were rounded up slightly for simplicity, resulting in girder loads of 1,780 kN. The maximum force capacity of the actuators corresponded to 140% ULS.

6.3.5 Experimental Performance

During experimental testing, it was possible to closely observe the specimens for the appearance of cracks. All longitudinal and transverse reinforcement and the corrugated pipe were drawn in pencil on the front face of each specimen prior to the test. The maximum width of each crack was measured using a crack comparator and documented. Figure 6-4 shows the extent of cracking and damage seen at the failure load patterns on the back face and on the most severely damaged region for all specimens, respectively.

In contrast to the reinforced concrete specimen (RCS-16-12) the prestressed bent cap specimens (PSS-16-12, PSS-16-24, and PSV-16-12) each displayed remarkably improved flexural cracking control capacity in both positive and negative moment regions by delaying the onset of the cracking and also limiting the overall crack widths. Only hairline cracks formed in the PSC bent caps under design loads. The voided specimens (PSV-16-12) displayed shear cracks along the interior void in the span prior to reaching to ultimate design loads. Shear-flexure failures were observed in all solid specimens showing severe crack damage along the principal diagonal arch (strut) at the span region in the reinforced bent cap (RCS-16-12) and at the square end region in the prestressed bent caps (PSS-16-12 and PSS-16-24). Failure of voided specimens (PSV-16-12) involved the crushing of concrete near the compression zone under the P2 actuator. Crack maps for each specimen at each load stage are drawn in Figure 6-5 and Figure 6-6.
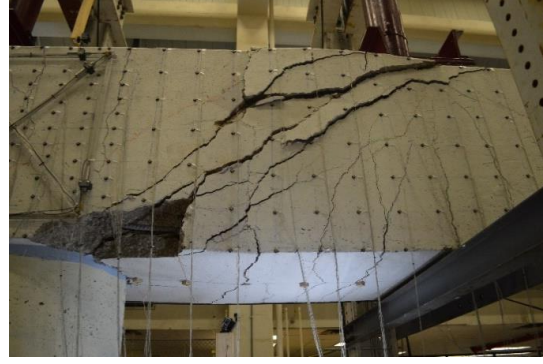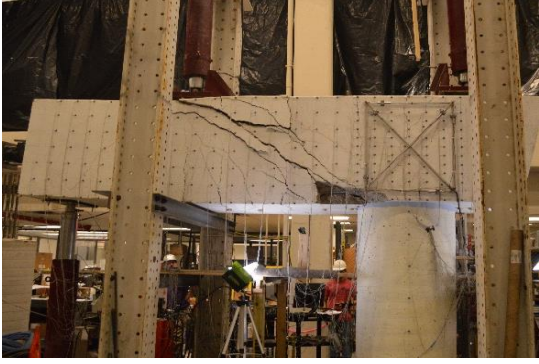
(a) RCS-16-12
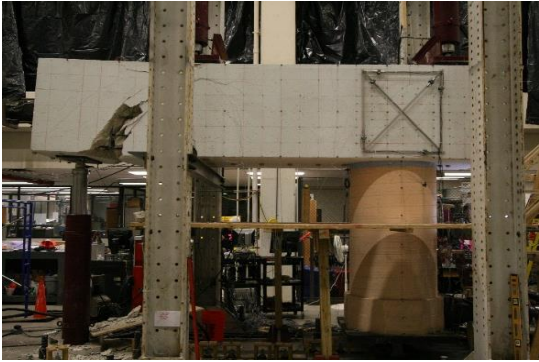
(b) PSS-16-12

(c) PSS-16-24
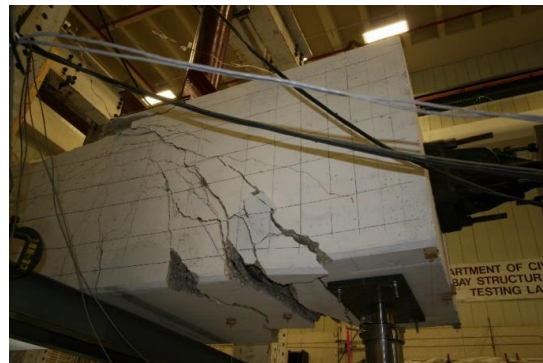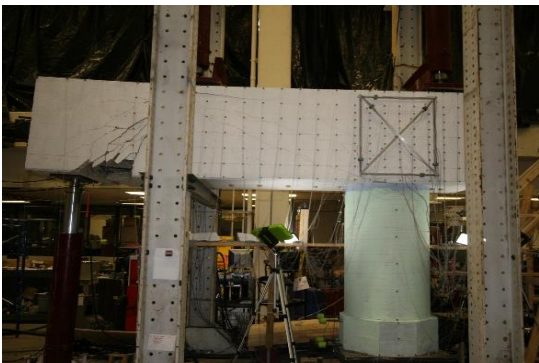
(d) PSV-16-24

Figure 6-4. Visual observation at failure (left: back face and right: failed region)
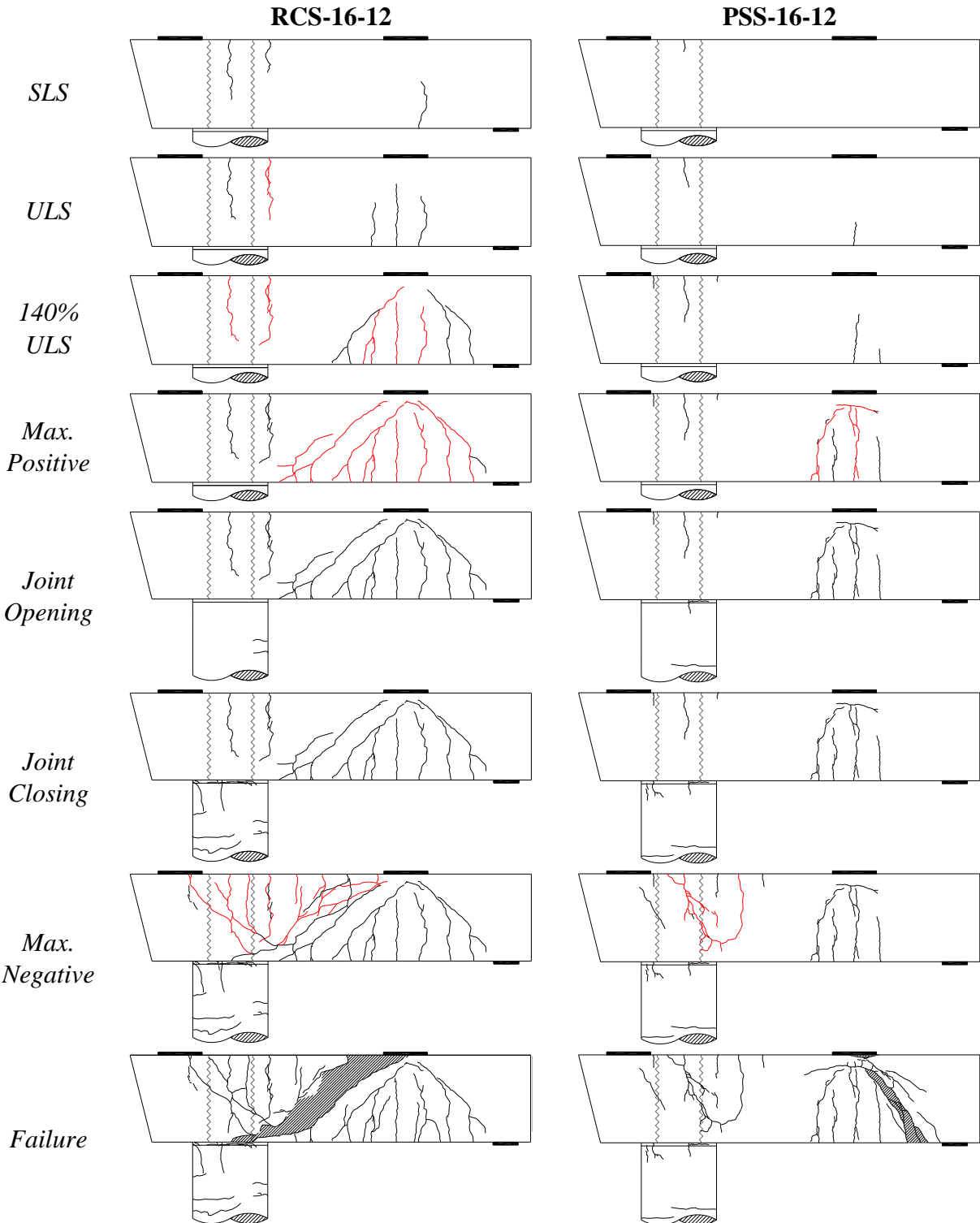
Note: Crack width exceeding AASHTO crack width limit colored in red

Figure 6-5. Crack maps of the reinforced concrete specimen (RCS-16-12) left, compared with the prestressed concrete specimen (PSS-16-12) right
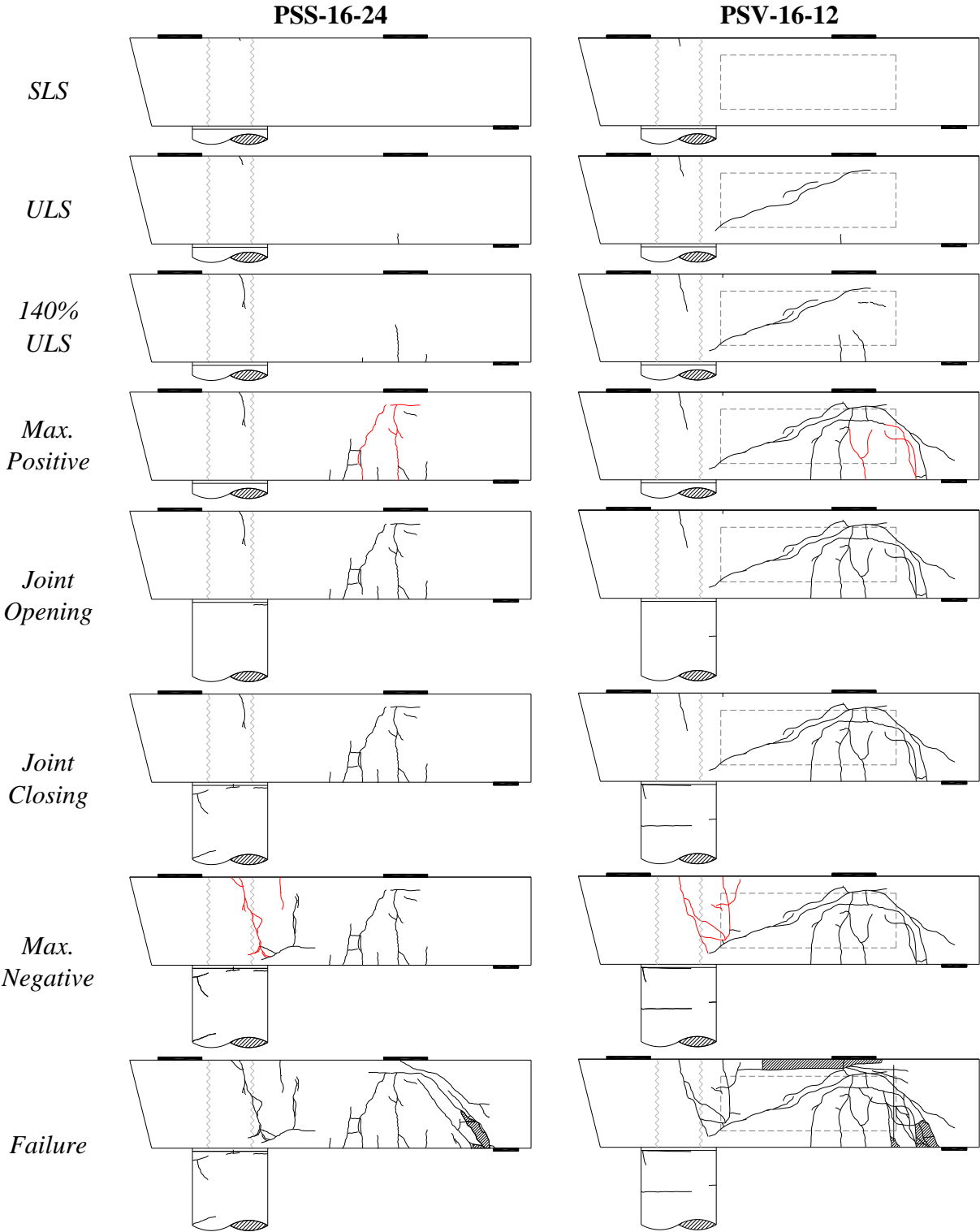
Note: Crack width exceeding AASHTO crack width limit colored in red

Figure 6-6. Crack maps for the prestressed concrete specimens with: the widely spaced hoops (PSS-16-24) left; and the voided specimen (PSV-16-12) right

159

6.3.6　Comparison of Design Parameters

The impact of design parameters is compared based on damage observation in this section. Parameters include a) types of concrete (RC vs. PSC), b) shear reinforcement spacing, and c) the existence of an interior void. Among the six load patterns, two patterns that were used to test the connections were not considered as they do not affect the bent cap behavior.

6.3.6.1　*Impact of Prestressing*

The test results of RC (RCS-16-12) and PSC (PSS-16-12) bent caps are compared to investigate the impact of prestressing force. Both specimens have the same flexural steel layout and shear reinforcement spacing. Concrete strengths were different for both specimens, and this was taken into account in the expected strength calculations.

Table 6-3 summarizes the predicted cracking moment, $M_{cr,pred}$, observed cracking moment, $M_{cr,test}$, and the ratio of them. The observed cracking moments were greater than predicted values except for the negative moment region in PSS-16-12. This might be caused by the nature of the pocket connection, given that the cross-section was hollow in that region. The cracking moments of RCS-16-12 were normalized by multiplying $\sqrt{f_{t,PSC}/f_{t,RC}}$ to consider the difference of concrete tensile strength. PSS-16-12 displayed 16% and 32% higher cracking moment in negative and positive moment regions, respectively, compared to RCS-16-12.

Figure 6-7 presents an overall summary of the front face crack progression. PSS-16-12 had fewer and finer cracks during the whole duration of the test. RCS-16-12 exhibited cracks wider than the AASHTO limit, but PSS-16-12 did not exceed the crack limit at 140 percent ULS demands. Flexure-shear failure was observed in both specimens; however, RCS-16-12 failed in the span region while PSS-16-12 failed in the square end region.

Table 6-3. Flexural cracking summary (RCS-16-12 vs. PSS-16-12)

Specimen	Region	f'_c (MPa)	f_r (MPa)	$M_{cr,test}$ (kN-m)	$M_{cr,pred}$ (kN-m)	$\dfrac{M_{cr,test}}{M_{cr,pred}}$	$\dfrac{M_{cr,test}}{M^*_{cr,pred}}$
RCS-16-12	Span	41.0	2.1	542	430	1.26	-
	End			702	430	1.63	-
PSS-16-12	Span	55.2	2.5	732	945	0.77	1.16
	End	51.4	2.4	1,041	927	1.12	1.32

Note: $M^*_{cr,RC}$ = normalized cracking moment of RC specimen by multiplying $\sqrt{f_{t,PSC}/f_{t,RC}}$ to consider the difference of concrete strength;
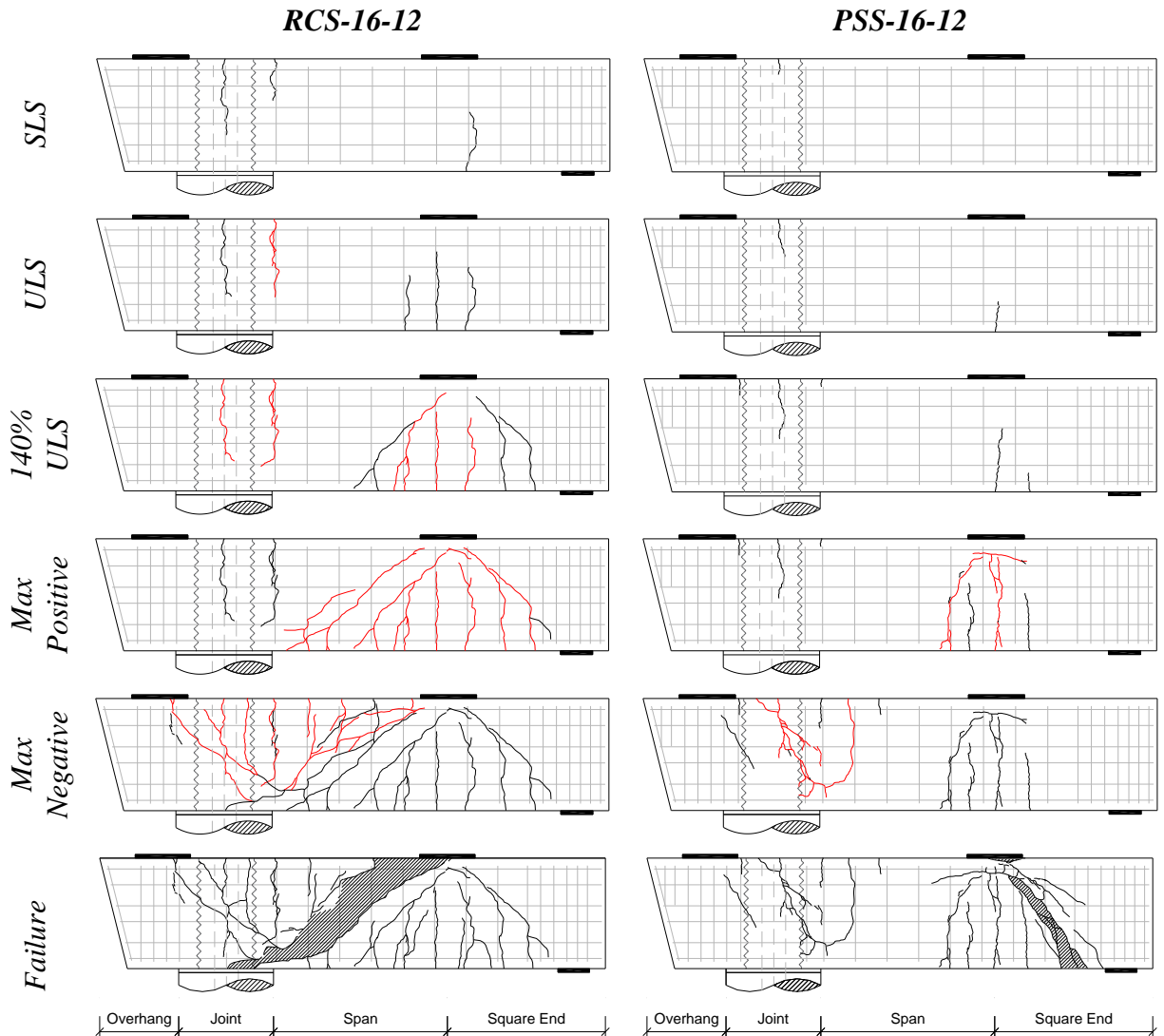
Figure 6-7. Crack progression comparison for RCS-16-12 and PSS-16-12

6.3.6.2   Impact of Shear Reinforcement

This section compares the results of specimens with different transverse reinforcement spacing. To reveal the effect of transverse reinforcement, two specimens were designed with different transverse reinforcement spacing; a) PSC bent cap with 305 mm (12 in.) spacing, PSS-16-12; and b) PSC bent cap with 610 mm (24 in.) spacing, PSS-16-24. The two specimens had the same strand layout and transverse reinforcement detailing.

Figure 6-8 presents the comparison of crack progression and widths of PSS-16-12 and PSS-16-24 specimens based on the visual observation. Figure 6-8(a) compares the crack propagations by various load stages in both specimens. As shown in the figure, the two specimens displayed a similar crack pattern for all loading stages in terms of a number of formed cracks and propagated length. This similar crack pattern was maintained at the end of the test, and both specimens had a flexural-shear failure in the square end region. Thus, no significant differences were observed in crack progression between PSS-16-12 and PSS-16-24.

Flexural crack widths in negative and positive moment regions are compared in Figure 6-8(b). In the figure, the hollow bars indicate the maximum crack width, and solid bars show the average crack width. As shown in the figure, both maximum and average flexural crack widths in PSS-16-24 tended to be slightly wider than those of PSS-16-12 generally, revealing that additional shear reinforcement can prevent cracks from being wider. Shear crack width is not presented here since no shear cracks appeared until failure demands when measuring crack width was not conducted for safety. Although the additional shear reinforcement slightly reduced flexural crack widths, the failure mode and ultimate failure load were almost the same. This result corresponds to the observation from the parameter study in Section 3.5 that providing more shear reinforcement does not necessarily increase the ultimate capacity within D-regions.
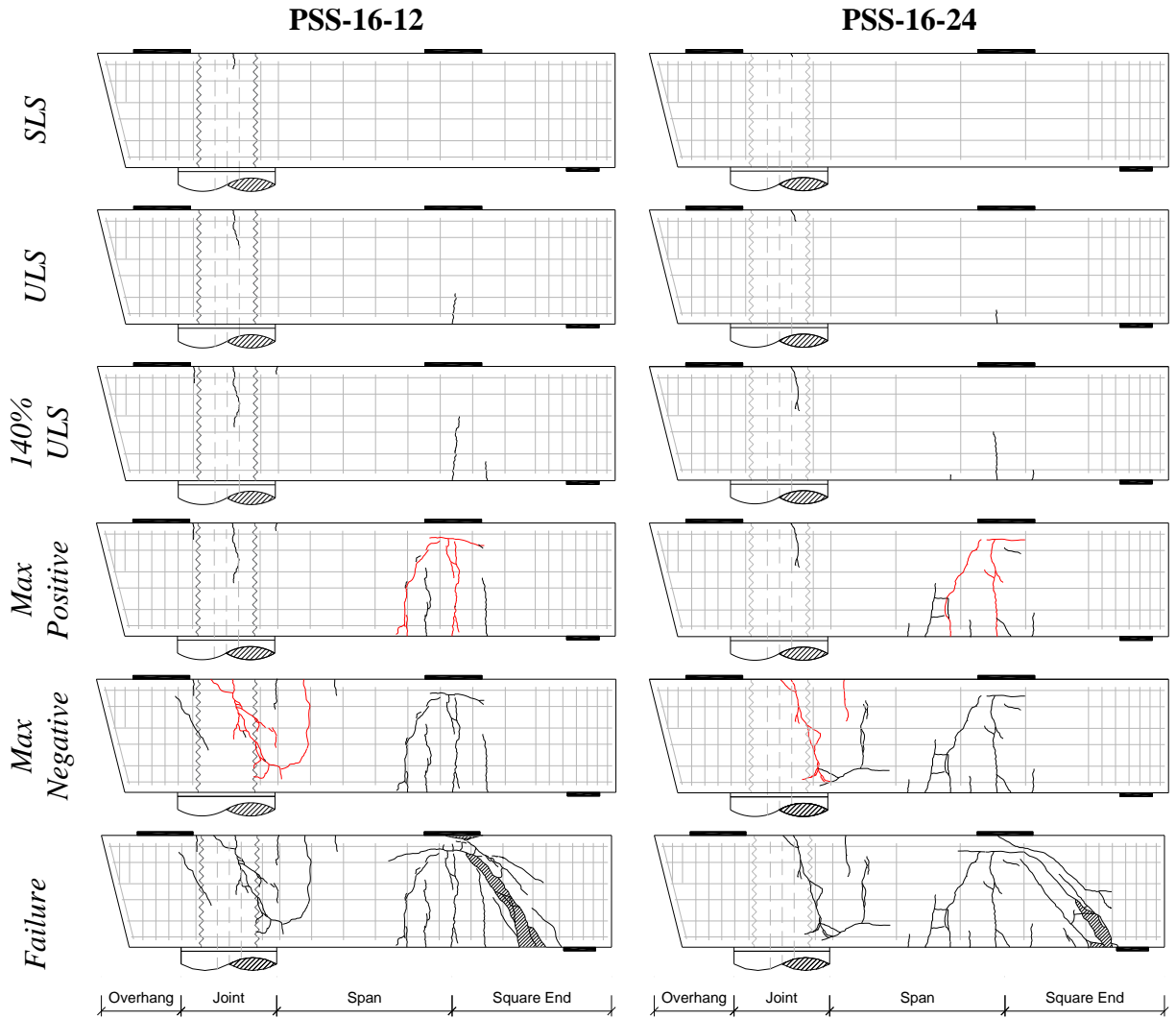
(a) Crack progression comparison for PSS-16-12 and PSS-16-24
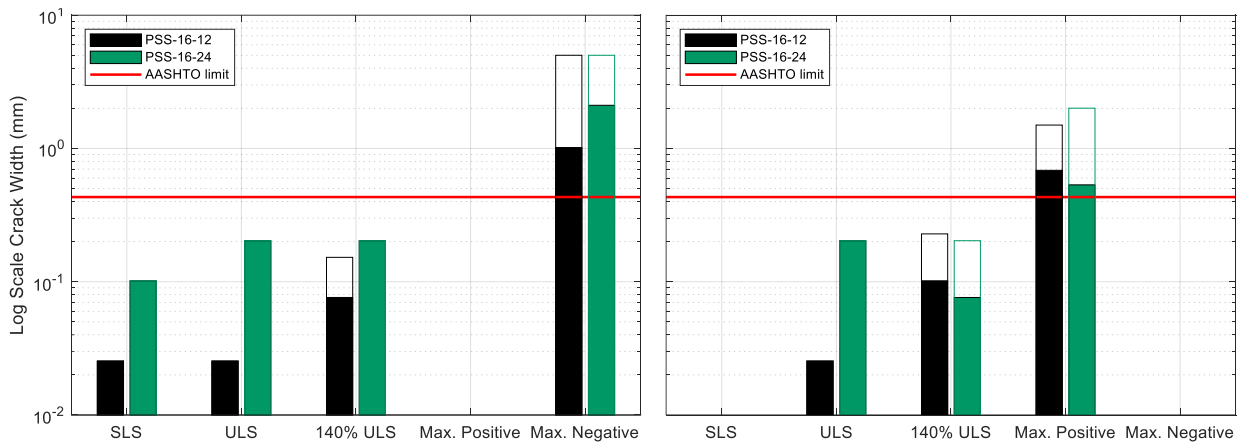
Negative moment region *Positive moment region*

(b) Crack progression comparison for PSS-16-12 and PSS-16-24

Figure 6-8. Crack progression comparison for PSS-16-12 and PSS-16-24

163

6.3.6.3 Impact of Interior Void

To evaluate the impact of an interior void, the test results of PSS-16-12 and PSV-16-12 specimens are compared. PSV-16-12 was designed in this experimental program to examine if PSC bent caps with a void can resist shear and moment demands, and control the cracking as effective as solid PSC bent caps. For this reason, all design detailing such as strand layout, shear reinforcement spacing, and end region detailing were the same for these two specimens, and the only difference was the existence of the interior void. Thus, it was thought that any differences in the results of both specimens were caused due to the interior void.

Figure 6-9(a) provides the comparisons of crack progression in the bent caps. As shown in the figure, both specimens showed a similar pattern of flexural cracking, but shear cracks formed along the interior void in PSV-16-12. The shear cracks were developed following the principal diagonal compression strut in both the span and square end regions as the applied load increased. Both specimens exhibited similar peak load carrying capacities under failure load, even though the square end regions were both severely damaged. At failure, concrete crushing occurred in the square end region in both specimens, but additional concrete crushed along the interior void line in PSV-16-12, resulting in a more abrupt decrease of the load-carrying capacity. Details of damages of these two specimens at failure can be found in Figure 6-4.

Crack width comparisons between PSS-16-12 (solid) and PSV-16-12 (voided) were made based on the type and location of cracks a) flexural crack in negative moment region; b) flexural crack in positive moment region; and c) shear cracks. Figure 6-9(b) summarizes each load case. In the figure, similar flexural crack formation, and average and maximum crack widths were observed in both specimens, but shear cracks formed only in the voided specimen.
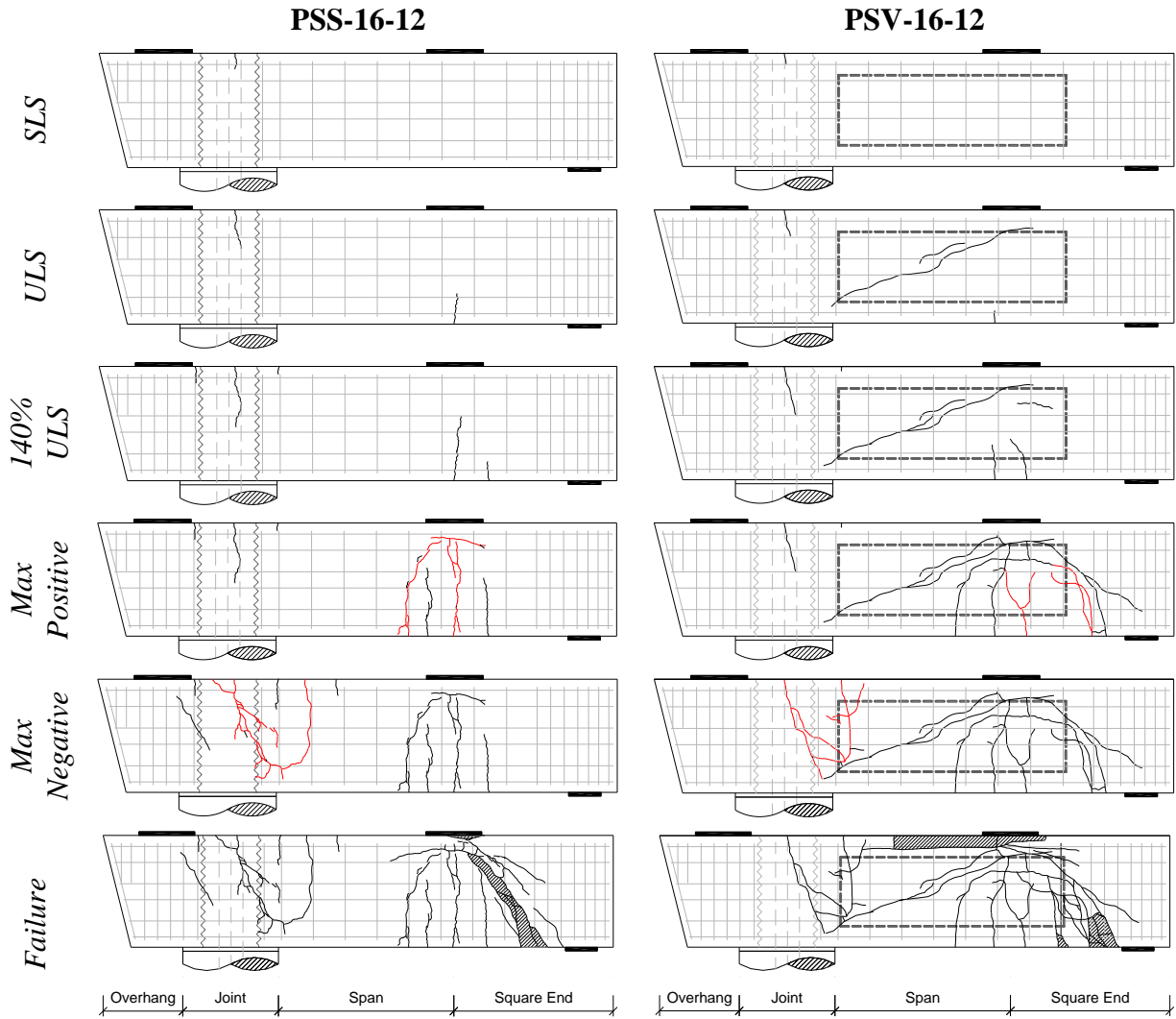
164

(a) Crack progression comparison for PSS-16-12 and PSV-16-12

Negative moment region   *Positive moment region*   *Shear crack*
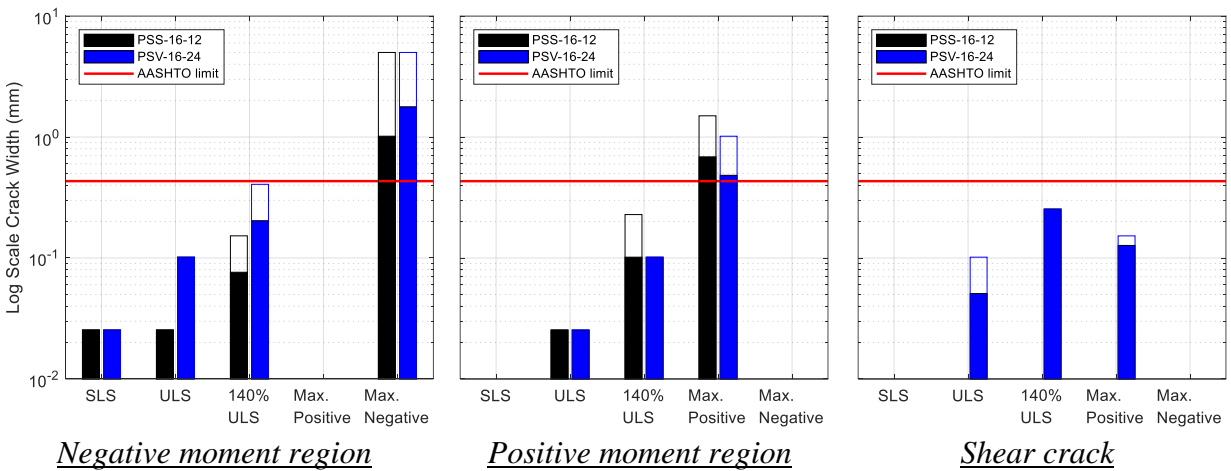
(b) Crack progression comparison for PSS-16-12 and PSV-16-12

Figure 6-9. Crack progression comparison for PSS-16-12 and PSV-16-12

6.4   Application of C-STM

The computational displacement-based Compatibility Strut and Tie Method (C-STM) analysis is used herein to assess the bent cap specimens as tested. From the test observation, it was found that all specimens failed along the diagonal arch (strut) either in the span or end region. The C-STM considers this type of failure mechanism as the failure of the principal diagonal concrete arch due to the softening effect by the transverse principal tensile strain as described in Figure 6-10(a). Based on Karthik et al. (2017), in the C-STM analysis, the concrete softening coefficient is taken into account by:

$$\zeta = \frac{1}{1 + 0.25|\varepsilon_1/\varepsilon_2|} \tag{6-1}$$

where ζ = concrete softening coefficient; ε_1 = principal tensile strain acting perpendicular to the principal diagonal arch and this is obtained using a dummy member in the C-STM analysis; and ε_2 = principal compressive strain in the diagonal concrete strut member;

The unconfined concrete model in Figure 6-10(b) is used for the principal diagonal arch and strut members in the C-STM model where f'_c = concrete compressive strength; ε_c = concrete strain at maximum strength; and ε_{cu} = concrete strain at crushing.

Based on Karthik et al. (2016), the prestressing effect is appropriately accounted for by applying external loads and modifying a constitutive model of prestressed strand. The modified stress-strain relation of strand is presented in Figure 6-10(c) where f_{py} = yield stresses; ε_{py} = yield strain; f_{ps} = prestressing stresses; ε_{ps} = prestrain corresponding to f_{ps}; and f_{pu} = ultimate stresses. It is noted that $0.6f_{pu}$ is used as prestressing stresses, f_{ps}, after losses in the analysis.

(a) Softening in the diagonal arch

(b) Softend concrete model
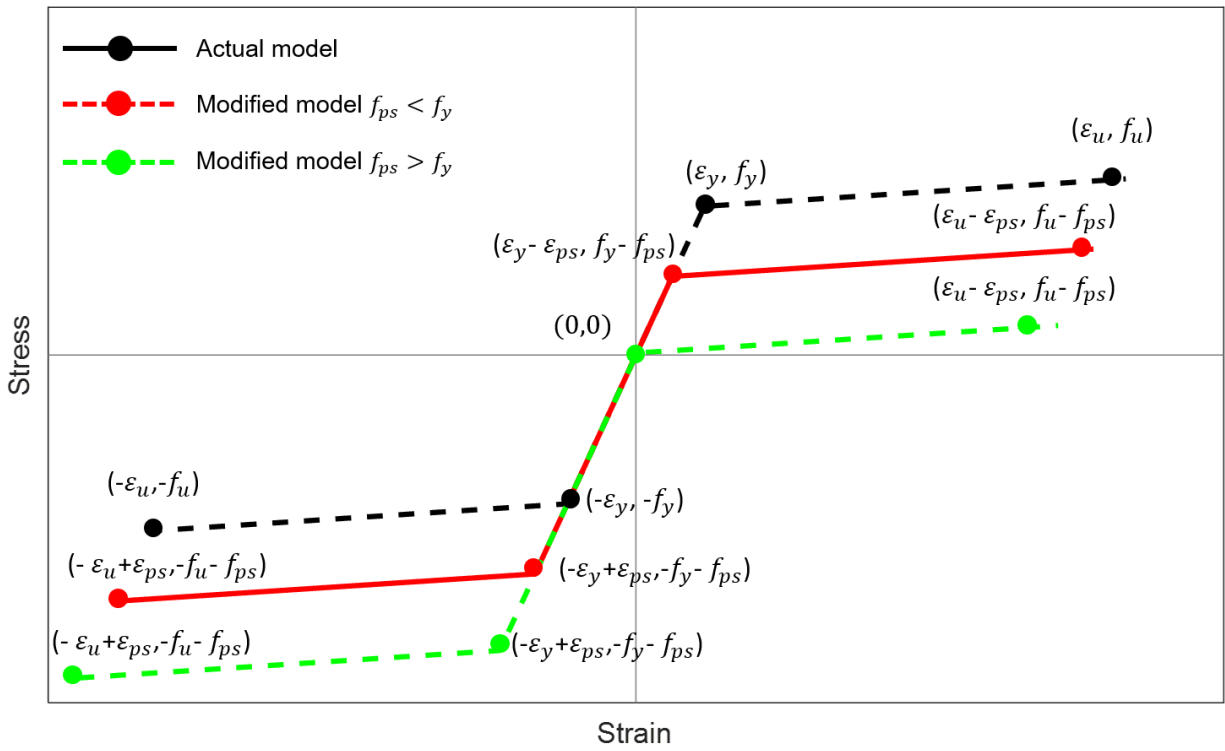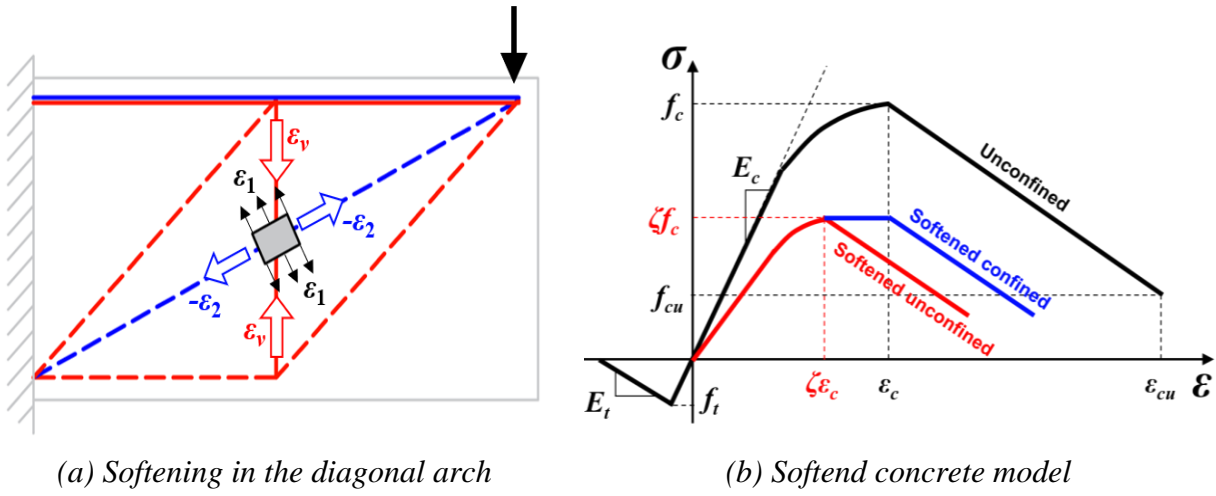
(c) Modified model for prestressed strand to account for prestressing effect

Figure 6-10. Softening effect and constitutive models used in C-STM analysis

All the specimens are analyzed using two load patterns: 1) bridge demand, and 2) failure demand. These two load patterns are selected to investigate overall behavior under actual bridge demand and the maximum capacity of bent caps, respectively. In the test, actuators were manipulated by force and displacement control as needed to achieve the target load and these loads are simulated in the C-STM modeling according to Table 6-2.

Figure 6-12(a) shows the truss and arch action of the C-STM model adapted in the analysis. This C-STM model is implemented using the nonlinear analysis program, *OpenSees* v. 3.2.2 (2020). Based on the modeling procedure and guidelines described in Scott et al. (2012a), the C-STM geometry and member axial rigidities are established. In this test, principal diagonal concrete arches are formed in three regions: 1) the overhang region, 2) the span region, and 3) the end region as shown in the figure. As the arch in the overhang region was small ($a/d = 0.35$), it is assumed that the force is transferred only by the arch action as truss action does not contribute significantly in this region.

Figure 6-12(b) presents cross-sections of the four specimens along with their corresponding distribution breadths of arch and truss action. The relative contribution of arch and truss action is determined by an arch breadth scalar, η, based on Scott et al. (2012a). The arch breadth scalar differs by not only the ratios of longitudinal and transverse reinforcement but also geometry, a/d ratio. Thus, span and end regions have respective arch breadth scalars even though they have the same cross-section. Arch and truss widths are provided in the figure for each specimen. The details of the elevation and cross-sections are previously provided in Figure 6-2, and material properties presented in Table 6-1 are used in the analysis.

(a) Bent cap model used to for C-STM
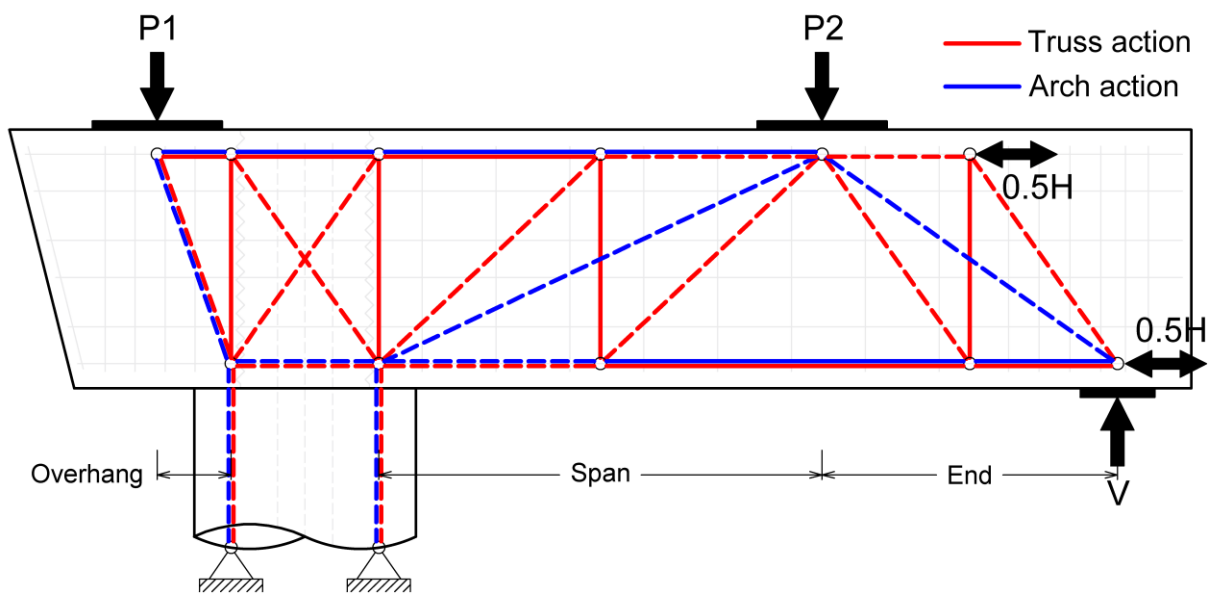
| Span : | 233mm | 602mm | 233mm | 233mm | 600mm | 233mm | 197mm | 674mm | 197mm | 89mm | 229mm | 89mm |
| End : | 240mm | 587mm | 240mm | 241mm | 585mm | 241mm | 217mm | 633mm | 217mm | 92mm | 223mm | 92mm |
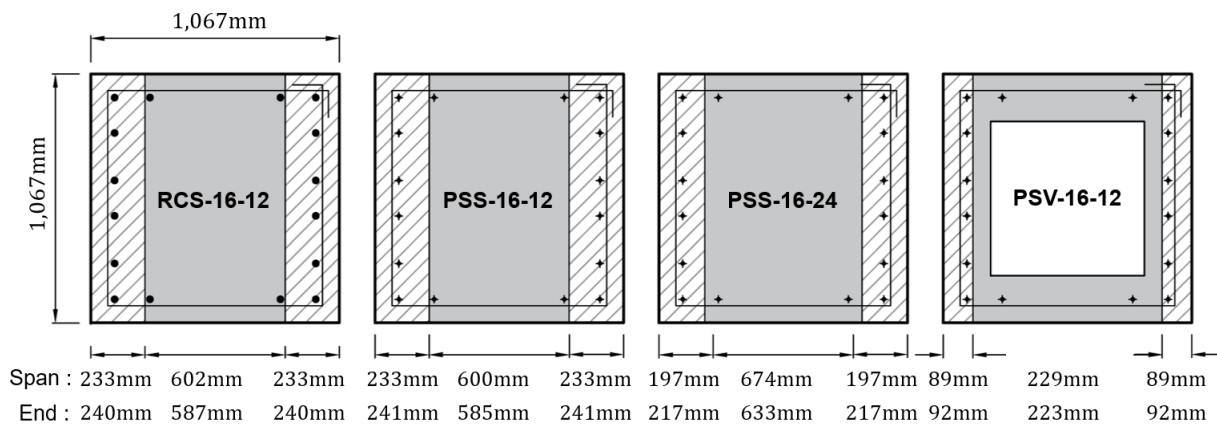
(b) Cross-section with distribution breadths of arch and truss

Figure 6-11. Representative C-STM for bent cap subassemblies

6.4.1 C-STM Analysis Results

6.4.1.1 Bridge Demand

Figure 6-12 presents the C-STM analysis results using the "bridge demand" loads. For this load case, P1 and P2 were increased simultaneously and V was set to be V = 0.48P2. Both actuators providing H had their displacements locked and served as a horizontal reaction. The C-STM modeling accounted for this load configuration. Figure 6-12(a) shows maximum actuator forces that would fail each specimen under the bridge load pattern. The line width and color drawn along C-STM members represent the magnitude of force applied to each member. As shown in the figure, a significant shear force was transferred through the principal diagonal arch in compression while only limited force was transferred to the truss members. All specimens are predicted to fail in the span region as indicated with a red point. For all specimens, the predicted failure loads exceed the maximum achievable force under this load configuration so that no failure was expected under this load pattern. This corresponds to the test observation as no specimen failure was observed during the "bridge demand" load case.

Figure 6-12(b) provides the force-deformation plot from the C-STM analysis for all the specimens. Since a force-controlled test was conducted without a reference point, the force-displacement relation was not obtained from the test. Thus, a direct comparison was not made between the C-STM analysis and the test result. Based on the force-displacement response from the C-STM, more ductile behavior is expected in the RC specimen while the PSC specimens have more rigid behavior due to the prestressing force. More ductile behavior of the RC specimen was evident in the test with significant crack formations. No difference between PSS-16-12 and PSS-16-24 is found in the analysis, implying a minor effect of shear reinforcement in D-regions. This corresponds to the test results and also findings in Section 3.5. The voided bent cap is expected to fail earlier with more ductile behavior than solid bent caps due to the reduced stiffness.
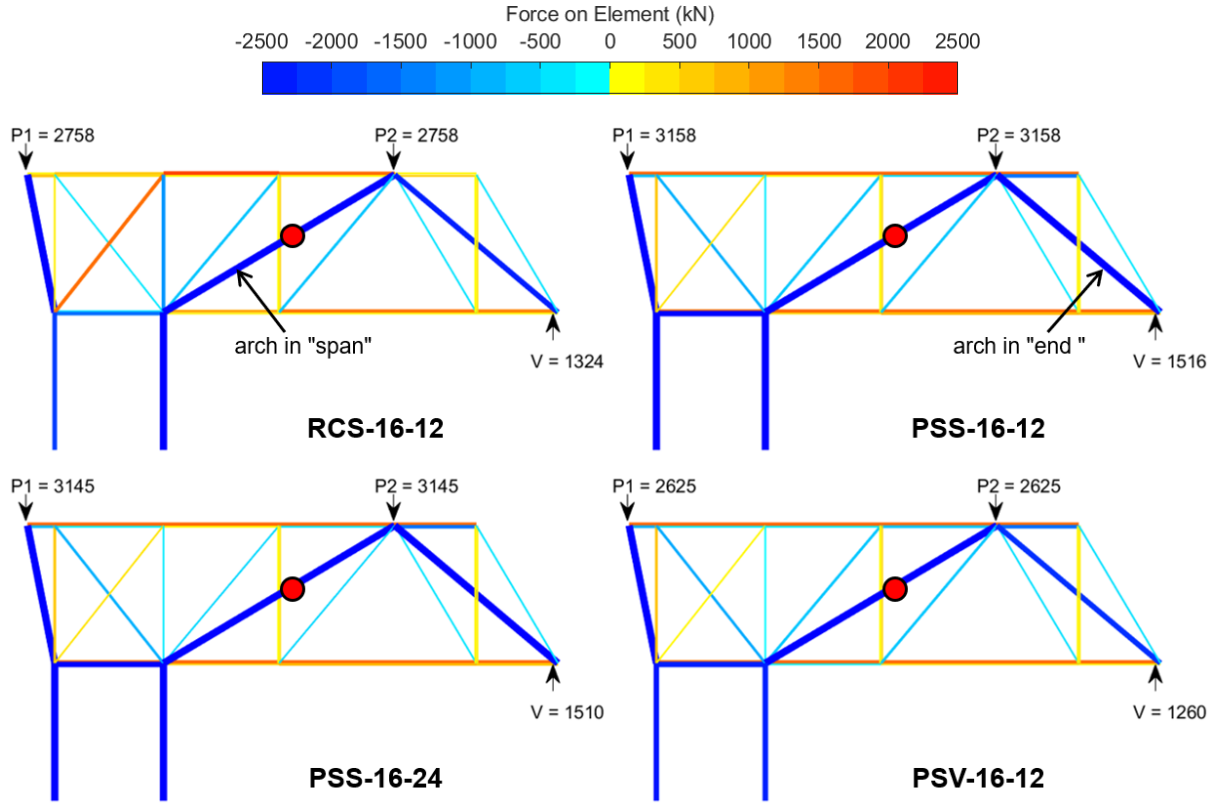
(a) Expected external and interior forces at failure
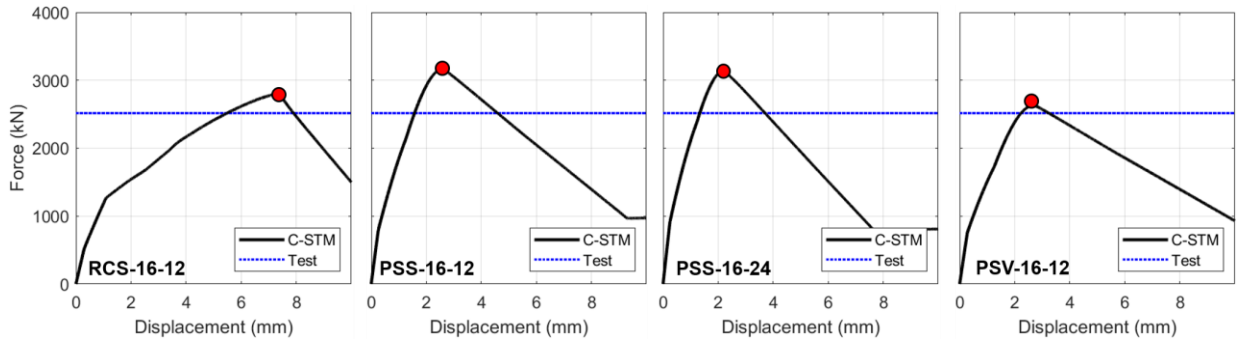
(b) Force vs. displacement beneath force P2
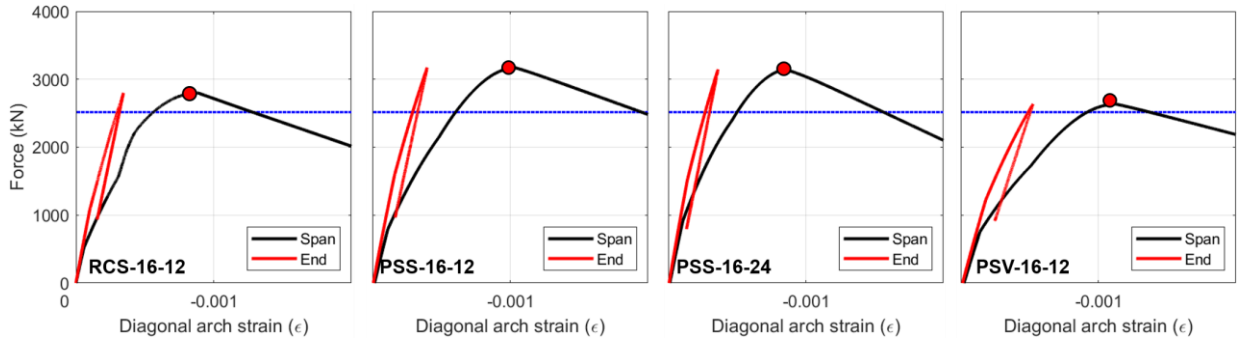
(c) Force vs. diagonal arch strain

Figure 6-12. Analysis results of all specimens under bridge demand

Figure 6-12(c) shows the force vs. strain of principal diagonal arch plots. Strains of both diagonal arch members in span and end regions are presented in black and red lines, respectively. As shown in the figure, the maximum load-carrying capacity is achieved when the diagonal concrete arch in the span region reaches the maximum strength. The displacement controlled-analysis captures the post-peak behavior of the specimens, including the descending branch due to the concrete arch. Overall PSC bent caps have higher strains at the peak load compared to the RC bent cap, and this is because of higher concrete softening coefficient, ζ, due to the prestressing effect. Also, the voided bent cap experiences a higher strain at the peak load than solid bent caps, due to the more effective prestressing force by the reduced area.

6.4.1.2   Failure Demand

The C-STM analysis results with the failure load demand are presented in Figure 6-13. To cause failure in each specimen, actuators P1, P2, HT (tension) were set to force control at their respective maximum load capacities while V was set to displacement control acting as a reaction in the test. Control of V was changed to force control near the final stages of this load pattern to increase the force provided by P2. Therefore, the ratios of V to other external forces (P1, H, and V) are differed by each specimen. Due to the different force ratios, it may not be appropriate to compare specimens directly. However, the maximum load-carrying capacity obtained from the C-STM can be compared with the experimental results.

Figure 6-13(a) shows the maximum loads of four actuators at the moment of failure predicted by the C-STM analysis. As mentioned earlier, each test has different ratios of P2 to other actuators and the C-STM analysis is conducted using the ratios found at the moment of failure in the test.

Based on the C-STM analysis, the failure may occur in the span region for the RC specimen and in the end region for the other PSC specimens, unlike the bridge demand in which all specimens may fail in the span region. Due to the large ratio of V to P2, more forces are applied in the end region, resulting in the failure in this region for PSC specimens. The predictions of failure locations coincide with the test observation as all the PSC specimens failed in the end region and the RC bent cap failed in the span region.

Figure 6-13(b) presents force and displacement curves for all specimens along with the maximum P2 load achieved in the test. As shown in the figure, the predicted maximum loads from the C-STM analysis are in good agreement with the measured peak loads. Since this is a displacement-controlled analysis model for the indeterminate structure, the analysis stops when the principal diagonal concrete arch reaches its maximum softened strength and loses its capacity. Thus, post-peak behavior is not obtained. Note the displacement at where P2 is applied is shown in the force-displacement curve, but no meaningful conclusion can be made as the ratios of P2 to V vary by each specimen.

The relationship of force vs. diagonal arch strain is plotted in Figure 6-13(c). Due to the large V to P2 ratio (indicated in Figure 6-13a), more shear force is applied in the end region, and the failure of the diagonal arch is expected in the end region for the PSC bent caps. Higher concrete softening coefficients are evident in the PSC specimens due to the prestressing effect, especially the voided bent cap (PSV-16-12) with the reduced section area.
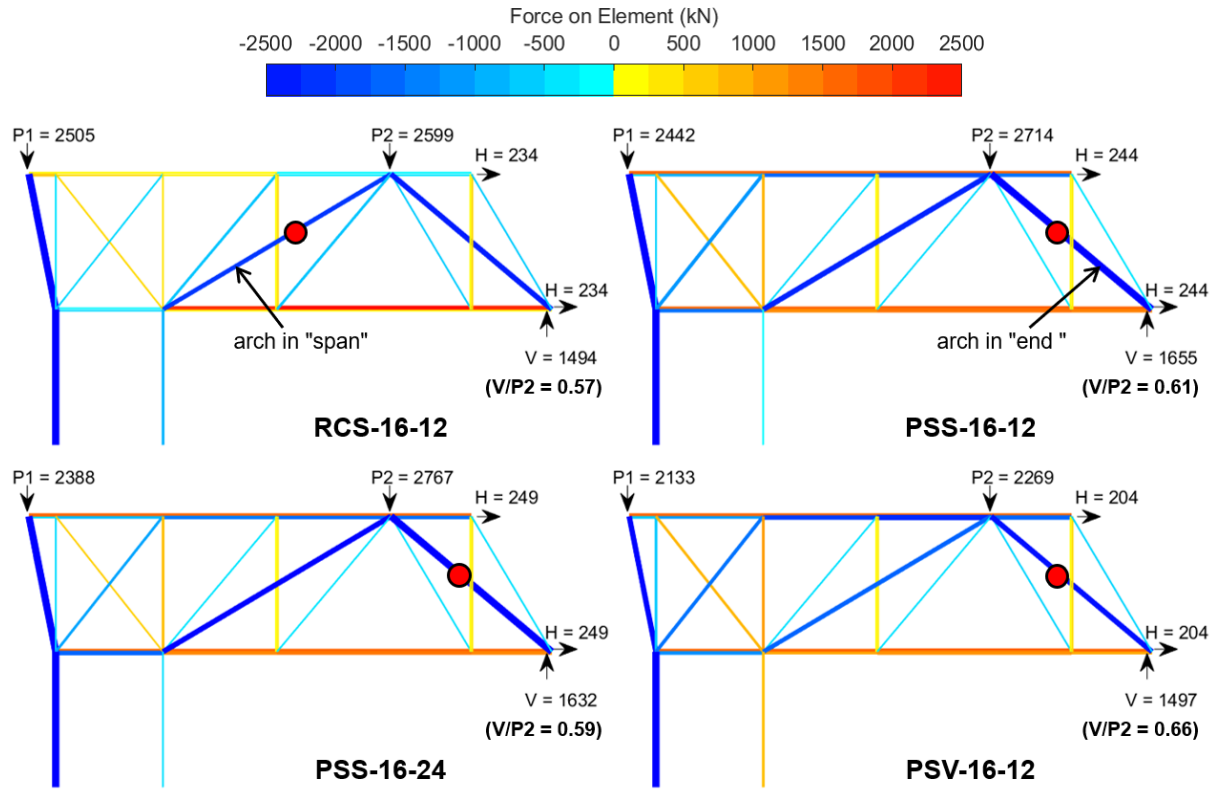
(a) Expected external and interior forces at failure
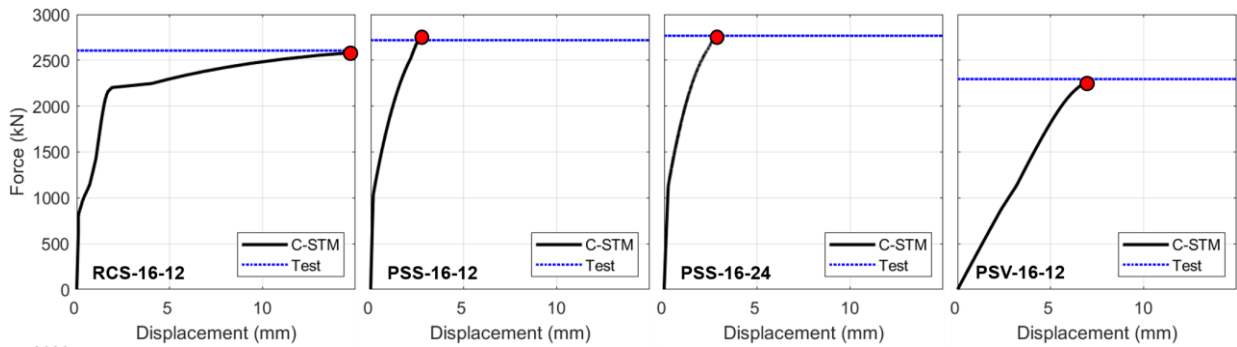
(b) Force vs. displacement beneath force P2
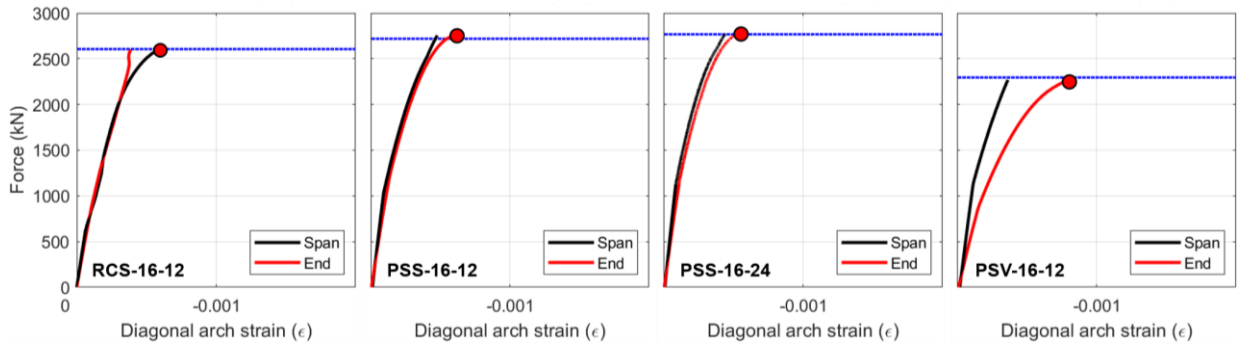
(c) Force vs. diagonal arch strain

Figure 6-13. Analysis results of all specimens under failure demand

174

6.5 Application of Truss-Arch Model Unified (*TAMU*)

The ultimate strengths of the bent cap specimens in the experimental program are predicted herein using the *TAMU* analysis. The *TAMU* is a strength analysis method to estimate the maximum load-carrying capacity of the shear-critical beams. Since the specimens have the a/d ratio of 2.0 and 1.4 for span and end regions, respectively, and failed by flexure-shear interaction along the principal diagonal arch, the use of the *TAMU* method for them is appropriate. The procedures and formulae to implement the *TAMU* analysis are summarized as follows.

The limit load governed by the critical diagonal arch/strut is calculated by:

$$V_n^{arch} = \frac{3}{8} \frac{\zeta \beta_1 f'_c b_w d}{\left(1 + \frac{\rho_v f_{yh}}{\rho_L f_y} \cot^2 \alpha\right)} \tan\alpha \left(1 + \frac{\psi_{arch}}{\psi_{truss}}\right) \qquad (6\text{-}2)$$

where V_n^{arch} = maximum nominal shear capacity of the principal diagonal arch; ζ = concrete softening coefficient; β_1 = ratio of the depth of the equivalent uniformly stressed compression zone; f'_c = concrete compressive strength; b_w = effective width of beam; d = effective depth; a = shear span length; ρ_L = volumetric ratio of longitudinal steel to concrete; ρ_v = ratio of transverse steel area to area of concrete for hoop spacing; f_y = yield strength of the longitudinal steel; and f_{yh} = yield strength of the transverse steel.

The concrete softening coefficient is a function of the principal strain ratio as:

$$\zeta = \frac{1}{1 + 0.25|\varepsilon_1/\varepsilon_2|} \qquad (6\text{-}3)$$

where ε_1 = principal diagonal tensile strain transverse to the axis of the arch; and ε_2 = principal diagonal compressive strain at the center of the arch.

From Mohr's circle analysis, the principal strain ratio $\varepsilon_1/\varepsilon_2$, is obtained by:

$$\left|\frac{\varepsilon_1}{\varepsilon_2}\right| = \left(\tan^2\alpha + \frac{|\varepsilon_v/\varepsilon_2|}{\cos^2\alpha}\right) \tag{6-4}$$

where $\varepsilon_v/\varepsilon_2$ the ratio of transverse strain to principal compressive strain given by:

$$\left|\frac{\varepsilon_v}{\varepsilon_2}\right| = \frac{0.375}{\rho_v n}\left(\frac{\rho_L f_y}{\rho_L f_y + \rho_v f_{yh}\cot^2\alpha}\right)\tan^2\alpha\left(\frac{\psi_{arch}}{\psi_{truss}}\right) \tag{6-5}$$

where ψ_{arch} and ψ_{truss} are the arch and truss mechanism flexibility coefficients. such that:

$$\psi_{arch} = \frac{\cot^2\alpha}{\rho_L n} + \frac{8}{3\sin^2\alpha}\left(1 + \cot^2\alpha\frac{f_{yh}\rho_v}{f_y\rho_L}\right) \tag{6-6}$$

$$\psi_{truss} = \cot^2\alpha\left(\frac{5k + \rho_L n}{8k\rho_L n}\right) + \frac{\tan^2\alpha}{\rho_v n} + \frac{\sqrt{8 + 16\tan^2\beta}}{\sin^3\beta\cot\alpha}\left(\frac{f_y\rho_L}{f_{yh}\rho_v}\tan^2\alpha + 1\right) \tag{6-7}$$

in which β = concrete strut angle in truss mechanism; and k = elastic compression zone coefficient defined by:

$$k = \sqrt{(\rho_L + \rho'_L)^2 n^2 + 2\left(\rho_L + \left(\frac{d'}{d}\right)\rho'_L\right)n} - (\rho_L + \rho'_L)n \tag{6-8}$$

where d' = depth from the extreme compression fiber to the centroid of the compression reinforcement; ρ'_L = ratio of compression reinforcement; and n = modular ratio of steel to concrete.

These flexibility coefficients are from unit displacement analyses for the arch and truss computation. Displacements for the unit load for the arch and truss mechanisms are given by:

$$\delta_{arch} = \frac{a}{E_c b_w d}\psi_{arch} \tag{6-9}$$

$$\delta_{truss} = \frac{a}{E_c b_w d} \psi_{truss} \tag{6-10}$$

Figure 6-14 shows strains induced by shear force and axial force, respectively. As shown in Eq.(6-3), the concrete softening coefficient, ζ, is determined by the principal strain ratio, $\varepsilon_1/\varepsilon_2$. The *TAMU* analysis uses Eq. (6-4) to estimate the principal strain ratio; however, this equation is derived from the shear mechanism in Figure 6-14(a), so that only strains caused by shear force are taken into account. Given that the axial force can also cause a significant change to the principal strain ratio due to axial elongation and lateral contraction as shown in Figure 6-14(b), additional strains by the axial force need to be addressed. The changes in the principal strain ratio due to the axial force, P, can be inferred by using plane strains, ε_x and ε_y in Figure 6-14(b). In elastic range, the longitudinal strain by the axial force is given by:

$$\varepsilon_{x\_P} = \frac{P}{b_w h E_c} \tag{6-11}$$

where ε_{x_P} = longitudinal strain by axial force; P = axial force (or prestressing force) applied to the member in the longitudinal axis; b_w = member width; h = member height; and E_c = elastic modulus of concrete.

Using Poisson's ratio, the lateral strain due to the longitudinal contraction is inferred as:

$$\varepsilon_{y\_P} = -\nu \varepsilon_x = -\frac{\nu P}{b_w h E_c} \tag{6-12}$$

where ε_{y_P} = transverse strain by axial force; and ν = Poisson's ratio
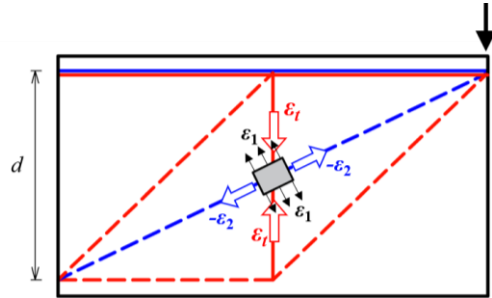
(a) strains induced by shear force, V
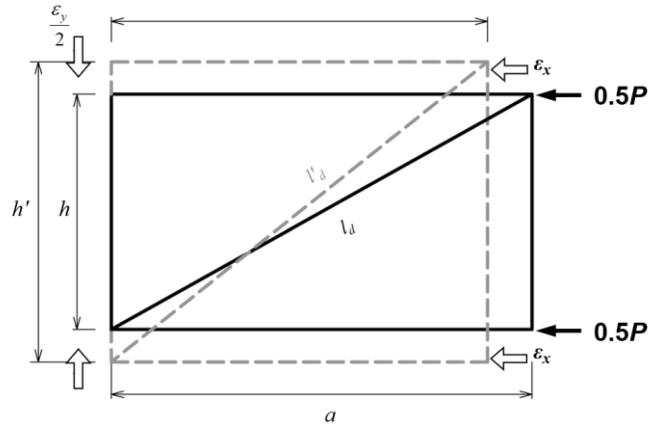
(b) strains induced by axial force, P

Figure 6-14. Strains by shear force, *V*, and axial force, *P*

2,607 kN / 2,718 kN / 2,767 kN / 2,295 kN

Span   End

489 kN
467 kN
445 kN
467 kN

—— Truss action
--- Arch action

1,557 kN / 1,677 kN / 1,633 kN / 1,512 kN
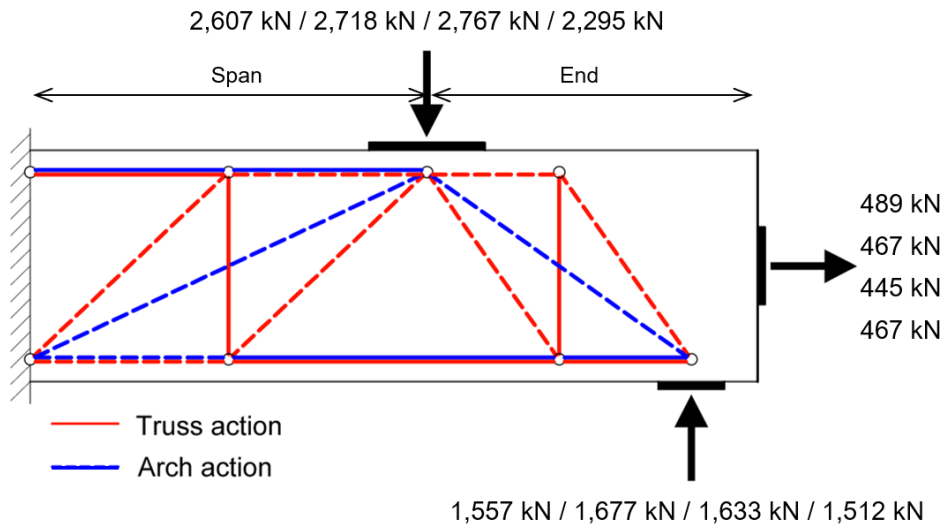
Note: Numbers indicate actuator forces at failure ordered by: RCS-16-12 / PSS-16-12 / PSS-16-24 / PSV-16-12

Figure 6-15. Truss and arch actions adapted in the *TAMU* analysis

According to geometry, the strain of the principal diagonal concrete strut by the axial force is calculated by:

$$\varepsilon_{2\_P} = \frac{l'_d}{l_d} - 1 = \sqrt{\frac{\left[a^2 + h^2\left(\dfrac{1 - \nu\varepsilon_{x\_P}}{1 + \varepsilon_{x\_P}}\right)^2\right]\left(1 + \varepsilon_{x\_P}\right)^2}{a^2 + h^2}} - 1 \tag{6-13}$$

where ε_{2_P} = principal compressive strain in the diagonal concrete strut member by axial force; l_d = diagonal length of the member before elongation; l'_d = diagonal length of the member after elongation; a = shear span length before elongation; and h = member height before elongation.

Based on the small (infinitesimal) strain theory, ε_2 may be considered as longitudinal strain, ε_x. By adding this principal diagonal strains by axial force to those by shear force in Eq. (6-5), the effect of axial force on the principal strain ratio can be adequately addressed.

The specimens in the experimental test are analyzed using the *TAMU* method. The effect of axial strain due to the prestressing force and horizontal load is addressed by following the above-mentioned procedures. The ultimate shear strengths are predicted for both span and end regions, and the smaller force is considered as a failure load. It is noted that the failure load pattern is only taken into account herein among six load patterns applied during the test because the *TAMU* method only focuses on the ultimate force inducing the shear failure.

Figure 6-15(c) presents truss and arch actions adapted in the *TAMU* analysis along with the maximum P2, V, and H loads measured at the moment of failure in the test for all the specimens. In the calculation of the principal strain ratio,$\varepsilon_1/\varepsilon_2$, shear force by vertical actuators and axial force by the horizontal actuator, and prestressing force are both considered. The ultimate strengths of the specimens and failure locations estimated by the *TAMU* method, three code-based analysis methods, and the C-STM analysis are provided in Table 6-4 along with the summary of comparison with the test results.

Table 6-4. Comparison of analysis and test results at failure load

ID	V_{pred} (kN)					V_{test} (kN)
	ACI	MCFT		*TAMU*	C-STM	
		Simplified	Full			
RCS-16-12	1,420 (End)	1,703 (End)	1,739 (End)	1,530 (Span)	1,579 (Span)	1,577 (Span)
PSS-16-12	1,792 (End)	1,470 (End)	1,957 (End)	1,695 (End)	1,702 (End)	1,677 (End)
PSS-16-24	1,566 (End)	1,248 (End)	1,637 (End)	1,552 (End)	1,606 (End)	1,633 (End)
PSV-16-12	1,347 (End)	1,101 (End)	1,183 (End)	1,401 (End)	1,464 (End)	1,512 (End)
Comparison (V_{test}/V_{pred})						
RCS-16-12	1.10	0.91	0.90	1.02	0.99	
PSS-16-12	0.94	1.14	0.86	0.99	0.99	
PSS-16-24	1.04	1.31	1.00	1.05	1.02	
PSV-16-12	1.12	1.37	1.28	1.08	1.03	
Avg.	1.05	1.18	1.01	1.03	1.01	
C.V	0.08	0.17	0.16	0.04	0.02	

Note: () indicates failure region observed from the test or predicted by each method

Both simplified and full MCFT methods account for axial force and prestressing force, respectively, when calculating the strain of the longitudinal steel. In the ACI method, the prestressing force is considered as an axial force using:

$$V_c = 0.17 \left(1 + \frac{N_u}{14A_g}\right) \sqrt{f'_{c\,(MPa)}}\, b_w d \tag{6-14}$$

where N_g = factored axial force normal to cross-section taken as positive for compression and negative for tension; and A_g = cross area of concrete section.

The failure locations of all specimens predicted by five analysis methods agree with the test results except for the ACI and both MCFT methods which expect the failure of the end region in RCS-16-12 specimen.

The comparison with the experimental results indicates that all shear analysis methods give overall conservative estimates of the ultimate shear capacities as the averages of V_{test}/V_{pred} from all methods are greater than 1.0. The C-STM analysis has the most accurate estimates among the considered shear analysis approaches as its mean value of V_{test}/V_{pred} for four specimens is 1.01 with the coefficient of variation value of 2%. The *TAMU* and ACI analyses have almost equivalent results as the mean values are 1.03 and 1.05, and their coefficient of variation values are 4% and 8%, respectively. The C-STM analysis shows slightly better prediction than the *TAMU* and ACI analyses, however, the difference is minor.

All code-based shear analysis approaches show reasonable predictions but fail to capture the failure location of RCS-16-12. Also, given the difference in the accuracy between PSS-16-12 and PSS-16-24 specimens, the effect of the transverse reinforcement spacing is not accurately addressed. All code-based analysis methods underestimate the resistance of the voided specimen. Among the code-based analysis methods, the ACI approach shows the most accurate predictions.

Based on the analysis results, it is considered that the effect of the prestressing, transverse reinforcement spacing, and interior void are appropriately addressed in the *TAMU* analysis.

6.6 Closure and Key Findings

Precast RC bent caps have been used in the construction of several Texas bridges to enable accelerated construction. Precast bent caps may offer greater flexibility with the use of prestressing by providing the additional benefit of improving performance. To enable the use of prestressed concrete for the construction of bridge piers, full-scale bent caps were tested under indeterminate demands. The experimental test results were further used to investigate the accuracy of the C-STM and *TAMU* analysis methods. The *TAMU* approach was extended to consider the axial force effect including prestressing force, and the C-STM analysis captured the overall force-deformation response of the specimens. The following key findings are drawn from the experimental and analytical study:

- PSC specimens delayed the onset of shear and flexural cracking and the limited crack formation and crack width compared to the traditional RC counterpart. After removal of service loads, the prestressed specimens led to the predominant closure of the previously open cracks.

- No significant difference was found based on transverse reinforcement spacing in crack formation at the various loading stages as similar cracks patterns were observed in both PSS-16-12 and PSS-16-24. The additional shear reinforcement might be effective to limit the crack widths.

- The voided specimen showed almost similar flexural resistance to the solid specimen counterpart under bridge demands. However, significantly reduced shear resistance was

detected by the shear crack along the interior void. The voided specimen exhibited additional concrete crushing and a more brittle post-peak behavior.

- The prestressing effect is appropriately accounted for by applying equivalent external axial loads representing the prestressing force and modifying the stress-strain behavior of the prestressed strand in the C-STM analysis. The C-STM analysis captures the overall force-displacement response including post-peak behavior. The failure load and its location are predicted by the C-STM and they agree well with test observations. The effect of several design variables is addressed adequately in the C-STM analysis.

- The *TAMU* analysis, originally derived by taking into account beam shear behavior, is extended to address the effect of axial force by superposing strains caused by shear force and axial or prestressing forces. The *TAMU* analysis results considering the axial force effect show good agreement with the experimental results, including maximum shear-carrying capacities and the failure locations. The effect of prestressing force, the transverse reinforcement spacing, and an interior void on the specimens is captured well.

- The shear capacities predicted by three existing code-based shear analysis methods are in good agreement with the test results. The predicted failure locations correspond to the test observation except for the reinforced concrete bent cap specimen. The ACI method shows more accurate predictions than two MCFT methods against the bent cap specimens. Although all code-based methods have reasonable predictions, the effect of prestressing force, shear reinforcement, and interior void is not captured adequately.

7. SUMMARY AND CONCLUSION

7.1 Summary

Based on force-deformation behavior computed using the Compatibility Strut and Tie Model (C-STM), a theoretical limit analysis model was developed to predict the ultimate shear-carrying capacity of shear-critical structural concrete beams with and without transverse reinforcement. The Truss-Arch Model Unified (*TAMU*) was validated based on experimental observations and from previous studies reported in the literature. The limit analysis approach assumes the failure mechanism occurs when the principal diagonal arch reaches its softened peak strength. Two truss models, with a vertical tie or an inclined tie, are used depending on whether the members are reinforced with or without shear steel, respectively. Explicit solutions for the principal strain ratio and ultimate shear strength were derived based on truss and arch contribution to flexibility and strength. A large database of test data consisting of 839 beams was assembled for the substantiation of the proposed method and also to conduct a comparative assessment of existing code-based shear analysis methods. The proposed *TAMU* approach predicted well the limit load capacities against the database. When compared with existing code-based shear analysis approaches, the *TAMU* based approach demonstrated superior accuracy with less dispersion due to modeling and aleatory uncertainty in both D-and B-regions.

The *TAMU* approach was further extended to account for axial strain effects which may be present due to the presence of either prestress, axial load, or both. A full-scale experimental program was conducted on reinforced and prestressed concrete bent caps to investigate the effect of prestressing force, shear reinforcement spacing, interior void, and axial loads on the bent cap. The specimens were analyzed by the *TAMU* method and other existing code-based analysis

methods. The C-STM and *TAMU* results are able to accurately predict the experimental test outcome, somewhat better than existing code analysis approaches.

7.2 Conclusions

The following key conclusions based on the research presented in this dissertation may be drawn as follows:

7.2.1 Proposed *TAMU* Method for RC Beams with Transverse Reinforcement

- The *TAMU* analysis with a vertical tie gave a reasonable prediction on the maximum shear capacities regardless of flexural and shear reinforcement ratios and concrete compressive strength against the large-scale experimental tests on RC bent caps.

- A parametric study on the concrete softening coefficient showed that the proposed explicit solution captured the trends in the ultimate shear stress associated with several parameters quite well. The predictive results corresponded well to observations made in experimental investigations.

- The versatility of the *TAMU* method for shear-critical beams with transverse reinforcement was verified, as reasonable predictions were made for the database consisting of 460 specimens. No significant trends were found on its accuracy by primary design variables, including a/d ratio, f'_c, b, h, ρ_L, and ρ_v for the range of values given. Therefore, it is considered that the *TAMU* approach adequately takes these variables into account.

- Even though the *TAMU* approach was originally conceived for D-regions when $a/d \leq 2.5$, its analysis results also demonstrated good agreement with experimental test results for B-regions when $a/d > 2.5$. This is because the failure mechanism is still mainly dominated by shear rather than flexure in transition regions, so the truss and arch model captures the force transfer path within the structure well, resulting in acceptably accurate predictions.

185

Thus, the use of the *TAMU* method for slender beams may be adequate, particularly when $a/d < 3.5$.

- The *TAMU* method is able to predict the ultimate shear strength with comparatively good accuracy for shear-critical reinforced concrete beams with transverse reinforcement regardless of various design parameters. Given that it is readily amenable to hand analysis, the *TAMU* approach may be used as a simple design checking method.

7.2.2   Proposed *TAMU* Method for RC Beams without Transverse Reinforcement

- The *TAMU* approach modeled with a diagonal tension tie (in lieu of the non-existing transverse steel) demonstrated good agreement with the test result of over 380 beams with both D- and B-regions. The *TAMU* approach demonstrated its versatility to predict the maximum shear-carrying capacity of shear-critical beams without transverse reinforcement, regardless of the a/d ratio. No trend was observed in the accuracy of the method associated with design variables, a/d ratio, ρ_L, f'_c, and b, implying the method adequately accounts for the contribution of each variable on the shear strength.

- The distinctly different trend associated with the a/d ratio was found in the accuracy of code-based methods. Each code-based strength approach showed a tendency to provide broad dispersion in accuracy (high β) with a significant percentage of conservative predictions, especially for D-regions. Conversely, reasonable predictions were made in B-regions which exhibited less dispersion. Because the code-based methods are based on tensile action, they did not adequately capture the shear mechanism in D-regions where the arch action governs the shear mechanism. Unlike code-based strength analysis methods, the *TAMU* method considered both arch and truss actions, so it provides reasonable predictions in both D- and B-regions.

7.2.3 Observations from the C-STM Displacement Analysis

- The C-STM analysis was conducted using the versatile nonlinear *OpenSees* analysis program which predicted the ultimate load-carrying capacity and failure mode of the large-scale experimental bridge bent caps accurately. The analysis results were consistent with the test results regardless of several design parameters, including longitudinal and shear reinforcement ratios and concrete compressive strength.

- The predicted responses of displacement and internal strain of longitudinal reinforcement showed good agreement with experimental responses, including the challenging post-peak behavior of the descending branch.

- The C-STM predicted the progression of several nonlinear hinge formations and also the final failure mode of RC bent cap specimens, and they were consistent with the experimental observations.

- The principal strain ratios obtained from the C-STM analysis were compared with those from the *TAMU* analysis which were reasonably close. Also, two methods showed only slight differences in predicting the ultimate shear capacities of the RC bent caps.

- The C-STM analysis took the prestressing effect into account by introducing initial strain in the longitudinal reinforcement, and the maximum load-carrying capacities of prestressed bent caps were captured well.

7.2.4 Verification of Code-Based Shear Analysis Methods

- In D-regions, overall predictions made by the code-based analysis methods were exceedingly conservative regardless of the beams were with or without transverse reinforcement, especially when the $a/d < 2.0$. Generally, all code-based analysis methods

tended to be more conservative for smaller a/d ratios. This trend contrasted with the *TAMU* method because it showed more conservatism for larger a/d ratios.

- In B-regions, each the code-based analysis method considered demonstrated acceptable accuracy in predicting ultimate shear strengths for beams with and without transverse reinforcement. In particular, remarkably good agreement with the test results was found for both full and simplified MCFT methods. Although the ACI method is not as an exacting analysis as the MCFT methods, it is still useful in B-regions considering it is a simple and straightforward procedure to use, particularly for design. This observation showed that the code-based analysis methods are capable of capturing the behavior of structural concrete quite well in B-regions.

- The distinct difference in the accuracy of code-based analysis methods between D- and B-regions is due to the simplistic shear mechanism they are based on. Each of the sectional shear methods is generally based on the tensile concrete strength and truss action and do not overtly take arch action into consideration. Therefore, the use of these code-based analysis methods, while appropriate for slender beams, is considered to be inadmissible for D-regions where a direct arch action dominates the shear mechanism behavior.

7.2.5   Experimental and Analytical Study on Prestressed Bent Caps

- PSC specimens delayed the onset of shear and flexural cracking and the limited crack formation and crack width compared to the traditional RC counterpart. No significant difference was found based on transverse reinforcement spacing in overall performance of prestressed concrete bent caps. The voided specimen had almost equivalent flexural resistance to the solid specimen under bridge demands. However, significantly reduced

188

shear resistance was detected by the shear crack along the interior void. The voided specimen exhibited additional concrete crushing and more brittle post-peak behavior.

- The prestressing effect was appropriately accounted for by applying equivalent external loads to the prestressing force and modifying the stress-strain behavior of the prestressed strand in the C-STM analysis. The C-STM analysis captured the overall force-displacement response, including post-peak behavior. The failure load and its location predicted by the C-STM analysis agreed well with the experimental test observations. The C-STM analysis addresses the effect of several design variables adequately.

- The *TAMU* analysis, originally conceived for by taking into account the shear-arch mechanism, was modified to address the effect of axial force in the model by superposing strains by shear force and axial force (or prestressing force). The *TAMU* analysis results which considered the axial force effect showed good agreement with the experimental results, including maximum shear-carrying capacities and the failure locations. The effect of prestressing force, the transverse reinforcement spacing, and an interior void on the specimens was well captured.

- The shear capacities predicted by three existing code-based shear analysis methods were in good agreement with the test results. The predicted failure locations corresponded to the test observation except for the reinforced concrete bent cap specimen. The ACI method showed more accurate predictions than two MCFT methods against the bent cap specimens. Although all code-based methods had reasonable predictions, the effect of prestressing force, shear reinforcement, and interior void was not adequately captured.

7.3   Future Work

Based on the findings of the analytical and experimental studies, the following research needs are identified:

The strength analysis method, *TAMU*, that was developed based on C-STM and validated in the present study, shows its ability to predict the maximum shear-carrying capacity of shear-critical beams. The benefit of the *TAMU* method is evident as it is amendable for hand methods of analysis and uses a few variables. However, there is still a possibility to simplify the method even more because the proposed equations for the implementation of the method are somewhat too long. This can be achieved by replacing several factors such as the arch breadth scalar and the force-distribution factor with simplified terms. Given the advantage of the method, more investigation may be deserved for broad use.

The present study proposed two *TAMU* approaches based on whether structural concrete beams are with or without transverse reinforcement. Both approaches were applicable to both D- and B-regions. Eventually, it may be beneficial to combine those two methods and develop a single unified shear method that can be used for both D-and B-regions regardless of whether beams possess shear reinforcement or not.

Also, the present study can be expanded to adopt the concept of capacity design. In general, ductile failure modes are preferable to brittle failure modes, and undesirable failure modes may be intentionally prevented by increasing their strength compared to those of the preferable failure modes; this is the basic philosophy of capacity design. In the present study, the diagonal principal arch failure which often leads to a sudden or brittle collapse was estimated. By knowing the failure load inducing the fracture of the diagonal arch, undesirable failure may be avoided through various approaches. Various approaches to effectively delay the diagonal arch failure can be further

investigated in a future study. To meet the philosophy of the capacity design, it is desirable that the force inducing arch failure is at least greater than the factored nominal flexural capacity, $\phi_f M_n$, as follows:

$$\phi_v V_n \geq \frac{\phi_o M_n}{a}$$

in which ϕ_o = overstrength factor that denotes strain-hardening potential.

Additionally, although the *TAMU* method focused on the failure of the principal diagonal arch in the present study, it can be further expanded to consider several nonlinear hinge formations, including concrete tensile cracking, and yielding of longitudinal and transverse reinforcement. This can be easily done by investigating strains or stresses of representative members in truss and arch models. Knowing respective forces inducing these nonlinear hinge formations, the hierarchy of failure mechanisms may be determined.

Experimental tests should be conducted on solid bent caps with moderate shear span ratios to establish shear behavior and enable the development of revisions for shear strength design. Research is needed to monitor the fabrication of future bent caps to better understand end region cracking and provide recommendations for avoidance or restraint of cracks. Inspection for cracks should occur after strand release and at regular intervals in the months following. Along with the visual inspection, concrete internal temperature, formwork temperature, and ambient temperature should be monitored. Data collection should be supplemented by computational modeling to better understand the mechanisms leading to cracking and to provide recommendations for avoidance of cracks, or restraint in the event cracks may occur.

An alternative to interior voided specimens should be explored to enable weight reduction but that would inhibit the formation of the diagonal flexure-shear cracks. One such option may be

the use of U-shaped shell beams that are infilled with site concrete to provide increased shear resistance. To provide further options for accelerated construction of bridge substructures, the use of precast columns should be explored along with appropriate connections to the adjoining bent caps.

REFERENCES

AASHTO LRFD. (1994). "Bridge Design Specifications," 1st Edition, American Association of State Highway Transportation Officials, Washington, D.C. Including interim revisions for 1996 through 2007.

AASHTO LRFD (2010). "Bridge Design Specifications," 5th edition, American Association of State Highway and Transportation Officials, Washington, DC.

AASHTO LRFD (2014). "Bridge Design Specifications," 7th edition. Washington, American Association of State Highway and Transportation Officials, Washington, DC.

AASHTO LRFD. (2017). "Bridge Design Specifications," 8th edition, American Association of State Highway and Transportation Officials, Washington, DC.

ACI Committee 318 (1963). "Commentary on Building Code Requirements for Reinforced Concrete (ACI 318 63)," SP 10, American Concrete Institute, Farmington Hills, MI.

ACI Committee 318 (2005). "Building Code Requirements for Structural Concrete (ACI 318-05) and Commentary (318R-05)," American Concrete Institute, Farmington Hills, MI.

ACI Committee 318. (2011). "Building Code Requirements for Structural Concrete (ACI 318-11) and Commentary," American Concrete Institute, Farmington Hills, MI.

ACI Committee 318. (2019). "Building Code Requirements for Structural Concrete (ACI 318-19) and Commentary," American Concrete Institute, Farmington Hills, MI.

Ahmad, A.H., and Lue, D.M. (1987). "Flexure-Shear Interaction of Reinforced High Strength Concrete Beams," ACI Structural Journal, V. 84(5), pp. 330-341.

Ang, B. G. (1985). "Seismic Shear Strength of Circular Bridge Piers," Ph.D. Dissertation, Department of Civil Engineering, University of Canterbury, Christchurch.

Angelakos, D., Bentz, E. C., and Collins, M. P. (2001). "Effect of Concrete Strength and Minimum Stirrups on Shear Strength of Large Members," ACI Structural Journal, V .98(3), pp. 290-300.

Baie, R. (2017). "In-Span Splicing for Continuous Prestressed Concrete Girder Bridges," Ph.D. Dissertation, Department of Civil Engineering, Texas A&M University, College Station.

Bentz, E. C. (2000). "Sectional Analysis of Reinforced Concrete Members," Ph.D. Dissertation, Department of Civil Engineering, University of Toronto, Toronto.

Bentz, E. C., Vecchio, F. J., and Collins, M. P. (2006). "Simplified Modified Compression Field Theory for Calculating Shear Strength of Reinforced Concrete Elements," ACI Structural Journal, V. 103(4), pp. 614-624.

Birely, A. C., Mander, J. B., Lee, J. D., McKee, C. D., Yole, K. J., and Barooah, U. R. (2018). "Precast, Prestressed Concrete Bent Caps: Volume 1 Preliminary Design Considerations and Experimental Test Program," Report No. FHWA/TX-18/0-6863-1, Texas A&M Transportation Institute, Texas A&M University, College Station, Texas. Copyright 2018 Texas A&M Transportation Institute.

Birely, A. C., Yole, K. J., Lee, J. D., McKee, C. D., and Mander, J. B. (2020). "Experimental Behavior of Reinforced Concrete and Pretensioned Concrete Bent Caps," Journal of Bridge Engineering, V. 25(2), 04019137.

Birrcher, D. B., Tuchscherer, R. G., Huizinga, M., and Bayrak, O. (2014). "Depth Effect in Deep Beams," ACI Structural Journal, V. 111(4), pp. 731-740.

Bracci, J.M., Keating, P.B., and Hueste, M.B.D. (2000). "Cracking in RC Bent Caps," Report No. FHWA/TX-01/1851-1, Texas Transportation Institute, The Texas A&M University System, College Station, Texas.

Brown, M. D., and Bayrak, O. (2008). "Design of Deep Beams Using Strut-and-Tie Models–Part I: Evaluating U.S Provisions," ACI Structural Journal, V. 105(4), pp. 395-404.

Brown, M.D, Sankovich, C.L., Bayrak, O., Jirsa, J.O., Breen, J.E., and Wood, S.L. (2006). "Design for Shear in Reinforced Concrete Using Strut-and-Tie Models," Report No. FHWA/TX-06/0-4371-2. CTR.

Chang, G.A., and Mander, J.B. (1994). "Seismic Energy Based Fatigue Damage Analysis of Bridge Columns, Part I: Evaluation of Seismic Capacity," Report No. NCEER-94-0006, National Center for Earthquake Engineering Research, State University of New York at Buffalo, New York.

Choi, K. K., Park, H., and Wight, J. K. (2007). "Unified Shear Strength Model for Reinforced Concrete Beams – Part I: Development," ACI Structural Journal, V. 104(2), pp. 142-152.

Choi, K.-K., Kim, J.-C., and Park, H.-G. (2016). "Shear Strength Model of Concrete Beams Based on Compression Zone Failure Mechanism," ACI Structural Journal, V. 113(5), pp. 1095-1106.

Clark, A.P. (1951). "Diagonal Tension in Reinforced Concrete Beams," ACI Journal, Proceedings V. 48(10), pp. 145-156.

Collins, M.P., Bentz, E.C., and Sherwood, E.G. (2008). "Where is Shear Reinforcement Required? Review of Research Results and Design Procedures," ACI Structural Journal, V. 105(5), pp. 590-600.

Collins, M. P., Mitchell, D., Adebar, P., and Vecchio, F. J. (1996). "A General Shear Design Method," ACI Structural Journal, V. 93(1), pp. 36-45.

Collins, M.P. (1978). "Towards a Rational Theory for RC Members in Shear," ASCE Journal of Structural Division, V. 104(4), pp. 649-666.

Collins, M.P., and Kuchma, D. (1999). "How Safe Are Our Large, Lightly Reinforced Concrete Beams, Slabs, and Footings?," ACI Structural Journal, V. 96(4), pp. 482-490.

Collins, M.P., and Mitchell, D. (1991). "Prestress Concrete Structures," Prentice Hall, Englewood Cliffs, New Jersey.

Cook, W. D., and Mitchell, D. (1988). "Studies of Disturbed Regions Near Discontinuities in Reinforced Concrete Members," ACI Structural Journal, V. 85(2), pp. 206-216.

CSA Committee A23.3 (1994). "Design of Concrete Structures," Canadian Standards Association, Rexdale, ON, Canada, 199 pp.

CSA Committee A23.3. (2010) "Design of Concrete Structures (Reaffirmed 2010)," Canadian Standards Association, Mississauga, ON, Canada, 214 pp.

Culmo, M. P. (2009). "Connection Details for Prefabricated Bridge Elements and Systems," Report FHWA-IF-09-010, Federal Highway Administration.

Demir, A., Caglar, N., and Ozturk, H. (2019). "Parameters Affecting Diagonal Cracking Behavior of Reinforced Concrete Deep Beams," Engineering Structures, V. 184, pp. 217-231.

Fenwick, R C., and Paulay, T. (1968). "Mechanisms of shear resistance of concrete beams," Journal of the Structural Division, ASCE, 94(10), pp. 2325-2350.

Ferguson, P.M. (1964). "Design Criteria for Overhanging Ends of Bent Caps – Bond and Shear," Research Report 3-5-63-52. Center of Highway Research, University of Texas, Austin, Texas.

fib, "Model Code 2010 First Complete Draft Vol. 1," fib Bulletin 55, International Federation for Structural Concrete (fib), Lausanne, Switzerland, 2010, 318 pp.

fib, "Model Code 2010 First Complete Draft Vol. 2," fib Bulletin 56, International Federation for Structural Concrete (fib), Lausanne, Switzerland, 2010, 312 pp.

FIP-Commission 3. (1996). "Practical Design of Structural Concrete," SETO, distributed by fib, London, UK.

Fonseca, F., and Rowe, M.D. (2003). "Flexural Performance of Deteriorated Reinforced Concrete Cantilevered Bent Caps – Part 1," Technical Report UT-03.33, Utah Department of Transportation.

Freeby, G., Hyzak, M., Medlock, R.D., Kenneth, O., Vogel, J., and Wolf, L.M. (2003). "Design and Construction of Precast Bent Caps at TxDOT," Texas Department of Transportation.

Hawkins, N. M., and D. A. Kuchma. (2005). "Simplified Shear Design of Structural Concrete Members," NCHRP Report 549. Transportation Research Board, National Research Council, Washington, DC.

He Z.-Q., Liu Z., and Ma Z.J. (2012). "Investigation of Load-Transfer Mechanisms in Deep Beams and Corbels," ACI Structural Journal, V. 109(4), pp. 467–476.

Hsu, T. T. C., Laskar, A., and Mo, Y. L. (2010). "Shear Strengths of Prestressed Concrete Beams Part 2: Comparisons with ACI and AASHTO Provisions," ACI Structural Journal, V. 107(3), pp. 340–345.

Hwang, S.-J., Lu, W.-Y., and Lee, H.-J. (2000). "Shear Strength Prediction for Deep Beams," ACI Structural Journal, V. 97(3), pp. 367-376.

Iida, T., Sumi, K., and Kawamata, S., (1984) "Behavior of Orthogonally Reinforced Walls Subjected to In-Plane Shear Force − Effectiveness of F. J. Vecchio and M. P. Collins' Theory," Proceedings, Annual Meeting, Architectural Institute of Japan, Yokohama, pp. 1807-1809.

Japan Society of Civil Engineers, "Standard Specifications for Concrete Structures 2007 Design," English Version, Japan Society of Civil Engineers, Tokyo, Japan, 2010, 469 pp.

Jeong, C.-Y., Kim, H.-G., Kim, S.-W., Lee, K.-S., and Kim, K.-H. (2017). "Size effect on shear strength of reinforced concrete beams with tension reinforcement ratio," Advances in Structural Engineering, V. 20(4), pp. 582-594.

Johnson, M.K., and Ramirez, J.A. (1989). "Minimum Shear Reinforcement in Beams with Higher Strength Concrete," ACI Structural Journal, V. 86(4), pp. 376-382.

Joint ACI-ASCE Committee 326 (1963) "Shear and Diagonal Tension," ACI Journal, Proceedings V. 59(1-3), pp. 1-30, 277-344, and 352-396.

Kang, T. H.-K., and Ibrahim Ary, M. (2012). "Shear-Strengthening of Reinforced & Prestressed Concrete Beams Using FRP: Part II – Experimental Investigation," International Journal of Concrete Structures and Materials, V. 6(1), pp. 49-57.

Kani, G. N. J. (1964). "The Riddle of Shear Failure and Its Solution," Journal of the American Concrete Institute, V. 61(4), pp. 441-467.

Kani, G. N. J. (1966). "Basic Facts Concerning Shear Failure," ACI Journal, V. 63(6), pp. 675-692.

Kani, G. N. J. (1967). "How Safe Are Our Large Reinforced Concrete Beams," ACI Journal, V.64(3), pp. 128-141.

Kapur, J., Yen, W.P., Dekelbab, W., Bardow, A., Keever, M., Sletten, J., Tobias, D., and Saiidi, M.S. (2012). "Best Practices Regarding Performance of ABC Connections in Bridges Subjected to Multihazard and Extreme Events," NCHRP Project 20-68A Scan 11-02, Arora and Associates P.C., American Association of State Highway and Transportation Officials, Lawrenceville, New Jersey.

Karthik, M. M., Mander, J. B., and Hurlebaus, S. (2016). "Displacement-Based Compatibility Strut-and-Tie Method and Application to Monotonic and Cyclic Loading," Journal of Structural Engineering, V. 142(6), 04016010.

Karthik, M.M. (2015). "Experimental Performance and Modeling of ASR and DEF Deteriorated Structural Concrete Bridges," Ph.D. Dissertation, Department of Civil Engineering, Texas A&M University.

Kim, J.H., and Mander, J.B. (1999). "Truss Modeling of Reinforced Concrete Shear-Flexure Behavior," Report No. MCEER-99–0005, State University of New York at Buffalo.

Kim, J.H., and Mander, J.B. (2000a). "Cyclic Inelastic Strut-Tie Modeling of Shear-Critical Reinforced Concrete Members," ACI Special Publication, V.193, pp. 707-728.

Kim, J.H., and Mander, J.B. (2000b). "Seismic Detailing of Reinforced Concrete Beam-Column Connections," Structural Engineering and Mechanics, V. 10(6), pp. 589-601.

Kim, J.H., and Mander, J.B. (2005). "Theoretical Shear Strength of Concrete Columns Due to Transverse Steel," Journal of Structural Engineering, V. 131(1), pp. 197-199.

Kim, J.H., and Mander, J.B. (2007). "Influence of Transverse Reinforcement on Elastic Shear Stiffness of Cracked Concrete Elements," Engineering Structures, V.29(8), pp. 1798-1807.

Krauthammer, T., and Hall, W. J. (1982). "Modified analysis of reinforced concrete beams," ASCE Journal of the Structural Division, V. 108(ST2), pp. 457-475.

Kupfer, H. (1964). "Erweiterung der Mörsch schen Fachwerkanalogie mit Hilfe des Prinzips vom Minimum der Formanderungsarbeit (Generalization of Mörsch's Truss Analogy Using the Principle of Minimum Strain Energy)," Comite Euro-Intemational du Beton, Bulletin d'lnformation No. 40, CEB, Paris, France, pp. 44-57.

Lampert, P., and Thurlimann, B. (1968). "Torsion tests of reinforced concrete beams (Torsionsversuche an Stahlbetonbalken)," Institute fur Baustatik, ETH, Zürich, Switzerland (in German).

Laskar, A., Hsu, T. T. C., and Mo, Y. L. (2010). "Shear Strengths of Prestressed Concrete Beams Part 1: Experiments and Shear Design Equations," ACI Structural Journal, V. 107(3), pp. 330-339.

Lee, J. D., Barooah, U. R., McKee, C. D., Birely, A. C., and Mander, J. B. (2019). "Recommendations for Design of Concentrically Pretensioned, Precast Concrete Bent Caps," Practical Periodical Structural Design and Construction, V.24(1), 04018034.

Lee, J.-Y., and Kim, U.-Y. (2008). "Effect of Longitudinal Tensile Reinforcement Ratio and Shear Span-Depth Ratio on Minimum Shear Reinforcement in Beams," ACI Structural Journal, V. 105(2), pp. 134-144.

Lee, J.-Y., and Watanabe, F. (2000). "Shear Design of Reinforced Concrete Beams with Shear Reinforcement Considering Failure Modes," ACI Struct. Journal, V. 97(3), pp. 477-484.

Leonhardt, F. (1965). "Reducing the Shear Reinforcement in Reinforced Concrete Beams and Slabs," Magazine of Concrete Research, V. 17(53), pp. 187-198.

Leonhardt, F., and Walther, R. (1962). "Contribution to Treatment of Shear Problems in Reinforced Concrete," Beton – Stahlbetonbau, V. 57(2) (in German).

Liu, S-H., Bracci, J. M., Mander, J. B., and Hurlebaus, S. (2017). "Performance of D-regions affected by alkali-silica reaction: Experimental and analytical study," Journal of Structural Engineering, V. 143 (9): 04017109.

MacGregor, J. G., Sozen, M. A., and Siess, C. P. (1965). "Strength of prestressed concrete beams with web reinforcement," ACI Journal, Proceedings V. 62(12), pp. 1503-1520.

MacGregor, J.G. (1992). Reinforced Concrete Mechanics and Design. 2nd Edition, Prentice-Hall, Englewood Cliffs, New Jersey.

Mander, J. B., Bracci, J. M., Hurlebaus, S., Grasley, Z., Karthik, M.M., Liu, S., and Scott R.M. (2012). "Structural Assessment of "D" Regions Affected by Premature Concrete Deterioration: Technical Report," Report No. FHWA/TX-12/0-5997-1, TTI.

Mander, J.B. (1983). "Seismic Design of Bridge Piers," Ph.D. Thesis, University of Canterbury, Christchurch, New Zealand.

Marsh, M.L., Wernli, M., Garrett, B.E., Stanton, J.F., Eberhard, M.O., and Weinert, M.D. (2011). "Application of Accelerated Bridge Construction Connections in Moderate-to-High Seismic Regions," Report 698, National Cooperative Highway Research Program, Transportation Research Board, Washington, D.C.

Marti, P. (1985). "Basic tools of reinforced concrete beam design," ACI Journal, Proceedings V. 82(1), pp. 46-56.

Massone, L.M., Gotschlich, N.J., Kang, T. H.-K., and Hong S.G. (2013). "Shear–Flexural Interaction for Prestressed Self-Consolidating Concrete Beams," Engineering Structures, V. 56, pp. 1464-1473.

Matamoros, A. B., and Wong, K. H. (2003). "Design of Simply Supported Deep Beams Using Strut-and-Tie Models," ACI Structural Journal, V. 100(6), pp. 704-712.

Matsumoto, E. E., Waggoner, M. C., Sumen, G., Kreger, M. E., Wood, S. L., and Breen, J. E. (2001). "Development of a Precast Bent Cap System," Report No. FHWA/TX-0-1748-2, Center for Transportation Research, University of Texas at Austin, Austin, Texas.

McKee, C. D., Lee, J. D., Birely, A. C., and Mander, J. B. (2020). "Experimental Behavior of Pretensioned Bent Caps with Internal Voids for Weight Reduction," Journal of Bridge Engineering, V.25(1), 04019110

Mehrsoroush, A., Saiidi, M., and Ryan, K. (2017). "Development of Earthquake-Resistant Precast Pier Systems for Accelerated Bridge Construction in Nevada," Report No. CCEER 17-03, Center for Civil Engineering Earthquake Research, University of Nevada, Reno.

Mihaylov, B.I., and Franssen, I. (2017). "Shear-Flexure Interaction in the Critical Sections of Short Coupling Beams," Engineering Structures, V. 152, pp. 370-380.

Mitchell, D., and Collins, M.P. (1974). "Diagonal Compression Field Theory-A Rational Model for Structural Concrete in Pure Torsion," ACI Structural Journal, V. 71(8), pp. 396-408.

Moody, K. G., Viest, I.M., Elstner, R.C., and Hognestad, E. (1954). "Shear Strength of Reinforced Concrete Beams Part 1 - Tests of Simple Beams," ACI Journal, Proceedings V. 51(12), pp. 317-332.

Moody, K. G., Viest, I.M., Elstner, R.C., and Hognestad, E. (1955). "Shear Strength of Reinforced Concrete Beams Part 2-Tests of Hestrained Beams without Web Reinforeemcnt," ACI Journal, Proceedings V. 51(21), pp. 417-434.

Moretto, O. (1945). "An Investigation of the Strength of Welded Stirrups in Reinforced Concrete Beams," ACI Journal, Proceedings V. 42(11). pp. 141-164.

Mörsch, E. (1909). "Concrete-Steel Construction," McGraw-Hill, New York.

Nakamura, E., Avendaño, A. R., and Bayrak, O. (2013). "Shear Database for Prestressed Concrete Members," ACI Structural Journal, V. 110(6), pp. 909-918.

Nielsen, M. P. (1967), "Am Forskydningsarmering I Jernbetonbjaelker (On shear reinforcement in reinforced concrete beams)," Bygningsstatiske Meddelelser, V. 38(2), pp. 33-58 (in German).

Oh, J. K., and Shin, S. W. (2001). "Shear Strength of Reinforced HighStrength Concrete Deep Beams," ACI Structural Journal, V. 98(2), pp. 164-173.

OpenSees v. 3.2.2. (2020). Open System for Earthquake Engineering Simulation. [Computer Software] Pacific Earthquake Engineering Research Center, University of California. Berkeley, California.

Park, R., and Paulay, T. (1975). "Reinforced Concrete Structures," John Wiley and Sons, New York.

Paulay, T, and Priestley, M. J. N. (1992). "Seismic Design of Reinforced Concrete and Masonry Buildings," John Wiley and Sons, New York.

Paulay, T. (1969). "The Coupling of Shear Walls," Ph.D. Thesis, University of Canterbury, Christchurch, New Zealand.

Paulay, T. (1971). "Coupling Beams of Reinforced Concrete Shear Walls," ASCE Journal of the Structural Division, V. 97(3), pp. 843-862.

Perera, S. V. T. J., and Mutsutoshi, H. (2013). "Shear Behavior of Reinforced High-Strength Concrete Beams," ACI Structural Journal, V. 110(1), pp. 43-52.

Reineck, K. H., Bentz, E. C., Fitik, B., Kuchma, D. A., and Bayrak, O. (2013). "ACI-DAfStb Database of Shear Tests on Slender Reinforced Concrete Beams without Stirrups," ACI Structural Journal, V.110(6), pp. 867-875.

Reineck, K. H., Bentz, E., Fitik, B., Kuchma, D. A., and Bayrak, O. (2014a). "ACI-DAfStb Databases for Shear Tests on Slender Reinforced Concrete Beams with Stirrups," ACI Structural Journal, V. 111(5), pp. 1147–1156.

Reineck, K.-H., and Todisco, L. (2014b). "Database of Shear Tests for Non-Slender Reinforced Concrete Beams without Stirrups," ACI Structural Journal, V. 111(6), pp. 1363-1372.

Restrepo, J. I., Tobolski, M. J., and Matsumoto, E. E. (2011). "Development of a Precast Bent Cap System for Seismic Regions," NCHRP Report 681, Transportation Research Board, Washington, D.C.

Richart, F. (1927). "An Investigation of Web Stresses in Reinforced Concrete Beams," University of Illinois Engineering Experiment Station, Bulletin No. 166, Urbana, Illinois.

Ritter, W. (1899). "Construction techniques of Hennebique (Die Bauweise Hennebique)," Schweizerische Bauzeitung, V. 33(7), pp. 59-61 (in German).

Roller, J.J., and Russell, H.G. (1990). "Shear Strength of High-Strength Concrete Beams with Web Reinforcement," ACI Structural Journal, V. 87(2), pp. 191-198.

Runzell, B., Shield, C., and French, C. (2007). "Shear Capacity of Prestressed Concrete Beams," Rep. No. MN/RC 2007 47, Minnesota Department of Transportation, University of Minnesota.

Russo, G., Zingone, G., and Puleri, G. (1991). "Flexure-Shear Interaction Model for Longitudinally Reinforced Beams," ACI Structural Journal, V. 88(1), pp. 60-68.

Sahoo, D.K., Sagi, M.S.V., Singh, B., and Bhargava, B. (2010). "Effect of detailing of web reinforcement on the behavior of bottle-shaped struts," Journal of Advanced Concrete Technology, V. 8(3), pp. 303-314.

SAP2000 v14. (2009). "SAP2000, Advanced 14.0.0," Computers and Structures, Inc., Berkeley, California, USA.

SAP2000 v17. (2014). "SAP2000, Advanced 17.0.0," Computers and Structures, Inc., Berkeley, California, USA.

Schlaich, J., Schaefer, K., and Jennewein, M. (1987). "Toward a Consistent Design of Structural Concrete," PCI Journal, V. 32 (3), pp.74-150.

Scott, R.M., Mander, J.B., and Bracci, J.M. (2012a). "Compatibility Strut-and-Tie Modeling: Part I—Formulation," ACI Structural Journal, V. 109(5), pp. 635–644.

Scott, R.M., Mander, J.B., and Bracci, J.M. (2012b). "Compatibility Strut-and-Tie Modeling: Part II —Implementation," ACI Structural Journal, V. 109(5), pp. 645–653.

Talbot, A. (1909). "Tests of Reinforced Concrete Beams: Resistance to Web Stresses, Series of 1907 and 1908," University of Illinois Engineering Experiment Station, Bulletin No. 29, Urbana, Illinois.

Taylor, A. W., Rowell, R. B., and Breen, J. E. (1995). "Behavior of Thin Walled Concrete Box Piers," ACI Structural Journal, V. 92(3), pp. 319 333.

To, N.H.T., Ingham, J.M., and Davidson, B.J. (2003). "Cyclic Strut-and-Tie Modeling of Reinforced Concrete Structures," 2003 Pacific Conference on Earthquake Engineering, pp. 102-110.

To, N.H.T., Ingham, J.M., and Sritharan, S. (2001). "Monotonic Nonlinear Strut-and-Tie Computer Models," Bulletin of the New Zealand Society for Earthquake Engineering, V. 34(3), pp. 169-190.

To, N.H.T., Ingham, J.M., and Sritharan, S. (2002). "Strut-and-Tie Computer Modelling of Reinforced Concrete Bridge Portal Frames," Bulletin of the New Zealand Society for Earthquake Engineering, V. 35(3), pp. 165-189.

Todisco, L., Reineck, K. H., and Bayrak, O. (2015). "Database with Shear Tests on Non-Slender Reinforced Concrete Beams with Vertical Stirrups," ACI Structural Journal, V. 112(6), pp. 761-769.

Tuchscherer, R. G., Birrcher, D. B., Williams, C. S., Deschenes, D. J., and Bayrak, O. (2014). "Evaluation of Existing Strut-and-Tie Methods and Recommended Improvements," ACI Structural Journal, V. 111(6), pp. 1451-1460.

Tureyen, A. K., and Frosch, R. J. (2003). "Concrete Shear Strength: Another Perspective," ACI Structural Journal, V. 100(5), pp. 609-615.

Ueda, T., and Stitmannaithum, B. (1991). "Shear Strength of Precast Prestressed Hollow Slabs with Concrete Topping," ACI Structural Journal, V. 88(4), pp. 402 410.

Vecchio, F. J., and Collins, M. P. (1986). "The Modified Compression Field Theory for Reinforced Concrete Elements Subjected to Shear," ACI Structural Journal, V. 83(2), pp. 219-231.

Vecchio, F. J., and Collins, M. P. (1988). "Predicting the Response of Reinforced Concrete Beams Subjected to Shear Using Modified Compression Field," ACI Structural Journal, V. 85(3), pp. 258-268.

Vecchio, F.J. (2000). "Analysis of Shear-Critical Reinforced Concrete Beams," ACI Structural Journal, V. 97(1), pp. 102–110.

Zararis, P. D., and Papadakis, G. C. (2001). "Diagonal Shear Failure and Size Effect in RC Beams without Web Reinforcement," ASCE Journal of Structural Engineering, V.127(7), pp. 733-742.

Zhu, R. R. H., Wanichakom, W., Hsu, T. T. C., and Vogel, J. (2004). "Crack Width Prediction Using Compatibility-Aided Strut-and-Tie Model," ACI Structural Journal, V. 100(4), pp. 413-421.

Ziehl, P.H., Caicedo, J.M., Rizos, D., Mays, T., Larosche, A., ElBatanouny, M., and Mustain, B. (2011). "Testing of Connections between Prestressed Concrete Piles and Precast Concrete Bent Caps," Department of Civil and Environmental Engineering, University of South Carolina, South Carolina Department of Transportation.

Zsutty, T. C. (1971). "Shear Strength Prediction for Separate Categories of Simple Beam Tests," ACI Journal, Proceedings V. 68(2), pp. 138-143.

APPENDIX A

SHEAR TEST DATABASE

The detailed information of the in this appendix. The database is consisted of four data sets, including a) deep beams with transverse reinforcement; b) slender beams with transverse reinforcement; c) deep beams without transverse reinforcement; and d) slender beams without transverse reinforcement. The data sets a) and b) are used to verify the *TAMU* method with a vertical tie for beams with transverse reinforcement, and (c) and (d) are used to validate for the *TAMU* method with an inclined tie for beams without transverse reinforcement. The information presented in the following tables are:

Ref.   =   reference number given for each database set

I.D.   =   identification of specimen used in original references

b =   effective width of the member

d =   effective depth of the member

a =   shear span length

a/d =   shear span to depth ratio

ρ_L =   ratio of area of longitudinal steel to area of concrete

ρ_v =   ratio of area of transverse steel to area of concrete for one hoop spacing

f'_c =   compressive strength of the concrete

f_y =   yield strength of the longitudinal steel

V_{test} =   maximum capacity measured in the test

A.1 Database of Deep Beams with Transverse Reinforcement

1. Anderson, N.S., and Ramirez, J.A. (1989). "Detailing of Stirrup Reinforcement," ACI Structural Journal, V.86(5), pp. 507-515.

2. Bracci, J.M., Keating, P.B., and Hueste, M.B.D. (2000). "Cracking in RC Bent Caps," Rep. No. FHWA/TX 01/1851, Texas Transportation Institute, Texas A&M University.

3. Brown M. D. (2005). "Design for Shear in Reinforced Concrete Using Strut-and-Tie and Sectional Models." Ph.D. dissertation. The University of Texas at Austin.

4. Clark, A.P. (1951). "Diagonal Tension in Reinforced Concrete Beams," ACI Journal, Proceedings V.48(10), pp. 145-156.

5. Gabrielsson, H. (1992). "Shear Capacity of Beams of Reinforced High Performance Concrete,", and "Bending and Shear Tests on Reinforced High-Performance Concrete Beams," (1993) Internal Report K1:1, Division of Structural Engineering, Lulea University of Technology, 52 and 59 pp.

6. Kong, F.K., Robins, P.J. and Cole, D.F. (1970). "Web Reinforcement Effects on Deep Beam," ACI Journal, Proceedings, Vol. 67 (12), pp. 1010-1017.

7. Kong, P. Y. L., and Rangan, B. V. (1998). "Shear Strength of High-Performance Concrete Beams," ACI Structural Journal, V.95(6), pp. 677-688.

8. Kriski, W. (1996). "Shear Strength of Reinforced Concrete Beams," Master Thesis, Department of Civil Engineering University of Calgary, Calgary, Alberta, Canada.

9. Oh, J. K., and Shin, S. W. (2001). "Shear Strength of Reinforced HighStrength Concrete Deep Beams," ACI Structural Journal, V.98(2), pp. 164-173.

10. Rodriguez, J. J., Bianchini, A. C., Viest, I. M., and Kesler, C. E. (1955). "Shear Strength of Two-Span Continuous Reinforced Concrete Beams," ACI Journal, Proceedings, V.55(10), pp. 1089-1130.

11. Roller, J.J., and Russell, H.G. (1990). "Shear Strength of High-Strength Concrete Beams with Web Reinforcement," ACI Structural Journal, V.87(2), pp. 191-198.

12. Sarsam, K.F., and Al-Musawi, J.M.S. (1992). "Shear Design of High- and Normal Strength Concrete Beams with Web Reinforcement," ACI Structural Journal, V.89(6), pp. 658-664.

13. Shin, S.-W., Lee, K.-S., Moon, J.-I., Ghosh, S.K. (1999). "Shear Strength of Reinforced HighStrength Concrete Beams with Shear Span-to-Depth Ratios between 1.5 and 2.5," ACI Structural Journal, V.96(4), pp. 549-556.

14. Smith, K. N., and Vantsiotis, A. S. (1982). "Shear Strength of Deep Beams," ACI Journal, Proceedings, V.79(3), pp. 201-213.

15. Tan, K. H., Kong, F., Teng, S., and Guan, L. (1995). "High-Strength Concrete Deep Beams with Effective Span and Shear Span Variations," ACI Structural Journal, V.92(4), pp. 1-11.

16. Tanimura, Y., and Sato, T. (2005). "Evaluation of Shear Strength of Deep Beams with Stirrups," Quarterly Report of the Railway Technical Research Institute, V.46(1), pp. 53-58.

17. Xie, Y., Ahmad, S.H., T. Yu, Hion, S., and Chung, W. (1994). "Shear Ductility of Reinforced Concrete Beams of Normal and High-Strength Concrete," ACI Structural Journal, V.91(2), pp. 140-149.

Table A-1. Database of deep beams with transverse reinforcement

Ref.	I.D	b (mm)	d (mm)	a (mm)	a/d	ρ_L	ρ_v	f'_c (MPa)	f_y (MPa)	V_{test} (kN)
No.1	W1	406	343	812	2.4	1.92	0.39	29.2	434	458
	W2	406	343	812	2.4	1.92	0.39	32.2	434	549
	W3	406	343	812	2.4	1.92	0.40	32.3	434	504
No.2	RC-1A	838	787	1102	1.4	0.53	0.30	42.8	448	1668
	RC-1B	838	787	1102	1.4	0.53	0.30	40.0	448	1815
	RC-2A	838	787	1102	1.4	0.53	0.30	42.8	448	1797
	RC-2B	838	787	1102	1.4	0.53	0.30	40.0	448	1695
	RC-3C	838	787	1102	1.4	0.56	0.30	41.4	448	1873
	RC-3D	838	787	1102	1.4	0.56	0.30	37.9	448	2042
	RC-4C	838	787	1102	1.4	0.75	0.30	41.4	448	1908
	RC-4E	838	787	1102	1.4	0.75	0.30	53.1	448	2024
	RC-5D	838	787	1102	1.4	0.73	0.30	37.9	448	2069
	RC-5E	838	787	1102	1.4	0.73	0.30	53.1	448	2140
	RC-6F	838	787	1102	1.4	0.53	0.60	37.9	448	1913
	RC-6G	838	787	1102	1.4	0.53	0.60	36.6	448	1788
	RC-7F	838	787	1102	1.4	0.73	0.60	37.9	448	2224
	RC-7H	838	787	1102	1.4	0.73	0.60	39.3	448	2126
	RC-8G	838	787	1102	1.4	0.53	0.60	36.6	448	1926
	RC-8H	838	787	1102	1.4	0.53	0.60	39.3	448	2104
No.3	I-2C-85-0	152	686	762	1.1	1.76	0.43	22.1	469	485
	I-CL-85-0	152	686	381	0.6	1.76	0.43	17.8	469	739
	II-N-E-58-8-N	457	406	686	1.7	1.95	0.15	19.7	469	457
	II-N-F-58-8-N	457	406	686	1.7	1.95	0.15	19.7	469	489
	II-N-C-58-8-N	457	406	686	1.7	1.95	0.15	19.7	469	680
	II-N-F-58-3-N	457	406	686	1.7	1.95	0.41	19.9	469	798
	II-N-C-46-8-N	457	406	686	1.7	1.95	0.15	19.9	469	832
	II-N-E-46-8-N	457	406	686	1.7	1.95	0.15	19.9	469	617
	II-N-F-46-8-N	457	406	686	1.7	1.95	0.15	21.6	469	494
	II-W-E-58-8-N	762	406	686	1.7	2.19	0.09	21.4	469	1186
	II-W-E-45-8-N	762	406	686	1.7	2.19	0.09	24.6	469	1048
	II-W-E-3-8-N	762	406	686	1.7	2.19	0.09	25.2	469	662

Ref.	I.D	b (mm)	d (mm)	a (mm)	a/d	ρ_L	ρ_v	f'_c (MPa)	f_y (MPa)	V_{test} (kN)
	A1-1	203	406	826	2.0	2.65	0.38	24.7	321	222
	A1-2	203	406	826	2.0	2.65	0.38	23.7	321	209
	A1-3	203	406	826	2.0	2.65	0.38	23.3	321	222
	A1-4	203	406	826	2.0	2.65	0.38	24.8	321	245
	B1-1	203	406	673	1.7	2.65	0.37	23.4	321	279
	B1-2	203	406	673	1.7	2.65	0.37	25.4	321	257
	B1-3	203	406	673	1.7	2.65	0.37	23.7	321	285
	B1-4	203	406	673	1.7	2.65	0.37	23.3	321	268
	B1-5	203	406	673	1.7	2.65	0.37	24.6	321	241
	B2-1	203	406	673	1.7	2.65	0.73	23.2	321	301
	B2-2	203	406	673	1.7	2.65	0.73	26.3	321	322
	B2-3	203	406	673	1.7	2.65	0.73	24.9	321	335
	B6-1	203	406	673	1.7	2.65	0.37	42.1	321	379
	C1-1	203	406	521	1.3	1.76	0.34	25.7	321	278
	C1-2	203	406	521	1.3	1.76	0.34	26.3	321	311
No.4	C1-3	203	406	521	1.3	1.76	0.34	24.0	321	246
	C1-4	203	406	521	1.3	1.76	0.34	29.0	321	286
	C2-1	203	406	521	1.3	1.76	0.69	23.7	321	290
	C2-2	203	406	521	1.3	1.76	0.69	25.0	321	301
	C2-3	203	406	521	1.3	1.76	0.69	24.1	321	324
	C2-4	203	406	521	1.3	1.76	0.69	27.0	321	288
	C3-1	203	406	521	1.3	1.76	0.34	14.1	321	224
	C3-2	203	406	521	1.3	1.76	0.34	13.8	321	200
	C3-3	203	406	521	1.3	1.76	0.34	13.9	321	188
	C4-1	203	406	521	1.3	2.65	0.34	24.5	321	309
	C6-2	203	406	521	1.3	2.65	0.34	45.2	321	424
	C6-3	203	406	521	1.3	2.65	0.34	44.7	321	435
	C6-4	203	406	521	1.3	2.65	0.34	47.6	321	429
	D1-1	203	406	368	0.9	1.39	0.46	26.2	321	301
	D1-2	203	406	368	0.9	1.39	0.46	26.1	321	357
	D1-3	203	406	368	0.9	1.39	0.46	24.6	321	257

Ref.	I.D	b (mm)	d (mm)	a (mm)	a/d	ρ_L	ρ_v	f'_c (MPa)	f_y (MPa)	V_{test} (kN)
No.4	D2-1	203	406	368	0.9	1.39	0.61	24.0	321	290
	D2-2	203	406	368	0.9	1.39	0.61	25.9	321	312
	D2-3	203	406	368	0.9	1.39	0.61	24.8	321	334
	D2-4	203	406	368	0.9	1.39	0.61	24.5	321	335
	D3-1	203	406	368	0.9	2.08	0.92	28.2	321	379
	D4-1	203	406	368	0.9	1.39	1.22	23.1	321	312
	D1-6	152	330	521	1.6	2.82	0.46	27.7	321	175
	D1-7	152	330	521	1.6	2.82	0.46	28.0	321	179
	D1-8	152	330	521	1.6	2.82	0.46	27.8	321	186
	E1-2	152	330	521	1.6	2.82	0.73	30.2	321	222
	D2-6	152	330	673	2.0	2.82	0.61	29.5	321	168
	D2-7	152	330	673	2.0	2.82	0.61	28.4	321	157
	D2-8	152	330	673	2.0	2.82	0.61	26.1	321	168
	D4-1	152	330	673	2.0	2.82	0.49	27.4	321	168
	D4-2	152	330	673	2.0	2.82	0.49	25.7	321	157
	D4-3	152	330	673	2.0	2.82	0.49	22.1	321	165
	D5-1	152	330	673	2.0	2.82	0.37	27.7	321	146
	D5-2	152	330	673	2.0	2.82	0.37	29.0	321	157
	D5-3	152	330	673	2.0	2.82	0.37	27.1	321	157
No.5	HB2	200	223	392	1.8	4.02	0.41	108.0	400	644
	HB3	200	223	392	1.8	4.02	0.76	108.0	400	749
	B1	200	257	473	1.8	2.01	0.15	126.0	400	482
	B2	200	257	432	1.7	2.01	0.20	129.0	400	483
	B3	200	257	391	1.5	2.01	0.25	149.0	400	600
	B4	200	257	370	1.4	2.01	0.29	149.0	400	661
	B5	200	257	288	1.1	2.01	0.34	149.0	400	850
	B6	200	257	391	1.5	2.01	0.39	147.0	400	578
	B7	200	257	391	1.5	2.01	0.44	147.0	400	581
	B8	200	257	391	1.5	2.01	0.48	147.0	400	576
	HPS1	200	225	432	1.9	3.22	0.34	123.0	600	648
	HPS2	200	225	432	1.9	3.22	0.34	129.0	600	610

Ref.	I.D	b (mm)	d (mm)	a (mm)	a/d	ρ_L	ρ_v	f'_c (MPa)	f_y (MPa)	V_{test} (kN)
No.6	1-30	76	724	254	0.4	0.49	2.44	21.5	287	217
	1-25	76	597	254	0.4	0.59	2.44	24.6	287	203
	1-20	76	470	254	0.5	0.73	2.44	21.2	287	172
	1-15	76	343	254	0.7	0.98	2.44	21.2	287	149
	1-10	76	216	254	1.2	1.47	2.44	21.7	287	81
	2-30	76	724	254	0.4	0.49	0.85	19.2	287	226
	2-25	76	597	254	0.4	0.59	0.85	18.6	287	203
	2-20	76	470	254	0.5	0.73	0.85	19.9	287	195
	2-15	76	343	254	0.7	0.98	0.85	22.8	287	127
	2-10	76	216	254	1.2	1.47	0.85	20.1	287	90
No.7	S1-1	250	292	730	2.5	2.34	0.16	63.6	452	228
	S1-2	250	292	730	2.5	2.34	0.16	63.6	452	208
	S1-3	250	292	730	2.5	2.34	0.16	63.6	452	206
	S1-4	250	292	730	2.5	2.34	0.16	63.6	452	278
	S1-5	250	292	730	2.5	2.34	0.16	63.6	452	253
	S1-6	250	292	730	2.5	2.34	0.16	63.6	452	224
	S2-1	250	292	730	2.5	2.34	0.11	72.5	452	260
	S2-2	250	292	730	2.5	2.34	0.13	72.5	452	233
	S2-3	250	292	730	2.5	2.34	0.16	72.5	452	253
	S2-4	250	292	730	2.5	2.34	0.16	72.5	452	219
	S2-5	250	292	730	2.5	2.34	0.21	72.5	452	282
	S2-6	250	292	730	2.5	2.34	0.26	72.5	452	359
	S3-1	250	297	740	2.5	1.41	0.10	67.4	450	209
	S3-2	250	297	740	2.5	1.41	0.10	67.4	450	178
	S3-3	250	293	730	2.5	2.34	0.10	67.4	452	229
	S3-4	250	293	730	2.5	2.34	0.10	67.4	452	175
	S3-5	250	299	720	2.4	3.15	0.10	67.4	442	297
	S3-6	250	299	720	2.4	3.15	0.10	67.4	442	283
	S4-1	250	542	1300	2.4	2.73	0.16	87.3	452	354
	S4-2	250	444	1070	2.4	2.63	0.16	87.3	433	573
	S4-3	250	346	830	2.4	2.46	0.16	87.3	450	243

Table A-1. Continued

(d) 5/11

Ref.	I.D	b (mm)	d (mm)	a (mm)	a/d	ρ_L	ρ_v	f'_c (MPa)	f_y (MPa)	V_{test} (kN)
No.7	S4-4	250	292	730	2.5	2.34	0.16	87.3	452	258
	S4-5	250	248	590	2.4	2.45	0.16	87.3	442	321
	S5-3	250	292	730	2.5	2.34	0.16	89.4	452	244
	S5-4	250	292	580	2.0	2.34	0.16	89.4	452	477
	S5-5	250	292	510	1.7	2.34	0.16	89.4	452	573
	S5-6	250	292	440	1.5	2.34	0.16	89.4	452	648
	S8-1	250	292	730	2.5	2.34	0.11	74.6	452	272
	S8-2	250	292	730	2.5	2.34	0.13	74.6	452	251
	S8-3	250	292	730	2.5	2.34	0.16	74.6	452	310
	S8-4	250	292	730	2.5	2.34	0.16	74.6	452	266
	S8-5	250	292	730	2.5	2.34	0.20	74.6	452	289
	S8-6	250	292	730	2.5	2.34	0.22	74.6	452	284
No.8	5	360	345	750	2.2	1.73	0.09	30.1	433	293
	8	360	345	750	2.2	1.73	0.09	77.8	433	391
	10	360	345	750	2.2	1.73	0.09	76.3	433	391
No.9	H41A2(1)	130	499	249	0.5	1.39	0.12	49.0	448	713
	H42A2(1)	130	499	432	0.9	1.39	0.12	49.0	448	488
	H43A2(1)	130	499	635	1.3	1.39	0.12	49.0	448	347
	H45A2	130	499	1016	2.0	1.39	0.12	49.0	448	211
	H41B2	130	499	249	0.5	1.39	0.22	49.0	448	706
	H42B2(1)	130	499	432	0.9	1.39	0.22	49.0	448	456
	H43B2	130	499	635	1.3	1.39	0.22	49.0	448	381
	H45B2	130	499	1003	2.0	1.39	0.22	49.0	448	237
	H41C2	130	499	249	0.5	1.39	0.35	49.0	448	709
	H42C2(1)	130	499	432	0.9	1.39	0.35	49.0	448	421
	H43C2	130	499	635	1.3	1.39	0.35	49.0	448	402
	H45C2	130	499	1016	2.0	1.39	0.35	49.0	448	235
	N42A2	130	500	425	0.8	1.40	0.12	23.7	448	284
	N42B2	130	500	425	0.8	1.40	0.22	23.7	448	377
	N42C2	130	500	425	0.8	1.40	0.35	23.7	448	358
	N33A2	130	500	625	1.2	1.40	0.12	23.7	448	228

Ref.	I.D	b (mm)	d (mm)	a (mm)	a/d	ρ_L	ρ_v	f'_c (MPa)	f_y (MPa)	V_{test} (kN)
	N43A2	130	500	625	1.2	1.40	0.12	23.7	448	255
	N53A2	130	500	625	1.2	1.40	0.12	23.7	448	207
	H41A2(1)*	130	500	250	0.5	1.40	0.12	49.1	448	713
	H41B2	130	500	250	0.5	1.40	0.22	49.1	448	706
	H41C2	130	500	250	0.5	1.40	0.35	49.1	448	709
	H42A2(1)	130	500	425	0.8	1.40	0.12	49.1	448	488
	H42B2(1)	130	500	425	0.8	1.40	0.22	49.1	448	456
	H42C2(1)	130	500	425	0.8	1.40	0.35	49.1	448	421
	H43A2(1)	130	500	625	1.2	1.40	0.12	49.1	448	347
	H43B2	130	500	625	1.2	1.40	0.22	49.1	448	381
	H43C2	130	500	625	1.2	1.40	0.35	49.1	448	402
	H45A2	130	500	1000	2.0	1.40	0.12	49.1	448	211
	H45B2	130	500	1000	2.0	1.40	0.22	49.1	448	237
	H45C2	130	500	1000	2.0	1.40	0.35	49.1	448	235
	H42A2(2)	120	500	425	0.8	1.15	0.13	50.7	448	392
No.9	H42B2(2)	120	500	425	0.8	1.15	0.24	50.7	448	361
	H42C2(2)	120	500	425	0.8	1.15	0.38	50.7	448	374
	H43A0	120	500	625	1.2	1.15	0.13	50.7	448	214
	H43A1	120	500	625	1.2	1.15	0.13	50.7	448	260
	H43A2(2)	120	500	625	1.2	1.15	0.13	50.7	448	277
	H43A3	120	500	625	1.2	1.15	0.13	50.7	448	291
	H45A2(2)	120	500	1000	2.0	1.15	0.13	50.7	448	165
	H31A2	130	500	250	0.5	1.40	0.12	49.1	448	746
	H41A2(1)*	130	500	250	0.5	1.40	0.12	49.1	448	713
	H51A2	130	500	250	0.5	1.40	0.12	49.1	448	702
	H32A2	130	500	425	0.8	1.40	0.12	49.1	448	530
	H42A2(1)	130	500	425	0.8	1.40	0.12	49.1	448	488
	H52A2	130	500	425	0.8	1.40	0.12	49.1	448	568
	H33A2	130	500	625	1.2	1.40	0.12	49.1	448	378
	H43A2(1)	130	500	625	1.2	1.40	0.12	49.1	448	347
	H53A2	130	500	625	1.2	1.40	0.12	49.1	448	363

Ref.	I.D	b (mm)	d (mm)	a (mm)	a/d	ρ_L	ρ_v	f'_c (MPa)	f_y (MPa)	V_{test} (kN)
	H45A2	130	500	1000	2.0	1.40	0.12	49.1	448	211
	N42A2	130	500	425	0.8	1.40	0.12	23.7	448	284
	N43A2	130	500	625	1.2	1.40	0.12	23.7	448	255
No.9	U41A2	130	500	250	0.5	1.45	0.12	73.6	448	548
	U42A2	130	500	425	0.8	1.45	0.12	73.6	448	418
	U43A2	130	500	625	1.2	1.45	0.12	73.6	448	338
	U45A2	130	500	1000	2.0	1.45	0.12	73.6	448	214
	E3H1	152	318	762	2.4	1.36	1.10	24.8	380	107
No.10	E3H2	152	311	762	2.5	1.33	0.87	27.5	377	95
	C3H1	152	318	762	2.4	1.36	1.10	22.6	385	95
	C3H2	152	323	762	2.4	1.38	0.87	22.8	410	87
	2	356	559	1194	2.1	2.50	0.43	120.1	431	1097
No.11	3	356	559	1194	2.1	3.55	0.88	120.1	431	1655
	4	356	559	1194	2.1	4.73	1.25	120.1	431	1940
	5	356	559	1194	2.1	5.24	1.74	120.1	462	2235
	AS2-N	180	241	587	2.4	1.94	0.09	39.3	448	189
	AS2-H	180	241	587	2.4	1.94	0.09	75.2	448	201
	AS3-N	180	241	587	2.4	1.94	0.14	40.0	448	199
	AS3-H	180	241	587	2.4	1.94	0.14	71.7	448	199
No.12	BS2-H	180	241	587	2.4	2.43	0.09	73.8	448	224
	BS3-H	180	241	587	2.4	2.43	0.14	73.1	448	228
	BS4-H	180	241	587	2.4	2.43	0.18	80.0	448	207
	CS2-H	180	241	587	2.4	3.03	0.09	70.3	448	247
	CS3-H	180	241	587	2.4	3.03	0.14	74.5	448	247
	CS4-H	180	241	587	2.4	3.03	0.18	75.7	448	221
	MHB-15-25	124	216	324	1.5	3.29	0.45	52.4	414	156
	MHB-15-50	124	216	324	1.5	3.29	0.91	52.4	414	208
No.13	MHB-15-75	124	216	324	1.5	3.29	1.36	52.4	414	240
	MHB-15-100	124	216	324	1.5	3.29	1.81	52.4	414	257
	MHB-20-25	124	216	432	2.0	3.29	0.32	52.4	414	111
	MHB-20-50	124	216	432	2.0	3.29	0.65	52.4	414	174

Ref.	I.D	b (mm)	d (mm)	a (mm)	a/d	ρ_L	ρ_v	f'_c (MPa)	f_y (MPa)	V_{test} (kN)
No.13	MHB-20-75	124	216	432	2.0	3.29	0.97	52.4	414	185
	MHB-20-100	124	216	432	2.0	3.29	1.29	52.4	414	193
	MHB-25-25	124	216	540	2.5	3.29	0.25	52.4	414	99
	MHB-25-50	124	216	540	2.5	3.29	0.47	52.4	414	139
	MHB-25-75	124	216	540	2.5	3.29	0.71	52.4	414	165
	MHB-25-100	124	216	540	2.5	3.29	0.94	52.4	414	164
	HB-15-25	124	216	324	1.5	3.29	0.45	73.1	414	214
	HB-15-50	124	216	324	1.5	3.29	0.91	73.1	414	246
	HB-15-75	124	216	324	1.5	3.29	1.36	73.1	414	266
	HB-15-100	124	216	324	1.5	3.29	1.81	73.1	414	280
	HB-20-25	124	216	432	2.0	3.29	0.32	73.1	414	143
	HB-20-50	124	216	432	2.0	3.29	0.65	73.1	414	196
	HB-20-75	124	216	432	2.0	3.29	0.97	73.1	414	230
	HB-20-100	124	216	432	2.0	3.29	1.29	73.1	414	242
	HB-25-25	124	216	540	2.5	3.29	0.24	73.1	414	115
	HB-25-50	124	216	540	2.5	3.29	0.47	73.1	414	149
	HB-25-75	124	216	540	2.5	3.29	0.71	73.1	414	167
	HB-25-100	124	216	540	2.5	3.29	0.94	73.1	414	184
No.14	1A1-10	102	305	133	0.4	1.66	0.27	18.7	431	161
	1A3-11	102	305	133	0.4	1.66	0.27	18.0	431	148
	1A4-12	102	305	133	0.4	1.66	0.27	16.1	431	141
	1A4-51	102	305	133	0.4	1.66	0.27	20.6	431	171
	1A6-37	102	305	133	0.4	1.66	0.27	21.1	431	184
	2A1-38	102	305	133	0.4	1.66	0.61	21.7	431	175
	2A3-39	102	305	133	0.4	1.66	0.61	19.8	431	171
	2A4-40	102	305	133	0.4	1.66	0.61	20.3	431	172
	2A6-41	102	305	133	0.4	1.66	0.61	19.1	431	162
	3A1-42	102	305	133	0.4	1.66	1.23	18.4	431	161
	3A3-43	102	305	133	0.4	1.66	1.23	19.2	431	173
	3A4-45	102	305	133	0.4	1.66	1.23	20.8	431	179
	3A6-46	102	305	133	0.4	1.66	1.23	19.9	431	168

Ref.	I.D	b (mm)	d (mm)	a (mm)	a/d	ρ_L	ρ_v	f'_c (MPa)	f_y (MPa)	V_{test} (kN)
	1B1-01	102	305	206	0.7	1.66	0.23	22.1	431	147
	1B3-29	102	305	206	0.7	1.66	0.23	20.1	431	143
	1B4-30	102	305	206	0.7	1.66	0.23	20.8	431	140
	1B6-31	102	305	206	0.7	1.66	0.23	19.5	431	153
	2B1-05	102	305	206	0.7	1.66	0.41	19.2	431	129
	2B3-06	102	305	206	0.7	1.66	0.41	19.0	431	131
	2B4-07	102	305	206	0.7	1.66	0.41	17.5	431	126
	2B4-52	102	305	206	0.7	1.66	0.41	21.8	431	150
	2B6-32	102	305	206	0.7	1.66	0.41	19.8	431	145
	3B1-08	102	305	206	0.7	1.66	0.61	16.2	431	131
	3B1-36	102	305	206	0.7	1.66	0.76	20.4	431	159
	3B3-33	102	305	206	0.7	1.66	0.76	19.0	431	158
	3B4-34	102	305	206	0.7	1.66	0.76	19.2	431	155
	3B6-35	102	305	206	0.7	1.66	0.76	20.7	431	166
	4B1-09	102	305	206	0.7	1.66	1.23	17.1	431	153
No.14	1C1-14	102	305	307	1.0	1.66	0.18	19.2	431	119
	1C3-02	102	305	307	1.0	1.66	0.18	21.9	431	123
	1C4-15	102	305	307	1.0	1.66	0.18	22.7	431	131
	1C6-16	102	305	307	1.0	1.66	0.18	21.8	431	122
	2C1-17	102	305	307	1.0	1.66	0.31	19.9	431	124
	2C3-03	102	305	307	1.0	1.66	0.31	19.2	431	104
	2C3-27	102	305	307	1.0	1.66	0.31	19.3	431	115
	2C4-18	102	305	307	1.0	1.66	0.31	20.4	431	125
	2C6-19	102	305	307	1.0	1.66	0.31	20.8	431	124
	3C1-20	102	305	307	1.0	1.66	0.55	21.0	431	141
	3C3-21	102	305	307	1.0	1.66	0.55	16.6	431	125
	3C4-22	102	305	307	1.0	1.66	0.55	18.3	431	128
	3C6-23	102	305	307	1.0	1.66	0.55	19.0	431	137
	4C1-24	102	305	307	1.0	1.66	0.76	19.6	431	147
	4C3-04	102	305	307	1.0	1.66	0.61	18.6	431	129
	4C3-28	102	305	307	1.0	1.66	0.76	19.2	431	152

Ref.	I.D	b (mm)	d (mm)	a (mm)	a/d	ρ_L	ρ_v	f'_c (MPa)	f_y (MPa)	V_{test} (kN)
No.14	4C4-25	102	305	307	1.0	1.66	0.76	18.5	431	153
	4C6-26	102	305	307	1.0	1.66	0.76	21.2	431	159
	4D1-13	102	305	511	1.7	1.66	0.41	16.1	431	87
No.15	Tan-A1	110	464	125	0.3	1.14	0.47	58.8	503	675
	Tan-A2	110	464	125	0.3	1.14	0.47	51.6	503	630
	Tan-A3	110	464	125	0.3	1.14	0.47	53.8	503	640
	Tan-A4	110	464	125	0.3	1.14	0.47	57.3	503	630
	Tan-B1	110	464	250	0.5	1.14	0.47	56.0	503	468
	Tan-B2	110	464	250	0.5	1.14	0.47	45.7	503	445
	Tan-B3	110	464	250	0.5	1.14	0.47	53.9	503	550
	Tan-B4	110	464	250	0.5	1.14	0.47	53.0	503	480
	Tan-C1	110	464	375	0.8	1.14	0.47	51.2	503	403
	Tan-C2	110	464	375	0.8	1.14	0.47	44.0	503	400
	Tan-D1	110	464	500	1.1	1.14	0.47	48.2	503	270
	Tan-D2	110	464	500	1.1	1.14	0.47	44.1	503	280
	Tan-D3	110	464	500	1.1	1.14	0.47	46.8	503	290
	Tan-D4	110	464	500	1.1	1.14	0.47	48.0	503	290
	Tan-E1	110	464	750	1.6	1.14	0.47	50.6	503	220
	Tan-E2	110	464	750	1.6	1.14	0.47	44.6	503	190
	Tan-E3	110	464	750	1.6	1.14	0.47	45.3	503	173
	Tan-F	110	464	1000	2.2	1.14	0.47	41.1	503	150
No.16	A-2	300	400	200	0.5	1.90	0.22	23.2	458	821
	A-3	300	400	200	0.5	1.90	0.47	23.2	458	833
	A-4	300	400	200	0.5	1.90	0.84	23.2	458	869
	A-6	300	400	400	1.0	1.90	0.22	29.1	458	731
	A-7	300	400	400	1.0	1.90	0.47	29.2	458	750
	A-8	300	400	400	1.0	1.90	0.84	29.3	458	804
	A-10	300	400	600	1.5	1.90	0.22	22.5	458	464
	A-11	300	400	600	1.5	1.90	0.47	23.0	458	491
	A-12	300	400	600	1.5	1.90	0.84	23.5	458	570
	B-14	300	400	400	1.0	1.90	0.22	32.0	458	751

Ref.	I.D	b (mm)	d (mm)	a (mm)	a/d	ρ_L	ρ_v	f'_c (MPa)	f_y (MPa)	V_{test} (kN)
No.16	B-15	300	400	400	1.0	1.90	0.47	32.0	458	774
	B-16	300	400	400	1.0	1.90	0.84	32.0	458	849
	C-17	300	400	400	1.0	1.90	0.22	31.3	458	570
	C-18	300	400	400	1.0	1.90	0.47	31.5	458	773
	C-19	300	400	400	1.0	1.90	0.84	31.8	458	756
	D-20	300	400	400	1.0	1.90	0.47	24.3	702	665
	D-21	300	400	400	1.0	1.90	0.84	26.9	702	661
	D-22	300	400	600	1.5	1.90	0.47	26.2	702	537
	D-23	300	400	600	1.5	1.90	0.84	26.3	702	566
	A-28	300	400	300	0.7	1.90	0.47	25.5	458	647
	A-29	300	400	300	0.7	1.90	0.84	26.2	458	666
	A-30	300	400	300	0.7	1.90	0.87	26.4	458	701
	A-31	300	400	800	2.0	1.90	0.47	26.6	702	416
	A-32	300	400	800	2.0	1.90	0.84	27.4	702	440
	A-33	300	400	400	1.0	1.90	0.95	24.7	458	647
	A-34	300	400	400	1.0	1.90	0.95	24.8	458	598
	E-36	300	400	200	0.5	0.37	0.47	24.5	1330	539
	E-37	300	400	200	0.5	0.37	0.84	25.8	1330	554
	E-39	300	400	400	1.0	0.37	0.47	25.4	1330	470
	E-40	300	400	400	1.0	0.37	0.84	25.9	1330	470
	A-41	300	400	1000	2.5	1.90	0.47	20.6	750	324
	A-42	300	400	1000	2.5	1.90	0.84	21.4	750	376
	F-46	300	400	400	1.0	1.90	0.22	97.5	750	1243
	F-47	300	400	400	1.0	1.90	0.47	96.3	750	1300
	F-48	300	400	600	1.5	1.90	0.22	94.5	750	932
	F-49	300	400	600	1.5	1.90	0.47	94.2	750	980
No.17	NNW1	127	203	152	0.8	2.56	0.49	42.4	421	478
	NNW2	127	203	305	1.5	2.56	0.49	43.4	421	246
	NHW1	127	198	149	0.8	3.52	0.50	97.7	421	647
	NHW2	127	198	297	1.5	3.52	0.50	99.7	421	356

A.2 Database of Intermediate Beams with Transverse Reinforcement

1. Angelakos, D., Bentz, E. C., and Collins, M. P. (2001). "Effect of Concrete Strength and Minimum Stirrups on Shear Strength of Large Members," ACI Structural Journal, V.98(3), pp. 290-300.

2. Bresler, B., and Scordelis, A.C. (1963). "Shear Strength of Reinforced Concrete Beams," ACI Journal, Proceedings V.60(1), pp.51-74.

3. Brown, M. D. (2005). "Design for Shear in Reinforced Concrete Using Strut-and-Tie and Sectional Models," Ph.D. dissertation. The University of Texas at Austin.

4. Collins, M.P., and Kuchma, D. (1999). "How Safe Are Our Large, Lightly Reinforced Concrete Beams, Slabs, and Footings?," ACI Structural Journal, V.96(4), pp. 482-490.

5. Debaiky, S.Y., and Elniema, E.I. (1982). "Behavior and Strength of Reinforced Concrete Haunched Beams in Shear," ACI Journal, Proceedings V.79(3), pp. 184-194.

6. Elzanaty, A. H., Nilson, A. H., and Slate, F.O. (1986). "Shear Capacity of Reinforced Concrete Beams Using High Strength Concrete," ACI Journal, Proceedings V.83(2), pp. 290-296.

7. Gabrielsson, H. (1992). "Shear Capacity of Beams of Reinforced High Performance Concrete,", and "Bending and Shear Tests on Reinforced High-Performance Concrete Beams," (1993) Internal Report K1:1, Division of Structural Engineering, Lulea University of Technology, 52 and 59 pp.

8. Johnson, M.K., and Ramirez, J.A. (1989). "Minimum Shear Reinforcement in Beams with Higher Strength Concrete," ACI Structural Journal, V.86(4), pp. 376-382.

9. Kong, P. Y. L., and Rangan, B. V. (1998). "Shear Strength of High-Performance Concrete Beams," ACI Structural Journal, V.95(6), pp. 677-688.

10. Kriski, W. (1996). "Shear Strength of Reinforced Concrete Beams," Master Thesis, Department of Civil Engineering University of Calgary, Calgary, Alberta, Canada.

11. Mphonde, A. G., and Frantz, C. C. (1984). "Shear Tests of High- and Low-Strength Concrete Beams Without Stirrups," ACI Journal, Proceedings V.81(4), pp. 350-357.

12. Ozcebe, G., Ersoy, U., and Tankut, T. (1999). "Evaluation of Minimum Shear Reinforcement Requirements for Higher Strength Concrete," ACI Structural Journal, V.96(3), pp. 361-368.

13. Peng, L. (1999). "Shear Strength of Beams by Shear-Friction," M.S. Thesis, Department of Civil Engineering, University of Calgary, Calgary, Canada

14. Podgorniak-Stanik, B.A. (1998). "The Influence of Concrete Strength, Distribution of Longitudinal Reinforcement, Amount of Transverse Reinforcement and Member Size on Shear Strength of Reinforced Concrete Members," M.S. Thesis. University of Toronto

15. Rodriguez, J.J., Bianchini, A.C., Viest, I. M., and Kesler, C E. (1959). "Shear Strength of Two-span Continuous Reinforced Concrete Beams," ACI Journal, Proceedings V.56(4), pp. 1089-1130.

16. Roller, J.J., and Russell, H.G. (1990). "Shear Strength of High-Strength Concrete Beams with Web Reinforcement," ACI Structural Journal, V.87(2), pp. 191-198.

17. Sarsam, K.F., and Al-Musawi, J.M.S. (1992). "Shear Design of High- and Normal Strength Concrete Beams with Web Reinforcement," ACI Structural Journal, V.89(6), pp. 658-664.

18. Tan, K. H., Kong, F., Teng, S., and Guan, L. (1995). "High-Strength Concrete Deep Beams with Effective Span and Shear Span Variations," ACI Structural Journal, V.92(4), pp. 1-11.

19. Xie, Y., Ahmad, S.H., T. Yu, Hion, S., and Chung, W. (1994). "Shear Ductility of Reinforced Concrete Beams of Normal and High-Strength Concrete," ACI Structural Journal, V.91(2), pp. 140-149.

20. Yoon, Y.S., Cook, W.D., and Mitchell, D. (1996). "Minimum Shear Reinforcement in Normal, Medium, and High-Strength Concrete Beams," ACI Structural Journal, V.93(5), pp. 576-584

Table A-2. Database of intermediate beams with transverse reinforcement

Ref.	I.D	b (mm)	d (mm)	a (mm)	a/d	ρ_L	ρ_v	f'_c (MPa)	f_y (MPa)	V_{test} (kN)
No.1	DB120M	300	925	2548	2.8	0.93	0.08	21.0	550	282
	DB140M	300	925	2548	2.8	0.93	0.08	38.0	550	277
	DB165M	300	925	2548	2.8	0.93	0.08	65.0	550	452
	DB180M	300	925	2548	2.8	0.93	0.08	80.0	550	395
	DB0.530M	300	925	2548	2.8	0.46	0.08	32.0	550	263
	BM100	300	925	2548	2.8	0.70	0.08	47.0	550	342
No.2	A-1	307	466	1827	3.9	1.50	0.10	24.1	552	234
	B-1	231	461	1821	4.0	2.21	0.15	24.8	552	222
	C-1	155	464	1831	4.0	1.79	0.20	29.6	552	156
No.3	II-W-E-45-8-S	762	406	1829	4.5	2.19	0.09	24.6	469	367
	II-W-E-3-8-S	762	406	1219	3.0	2.19	0.09	25.2	469	372
No.4	BM100	300	850	2700	3.2	0.70	0.08	47.0	550	342
	BM100D	300	850	2700	3.2	0.97	0.08	47.0	550	461
No.5	A1	120	260	900	3.5	2.50	0.20	24.5	408	72
	B1	120	260	700	2.7	2.50	0.20	24.5	408	68
	CI	120	260	900	3.5	2.50	0.20	28.0	408	71
	D	120	260	900	3.5	2.50	0.39	29.8	408	82
	D2	120	260	900	3.5	2.50	0.42	30.6	408	74
	F5	120	260	900	3.5	2.09	0.24	20.2	408	66
	C3H2	120	260	900	3.5	1.66	0.24	20.5	408	61
No.6	G4	178	267	967	3.6	2.89	0.19	62.7	434	147
	G5	178	267	967	3.6	2.19	0.19	40.0	434	113
	C3H2	178	267	967	3.6	2.19	0.19	20.7	434	78
No.7	S2	200	152	401	2.6	2.51	0.24	91.0	600	345
	S3	200	152	401	2.6	2.51	0.32	113.0	600	420
	S4	200	152	401	2.6	2.51	0.44	105.0	600	400
	HS1	200	260	645	2.5	2.68	0.30	102.0	600	501
	HS2	200	260	874	3.4	2.68	0.26	102.0	600	400
	SAR4	200	260	874	3.4	2.68	0.57	136.0	600	459
	HP2	200	200	640	3.2	2.41	0.54	113.0	600	368

Ref.	I.D	b (mm)	d (mm)	a (mm)	a/d	ρ_L	ρ_v	f'_c (MPa)	f_y (MPa)	V_{test} (kN)
No.7	HP4	200	200	640	3.2	3.22	0.91	121.0	600	451
	HP6	200	200	640	3.2	3.22	0.72	108.0	600	438
No.8	No.1	305	539	1505	2.8	2.21	0.16	36.4	525	339
	No.2	305	539	1505	2.8	2.21	0.08	36.4	525	222
	No.4	305	539	1505	2.8	2.21	0.08	72.3	525	316
	No.5	305	539	1505	2.8	2.21	0.16	55.8	525	383
	No.7	305	539	1505	2.8	2.21	0.08	51.3	525	281
	C3H2	305	539	1505	2.8	2.21	0.08	51.3	525	258
No.9	S4-6	250	198	500	2.5	2.21	0.16	87.3	442	203
	S5-1	250	292	880	3.0	2.34	0.16	89.4	452	242
	S5-2	250	292	800	2.7	2.34	0.16	89.4	452	260
	S6-1	250	297	810	2.7	1.41	0.10	68.9	450	155
	S6-2	250	297	810	2.7	1.41	0.10	68.9	450	155
	S6-3	250	293	800	2.7	2.34	0.10	68.9	452	178
	S6-4	250	293	800	2.7	2.34	0.10	68.9	452	214
	S6-5	250	299	790	2.6	3.15	0.10	68.9	442	297
	S6-6	250	299	790	2.6	3.15	0.10	68.9	442	287
	S7-1	250	294	970	3.3	3.75	0.11	74.8	433	217
	S7-2	250	294	970	3.3	3.75	0.13	74.8	433	205
	S7-3	250	294	970	3.3	3.75	0.13	74.8	433	247
	S7-4	250	294	970	3.3	3.75	0.20	74.8	433	274
	S7-5	250	294	970	3.3	3.75	0.22	74.8	433	304
	S7-6	250	294	970	3.3	3.75	0.26	74.8	433	311
No.10	1	360	345	900	2.6	1.73	0.09	28.9	433	249
	3	360	345	900	2.6	1.73	0.09	28.9	433	225
	7	360	345	900	2.6	1.73	0.09	74.3	433	305
	9	360	345	900	2.6	1.73	0.09	77.0	433	242
No.11	B50-3-3	152	298	1074	3.6	2.98	0.12	22.1	414	76
	B50-7-3	152	298	1074	3.6	2.98	0.12	39.9	414	93
	B50-11-3	152	298	1074	3.6	2.98	0.12	59.7	414	98

Ref.	I.D	b (mm)	d (mm)	a (mm)	a/d	ρ_L	ρ_v	f'_c (MPa)	f_y (MPa)	V_{test} (kN)
No.11	B50-15-3	152	298	1074	3.6	2.98	0.12	82.8	414	111
	B100-3-3	152	298	1074	3.6	2.98	0.26	27.9	414	95
	B100-7-3	152	298	1074	3.6	2.98	0.26	47.1	414	120
	B100-11-3	152	298	1074	3.6	2.98	0.26	68.6	414	152
	B100-15-3	152	298	1074	3.6	2.98	0.26	81.4	414	116
	B150-3-3	152	298	1074	3.6	2.98	0.38	28.7	414	139
	B150-7-3	152	298	1074	3.6	2.98	0.38	46.6	414	133
	B150-11-3	152	298	1074	3.6	2.98	0.38	69.7	414	161
	B150-15-3	152	298	1074	3.6	2.98	0.38	82.8	414	150
	C50-3-3	152	298	1074	3.6	2.98	0.12	23.7	414	62
	C50-7-3	152	298	1074	3.6	2.98	0.12	46.9	414	76
	C50-11-3	152	298	1074	3.6	2.98	0.12	70.3	414	129
	C50-15-3	152	298	1074	3.6	2.98	0.12	83.4	414	107
	C100-3-3	152	298	1074	3.6	2.98	0.26	23.9	414	80
	C100-7-3	152	298	1074	3.6	2.98	0.26	39.2	414	93
	C100-11-3	152	298	1074	3.6	2.98	0.26	71.7	414	152
	C100-15-3	152	298	1074	3.6	2.98	0.26	82.8	414	134
No.12	ACI36	150	310	930	3.0	2.23	0.14	75.0	425	105
	TH36	150	310	930	3.0	2.23	0.17	75.0	425	141
	TS36	150	310	930	3.0	2.23	0.24	75.0	425	156
	ACI39	150	310	930	3.0	2.65	0.14	73.0	425	112
	TH39	150	310	930	3.0	2.65	0.21	73.0	425	143
	TS39	150	310	930	3.0	2.65	0.28	73.0	425	179
	ACI26	150	325	975	3.0	1.75	0.14	70.0	425	344
No.13	B-1	280	274	848	3.1	2.31	0.05	31.3	478	114
	B-2	280	274	848	3.1	2.31	0.06	31.8	478	119
	B-3	280	274	848	3.1	2.31	0.07	32.7	478	121
	B-4	280	274	848	3.1	2.31	0.09	33.0	478	143
	B-5	280	274	848	3.1	2.31	0.20	32.4	478	181
	B-6	280	274	848	3.1	2.31	0.24	29.3	478	191

Table A-2. Continued
(c) 4/4

Ref.	I.D	b (mm)	d (mm)	a (mm)	a/d	ρ_L	ρ_v	f'_c (MPa)	f_y (MPa)	V_{test} (kN)
No.13	B-7	280	274	848	3.1	2.31	0.29	32.2	478	187
No.14	BM100	300	925	2548	2.8	0.70	0.08	47.0	550	342
	BM100D	300	925	2548	2.8	0.70	0.08	47.0	550	461
No.15	E2A1	152	318	1193	3.8	1.36	0.37	25.5	320	65
	E2A2	152	321	1193	3.7	1.37	0.37	19.3	325	60
	E2A3	156	321	1193	3.7	1.37	0.36	20.1	331	64
	C2A1	154	318	1193	3.8	1.36	0.36	22.6	318	50
	C2A2	157	321	1193	3.7	1.37	0.36	22.1	324	61
No.16	6	457	762	2083	2.7	1.52	0.08	72.4	464	665
	7	457	762	2083	2.7	1.65	0.16	72.4	483	788
No.17	C3H2	457	762	2083	2.7	2.53	0.24	125.3	464	1172
	AL2-N	180	241	940	3.9	1.94	0.09	40.4	448	115
	AL2-H	180	241	940	3.9	1.94	0.09	75.2	448	123
	BL2-H	180	241	940	3.9	2.43	0.09	75.7	448	138
	CL2-H	180	241	940	3.9	3.03	0.09	70.3	448	147
No.18	Tan-G	110	464	1250	2.7	1.14	0.47	42.8	503	105
No.19	NNW3	127	203	457	2.3	2.56	0.49	43.7	421	174
	NHW3	127	198	446	2.3	3.52	0.50	103.4	421	205
	NHW3a	127	198	446	2.3	3.52	0.65	94.8	421	216
	NHW3b	127	198	446	2.3	3.52	0.79	108.7	421	245
	NHW4	127	198	594	3.0	3.52	0.50	104.1	421	187
No.20	N1N	375	655	2000	3.1	2.49	0.08	36.0	400	457
	N2S	375	655	2000	3.1	2.49	0.08	36.0	400	363
	N2N	375	655	2000	3.1	2.49	0.12	36.0	400	483
	M1N	375	655	2000	3.1	2.49	0.08	67.0	400	405
	M2S	375	655	2000	3.1	2.49	0.12	67.0	400	552
	M2N	375	655	2000	3.1	2.49	0.16	67.0	400	689
	H1N	375	655	2000	3.1	2.49	0.08	87.0	400	483
	H2S	375	655	2000	3.1	2.49	0.14	87.0	400	598
	H2N	375	539	2000	3.7	2.05	0.24	87.0	400	721

A.3 Database of Deep Beams without Transverse Reinforcement

1. Ahmad, S.H., Khaloo, A.R., and Poveda, A. (1986). "Shear Capacity of reinforced High Strength Concrete Beams," ACI Journal, Proceedings V.83(2), pp. 297-305.

2. Brown, M. D. (2005). "Design for Shear in Reinforced Concrete Using Strut-and-Tie and Sectional Models," Ph.D. dissertation. The University of Texas at Austin.

3. Clark, A.P. (1951). "Diagonal Tension in Reinforced Concrete Beams," ACI Journal, Proceedings V.48(10), pp. 145-156.

4. Gabrielsson, H. (1992). "Shear Capacity of Beams of Reinforced High Performance Concrete,", and "Bending and Shear Tests on Reinforced High-Performance Concrete Beams," (1993) Internal Report K1:1, Division of Structural Engineering, Lulea University of Technology, 52 and 59 pp.

5. Kani, G. N. J. (1967). "How Safe Are Our Large Reinforced Concrete Beams," ACI Journal, V.64 (3), pp. 128-141.

6. Kani, G. N. J. (1966). "Basic Facts Concerning Shear Failure," ACI Journal, V.63(6), pp. 675-692.

7. Leonhardt, F., and Walther, R. (1962), "Schulversuche an Einfeldrigen Stahlbetonbalken mit und ohne Schubbewehrung zur Ermittlung der Schubtragfahigkeit und der Oberen Schubspannungsgrenze," DAfStb, Berlin, Germany, (in German).

8. Moody, K. G., Viest, I.M., Elstner, R.C., and Hognestad, E. (1954). "Shear Strength of Reinforced Concrete Beams Part 1 - Tests of Simple Beams," ACI Journal, Proceedings V.51(12), pp. 317-332.

9. Mphonde, A. G., and Frantz, C. C. (1984). "Shear Tests of High- and Low-Strength Concrete Beams Without Stirrups," ACI Journal, Proceedings V.81(4), pp. 350-357.

10. Oh, J. K., and Shin, S. W. (2001). "Shear Strength of Reinforced HighStrength Concrete Deep Beams," ACI Structural Journal, V.98(2), pp. 164-173.

11. Shin, S.-W., Lee, K.-S., Moon, J.-I., Ghosh, S.K. (1999). "Shear Strength of Reinforced HighStrength Concrete Beams with Shear Span-to-Depth Ratios between 1.5 and 2.5," ACI Structural Journal, V.96(4), pp. 549-556.

12. Smith, K. N., and Vantsiotis, A. S. (1982). "Shear Strength of Deep Beams," ACI Journal, Proceedings V.79(3), pp. 201-213.

13. Tanimura, Y., and Sato, T. (2005). "Evaluation of Shear Strength of Deep Beams with Stirrups," Quarterly Report of the Railway Technical Research Institute, V.46(1), pp. 53-58.

14. Xie, Y., Ahmad, S.H., T. Yu, Hion, S., and Chung, W. (1994). "Shear Ductility of Reinforced Concrete Beams of Normal and High-Strength Concrete," ACI Structural Journal, V.91(2), pp. 140-149.

Table A-3. Database of deep beams with transverse reinforcement

Ref.	I.D	b (mm)	d (mm)	a (mm)	a/d	ρ_L	f'_c (MPa)	f_y (MPa)	V_{test} (kN)
No.1	A4	127	203	467	2.3	3.95	66.1	414	93
	A5	127	203	406	2.0	3.95	66.1	414	167
	A6	127	203	203	1.0	3.95	66.1	414	400
	A10	127	208	478	2.3	1.78	66.1	414	82
	A11	127	208	416	2.0	1.78	66.1	414	56
	A12	127	208	208	1.0	1.78	66.1	414	222
	A16	127	213	490	2.3	0.36	66.1	414	24
	A17	127	213	426	2.0	0.36	66.1	414	27
	A18	127	213	213	1.0	0.36	66.1	414	62
	B4	127	202	464	2.3	5.04	72.8	414	143
	B5	127	202	403	2.0	5.04	72.8	414	107
	B6	127	202	202	1.0	5.04	72.8	414	206
	B10	127	208	478	2.3	2.27	72.8	414	64
	B11	127	208	416	2.0	2.27	72.8	414	122
	B12	127	208	208	1.0	2.27	72.8	414	214
	B16	127	213	490	2.3	0.48	72.8	414	31
	B17	127	213	426	2.0	0.48	72.8	414	36
	B18	127	213	213	1.0	0.48	72.8	414	82
	C4	127	184	424	2.3	6.62	69.9	414	89
	C5	127	184	368	2.0	6.62	69.9	414	247
	C6	127	184	184	1.0	6.62	69.9	414	311
	C10	127	207	475	2.3	3.25	69.9	414	57
	C11	127	207	413	2.0	3.25	69.9	414	107
	C12	127	207	207	1.0	3.25	69.9	414	245
	C16	127	211	485	2.3	0.53	69.9	414	30
	C17	127	211	422	2.0	0.53	69.9	414	34
No.2	I-2C-0-0	152	686	762	1.1	1.95	22.1	469	559
	I-CL-0-0	152	686	381	0.6	1.95	16.3	469	554
No.3	A0-1	203	406	826	2.0	0.94	21.5	321	89
	A0-2	203	406	826	2.0	0.94	26.0	321	108

Ref.	I.D	b (mm)	d (mm)	a (mm)	a/d	ρ_L	f'_c (MPa)	f_y (MPa)	V_{test} (kN)
No.3	A0-3	203	406	826	2.0	0.94	23.7	321	119
	B0-1	203	406	673	1.7	0.94	23.6	321	121
	B0-2	203	406	673	1.7	0.94	23.9	321	94
	B0-3	203	406	673	1.7	0.94	23.5	321	128
	C0-1	203	406	521	1.3	0.94	24.7	321	174
	C0-2	203	406	521	1.3	0.94	23.5	321	178
	C0-3	203	406	521	1.3	0.94	23.6	321	167
	D0-1	203	406	368	0.9	0.94	25.9	321	222
	D0-2	203	406	368	0.9	0.94	26.2	321	260
	D0-3	203	406	368	0.9	0.94	26.0	321	223
No.4	HB1	200	223	357	2.0	4.51	108.0	400	522
No.5	Kani1	152	255	267	1.0	2.93	26.2	448	256
	Kani2	152	255	400	1.6	2.93	26.2	448	108
	Kani3	152	255	533	2.1	2.93	26.2	448	70
	Kani6	152	255	267	1.0	1.96	26.2	448	197
	Kani7	152	255	400	1.6	1.96	26.2	448	137
	Kani8	152	255	533	2.1	1.96	26.2	448	76
	Kani11	152	255	267	1.0	0.84	26.2	448	125
	Kani12	152	255	533	2.1	0.84	26.2	448	57
	Kani15	152	255	267	1.0	0.52	26.2	448	80
	Kani16	152	255	400	1.6	0.52	26.2	448	53
	Kani17	152	255	533	2.1	0.52	26.2	448	40
No.6	265	153	269	407	1.5	0.52	18.1	400	53
	266	153	272	673	2.5	0.50	18.1	396	32
	269	154	274	270	1.0	0.49	18.1	396	89
	270	152	273	542	2.0	0.50	20.1	396	41
	248	153	282	678	2.4	0.49	27.6	400	37
	249	153	276	270	1.0	0.49	28.0	376	84
	250	152	274	406	1.5	0.50	28.0	376	55
	251	154	276	544	2.0	0.48	26.2	391	42

Table A-3. Continued
(b) 3/6

Ref.	I.D	b (mm)	d (mm)	a (mm)	a/d	ρ_L	f'_c (MPa)	f_y (MPa)	V_{test} (kN)
	174	153	272	270	1.0	0.51	36.4	396	87
	178	153	269	407	1.5	0.52	34.5	400	59
	141	151	270	544	2.0	0.81	19.3	382	49
	142	156	276	544	2.0	0.77	19.3	382	58
	145	153	272	425	1.6	0.74	16.2	424	83
	146	154	272	271	1.0	0.73	16.2	407	128
	147	152	287	678	2.4	0.70	16.8	417	42
	148	152	274	408	1.5	0.79	19.9	382	80
	150	153	273	678	2.5	0.77	18.0	380	46
	151	154	273	679	2.5	0.78	19.3	382	36
	102	153	269	543	2.0	0.76	25.3	423	49
	105	152	272	679	2.5	0.76	26.2	383	42
	108	154	269	271	1.0	0.76	25.0	422	147
	109	153	271	407	1.5	0.76	25.0	457	72
	111	154	272	678	2.5	0.76	27.0	368	43
No.6	112	153	273	678	2.5	0.76	27.0	368	39
	113	152	274	408	1.5	0.77	25.5	486	87
	114	153	270	544	2.0	0.80	25.5	486	61
	162A	153	272	543	2.0	0.77	34.3	377	59
	162B	154	267	543	2.0	0.76	34.3	379	62
	163A	156	273	678	2.5	0.76	35.4	378	40
	163B	152	272	678	2.5	0.78	35.4	378	38
	167	154	274	272	1.0	0.76	36.4	381	128
	169	152	274	272	1.0	0.76	36.4	381	128
	127	154	271	271	1.0	1.81	15.7	345	201
	129	155	275	407	1.5	1.78	17.6	345	143
	131	151	274	679	2.5	1.85	18.1	400	50
	134	154	273	544	2.0	1.81	17.4	421	60
	135	149	274	544	2.0	1.86	17.4	414	77
	23	152	271	407	1.5	1.87	26.9	396	164

Table A-3. Continued
(c) 4/6

Ref.	I.D	b (mm)	d (mm)	a (mm)	a/d	ρ_L	f'_c (MPa)	f_y (MPa)	V_{test} (kN)
	24	152	271	407	1.5	1.87	27.9	396	182
	25	152	271	543	2.0	1.87	24.6	396	104
	26	152	271	543	2.0	1.87	27.1	396	78
	27	152	271	678	2.5	1.87	29.8	396	51
	28	152	271	678	2.5	1.87	29.2	396	54
	181	154	272	542	2.0	1.79	33.9	386	65
	183	154	269	271	1.0	1.80	35.4	394	260
	184	154	271	407	1.5	1.80	35.1	394	163
	188	153	277	543	2.0	1.76	33.1	384	93
	193	153	278	678	2.4	1.80	34.6	352	57
	197	150	274	679	2.5	1.84	36.0	376	53
	199	152	273	544	2.0	1.83	36.0	410	76
	85	154	274	272	1.0	2.69	25.5	381	234
No.6	87	154	269	272	1.0	2.72	27.6	366	240
	88	153	266	271	1.0	2.81	31.4	400	360
	94	153	273	543	2.0	2.77	25.3	352	111
	95	153	275	678	2.5	2.75	25.3	338	73
	98	153	275	679	2.5	2.68	26.2	366	128
	99	152	272	679	2.5	2.73	26.2	366	77
	100	153	270	544	2.0	2.75	27.6	366	112
	201	155	274	272	1.0	2.65	35.2	379	254
	203	152	268	271	1.0	2.75	34.8	369	357
	204	152	275	543	2.0	2.69	34.8	369	147
	205	153	275	544	2.0	2.66	35.2	381	125
	210	154	272	679	2.5	2.67	35.2	381	79
	214	153	272	679	2.5	2.71	36.0	412	82
	215	154	274	679	2.5	2.67	36.0	412	66
	1	190	270	270	1.0	2.07	29.6	465	388
No.7	2	190	270	400	1.5	2.07	29.6	465	260
	3	190	270	540	2.0	2.07	29.6	465	147

Ref.	I.D	b (mm)	d (mm)	a (mm)	a/d	ρ_L	f'_c (MPa)	f_y (MPa)	V_{test} (kN)
No.7	4	190	270	670	2.5	2.07	29.6	465	82
No.8	24a	178	533	813	1.5	2.72	17.8	321	296
	24b	178	533	813	1.5	2.72	20.6	321	302
	25a	178	533	838	1.6	3.46	24.3	321	267
	25b	178	533	838	1.6	3.46	17.2	321	289
	26a	178	533	864	1.6	4.24	21.7	321	420
	26b	178	533	864	1.6	4.24	20.6	321	396
	27a	178	533	889	1.7	2.72	21.4	321	347
	27b	178	533	889	1.7	2.72	22.9	321	356
	28a	178	533	914	1.7	3.46	23.3	321	302
	28b	178	533	914	1.7	3.46	22.4	321	340
	29a	178	533	940	1.8	4.24	21.7	321	389
	29b	178	533	940	1.8	4.24	25.0	321	436
	30	178	533	965	1.8	4.24	25.4	321	478
	31	178	533	991	1.9	4.24	22.4	321	507
No.9	A0-3-2	152	298	746	2.5	3.36	20.6	414	82
	A0-7-2	152	298	746	2.5	3.36	45.2	414	118
	A0-11-2	152	298	746	2.5	3.36	79.3	414	111
	A0-15-2a	152	298	746	2.5	3.36	83.4	414	178
	A0-15-2b	152	298	746	2.5	3.36	69.7	414	206
	A0-3-1	152	298	448	1.5	3.36	23.1	414	112
	A0-7-1	152	298	448	1.5	3.36	41.4	414	311
	A0-11-1	152	298	448	1.5	3.36	65.8	414	433
	A0-15-1a	152	298	448	1.5	3.36	79.3	414	276
	A0-15-1b	152	298	448	1.5	3.36	81.4	414	495
No.10	H4100	130	499	249	0.5	1.56	49.0	448	642
	H4200	130	499	432	0.9	1.56	49.0	448	401
	H4300	130	499	635	1.3	1.56	49.0	448	337
	H4500	130	499	1016	2.0	1.56	49.0	448	112
	N4200	130	500	425	0.8	1.56	23.7	448	265

Ref.	I.D	b (mm)	d (mm)	a (mm)	a/d	ρ_L	f'_c (MPa)	f_y (MPa)	V_{test} (kN)
No.10	H4100	130	500	250	0.5	1.56	49.1	448	642
	H4200	130	500	425	0.8	1.56	49.1	448	401
	H4300	130	500	625	1.2	1.56	49.1	448	337
	H4500	130	500	1000	2.0	1.56	49.1	448	112
No.11	MHB-15-0	124	216	324	1.5	3.79	52.4	414	113
	MHB-20-0	124	216	432	2.0	3.79	52.4	414	88
	MHB-25-0	124	216	540	2.5	3.79	52.4	414	56
	HB-15-0	124	216	324	1.5	3.79	73.1	414	142
	HB-20-0	124	216	432	2.0	3.79	73.1	414	99
	HB-25-0	124	216	540	2.5	3.79	73.1	414	80
No.12	0B0-49	102	305	206	1.0	1.94	21.7	421	149
	0C0-50	102	305	307	1.3	1.94	20.7	421	116
	0D0-47	102	305	511	2.0	1.94	19.5	421	73
No.13	A-1	300	400	200	0.5	2.14	23.2	458	853
	A-5	300	400	400	1.0	2.14	29.0	458	632
	A-9	300	400	600	1.5	2.14	22.9	458	284
	B-13	300	400	600	1.5	2.14	32.0	458	661
	F-24	300	400	200	0.5	2.14	79.9	702	1958
	F-25	300	400	400	1.0	2.14	76.4	702	1403
	F-26	300	400	600	1.5	2.14	78.3	702	904
	F-27	300	400	800	2.0	2.14	77.8	702	752
	E-35	300	400	200	0.5	0.42	25.3	1330	588
	E-38	300	400	400	1.0	0.42	25.2	1330	358
	F-45	300	400	1000	2.5	2.14	97.2	750	345
No.14	NNN1	127	216	162	1.0	2.07	47.0	421	312
	NNN2	127	216	324	2.0	2.07	41.4	421	113
	NHN1	127	216	162	1.0	2.07	103.8	421	483
	NHN2	127	216	324	2.0	2.07	103.4	421	203

A.4 Database of Intermediate Beams without Transverse Reinforcement

1. Ahmad, S.H., Khaloo, A.R., and Poveda, A. (1986). "Shear Capacity of reinforced High Strength Concrete Beams," ACI Journal, Proceedings V.83(2), pp. 297-305.

2. Angelakos, D., Bentz, E. C., and Collins, M. P. (2001). "Effect of Concrete Strength and Minimum Stirrups on Shear Strength of Large Members," ACI Structural Journal, V.98(3), pp. 290 300.

3. Bresler, B., and Scordelis, A.C. (1963). "Shear Strength of Reinforced Concrete Beams," ACI Journal, Proceedings V.60(1), pp.51-74.

4. Collins, M.P., and Kuchma, D. (1999). "How Safe Are Our Large, Lightly Reinforced Concrete Beams, Slabs, and Footings?," ACI Structural Journal, V.96(4), pp. 482-490.

5. Gabrielsson, H. (1992). "Shear Capacity of Beams of Reinforced High Performance Concrete,", and "Bending and Shear Tests on Reinforced High-Performance Concrete Beams," (1993) Internal Report K1:1, Division of Structural Engineering, Lulea University of Technology.

6. Kani, G. N. J. (1966). "Basic Facts Concerning Shear Failure," ACI Journal, V.63(6), pp. 675-692.

7. Kani, G. N. J. (1967). "How Safe Are Our Large Reinforced Concrete Beams," ACI Journal, V.64 (3), pp. 128-141.

8. Leonhardt, F., and Walther, R. (1962), "Schulversuche an Einfeldrigen Stahlbetonbalken mit und ohne Schubbewehrung zur Ermittlung der Schubtragfahigkeit und der Oberen Schubspannungsgrenze," DAfStb, Berlin, Germany, (in German).

9. Moody, K. G., Viest, I.M., Elstner, R.C., and Hognestad, E. (1954). "Shear Strength of Reinforced Concrete Beams Part 1 - Tests of Simple Beams," ACI Journal, Proceedings V.51(12), pp. 317-332.

10. Mphonde, A. G., and Frantz, C. C. (1984). "Shear Tests of High- and Low-Strength Concrete Beams Without Stirrups," ACI Journal, Proceedings V.81(4), pp. 350-357.

11. Van Den Berg, F.J. (1962). "Shear Strength of Reinforced Concrete Beams without Web Reinforcement Part 2 - Factors Affecting Load at diagonal Cracking," ACI Journal, Proceedings V.59(11), pp. 1587-1599.

12. Xie, Y., Ahmad, S.H., T. Yu, Hion, S., and Chung, W. (1994). "Shear Ductility of Reinforced Concrete Beams of Normal and High-Strength Concrete," ACI Structural Journal, V.91(2), pp. 140-149.

13. Yoon, Y.S., Cook, W.D., and Mitchell, D. (1996). "Minimum Shear Reinforcement in Normal, Medium, and High-Strength Concrete Beams," ACI Structural Journal, V.93(5), pp. 576-584

Table A-4. Database of intermediate beams without transverse reinforcement

Ref.	I.D	b (mm)	d (mm)	a (mm)	a/d	ρ_L	f'_c (MPa)	f_y (MPa)	V_{test} (kN)
No.1	A1	203	813	40	4.0	0.04	66.1	414	58
	A2	203	610	40	3.0	0.04	66.1	414	69
	A3	203	549	40	2.7	0.04	66.1	414	69
	A7	208	832	19	4.0	0.02	66.1	414	47
	A8	208	624	19	3.0	0.02	66.1	414	49
	A9	208	562	19	2.7	0.02	66.1	414	80
	A13	213	851	4	4.0	0.00	66.1	414	13
	A14	213	639	4	3.0	0.00	66.1	414	18
	A15	213	575	4	2.7	0.00	66.1	414	20
	B1	202	807	51	4.0	0.05	72.8	414	50
	B2	202	605	51	3.0	0.05	72.8	414	69
	B3	202	545	51	2.7	0.05	72.8	414	100
	B7	208	832	24	4.0	0.02	72.8	414	44
	B8	208	624	24	3.0	0.02	72.8	414	47
	B9	208	562	24	2.7	0.02	72.8	414	80
	B13	213	851	5	4.0	0.00	72.8	414	17
	B14	213	639	5	3.0	0.00	72.8	414	24
	B15	213	575	5	2.7	0.00	72.8	414	27
	C1	184	737	61	4.0	0.07	69.9	414	54
	C2	184	552	61	3.0	0.07	69.9	414	76
	C3	184	497	61	2.7	0.07	69.9	414	69
	C7	207	826	34	4.0	0.03	69.9	414	45
	C8	207	620	34	3.0	0.03	69.9	414	44
	C9	207	558	34	2.7	0.03	69.9	414	45
	C13	211	844	6	4.0	0.01	69.9	414	16
	C14	211	633	6	3.0	0.01	69.9	414	22
	C15	211	570	6	2.7	0.01	69.9	414	24
No.2	DB120	850	2700	110	3.2	0.01	21.0	550	179
	DB130	850	2700	110	3.2	0.01	32.0	550	185
	DB140	850	2700	110	3.2	0.01	38.0	550	180

Ref.	I.D	b (mm)	d (mm)	a (mm)	a/d	ρ_L	f'_c (MPa)	f_y (MPa)	V_{test} (kN)
No.2	DB165	850	2700	110	3.2	0.01	65.0	550	185
	DB180	850	2700	110	3.2	0.01	80.0	550	172
	DB230	850	2700	220	3.2	0.02	32.0	550	257
	DB0.530	850	2700	55	3.2	0.01	32.0	550	165
	B100	850	2700	110	3.2	0.01	36.0	550	225
	B100H	850	2700	110	3.2	0.01	98.0	550	193
	B100HE	850	2700	110	3.2	0.01	98.0	550	217
	B100L	850	2700	110	3.2	0.01	39.0	550	223
	B100B	850	2700	110	3.2	0.01	39.0	550	204
	BN100	850	2700	83	3.2	0.01	37.0	550	192
	BH100	850	2700	83	3.2	0.01	99.0	550	193
	BRL100	850	2700	55	3.2	0.01	94.0	550	163
No.3	OA-1	461	1830	102	4.0	0.02	22.6	552	167
No.4	B100	850	2700	110	3.2	0.01	36.0	550	225
	B100-R	850	2700	110	3.2	0.01	36.0	550	249
	B100D	850	2700	130	3.2	0.01	36.0	550	320
	B100H	850	2700	110	3.2	0.01	98.0	550	193
	B100HE	850	2700	110	3.2	0.01	98.0	550	217
	B100L	850	2700	110	3.2	0.01	39.0	483	223
	B100L-R	850	2700	110	3.2	0.01	39.0	550	235
	B100B	850	2700	110	3.2	0.01	39.0	550	204
	BN100	850	2700	83	3.2	0.01	37.2	550	192
	BN50	400	1350	43	3.4	0.01	37.2	480	132
	BN25	200	675	24	3.4	0.01	37.2	483	73
	BN12	95	338	12	3.6	0.01	37.2	522	40
	BND100	850	2700	114	3.2	0.01	37.2	550	258
	BND50	400	1350	59	3.4	0.01	37.2	480	163
	BND25	200	675	35	3.4	0.01	37.2	483	112
	BH100	850	2700	83	3.2	0.01	98.8	550	193
	BH50	400	1350	43	3.4	0.01	98.8	480	132

Ref.	I.D	b (mm)	d (mm)	a (mm)	a/d	ρ_L	f'_c (MPa)	f_y (MPa)	V_{test} (kN)
No.4	BH25	200	675	24	3.4	0.01	98.8	483	85
	BHD100	850	2700	114	3.2	0.01	98.8	550	278
	BHD100R	850	2700	114	3.2	0.01	98.8	550	334
	BHD50	400	1350	59	3.4	0.01	98.8	480	193
	BHD50R	400	1350	59	3.4	0.01	98.8	480	205
	BHD25	200	675	35	3.4	0.01	98.8	483	111
	BRL100	850	2700	55	3.2	0.01	94.0	550	163
No.5	A1	268	879	32	4.1	0.02	126.0	400	184
	A2	268	879	32	4.1	0.02	129.0	600	183
	M1	268	879	24	4.1	0.01	90.0	400	138
	M2	268	879	24	4.1	0.01	91.0	400	141
	M3	268	879	24	4.1	0.01	113.0	600	193
	M4	268	879	24	4.1	0.01	105.0	600	194
	HPM1	268	879	32	4.1	0.02	123.0	600	177
	HPM2	268	879	32	4.1	0.02	129.0	600	153
	SAR3	260	874	63	4.2	0.03	137.0	600	214
	HP1	200	640	47	4.0	0.03	139.0	600	217
	HP3	200	640	63	4.0	0.04	125.0	600	203
	HP5	200	640	63	4.0	0.04	108.0	600	218
No.6	29	271	1221	30	4.5	0.02	24.6	350	43
	30	271	1221	30	4.5	0.02	25.2	350	46
	35	269	953	30	3.5	0.02	26.1	491	45
	36	273	953	30	3.5	0.02	26.1	491	52
	83	271	814	46	3.0	0.03	27.6	345	65
	84	271	1085	46	4.0	0.03	27.6	345	55
	96	275	1085	46	3.9	0.03	25.3	335	56
	97	276	815	44	3.0	0.03	27.6	366	63
	103	274	814	12	3.0	0.01	29.4	423	39
	104	269	1085	12	4.0	0.01	25.3	423	34
	106	268	678	13	2.5	0.01	28.8	422	45

Ref.	I.D	b (mm)	d (mm)	a (mm)	a/d	ρ_L	f'_c (MPa)	f_y (MPa)	V_{test} (kN)
	115	272	679	13	2.5	0.01	26.2	383	45
	116	271	815	13	3.0	0.01	26.4	384	39
	117	275	1087	13	4.0	0.01	26.4	384	33
	121	272	815	30	3.0	0.02	20.3	330	49
	122	276	1087	30	3.9	0.02	19.9	343	39
	123	271	1085	30	4.0	0.02	15.4	345	38
	126	272	814	30	3.0	0.02	16.3	345	43
	132	271	679	30	2.5	0.02	18.5	414	52
	143	274	1085	12	4.0	0.01	17.7	428	30
	149	271	678	13	2.5	0.01	18.0	380	44
	152	270	815	13	3.0	0.01	19.7	384	32
	153	273	815	12	3.0	0.01	19.7	384	33
	164	271	1085	12	4.0	0.01	33.8	412	36
	166A	271	815	13	3.0	0.01	35.4	377	40
	166B	274	815	13	3.0	0.01	35.4	379	38
No.6	168	290	1221	12	4.2	0.01	34.6	412	33
	170	285	1221	13	4.3	0.01	33.9	396	32
	179	264	678	8	2.6	0.01	32.3	400	34
	180	269	949	8	3.5	0.01	34.5	400	25
	186	272	1085	29	4.0	0.02	35.1	394	55
	191	275	815	30	3.0	0.02	34.0	497	53
	194	278	814	30	2.9	0.02	34.6	352	51
	195	275	1085	30	3.9	0.02	34.6	352	47
	206	270	933	44	3.5	0.03	35.2	381	100
	208	274	1221	45	4.5	0.03	35.7	379	60
	211	269	815	44	3.0	0.03	35.2	381	57
	212	273	815	44	3.0	0.03	35.2	381	60
	213	278	1223	44	4.4	0.03	36.7	381	57
	246	274	952	8	3.5	0.01	27.6	400	25
	267	269	949	8	3.5	0.01	20.7	400	24

Ref.	I.D	b (mm)	d (mm)	a (mm)	a/d	ρ_L	f'_c (MPa)	f_y (MPa)	V_{test} (kN)
No.6	268	274	816	8	3.0	0.00	20.1	396	27
No.7	Kani4	255	667	45	2.6	0.03	26.2	448	76
	Kani5	255	800	45	3.1	0.03	26.2	448	63
	Kani9	255	667	30	2.6	0.02	26.2	448	51
	Kani10	255	800	30	3.1	0.02	26.2	448	41
	Kani13	255	667	13	2.6	0.01	26.2	448	38
	Kani14	255	800	13	3.1	0.01	26.2	448	36
	Kani18	255	667	8	2.6	0.01	26.2	448	35
	Kani19	255	800	8	3.1	0.01	26.2	448	24
No.8	5	270	810	42	3.0	0.02	29.6	465	60
	6	270	1100	42	4.1	0.02	29.6	465	61
No.9	A1	262	800	40	3.1	0.02	30.3	317	60
	A2	267	800	40	3.0	0.02	31.0	317	67
	A3	268	800	42	3.0	0.02	31.0	317	76
	A4	270	800	45	3.0	0.02	31.5	317	71
	B1	267	800	30	3.0	0.02	21.2	317	56
	B2	268	800	30	3.0	0.02	21.6	317	60
	B3	270	800	30	3.0	0.02	19.2	317	56
	B4	272	800	32	2.9	0.02	16.8	317	56
	C1	268	800	15	3.0	0.01	6.3	317	20
	C2	272	800	16	2.9	0.01	6.1	317	24
	C3	273	800	15	2.9	0.01	6.9	317	25
	C4	274	800	16	2.9	0.01	6.8	317	25
	B-1	268	914	30	3.4	0.02	36.7	317	58
	B-2	268	914	30	3.4	0.02	16.7	317	36
	B-3	268	914	30	3.4	0.02	25.8	317	52
	B-4	268	914	30	3.4	0.02	15.4	317	40
	B-5	268	914	30	3.4	0.02	30.7	317	52
	B-6	268	914	30	3.4	0.02	15.8	317	34
	B-7	268	914	30	3.4	0.02	30.9	317	51

Ref.	I.D	b (mm)	d (mm)	a (mm)	a/d	ρ_L	f'_c (MPa)	f_y (MPa)	V_{test} (kN)
No.9	B-8	268	914	30	3.4	0.02	12.2	317	31
	B-9	268	914	30	3.4	0.02	41.2	317	53
	B-10	268	914	30	3.4	0.02	23.9	317	49
	B-11	268	914	30	3.4	0.02	38.1	317	60
	B-12	268	914	30	3.4	0.02	20.2	317	47
	B-13	268	914	30	3.4	0.02	37.8	317	56
	B-14	268	914	30	3.4	0.02	22.6	317	43
	B-15	268	914	30	3.4	0.02	37.4	317	51
	B-16	268	914	30	3.4	0.02	16.3	317	38
No.10	A0-3-3b	298	1074	60	3.6	0.03	20.8	414	65
	A0-3-3c	298	1074	42	3.6	0.02	27.2	414	67
	A0-7-3a	298	1074	60	3.6	0.03	37.7	414	82
	A0-7-3b	298	1074	60	3.6	0.03	41.7	414	83
	A0-11-3a	298	1074	60	3.6	0.03	75.0	414	90
	A0-11-3b	298	1074	60	3.6	0.03	74.7	414	89
	A0-15-3a	298	1074	60	3.6	0.03	81.4	414	93
	A0-15-3b	298	1074	60	3.6	0.03	93.8	414	100
	A0-15-3c	298	1074	60	3.6	0.03	91.7	414	98
No.11	A4-1	359	991	147	2.8	0.05	43.6	310	178
	A4-2	359	1372	147	3.8	0.05	38.9	310	133
	A4-3	359	1448	147	4.0	0.05	41.8	310	134
	A4-4	359	1524	147	4.2	0.05	38.9	310	135
	A4-5	359	1257	147	3.5	0.05	39.6	310	133
	A4-6	359	1524	147	4.2	0.05	44.9	310	142
	A4-7	359	1257	147	3.5	0.05	50.3	310	142
	A4-8	359	1600	147	4.5	0.05	42.8	310	125
	A4-12	359	991	147	2.8	0.05	44.0	310	178
	Dl	359	1257	147	3.5	0.05	49.8	310	151
	D2	359	1257	147	3.5	0.05	43.0	310	131
	D3	359	1257	147	3.5	0.05	36.1	310	129

Ref.	I.D	b (mm)	d (mm)	a (mm)	a/d	ρ_L	f'_c (MPa)	f_y (MPa)	V_{test} (kN)
No.11	D4	359	1257	147	3.5	0.05	35.5	310	145
	D5	359	1257	147	3.5	0.05	43.0	310	131
	D6	359	1257	147	3.5	0.05	41.3	310	140
	D7	359	1257	147	3.5	0.05	32.2	310	140
	D8	359	1257	147	3.5	0.05	25.5	310	118
	D9	359	1257	147	3.5	0.05	26.7	310	127
	D10	359	1257	147	3.5	0.05	19.1	310	109
	D12	359	1257	147	3.5	0.05	23.3	310	107
	D13	359	1257	147	3.5	0.05	20.8	310	99
	D14	359	1257	147	3.5	0.05	23.9	310	107
	D15	359	1257	147	3.5	0.05	22.3	310	102
	D16	359	1257	147	3.5	0.05	25.9	310	111
	D17	359	1257	147	3.5	0.05	22.2	310	105
	D18	359	1257	147	3.5	0.05	24.4	310	105
	D19	359	1257	147	3.5	0.05	27.4	310	116
	D20	359	1257	147	3.5	0.05	24.2	310	107
No.12	NNN3	216	486	22	3.0	0.02	39.7	421	73
	NHN3	216	486	22	3.0	0.02	104.2	421	91
No.13	N1-S	655	2150	271	3.3	0.03	36.0	400	249
	M1-S	655	2150	271	3.3	0.03	67.0	400	296
	H1-S	655	2150	271	3.3	0.03	87.0	400	327

APPENDIX B

MATERIAL PROPERTIES

B.1 Concrete Material Properties and Test Setup

To obtain measured material properties, each concrete batch was sampled to perform the following material properties tests: slump, compressive strength, modulus of elasticity, indirect tensile strength, and modulus of rupture. The fresh concrete was sampled following ASTM C172/C172M standards. Molded cylinder and beam specimens were sampled following ASTM C31/C31M standards. Slump tests were performed on every batch of concrete following ASTM C143/C143M standards to determine the consistency and flowability of the concrete. Table B-1 shows the results of the slump tests.

Concrete compressive tests were performed for every batch according to the sampling plan following ASTM C39/C39M standards. The results of three 152 mm x 305 mm cylinder specimens were averaged to indicate the representative compressive strength, f'_c. Table B-1 shows the results of the concrete strength tests. Deviation from the target testing dates is noted where applicable.

Tests of modulus of elasticity, E_c, indirect tensile, f_{ct}, and modulus of rupture, f_r, were conducted in conjunction with the 28-day compressive strength tests. These tests were performed following ASTM C469/C469M, ASTM C496/C496M, and ASTM C78/C78M standards, respectively. Additional indirect tensile tests were conducted on, or close to, the date of experimental testing for each specimen. Table B-2 summarizes the results of the modulus of elasticity, indirect tensile, and modulus of rupture for each batch of concrete. It is noted that only Batch C was tested for 28-day E_c, f_{ct}, and f_r.

Table B-1. Concrete compressive strength results.

Specimen	Component	Slump (mm.)	f'_c (MPa) 3 Day	7 Day	14 Day	28 Day	Test Day
RCS-16-12	Cap	140	*16.3	26.9	26.9	31.8	38.6
PSS-16-12	Batch A	178	28.0	-	-	47.2	51.4
	Batch B	178	28.5	-	-	49.6	55.2
PSS-16-24	Batch B	178	28.5	-	-	49.6	-
	Batch C	178	33.2	40.3	44.9	52.8	-
	Batch D	178	31.7	-	-	52.1	-
PSV-16-12	Batch E	178	26.6	-	-	54.5	60.8
	Batch F	178	27.9	-	-	52.8	57.8

Note: *4 day

Table B-2. Modulus of elasticity, indirect tensile, and modulus of rupture results.

Specimen	Component	E_c (MPa) 28 Day	Test Day	f_{ct} (MPa) 28 Day	Test Day	f_r (MPa) 28 Day	Test Day
RCS-16-12	Cap	37,255	42,724	4.6	5.0	4.6	5.4
PSS-16-12	Batch A	-	33,931	-	6.6	-	-
	Batch B	-	26,993	-	6.0	-	-
PSS-16-24	Batch B	-	-	-	-	-	-
	Batch C	27,421	-	5.7	-	5.9	-
	Batch D	-	-	-	-	-	-
PSV-16-12	Batch E	-	-	-	6.3	-	-
	Batch F	-	-	-	6.2	-	-

B.2 Steel Material Properties

Tensile testing of reinforcing bar specimens was conducted to determine yield strength, f_y, ultimate strength, f_u, modulus of elasticity, E_s, and yield strain, ε_y, of the mild steel reinforcement used in the construction of the columns and prestressed bent caps. Rebar specimens were sent to Applied Technical Services for testing. Tensile tests were conducted on samples of D16 (#5) transverse reinforcing bars, D25 (#8) longitudinal reinforcing bars (RCS-16-12), and D36 (#11) dowel bars. Three specimens from each rebar type were tested, and the results for each parameter were averaged to determine the material properties of the steel. Table B-3. summarizes the results.

Table B-3. Steel tensile test results.

Rebar	f_y (MPa)	f_u (MPa)	E_s (GPa)	ε_y (mm/mm)
D16 (#5)	441	710	196	0.00225
D25 (#8)	455	738	203	0.00225
D36 (#11)	469	731	194	0.00240

B.3 Connection Details

The laboratory floor has a 914 mm x 914 mm (3 ft × 3 ft) grid of 76.2 mm (3 in.) diameter holes. Each hole travels the thickness of the laboratory strong floor and allows the use of dywidags to secure reaction frames and towers. The vertical reaction towers (Figure B-1), reaction plate, and horizontal reaction frames (Figure C-3) for the specimens were attached to the laboratory strong floor by 63.5 mm (2.5 in.) dywidag threaded bars, with each tensioned to 20.7 MPa (3,000 psi). The specimen was aligned above a strong floor foundation wall to accommodate the large forces acting during testing.

(a) Vertical Reaction Towers

(b) Vertical Reaction Towers

Figure B-1. Vertical reaction towers.

(a) Bottom Horizontal Actuator Reaction Frame

(b) Top Horizontal Actuator Reaction Frame

Figure B-2. Horizontal reaction frames.

APPENDIX C

SPECIMEN DESIGNS

C.1 Flexural Design

The flexural design of the specimens was governed by the maximum demands of the test setup (2,000 kN-m). A 1,067 mm (42 in.) square section with 41.4 MPa (6 ksi) concrete and 16 strands had a moment capacity of 1,870 kN-m. To avoid interference between flexural reinforcement and the pocket connection, a side configuration of strands was used. Side reinforcement was uniformly distributed to control cracks effectively. To allow comparison of the overall performance of prestressed bent caps to RC bent caps, an RC prototype was designed to have the same steel configuration and similar strength to the prestressed prototype, leading to the use of 16-D25 bars. Figure C-1 shows the moment-curvature analysis results of the PSC and RC specimens from the nonlinear analysis program, *OpenSees* v. 3.2.2 (2020), along with the cross-section of the RC specimen. The layout of the bars was identical to the strand layout for the prestressed section.
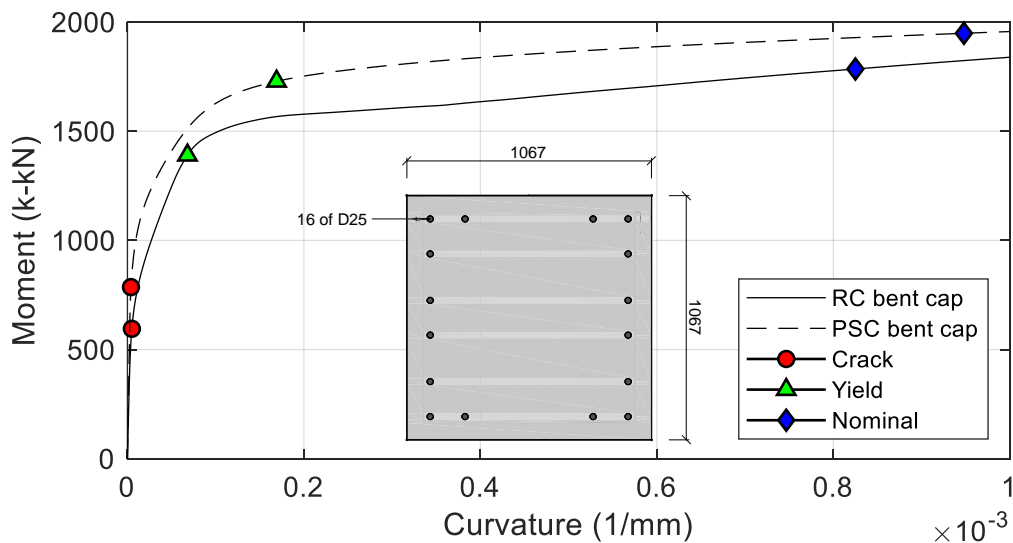

Figure C-1. Moment-curvature response of RC and PSC bent caps

C.2 Prototype Selection

Having established a flexural design, it was necessary to identify prototype bridge(s) that would result in the selected design. For the prestressing force from 16 strands, the zero-tension moment was 444 kN-m. This established the selection criterion for the prototype bridge; the prestressed bent cap should have a maximum flexural demand under a dead load of 444 kN-m.

From a preliminary study of the bent configuration in the TxDOT bridge inventory with I-girders, the 9.75 m (32-ft) and 12.2 m (40-ft) roadway width bridges were observed to be a close representation of the specimen that could be built in the laboratory. Iterative analysis of the bridge with different span lengths was done in CAP18 (CAP18 Version 6.2.2) to find the span length producing these demands. The maximum dead load moment for a 20.1 m (66-ft) span was close to the required moment for the prototype. Figure C-2 shows the configuration of the two prototype bridges. Maximum ultimate demands of both 9.75m (32-ft) and 12.2 m (40-ft) roadway width bridges were -1,040 kN-m and 1,360 kN-m, respectively, and did not the exceed moment capacity of the specimens.
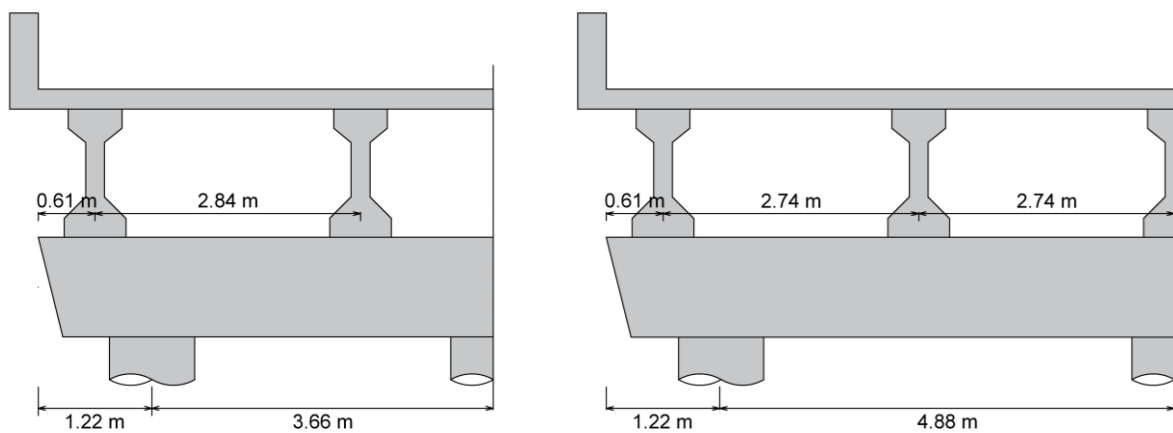
(a) BIG-32 interior bent in TxDOT standard (b) BIG-40 interior bent in TxDOT standard

Figure C-2. Prototype bridge configuration

C.3 Shear Design

The shear design of the specimens was in accordance with AASHTO LRFD Bridge Design Specification (AASHTO 2017), the general procedure of sectional design, in Appendix B5. According to AASHTO LRFD, the sectional design method is appropriate for the design of components where the assumptions of beam theory are valid. For this reason, the shear design was conducted only in the spans between columns.

AASHTO LRFD shear design requires both moment and shear demands, M_u and V_u, to evaluate the shear strength of the section. Demands from the prototype bridge were considered. Three points where shear and moment demands were significantly higher than other locations were selected as critical locations, including the interior face of the exterior column, interior girder location, and the interior column face in the prototype, as shown in Figure C-3. Concrete compressive strengths of 24.8 MPa (3.6 ksi) and 41.3 MPa (6 ksi) were used for RC and PSC bent caps, respectively. Two legs of D16 reinforcing steel bars were used as a transverse reinforcement.
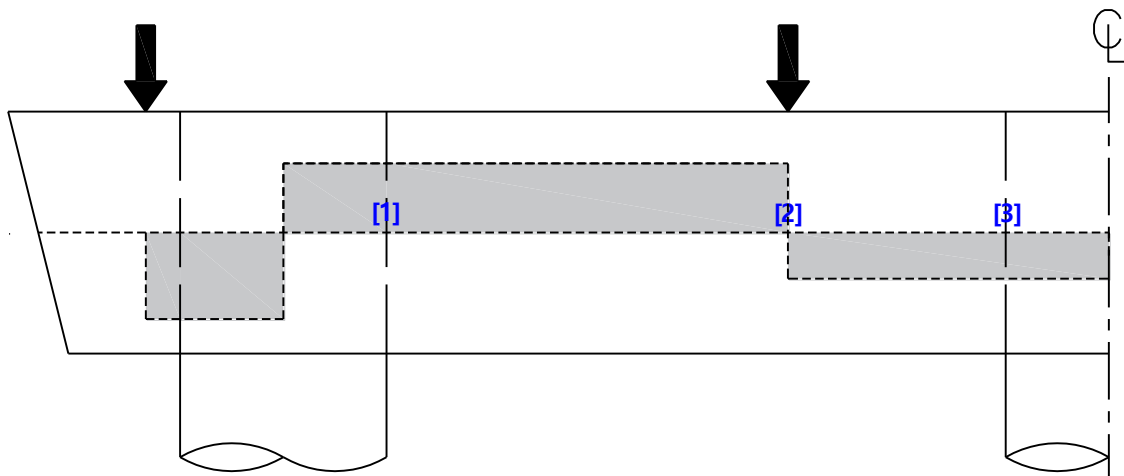

Figure C-3. Shear force diagram and three shear critical section locations.

TxDOT uses a spreadsheet for designing shear based on the general procedure for shear design with tables in AASHTO LRFD provisions. The spreadsheet was used to design shear for both RC and PSC bent caps. Table C-1 summarizes the results. The table provides moment and shear demands, M_u and V_u, longitudinal tensile strain at mid-depth of the member, ε, angle of inclination of diagonal compressive stresses, θ, factor indicating the ability of diagonally cracked concrete to transmit tension and shear, β, shear strengths provided by concrete and steel, V_c and V_s, factored shear strength, ϕV_n, and required spacing at each critical section.

As shown in Table C-1, 376 mm and 290 mm transverse reinforcement spacing were required for RC and PSC bent caps regardless of the critical section considered for both prototype bridges. These required spacing values highlighted a shortcoming of the AASHTO design procedures, in that it did not reflect the fact that prestressing improves shear resistance (Collins et al. 1996; Runzell et al. 2007). The design spacing for the prototype bridges were governed by the requirements for the minimum area of steel. AASHTO requirements for a minimum area of steel were dependent on the concrete compressive strength. The design concrete strength was higher in prestressed bent caps than in RC bent caps, leading to the smaller spacing for the same area of steel.

For this reason, additional shear spacing was calculated considering shear strength requirement without satisfying the requirement of maximum spacing limit and minimum area of steel and compared with design values in

Table C-2. In the table, the first column ($V_u > \phi V_c$) indicates if the demand exceeded the capacity provided by the concrete, that is, is shear reinforcement needed to provide strength. The second value, s_{design}, is the spacing by design following the AASHTO provisions. The third value, $s_{strength}$, is the spacing that would be required to provide the necessary strength, ignoring any requirements on a minimum area of steel or maximum spacing limits.

247

Table C-1. Summary of demands and shear design results.

Design	RC			PSC		
	Critical 1[1]	Critical 2[2]	Critical 3[3]	Critical 1[1]	Critical 2[2]	Critical 3[3]
9.7 m (32 ft) prototype						
M_u (kN-m)	796	633	735	796	633	735
V_u (kN)	547	1125	1161	547	1,125	1,161
ε	8.4×10^{-4}	1.0×10^{-3}	1.0×10^{-3}	2.7×10^{-4}	9.9×10^{-4}	1.0×10^{-3}
θ	34.7	36.4	36.4	26.8	36.3	36.4
β	2.33	2.23	2.23	2.9	2.24	2.23
V_c (kN)	841	805	805	1277	979	974
V_s (kN)	641	601	601	823	569	565
ϕV_n (kN)	1,335	1,263	1,263	1,891	1,392	1,388
$s_{req'd}$ (mm)	376	376	376	610	290	290
12.2 m (40 ft) prototype						
M_u (kN-m)	625	1,223	913	625	1,223	913
V_u (kN)	1,001	956	867	1,001	956	867
ε	1.0×10^{-3}	1.0×10^{-3}	1.0×10^{-3}	9.1×10^{-4}	1.0×10^{-3}	8.2×10^{-4}
θ	36.4	36.4	36.4	35.5	36.4	34.5
β	2.23	2.23	2.23	2.28	2.23	2.34
V_c (kN)	805	805	805	996	974	1,023
V_s (kN)	601	601	601	583	565	609
ϕV_n (kN)	1,263	1,263	1,263	1,423	1,388	1,468
$s_{req'd}$ (mm)	376	376	376	290	290	290

Note: [1] interior face of exterior column; [2] interior girder location; and [3] interior column face

Table C-2. Key values for shear spacing selection.

Prototype	RC Bent Cap			PSC Bent Cap		
	$V_u > \phi V_c$	s_{design}	$s_{strength}$	$V_u > \phi V_c$	s_{design}	$s_{strength}$
BIG-32	Yes	376 mm	376 mm	No	290 mm	None
BIG-40	Yes	376 mm	610 mm	Yes	290 mm	610 mm

Note: s_{design} = spacing satisfying all minimum spacing requirement in AASHTO LRFD specification including minimum area of steel (AASHTO 5.8.2.5) and maximum spacing of transverse reinforcement (AASHTO 5.8.2.7); $s_{strength}$ = required spacing to resist demands without considering minimum area of steel and maximum spacing of transverse reinforcement.

TxDOT uses a maximum spacing of 305 mm (12-in.), which would lead to a revision of the RC design. For simplicity, the transverse reinforcement was not varied along the spans rather the smallest required was used so that both RC and prestressed prototype designs are considered to have a 305 mm (12-in.) spacing.

As an alternative to the design spacing, the spacing needed to only provide adequate strength for the section was considered. As shown in

Table C-2, when the minimum area requirements were ignored, the spacing of the transverse reinforcement for the prestressed bent cap increases dramatically, requiring 610 mm (24-in.) for one prototype, while the other, theoretically, had sufficient strength from the concrete alone and did not require shear reinforcement. While a design with no transverse reinforcement or 610 mm (24-in.) spacing would not meet design requirements in a TxDOT bridge, they were considered in establishing the experimental test matrix.

A section with an interior void was considered as another alternative design. As mentioned earlier, the use of the interior void may bring many advantages by the reduction of the bent cap weight (Taylor et al. 1995; Ueda and Stitmannaithum 1991). A 660 mm (26-in.) size void was regarded to be appropriate to ensure the cover thickness in both interior and exterior sides. Shear design results for a section with 660 mm (26-in.) void from the spreadsheet were summarized for both prototypes in Table C-3. The table only shows the shear design results in critical section 2. This is because a solid section was used in critical sections 1 and 3 so they had the same design result in

Table C-2. Although required spacing was 229 mm (9.0-in.) and 287 mm (11.3-in.) for BIG-32 and BIG-40 prototypes, respectively, 305 mm (12-in.) spacing was used for voided to be consistent with other specimens.

Table C-3. Summary of demands and shear design results for voided bent cap.

Design	BIG-32	BIG-40
	Critical 2	Critical 2
M_u (kN-m)	633	1,223
V_u (kN)	1,125	956
ε	9.3×10^{-3}	1.0×10^{-3}
θ	36.3	36.4
β	2.23	2.23
V_c (kN)	463	463
V_s (kN)	569	565
ϕV_n (kN)	930	925
$s_{req'd}$ (mm)	229	287